Analysis of Ukulele Tones with Comparisons to the Pipa and Classical Guitar

KIRSTEN WONG PIK SOON

A0074846U

Department of Physics

National University of Singapore

2013/2014

Supervisor: Professor Bernard Tan

In partial fulfillment of the requirements for the Degree of Bachelor of Science with Honours

ABSTRACT

In this project, the harmonics of the ukulele strings were analyzed using the Fast Fourier Transform. Using a stereo microphone and an audio interface, recordings were obtained and the Fast Fourier Transform was then performed on the sample using the MATLAB program. This project also serves to examine the variation for amplitudes for each harmonic frequency over the duration of the note. In addition, the inharmonicity coefficients and the deviations between experimental and theoretical data were determined.

These analysis were performed using three different types of ukuleles: Kala Spruce/Rosewood Soprano (Model KA-SRS), Makala Soprano (Model MK-S) and Outdoor Ukulele. Comparisons between two different types of strings were made: Aquila AQ-4U New Nylgut® Regular GCEA Set Soprano and D'Addario T2 Soprano Strings. The thickness of the string was also varied. The Spruce Wood Shanghai Pipa and CG151S Yamaha Classical Guitar were also analyzed and compared with the ukuleles.

ACKNOWLEDGEMENTS

First of all, I would like to express my deepest gratitude to my supervisor, Professor Bernard Tan Tiong Gie, for his guidance and constant supervision in completing this project. I am truly grateful for the opportunity to work on a project which combines my two passions, music and physics, together. His patience in teaching me this field of Physics has enabled me to understand and appreciate Physics better.

I would also like to thank Dr Soh Min and Nicholas Wong who has so patiently and willingly provided advice in this project. I would not have been able to complete this project without their guidance.

Lastly, I am blessed and eternally grateful for my family who has showed me never ending support. I would also like to thank my friends for the encouragement that they have given me throughout my study in NUS.

CONTENTS

Chapter 1

INTRODUCTION

Notes are like letters in a language and are the most basic structure in music. Each note expresses a certain pitch and duration of a musical sound. A real world note does not consist of a single pure tone or frequency but rather a combination of several frequencies known as harmonics. The relative amplitudes of these frequencies give each musical instrument its unique sound. The lowest frequency produced in a note determines its pitch and is also known as the fundamental frequency or first harmonic.

The ukulele is a Hawaiian string musical instrument and is also a member of the guitar family of instruments. The ukulele is known to produce bright sounds and is made out of various types of wood including rosewood, ebony, maple and spruce. It employs four strings and comes in four different sizes: Soprano, Tenor, Concert and Baritone. In this project, the soprano ukulele was selected to be analyzed. Modern ukuleles commonly use synthetic strings such as the nylon strings and thus are the focus of this project.

This project serves to investigate the harmonic frequencies produced by various ukuleles, pipa and classical guitar across strings of different thickness. This project also determines the inharmonicity coefficients of each string used and the amplitudes of the harmonic frequencies were also observed over the duration of the note. The results obtained are then compared with those of the pipa and classical guitar. These analyses may be used as reference in the digital synthesis of ukulele waveforms such as the frequency modulation synthesis.

Chapter 2

THEORY

2.1 The Ukulele

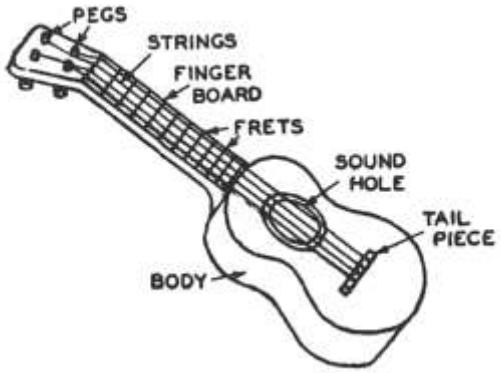

Figure 2.1: Perspective view of a ukulele [1]

The ukulele is often regarded as a smaller version of a guitar. It consists of pegs, strings, a finger board, frets, a sound hole and a tail piece similar to the guitar as indicated in Figure 2.1. The four strings of the ukulele are stretched over the finger board, frets and sound hole, beginning from the pegs all the way down to the tail piece which is fastened to the flat top of the body of the ukulele. The pegs are used to tune the strings according to the specific frequencies which are commonly noted as A4, E4, C4 and G4 and are also used to raise the strings so that they are not in contact with the frets. The resonant frequency of each string can be varied by pressing against the fret. Each fret is separated by a distance in which the sounds produced by pressing against two adjacent frets are a semitone apart [1].

Sound is produced when the strings are allowed to vibrate. These vibrations travel to the tail piece and then to the soundboard which are then amplified through the hollow body of the ukulele. Sound waves then travel out of the sound hole and are heard by listeners.

2.2 The Pipa

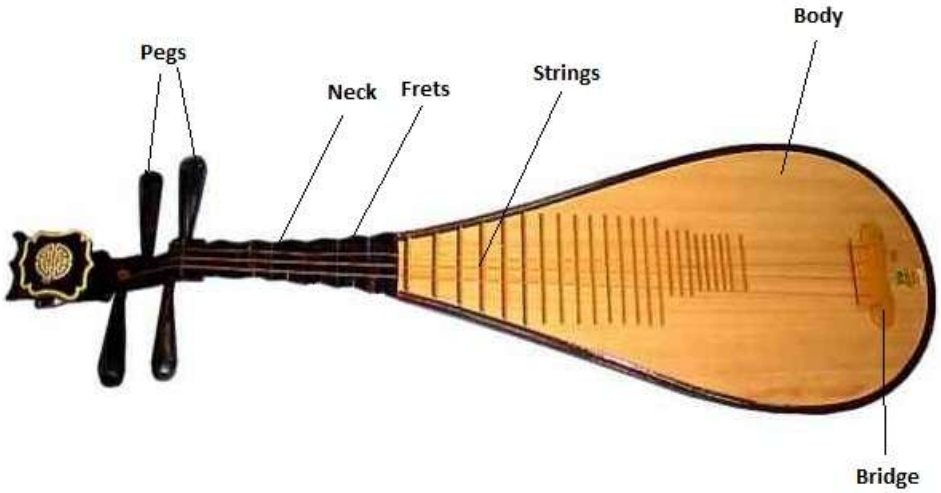

Figure 2.2: Components of a pipa

The pipa, also known as the Chinese lute, is a four-stringed short-necked Chinese instrument and has three segments – the head, neck and body. The head consists of tuning pegs in the sides of the bent-back pegbox whereas the neck consists of 6 frets. The pear-shaped body of the pipa includes the frets, soundboard, the back of the instrument and the bridge [2]. The frets which are made out of bamboo holds the strings in place and allow different notes to be played. The strings of the pipa run along the instrument from the bridge right up to the conical tuning pegs. It is commonly tuned to the notes A2, D3, E3 and A3 [3]. The primary material used for the body, pegs and frets of the pipa in this project is Spruce. The components of the pipa are shown in Figure 2.2.

Traditional pipas are played using silk strings. However, modern pipas use steel core strings coated with nylon, copper or nickel and are plucked with a fake nail made out of turtle shell or special plastics [4]. Similar to the ukulele, the sound production of the pipa begins with the vibration of strings. These vibrations travel to the tail piece and then to the soundboard.

2.3 The Classical Guitar

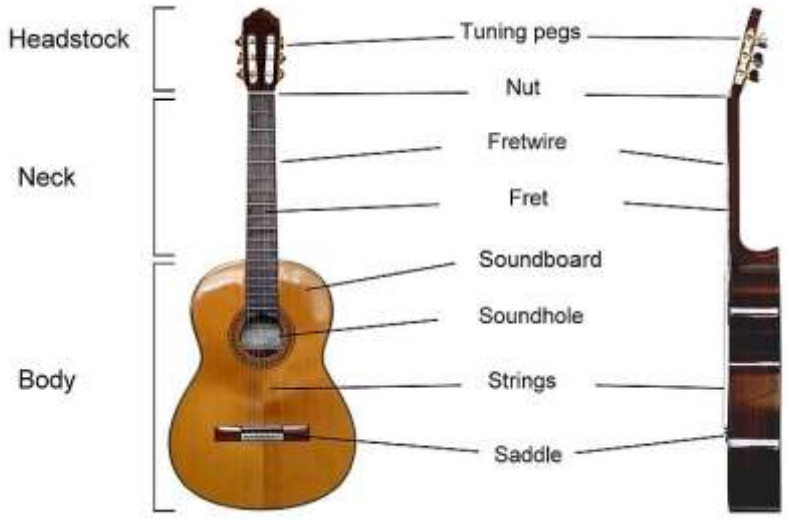

Figure 2.3: Components of the Classical Guitar [5]

The classical guitar is another member of the guitar family which has six strings and may be divided into three sections: Headstock or head, neck and body. The head of the guitar contains the tuning pegs and nut. The tuning peg is used to tune the strings to the notes E4, B3, G3, D3, A2, E2 whereas the nut is a thin, white piece of ebony which holds the strings in place. The neck of the guitar consists of the fretwires and frets. Each fret is separated by a distance in which the sounds produced by pressing against two adjacent frets are a semitone apart. [1] The soundboard, soundhole and saddle make up the body. The strings of the classical guitar are tied onto the bridge which is attached to the saddle and run along the guitar right up to the tuning pegs.

When the guitar is plucked using a finger, the guitar strings are excited and begins to vibrate. The vibrations of the strings bring the bridge into movement [6]. The vibrations then move from the bridge to the soundboard and is amplified by the hollow body of the guitar. The sound waves are then transmitted through the sound hole and are perceived by the listener.

2.4 Physics of Sound: Ideal String Model

Sound is an alteration in pressure, particle displacement, or particle velocity which is propagated in an elastic medium, or the superposition of such propagated alterations [1]. The production of perceived sound begins through various motions such as a vibrating body, intermittent throttling of an air stream or even through an explosion of an inflammable gas [1]. The motion of repetitive variation with time is known as a harmonic oscillator given that the motion is in a system

with a degree of freedom and the capability of oscillation. The number of oscillations produced in one second is known as the frequency and one oscillation per second is known as Hertz (Hz). When in contact with a physical medium such as the atmosphere, the motion of the oscillator transmits mechanical waves in the form of longitudinal compression and rarefaction and thus producing sound [7].

In string musical instruments, the production of perceived sound begins with the transverse vibrations of strings. When a string experiences an increase in amplitude of oscillation and its frequency is equal or very close to the natural undamped frequency, the string is said to be experiencing resonance and is known as a resonator. The frequencies to which the string oscillates are known as resonant frequencies.

2.4.1 The Wave Equation

In order to understand the physical properties which determine the frequencies, Newton's Law is applied to an elastic string and it is found that it obeys the wave equation at small amplitude transverse vibrations.

Plucking can be described as applying a tension force T on an elastic string in which the force applied is larger than the weight of the string. The string has a mass per unit length or linear density, σ and its equilibrium position lies along the x-axis. Figure 2.4 shows the infinitesimal segment of a string, dm. [8]

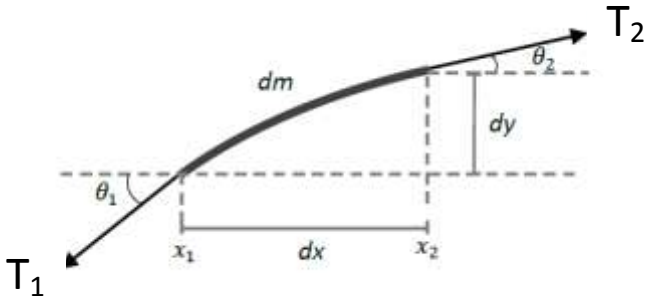

Figure 2.4: Infinitesimal segment of a plucked string [8]

The mass element of the string, $dm = \sigma\sqrt{dx^2 + dy^2}$. Applying Newton's Law to the y-component, we obtain

$$\boldsymbol{\sigma\sqrt{dx^2 + dy^2}\,\frac{\partial^2 y}{\partial t^2} = T_2 \sin\theta_2 - T_1 \sin\theta_1 + Fdx} \quad \textbf{(1)}$$

Fdx is the magnitude of the external forces which act vertically on the string.
Dividing (1) by dx and taking the limit $dx \to 0$,

$$\sigma\sqrt{1+\left(\frac{dy}{dx}\right)^2}\frac{\partial^2 y}{\partial t^2} = \frac{\partial}{\partial x}(T_1 \sin\theta_1) + F$$

$$= \frac{\partial T_1}{\partial x}\sin\theta_1 + T_1\cos\theta_1\frac{\partial \theta_1}{\partial x} + F \quad (2)$$

Comparing the small segment of the string, dm, with the right angle triangle in Figure 2.4 gives

$$\tan\theta_1 = \frac{\partial y}{\partial x} \quad (3)$$

Since y is a function of both x and t, the partial derivative is used in the equation above.

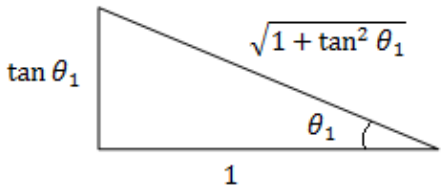

Figure 2.5: Tangent Trigonometric

Using trigonometric relations as shown in Figure 2.5, it can be seen that

$$\sin\theta_1 = \frac{\frac{\partial y}{\partial x}}{\sqrt{1+\left(\frac{\partial y}{\partial x}\right)^2}} \quad (4) \qquad \cos\theta_1 = \frac{1}{\sqrt{1+\left(\frac{\partial y}{\partial x}\right)^2}} \quad (5)$$

$$\theta_1 = \tan^{-1}\frac{\partial y}{\partial x} \quad (6)$$

Differentiating (6),

$$\frac{\partial \theta_1}{\partial x} = \frac{\frac{\partial^2 y}{\partial x^2}}{1+\left(\frac{\partial y}{\partial x}\right)^2} \quad (7)$$

When considering small vibrations such that $|\theta_1| \ll 1$ for all x at any time t, it is implied that $|\tan\theta_1| \ll 1$ and therefore, $\left|\frac{\partial y}{\partial x}\right| \ll 1$. This shows that (7) can be written as

$$\frac{\partial \theta_1}{\partial x} \approx \frac{\partial^2 y}{\partial x^2} \quad (8)$$

Since $\sqrt{1+\left(\frac{\partial y}{\partial x}\right)^2} \approx 1$, $\sin\theta_1 \approx \frac{\partial y}{\partial x}$ and $\cos\theta_1 \approx 1$.

Using these approximations, equation 2 becomes

$$\sigma\frac{\partial^2 y}{\partial t^2} = \frac{\partial T_1}{\partial x}\frac{\partial y}{\partial x} + T_1\frac{\partial^2 y}{\partial x^2} + F \quad (9)$$

Applying Newton's Law to the x-component,

$$\boldsymbol{T_2 \cos\theta_2 - T_1 \cos\theta_1 = 0} \text{ (10)}$$

Assuming that only transverse vibrations occur, (10) can be divided by dx and limited by $dx \to 0$.

$$\boldsymbol{\frac{\partial}{\partial x}(T_1 \cos\theta_1) = 0} \text{ (11)}$$

By using the small amplitude vibrations approximation from before, it is found that $\frac{\partial T_1}{\partial x} \approx 0$ which shows that T is a function t. Therefore, $T_1 \approx T_2 \approx T(t)$. This simplifies (9) further to

$$\boldsymbol{\sigma \frac{\partial^2 y}{\partial t^2} = T(t) \frac{\partial^2 y}{\partial x^2} + F} \text{ (12)}$$

If the string has a constant string density which is independent of x, a string tension T_1 which is independent of t and has no external forces acting on it, the wave equation for an ideal string is obtained as shown below

$$\boldsymbol{\frac{\partial^2 y}{\partial t^2} = c^2 \frac{\partial^2 y}{\partial x^2}} \text{ (13)}$$

The variable c is introduced here as $c = \sqrt{\frac{T}{\sigma}}$ which is also the characteristic speed of travelling waves.

2.4.2 Superposition

The principle of superposition states that the displacement at any point is the sum of the displacements of the two individual waves [4]. Mathematically, it can be described as:

If $y_1(x,t), y_2(x,t), \ldots$ are solutions to the wave equation, then the sum $y_s(x,t) = K_1 y_1(x,t) + K_2 y_2(x,t) + \cdots$ is another solution where K_i are arbitrary constants.

Applying this principle to the wave equation, the following equation is obtained.

$$\boldsymbol{\frac{\partial^2 y_s}{\partial t^2} = c^2 \frac{\partial^2 y_s}{\partial x^2}} \text{ (14)}$$

2.4.3 Solution to the Wave Equation

The general solution of the wave equation can be written in the form

$$\boldsymbol{y(x,t) = f_1(ct - x) + f_2(ct + x)} \text{ (15)}$$

The nature of functions f_1 and f_2 are arbitrary here as this is a general solution for waves on an infinite string. The function $f_1(ct - x)$ represents a wave travelling to the right and the function $f_2(ct + x)$ represents a wave travelling to the left. Both waves are travelling with the velocity of c. The wave equation may also be solved using the method of separation of variables which assumes that the function for distance of position and time, $y(x, t)$ can be written as the product of the function of position, $X(x)$ and the function of time $T(t)$.

In other words,

$$\boldsymbol{y(x,t) = X(x) \times T(t)} \quad \textbf{(16)}$$

Applying this to equation 13,

$$\boldsymbol{\frac{\delta^2 X(x)}{\delta t^2} T(t) + \frac{\delta^2 T(t)}{\delta t^2} X(x) = c^2 \frac{\delta^2 X(x)}{\delta x^2} T(t) + c^2 \frac{\delta^2 T(t)}{\delta x^2} X(x)} \quad \textbf{(17)}$$

Since $X(x)$ is independent of t and $T(t)$ is independent of x, equation 16 becomes

$$\boldsymbol{\frac{\delta^2 T(t)}{\delta t^2} X(x) = c^2 \frac{\delta^2 X(x)}{\delta x^2} T(t)} \quad \textbf{(18)}$$

Letting $\frac{\delta^2 T(t)}{\delta t^2} = T''(t)$ and $\frac{\delta^2 X(x)}{\delta x^2} = X''(x)$,

$$\boldsymbol{\frac{X''(x)}{X(x)} = \frac{T''(t)}{T(t)} \frac{1}{c^2}} \quad \textbf{(19)}$$

In (19), the left hand side of the equation is independent of t whereas the right hand side of the equation is independent of x. This means that both sides are equal to a constant, μ.

The solutions of the differential equations $\frac{X''(x)}{X(x)} = \mu$ and $\frac{T''(t)}{T(t)} \frac{1}{c^2} = \mu$ are

$$\boldsymbol{X(x) = a_1 e^{\sqrt{\mu} x} + a_2 e^{-\sqrt{\mu} x}} \quad \textbf{(20)}$$

$$\boldsymbol{T(t) = a_3 e^{c\sqrt{\mu} x} + a_4 e^{-c\sqrt{\mu} x}} \quad \textbf{(21)}$$

2.4.4 The Standing Wave

Consider a string of length L fixed at $x = 0$ and $x = L$. Applying these boundary conditions to (19), it is found that $a_1 = -a_2$ and $a_1(e^{\sqrt{\mu} L} - e^{-\sqrt{\mu} L}) = 0$. Ignoring solutions with $a_1 = 0$ which implies the trivial case $X(x) = 0$ for all x,

$$\boldsymbol{e^{2\sqrt{\mu} L} = 1} \quad \textbf{(22)}$$

Assuming that σ is nonzero and using the equation $e^{2n\pi i} = 1$ for any integer n, this implies that

$$\sqrt{\boldsymbol{\mu}} = \frac{\boldsymbol{n\pi}}{\boldsymbol{L}}\boldsymbol{i} \quad \textbf{(23)}$$

Since only certain values of n are allowed, the frequencies for the string of fixed ends are discrete:

$$\boldsymbol{\omega_n = ck_n = \frac{cn\pi}{L}} \quad \textbf{(24)}$$

where k_n is the wave vector.

Using Euler's formula, the complete solution for a normal mode is

$$\boldsymbol{y(x,t) = X_i(x)T_i(t) = \sin\left(\frac{n\pi}{L}x\right)\left[\alpha\cos\left(c\frac{n\pi}{L}t\right) + \beta\sin\left(c\frac{n\pi}{L}t\right)\right]} \quad \textbf{(25)}$$

The oscillation of a string is a complex standing wave as it is a linear superposition of normal modes. [11] Therefore, the general solution for a string is

$$y(x,t) = \sum_i X_i(x)T_i(t) = \sum_{n=1}^{\infty} \sin\left(\frac{n\pi}{L}x\right)\left[\alpha_n\cos\left(c\frac{n\pi}{L}t\right) + \beta_n\sin\left(c\frac{n\pi}{L}t\right)\right]$$
$$= \boldsymbol{\sum_{n=1}^{\infty} \sin(k_n x)[\alpha_n \cos(\omega_n t) + \beta_n \sin(\omega_n t)]} \quad \textbf{(26)}$$

Mathematically, the wavelength of the standing wave is defined as

$$\boldsymbol{\lambda_n = \frac{2\pi}{k_n} = \frac{2L}{n}} \quad \textbf{(27)}$$

The longest wavelength possible is $2L$. This corresponds to the smallest frequency which is also known as the fundamental frequency, f_1.

$$\boldsymbol{f_1 = \frac{\omega_1}{2\pi} = \frac{c}{2L}} \quad \textbf{(28)}$$

The resonant frequencies are all integer multiples of the fundamental frequency and may be expressed as

$$\boldsymbol{f_n = n\frac{c}{2L} = nf_1} \quad \textbf{(29)}$$

These frequencies are called harmonics and the series is called a harmonic series. Overtones consist of frequencies from all harmonics except for the fundamental frequency or the first harmonic.

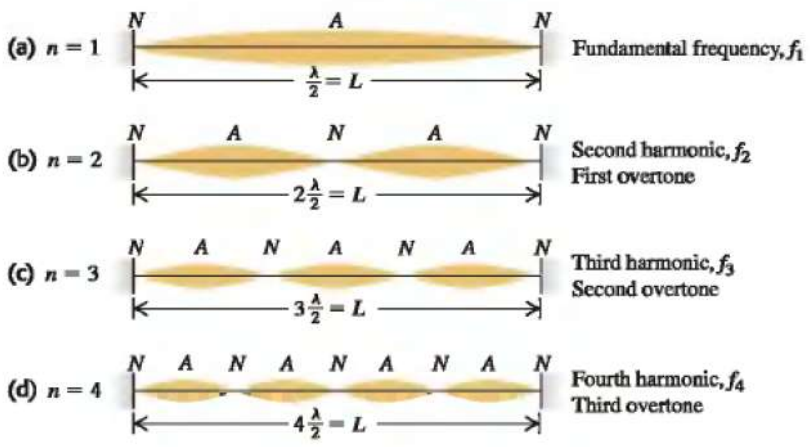

Figure 2.6: The first four normal modes of a string fixed at both ends [12]

Figure 2.6(a) shows the standing waves which produces the fundamental frequency, f_1 whereas Figure 2.6(b), (c) and (d) show the configurations for the first, second and third overtone. Nodes are points on the string which do not move throughout oscillation and noted as N in Figure 2.6. Antinodes are points in between two nodes and are noted as A.

When a string is plucked, the displacement of the string is not as simple as the ones in Figure 2.6. Instead, a complex standing wave is formed in which the fundamental and overtones are present in the vibration. As mentioned previously, it is a superposition of many normal modes. In addition, the harmonic content of the standing wave of the string is not exactly the same as the travelling sound wave in the air but are very similar. The harmonic content depends on the location in which the string is plucked.

2.5 Physics of Sound: Stiff String Model

2.5.1 Stiff String Model

In the paper titled "Normal Vibration Frequencies of a Stiff Piano String" [13], Harvey Fletcher modified the ideal string model so that it applies to stiff strings. Fletcher's model appears to be a commonly accepted model up to this day because it has been proven to agree better with the realistic string musical instrument.

Consider a string with a displacement y at a position x. If a tension T is applied, the restoring force is given by

$$\boldsymbol{T\left(\frac{\partial^2 y}{\partial x^2}\right)} \quad \textbf{(30)}$$

If Q is the Young's modulus of material, A is the cross-sectional area of the string and K is the radius of gyration, the restoring force due to the elastic stiffness of the string is

$$-\boldsymbol{QAK^2}\left(\frac{\partial^4 y}{\partial x^4}\right) \text{ (31)}$$

Using the equation $F = ma$, the differential equation describing the motion of the string becomes

$$\boldsymbol{\sigma}\left(\frac{\partial^2 y}{\partial t^2}\right) = \boldsymbol{T}\left(\frac{\partial^2 y}{\partial x^2}\right) - \boldsymbol{QAK^2}\left(\frac{\partial^4 y}{\partial x^4}\right) \text{ (32)}$$

where σ is the linear density of the string.

Fletcher also noted that the frictional term of the form

$$\boldsymbol{R}\left(\frac{\partial y}{\partial t}\right) \text{ (33)}$$

should be included to the right hand side of (30) but is neglected due to its small contributions to the values of partial frequencies.

The following substitutions were made for convenience

$$\boldsymbol{B} = \frac{\pi^2 QAK^2}{Tl^2} \text{ (34)}$$

$$\boldsymbol{f_1} = \frac{1}{2l}\sqrt{\frac{T}{\sigma}} \text{ (35)}$$

where l is the length of the string between its supports and B is labelled as the inharmonicity coefficient. For a string which has no stiffness and negligible retarding force, the value of f_1 is taken to be the fundamental vibration of the string.

Assuming the solution to the differential equation (32) is a sum of terms of the form

$$\boldsymbol{y = Ce^{2\pi kx}e^{-2\pi ift}} \text{ (36)}$$

Where C, k and f are constants to be determined from the initial and boundary conditions.

Substituting (36) into (32), it is found that

$$\boldsymbol{k^4 - \left(\frac{1}{4Bl^2}\right)k^2 - \left(\frac{f^2}{16Bl^4 {f_1}^2}\right) = 0} \text{ (37)}$$

By solving this equation, 4 solutions are produced:

$$\boldsymbol{k = \pm\sqrt{\frac{1}{8Bl^2}\left(\sqrt{1 + \frac{4Bf^2}{{f_1}^2}} + 1\right)} \equiv \pm k_1} \text{ (38)}$$

$$\boldsymbol{k = \pm i\sqrt{\frac{1}{8Bl^2}\left(\sqrt{1 + \frac{4Bf^2}{{f_1}^2}} - 1\right)} \equiv \pm ik_2} \text{ (39)}$$

in which k_1 is related to k_2 as

$$\boldsymbol{k_1}^2 - \boldsymbol{k_2}^2 = \frac{\mathbf{1}}{\mathbf{4}\boldsymbol{Bl}^2} \text{ (40)}$$

The general solution can be written as

$$\boldsymbol{y = e^{-2\pi ift}[K_1 \cosh(2\pi k_1 x) + K_2 \sinh(2\pi k_1 x) + K_3 \cos(2\pi k_2 x) + K_4 \sin(2\pi k_2 x)]} \text{ (41)}$$

These relations are independent of the boundary conditions. Therefore, the values of k_2 and f can be obtained if the corresponding $k_1$value is found. The boundary conditions may be selected based on how the coordinates are defined. For example, if the midpoint of the string is selected to be the origin, the boundary conditions will be symmetrical with its ends at $\frac{l}{2}$ and $-\frac{l}{2}$. The first two terms in (41) will be even functions whereas the last two terms will be odd functions.

2.5.2 Pinned Boundary Conditions

For the ukulele, pipa and classical guitar, the two ends of the strings are pinned down at the head and bridge of the respective musical instruments similar to a string which is pinned by knife edges.Then,

$$\boldsymbol{y = \frac{\partial^2 y}{\partial x^2} = 0} \text{ at } \boldsymbol{x = \frac{l}{2}} \text{ and } \boldsymbol{-\frac{l}{2}} \text{ (42)}$$

Considering only even functions that is to take K_2 and K_4 as zero, these boundary conditions will fit if $K_1 = 0$ and $\cos(\pi kl) = 0$. This means

$$\boldsymbol{k = \frac{n}{2l}} \text{ (43)}$$

where $n = 1,3,5,7$ or any odd integer.

There is a corresponding frequency f of the odd partials obtained for each value of k, that is

$$\boldsymbol{f_n = nf_1(1 + Bn^2)^{\frac{1}{2}}} \text{ (44)}$$

The corresponding displacement equation will then be

$$\boldsymbol{y = K_3 \cos\left(\frac{\pi n x}{l}\right) \cos(2\pi f_n t)} \text{ (45)}$$

The value of K_3 is different for each off partial and is determined by the amplitude of that partial. However, if only odd functions are considered, K_1, K_2 and K_3 are zero and $\sin(\pi kl) = 0$. In other words,

$$k = \frac{n}{2l} \text{ (43)}$$

where $n = 2,4,6,8$ or any even integer.

Similar to the case in which even functions are considered, the frequencies corresponding to these values of k are

$$\boldsymbol{f_n = nf_1\left(1 + Bn^2\right)^{\frac{1}{2}}} \quad \textbf{(46)}$$

The displacement equation is

$$\boldsymbol{y = K_4 \sin\left(\frac{\pi n x}{l}\right) \cos(2\pi f_n t)} \quad \textbf{(47)}$$

The value of K_4 is different for each even partial and is determined by the amplitude of that partial.

2.5.3 Inharmonicity Coefficient

In the ideal string model, it is seen that the series of frequencies produced are harmonic but this is not the case in reality. The resonant frequencies produced by a string musical instrument deviate from the ideal harmonic series. This phenomenon is also known as inharmonicity. The degree to which it deviates is quantified through the inharmonicty coefficient and is dependent on several variables such as the thickness of the string.

In Fletcher's stiff string model, the constant B was introduced in (34) and is defined as follows

$$\boldsymbol{B = \frac{\pi^2 Q A K^2}{T l^2} = \frac{\pi^3 Q d^4}{64 T l^2}} \quad \textbf{(48)}$$

where d is the diameter of the string.

Young's modulus is a measure of stiffness of an elastic isotropic material. Since each material has a unique Young's modulus, it is also used as a quantity to characterize materials.

2.5.4 String Characteristics

In this project, the correlation of the string's thickness to its inharmonicity coefficient is examined. The inharmonicity coefficient is expected to correlate linearly to the 4th power of the diameter of the strings according to the stiff string model. The theoretical inharmonicity coefficients were obtained through two methods, one by using the tensions of the strings obtained from the manufacturer's data and another by using the linear densities of the strings.

All ukuleles strings and 3 out of the 6 strings of the classical guitar are round solid plain strings which are similar to nylon or gut strings. The ukulele strings in this project have diameters ranging from $0.5265mm$ to $1.0025mm$ and the nylon strings of the classical guitar have diameters ranging from $0.6928mm$ to $0.9863mm$. The thinnest string of the pipa is also a round solid plain string but is made out of steel and has a diameter of $0.2555mm$.

The remaining strings of the guitar are steel core strings wound with nylon and coated with a helical coil of plastic as shown in Figure 2.7.

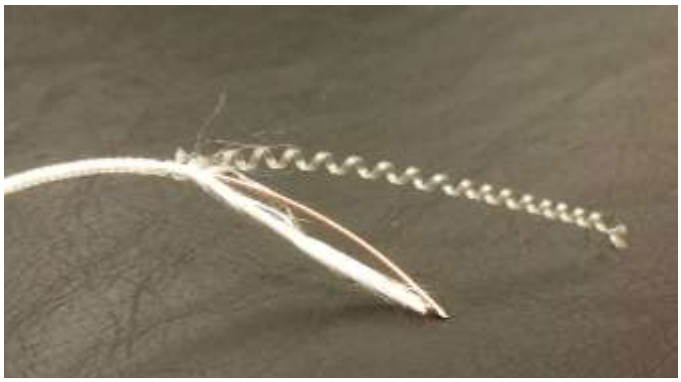

Figure 2.7: Components of the Pipa String

The wound strings of the guitar have a nylon core which is wound using silver-plated copper on a multi-filament nylon core as shown in Figure 2.8.

Figure 2.8: Components of the Wound Classical Guitar String

According to Fletcher, windings contributed negligibly to the stiffness of the string. Therefore, windings are said to increase the mass of a string and lowers the pitch of the tone produced without increasing the stiffness and thus, the inharmoncity of the string.

As defined before, the fundamental frequency of a string is

$$\boldsymbol{f_1 = \frac{1}{2l}\sqrt{\frac{T}{\sigma}}} \textbf{ (35)}$$

Substituting this into equation (48), the inharmonicity coefficient can be written as

$$B = \frac{\pi^3 Q d^4}{256 {f_1}^2 \sigma l^4} \text{ (49)}$$

Solid Strings

For solid strings, the theoretical calculations made using equation (49) are relatively simple. The linear density,σ is calculated by

$$\sigma = cross\ sectional\ area\ \times volume\ density \text{ (50)}$$

Wound Strings

The calculations for these complex strings are not as simple as the case of solid strings. Fletcher introduced a model of calculation by assuming that the restoring elastic torque is due to the core of strings but the linear density is due to the core and windings.

Letting the diameter of the string including its windings be D and the diameter of the core be d and assuming that the windings were a sheaf, the cross sectional area of the windings would be

$$\frac{\pi D^2}{4} - \frac{\pi d^2}{4} \quad (51)$$

If the wire is round, this value would be reduced to $\frac{\pi}{4}$ of this value.

The linear density is then calculated by

$$\sigma = (core\ cross\ sectional\ area\ \times core\ volume\ density) + (windings\ cross\ sectional\ area\ \times windings\ volume\ density) \quad (52)$$

Fletcher experimented on the values of QSK^2 and found that the measure value of QSK^2 is only about 7% higher than that for the core alone. Although Fletcher determined this using steel core wires wound with copper windings, this estimation is used to obtain approximate calculations for the wrapped strings of the pipa.

2.6 Recording

2.6.1 Sampling

A sample is defined as a value or set of values at a point in time and/or space. Sampling refers to the process of converting a continuous signal of a sound wave into a numeric sequence which is a function of discrete time or space. This is then used in the Fast Fourier Transform (FFT) analysis. The sampling interval is denoted as T_s . The sampling-rate or sampling frequency refers to the number of samples obtained in one second or in other words, $f_s = \frac{1}{T_s}$

If the highest frequency of the original signal is f, the Nyquist-Shannon sampling theorem shows that a signal that has been sampled can be reconstructed from an infinite sequence of samples if the sampling rate exceeds $2f$ samples per second. The sampling rate selected for this project is 48000Hz. From the sampling theorem, the reconstructed sample will have a maximum frequency of 24000Hz which lies well within the range of human hearing.

2.6.2 Harmonic Analysis

A Fourier transform decomposes a function into an alternate representation. There are various types of Fourier transforms which are characterized based on their input and output functions [14]. In this project, the Fast Fourier Transform (FFT) was applied in order to determine the

frequency components of a signal buried in a time domain signal. The FFT is an algorithm that computes the Discrete Fourier Transform (DFT) and its inverse.

DFTs, as its name implies, map periodic sequences in the time domain to periodic sequences in the frequency domain [8]. Since the input function of the DFT is a finite sequence of discrete values, it is a suitable method for processing digital data stored in computers.

Consider a sequence x_n of length N which is transformed into another sequence X_k of N complex numbers using DFT, the general equation is

$$X_k = \sum_{n=0}^{N-1} x_n e^{-\frac{i2\pi kn}{N}} = \sum_{n=0}^{N-1} x_n W_N^{kn}, \qquad 0 \leq k \leq N-1 \quad (53)$$

where $W_N = e^{-\frac{i2\pi}{N}}$. This equation implies that the there are N complex multiplications and $N-1$ complex additions for each value of k. Therefore, to compute X_k, the DFT requires N^2 complex multiplications and $N \cdot N - 1$ complex additions. Direct computation of X_k is inefficient because it does not apply the symmetry and periodicity properties of the phase factor, W_N. The two properties can be represented as follows:

$$\text{Symmetry property: } W_N^{k+\frac{N}{2}} = -W_N^k$$

$$\text{Periodicity property: } W_N^{k+N} = W_N^k$$

The FFT utilizes these two properties in order to reduce the number of complex multiplications and additions in the transformation matrix. The most common FFT algorithm used is the Cooley-Tukey algorithm which recursively breaks down the DFT into many smaller DFTs of sizes N_1 and N_2.

One form of the Cooley-Tukey algorithm is the radix-2 decimation-in-time (DIT) FFT. The Radix-2 DIT considers the computation of the $N = 2^v$ sample DFT by dividing the N sample data sequence into two $\frac{N}{2}$-sample data sequences x_{2m} and x_{2m+1} corresponding to the even-indexed samples and odd-indexed samples of x_n. In other words, it decimates the x_n function by a factor of 2 just as its name suggests.

$$X_k = \sum_{m=0}^{\frac{N}{2}-1} x_{2m} e^{-\frac{i2\pi k(2m)}{N}} + \sum_{m=0}^{\frac{N}{2}-1} x_{2m+1} e^{-\frac{i2\pi k(2m+1)}{N}}$$

$$= \sum_{m=0}^{\frac{N}{2}-1} x_{2m} e^{-\frac{i2\pi k(2m)}{N}} + e^{-\frac{i2\pi k}{N}} \sum_{m=0}^{\frac{N}{2}-1} x_{2m+1} e^{\frac{i2\pi k(2m)}{N}} \quad (54)$$

$$X_k = E_k + e^{-\frac{i2\pi k}{N}} O_k \quad (55)$$

where E_k and O_k are the DFTs of the even-indexed inputs and odd-indexed inputs. $e^{-\frac{i2\pi k}{N}}$ is a phase factor which is also known as the twiddle factor and obeys the following relation:

$$e^{-\frac{i\pi}{N}\left(k+\frac{N}{2}\right)} = e^{-\frac{i\pi k}{N}} e^{-i\pi} = -e^{-\frac{i\pi k}{N}} \quad (56)$$

Due to the periodicity property of DFT,

$$E_{k+\frac{N}{2}} = E_k \text{ and } O_{k+\frac{N}{2}} = O_k \quad (57)$$

Therefore, the DFT equation can now be expressed as

$$X_k = \begin{cases} E_k + e^{-\frac{2\pi i}{N}k} O_k & if\ k < \frac{N}{2} \\ E_{k-\frac{N}{2}} - e^{-\frac{2\pi i}{N}(k-\frac{N}{2})} O_{k-\frac{N}{2}} & if\ k \geq \frac{N}{2} \end{cases} \quad (58)$$

This result is the core of the radix-2 DIT fast Fourier transform. The direct computation of E_k and O_k requires $\left(\frac{N}{2}\right)^2$ complex multiplications whereas the computation of $e^{-\frac{2\pi i}{N}k} O_k$ requires an additional $\frac{N}{2}$ complex multiplications. Therefore, the overall computation of X_k requires $2\left(\frac{N}{2}\right)^2 + \frac{N}{2}$ which is a reduction from the initial results of N^2. This reduction is about a factor of 2 for large N. The decimation of the data sequence can be repeated again by reducing it to two $\frac{N}{4}$ sample length DFTs using E_k and O_k. This decimation can be performed $v = \log_2 N$ times and thus reducing the total number of complex multiplications to $\frac{N}{2}\log_2 N$. The number of complex additions will be reduced to $N \log_2 N$.

Taking $N = 8$ sample DFT as an example, the computation is carried out in three stages. The first stage is the computation of four two sample length DFTs or two-point DFTs followed by two four sample long DFT. Lastly, the computation of one eight sample long DFT. These three stages are illustrated in Figure 2.9.

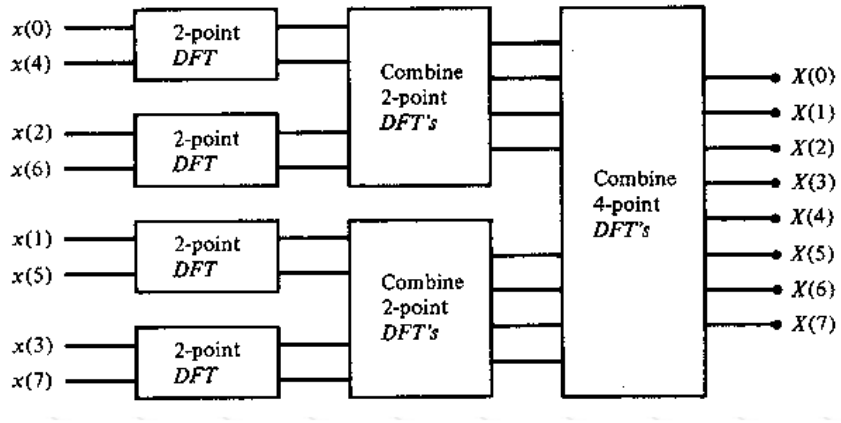

Figure 2.9: Three stages in the computation of an $N = 8$-point DFT

The Cooley-Tukey algorithm is applied with any decimation that recursively re-expresses a DFT of a composite size $N = N_1 N_2$ in the computational program used in this project, MATLAB®. The decimation does not necessarily have to be fixed to a factor of 2 and the function used in MATLAB® deals with a combination of decimations that offers decent optimization.

Chapter 3

EXPERIMENTAL METHODOLOGY

3.1 Equipment

3.1.1 Musical Instruments and Strings

Three types of ukuleles were used in this experiment in order to study the effects of the quality of ukulele on its frequencies. The ukuleles used are shown in Figure 8.

Figure 3.1: (a) Kala Spruce/Rosewood Soprano Ukulele (b) Makala Soprano (c) Outdoor Ukulele

Figure 3.1(a) shows the Kala Spruce/Rosewood Soprano (Model KA-SRS). The Kala ukulele has a solid spruce top and its back, fingerboard, sides and bridge are made out of rosewood. The second ukulele used is the Makala Soprano (Model MK-S) which mainly consists of agathis. Similar to the Kala Ukulele, its fingerboard and bridge is made out of rosewood [16]. Lastly, the most unique ukulele was selected which is the Outdoor Ukulele. Its injection molded composite polycarbonate creates a sturdy structure and tonal quality similar to a traditional ukulele [17]. All ukuleles were tuned according to the frequencies of the Equal-tempered scale. The two sets of strings compared in this experiment for each ukulele are the Aquila AQ-4U New Nylgut® Regular GCEA Set Soprano and D'Addario T2 Soprano Strings as shown in Figure 3.2 (a) and (b) respectively.

Figure 3.2: (a) Aquila AQ-4U New Nylgut® Regular GCEA Set Soprano **(b)** D'Addario T2 Soprano Strings **(c)** Pipa Strings **(d)** D'addario EJ45 Pro-Arte Nylon, Normal Tension

The Aquila AQ-4U New Nylgut® Regular GCEA Set Soprano is constructed out of Nylgut which has a specific density and acoustical qualities which are nearly identical to the traditional gut strings. It also has improved resistance under tension than that of gut and is known to be considerably better than that of Nylon and thus is given the name Nylgut [18]. The D'addario T2 Soprano Strings are made from a dense monofilament which is similar to nylon. This unique material is suitable for the Ukulele because of its brighter tone and increased projection [19].

The Spruce Wood Shanghai Pipa was also selected for analysis in this experiment. The Shanghai pipa string is made of a steel core which is wound together with nylon within a helical coil of plastic except for the first string [2] [4]. Figure 3.2(c) shows the set of pipa strings used in this project. The pipa was tuned according to the frequencies of the Just scale.

The classical guitar used in this experiment is the CG151S Yamaha Classical Guitar. The strings used for this guitar is the EJ45 Pro-Arte Nylon, Normal Tension as shown in Figure 3.3(d). The treble set of strings (E4, B3, G3) are made out of nylon whereas the bass strings are wound using silver-plated copper on a multi-filament nylon core [23]. The classical guitar was tuned according to the frequencies of the Equal-tempered scale.

3.1.2 Microphone and Audio Interface

The microphone used in this project is RODE® NT4 microphone which is a stereo microphone that contains two audio channels. Sounds are detected from its right and left channels and its signals are sent to the audio interface. Before analyzing the sound waves, the two audio signals were combined into one signal. The M-audio® FAST TRACK PRO audio interface is used to convert incoming analog audio signals into digital audio data and sends this data to the operation system. In this project, the Windows 7 Vista operating system was used. All recordings were made in the acoustic laboratory of National University of Singapore (NUS).

3.1.3 Software

Audacity is a multi-track audio recorder which was used in this experiment to interface with the RODE® NT4 microphone. This software was used to record and save the waveforms produced by the string musical instruments. The waveforms were also exported into the Waveform Audio File Format (.wav) using a Pulse-code modulation (PCM) method as digital data which was then used for the Fast Fourier Transform analysis in MATLAB® R2012b. MATLAB® R2012b is a programming platform used for numerical computation, data analysis, algorithm development and visualization. [10] Two algorithms were written and used to perform the FFT on the samples in order to obtain the

harmonic spectrum of the samples and to determine the amplitudes of the harmonic frequencies over time.

3.2 Setup

When the strings of the ukulele, pipa and guitar are plucked, the vibrations of the strings excite the bridge and top plate as mentioned previously [24]. Therefore, it is important that the hollow body of these musical instruments should be in minimal contact with any other object. In this experiment, the instruments were supported by tripod stands. One end of the instrument was clamped by a tripod stand while the hollow body of the instrument was supported by the stem of another tripod stand. The experiment set up is shown in Figure 3.5.

Figure 3.5: Experimental Setup

The microphone was set up onto a microphone stand and was placed near the sound-hole for the ukulele and guitar and near the region in between the neck and bridge for the pipa. Since the microphone used is directional, the laptop used to record sound samples were placed behind the microphone so that it would not affect the recordings made.

3.3 Procedure

1. The RODE®NT4 microphone was set up as stated in section 3.2.
2. The first string of the ukulele was plucked by a finger.
3. The sustained sounds produced were recorded and stored using the program Audacity.
4. The remaining strings of the ukulele were each plucked and recorded at a sampling rate of 48000Hz with a bit depth of 32 bits.
5. The variables were varied and repeated for

a. Three different types of ukuleles

b. Two different types of strings

6. Steps 1 to 4 were then repeated for the pipa and classical guitar.

7. An algorithm was written in the MATLAB language to perform the FFT function on the entire wav file (Appendix A). The amplitudes graphs of the samples were plotted in both time and frequency domains. A calibration spectrum was used to identify the range in which the harmonics were present.
8. The frequencies of harmonics for several samples were determined for each string from the frequency domain graph and were recorded. The average of these values was calculated.
9. The ideal harmonic series is obtained through calculation using the value of the fundamental frequency from the sample.
10. The equation $f_n = nf_1(1 + Bn^2)^{\frac{1}{2}}$ (46) is rearranged as

$$\frac{{f_n}^2}{n^2} = Bn^2{f_1}^2 + {f_1}^2$$

The graph of $\frac{{f_n}^2}{n^2}$ against $n^2{f_1}^2$ is plotted and a best line is fitted using the method of least squares. The gradient of the graph is equivalent to the inharmonicity coefficient.

11. The theoretical values of the inharmonicity coefficient of the ukulele, pipa and classical guitar strings were calculated using the following equations

$$B = \frac{\pi^3 Q d^4}{64Tl^2} \quad (48)$$

$$B = \frac{\pi^3 Q d^4}{256{f_1}^2 \sigma l^4} \quad (49)$$

12. Equation (46) may also be arranged accordingly

$$\sqrt{{f_n}^2 - n^2{f_1}^2} = B^{\frac{1}{2}} f_1 n^2$$

The graph of $\sqrt{{f_n}^2 - n^2{f_1}^2}$ is plotted against n in order to observe the degree to which the experimental frequencies deviate from the ideal harmonic frequencies and to compare among the different instruments and strings used in this project.

13. An algorithm is written in the MATLAB language in order to observe the variation of amplitudes of the harmonic frequencies over the duration of the sample (Appendix B).

Chapter 4

RESULTS AND DISCUSSION

4.1 Inharmonicity Coefficient

Due to the unavailability of the actual values of the tension, T of the Aquila AQ-4U New Nylgut® and Pipa set of strings, the theoretical values of the inharmonicity coefficient were calculated using two different equations. The first being

$$B = \frac{\pi^3 Q d^4}{64 T l^2} \quad (48)$$

The tensions of the D'addario T2 Soprano Strings were used for the Aquila set of strings for comparisons of the inharmonicity coefficients. The second equation used is

$$B = \frac{\pi^3 Q d^4}{256 {f_1}^2 \sigma l^4}$$

The diameters of all strings and lengths of all instruments were measured and the mean values were calculated. The cross sectional areas and linear density were also calculated. Several values of the Young's modulus of nylon ranging from $4.41 - 5.40GPa$ [7] were used as the specific Young's moduli of the strings used in this project have not been determined yet. The Young's modulus of the steel core of the Pipa strings E3, D3 and A2 used is $195GPa$ [13].

The experimental and theoretical values of the inharmonicity coefficient, B were plotted on a graph against its diameter in order to observe the correlation of points.

The diameters of the ukulele strings were found to increase in the order of A4, G4, E4 and C4. The inharmonicity coefficients were compared across the various types of ukuleles using a low, medium and high value of the Young's modulus of nylon based on the range obtained from the *Manual of guitar technology: The history and technology of plucked string instrument.*

4.1.1 Inharmonicity Coefficient Calculated Using Tension

(a) Ukulele Strings

Figures 4.1.1 and 4.1.2 show the graphs of B against d with $Q = 4.41GPa$ for both Aquila and D'addario strings respectively.

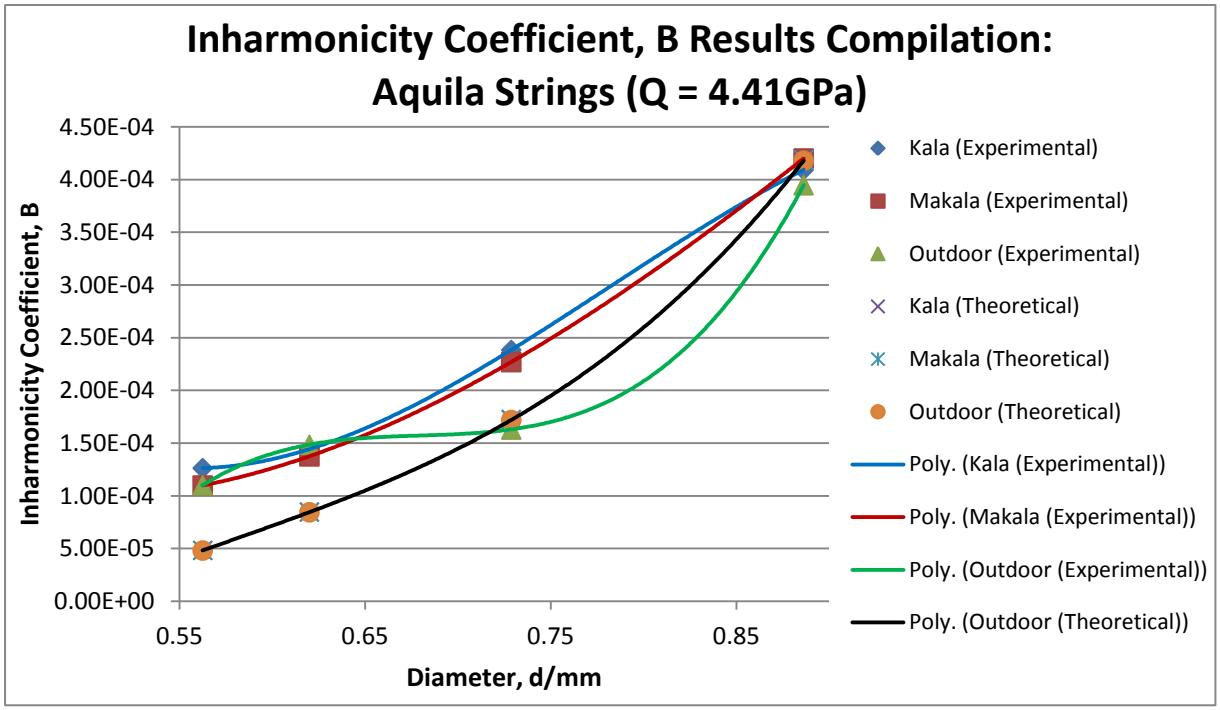

Figure 4.1.1: Plot of Inharmonicity Coefficient, B against diameter, d/mm for the Aquila Strings

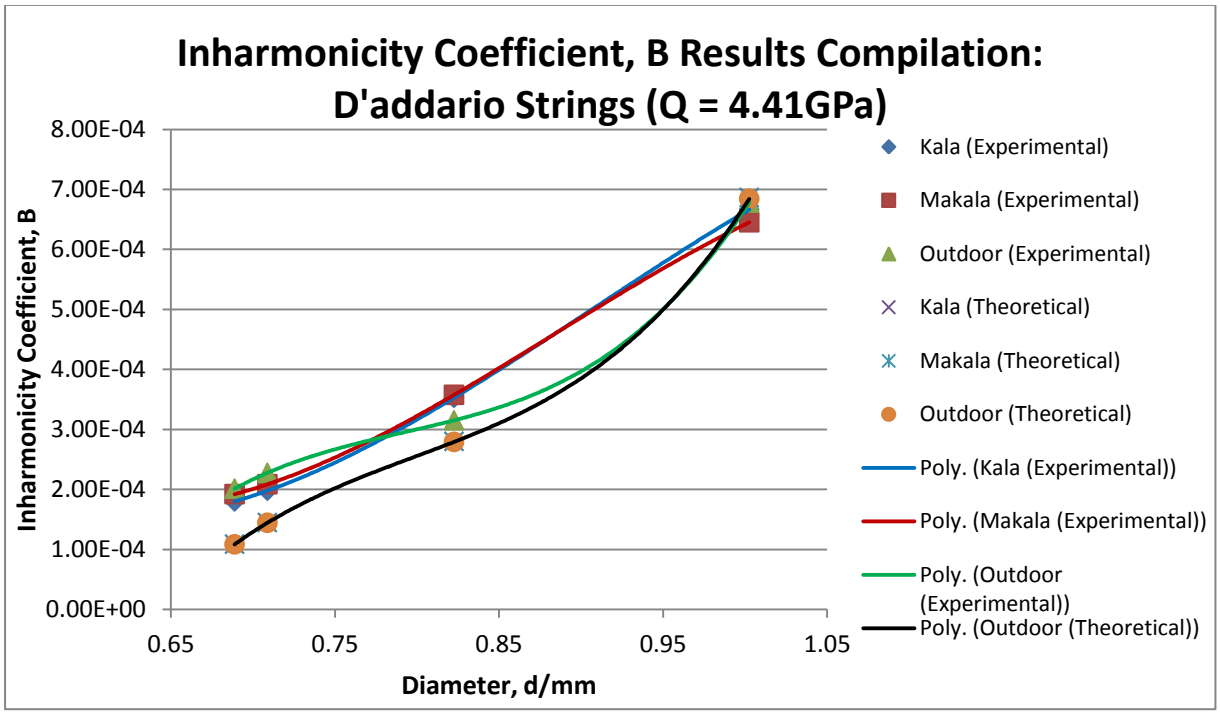

Figure 4.1.2: Plot of Inharmonicity Coefficient, B against diameter, d/mm for the D'addario Strings

Figures 4.1.3 and 4.1.4 show the graphs of B against d with $Q = 4.905GPa$ for both Aquila and D'addario strings respectively.

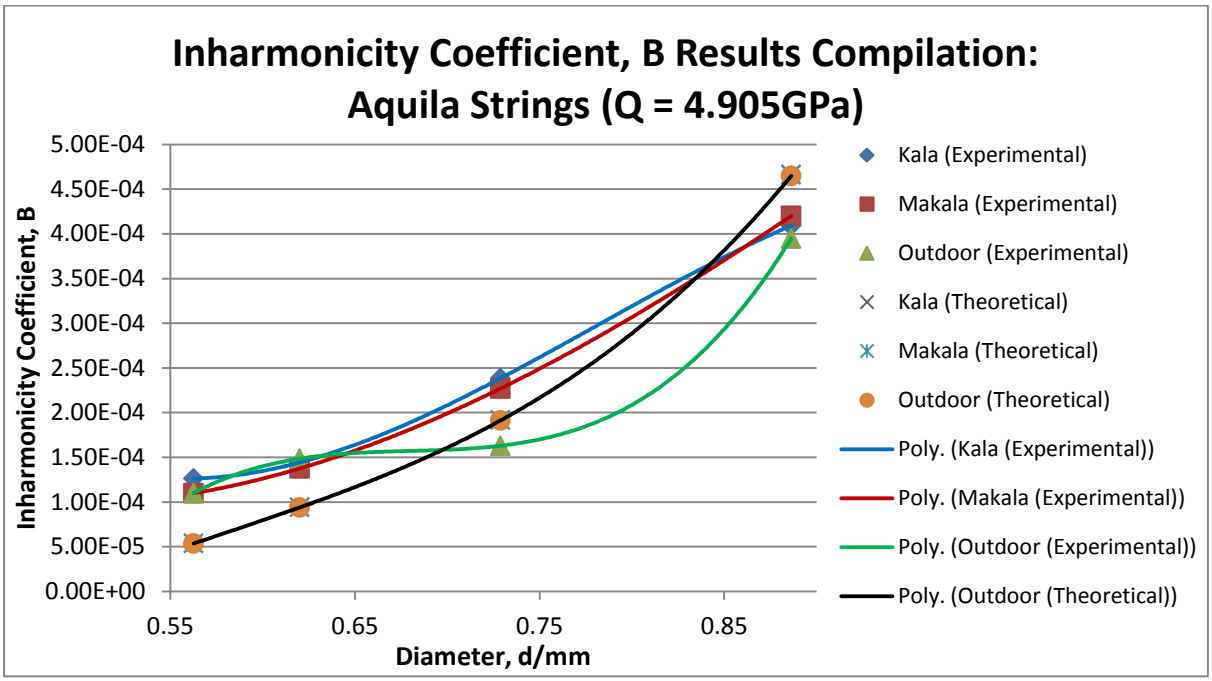

Figure 4.1.3: Plot of Inharmonicity Coefficient, B against diameter, d/mm for the Aquila Strings

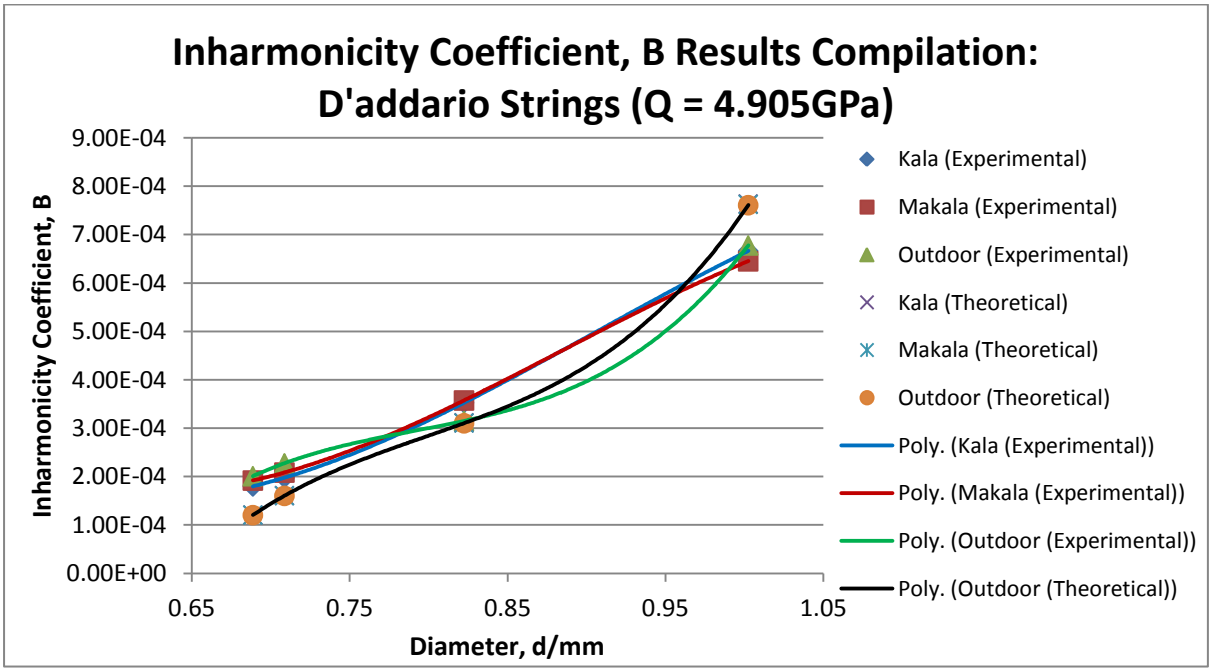

Figure 4.1.4: Plot of Inharmonicity Coefficient, B against diameter, d/mm for the D'addario Strings

Figures 4.1.5 and 4.1.6 show the graphs of B against d with $Q = 5.40GPa$ for both Aquila and D'addario strings respectively.

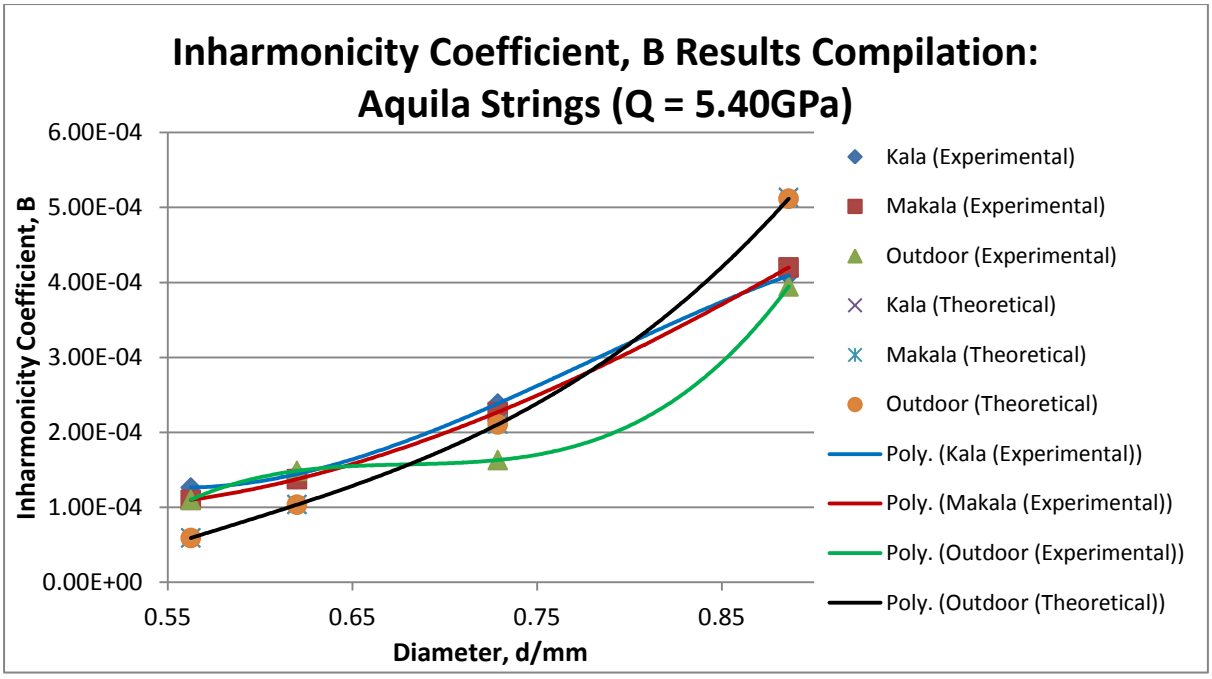

Figure 4.1.5: Plot of Inharmonicity Coefficient, B against diameter, d/mm for the Aquila Strings

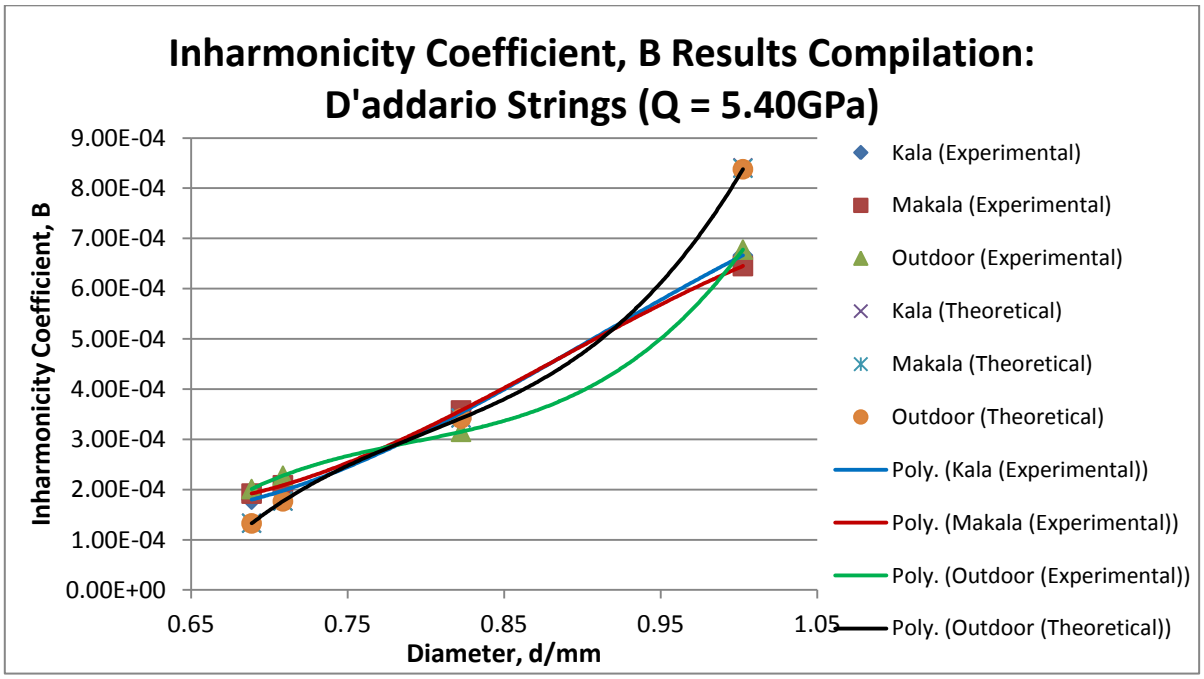

Figure 4.1.6: Plot of Inharmonicity Coefficient, B against diameter, d/mm for the D'addario Strings

The black trendline in Figures 4.1 to 4.6 represent the relationship of theoretical values of inharmonicity coefficients for all ukuleles as the difference between their values are negligible. From Figures 4.1.1 to 4.1.6, it is observed that the relationship between the inharmonicity coefficient and its diameter models a polynomial to the order of 4 as expected from the equation $B = \left(\frac{\pi^3 Q}{64Tl^2}\right) d^4$. The increase in value of the inharmonicity coefficients as the diameters increases suggests that thicker strings deviate more from the expected or ideal value. It is noted that the

results for the Kala and Makala ukulele are very similar suggesting that the strings largely contribute to the inharmonicity coefficients. However, the results of the Outdoor ukulele differ from that of the Kala and Makala.

In order to compare the experimental values of the inharmonicity coefficient for the Aquila or D'addario set of strings among the ukuleles used, the percentage differences for each string were calculated and were found to range from 0.13% to 32.8%, in which about 79% of the values had percentage differences less than 15%. It is also noted that the remaining 21% of the values were obtained when the inharmonicity coefficients were compared to those of the Outdoor ukulele. The reason for this is due to the fact that several harmonic frequencies determined from the frequency domain graph had values less than the ideal harmonic series and thus, affecting the values of the inharmonicity coefficients. This negative deviation is seen to impact the E4 string most and it is explained in further detail in section 4.3. In the calculation of percentage differences, the lengths of strings were treated to be equal. This is because the variations in length only contribute to at most 0.2% to the percentage differences and are therefore negligible. The remaining percentage difference may be attributed to the difference in shapes and composition of the ukuleles.

The percentage discrepancies between the experimental and theoretical values were found to range from as low as 0.29% to 161%. It was also observed that the high percentage discrepancies were mainly due to the A4 string.

(b) Classical Guitar Strings

Figure 4.1.7 shows the experimental and theoretical inharmonicity coefficients calculated.

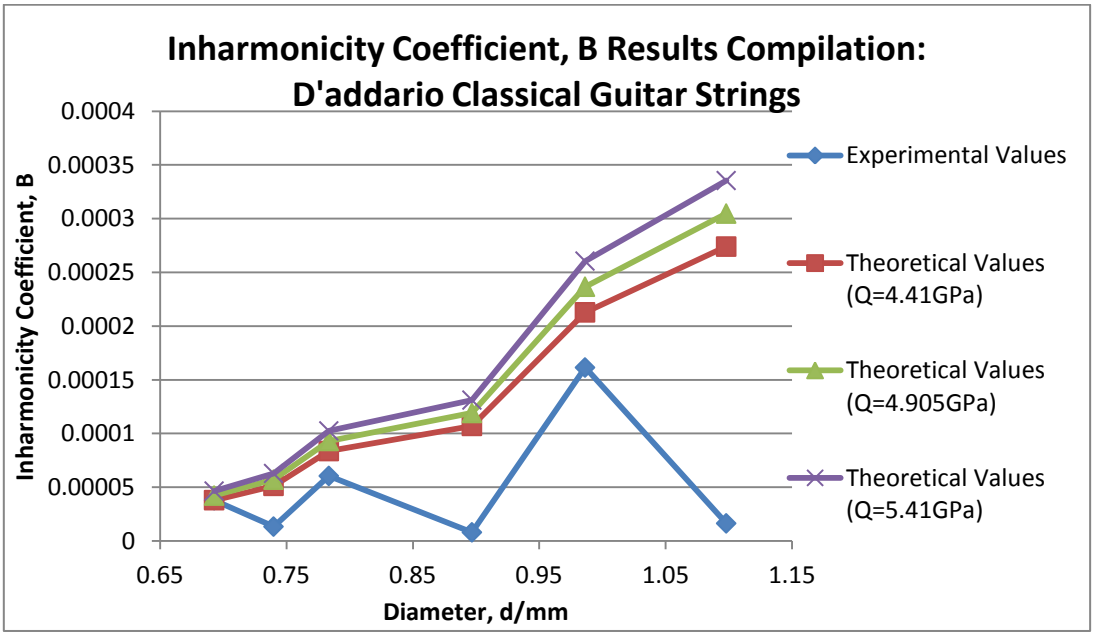

Figure 4.1.7: Plot of Inharmonicity Coefficient, B against diameter, d/mm for the D'addario Strings of the Classical Guitar

Figure 4.1.7 is plotted to see the correlation of the points to a straight line fit as predicted by plotting $B = \left(\frac{\pi^3 Q}{64Tl^2}\right) d^4$. The E4, B3 and G4 nylon strings which are represented by the first, third and fifth point from the left of Figure 4.1.7 is found to have experimental values closer to the theoretical values. The percentage discrepancies were found to be below 41% which is much lower than those of the wound strings as expected. However, the percentage discrepancies for the wound strings ranged from 74% to 95% due to the fact that the Young's modulus of nylon was used in the calculations but in actuality, this is not true.

4.1.1 Inharmonicity Coefficient Calculated Using Linear Density

The second method of determining the inharmonicity coefficient is performed in order to compare the experimental values and theoretical values in a more consistent manner. Comparisons could not be made for the pipa using the first method but can be estimated using this method.

(a) Ukulele Strings

Figures 4.1.8 and 4.1.9 show the graphs of B against d with $Q = 4.41GPa$ for both Aquila and D'addario strings respectively.

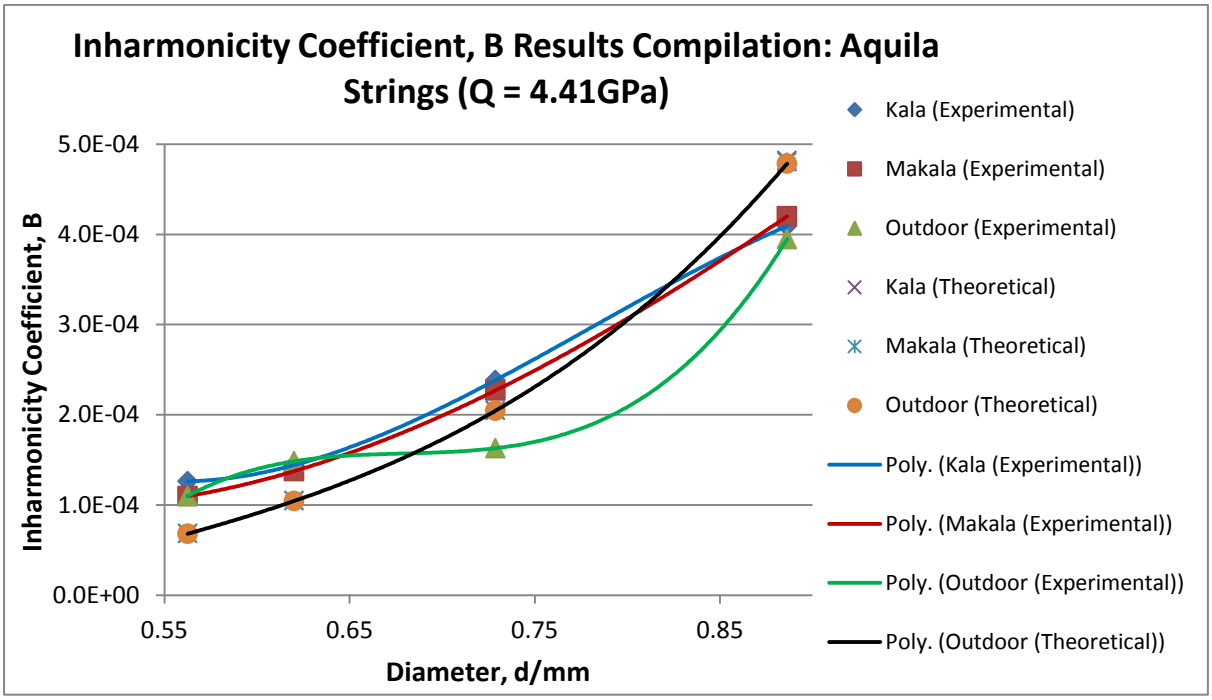

Figure 4.1.8: Plot of Inharmonicity Coefficient, B against diameter, d/mm for the Aquila Strings

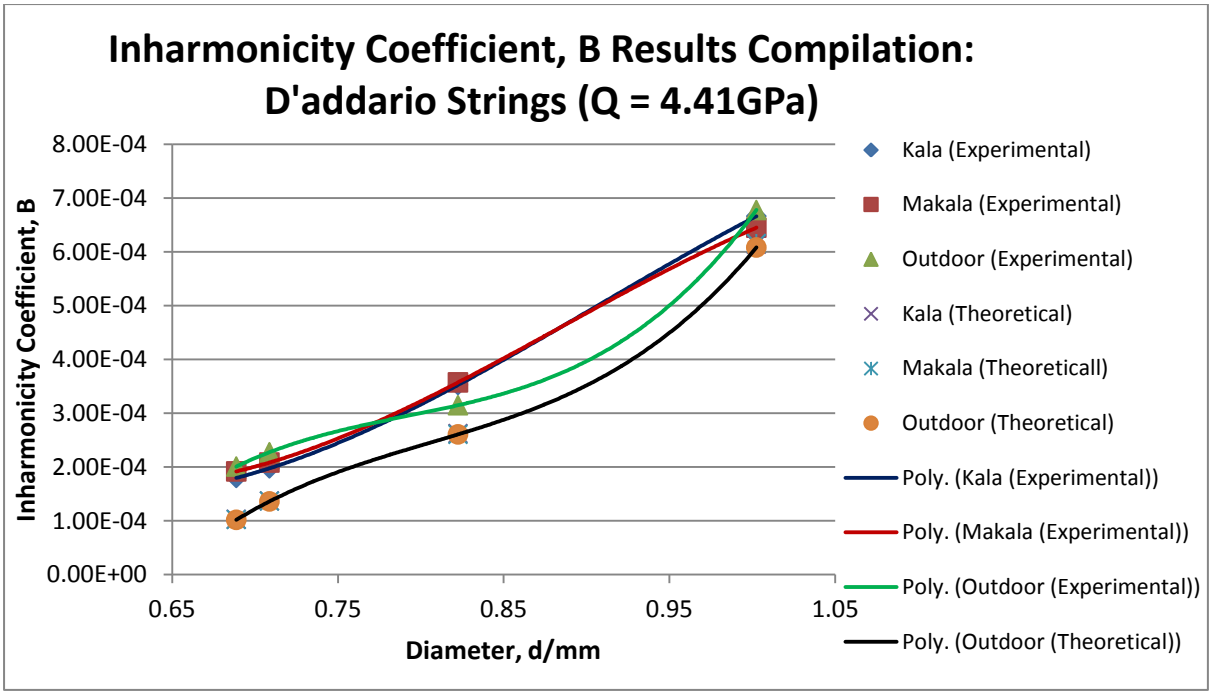

Figure 4.1.9: Plot of Inharmonicity Coefficient, B against diameter, d/mm for the D'addario Strings

Figures 4.1.10 and 4.1.11 show the graphs of B against d with $Q = 4.905GPa$ for both Aquila and D'addario strings respectively.

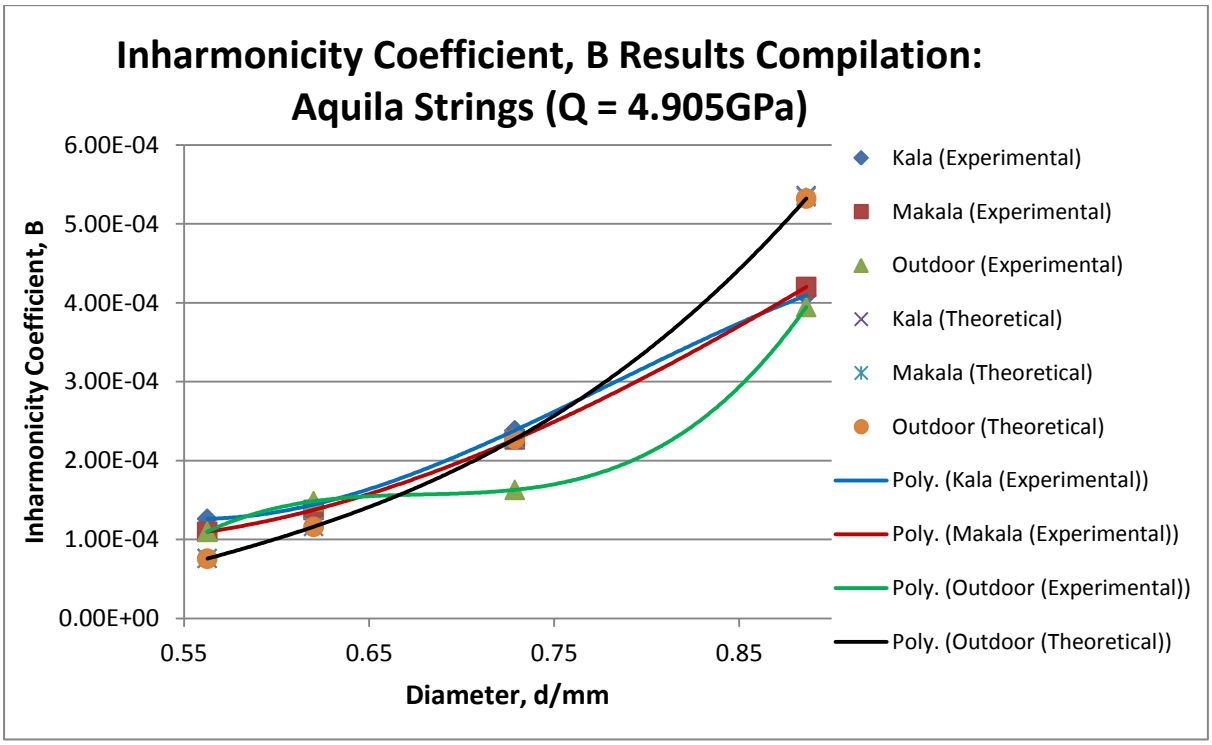

Figure 4.1.10: Plot of Inharmonicity Coefficient, B against diameter, d/mm for the Aquila Strings

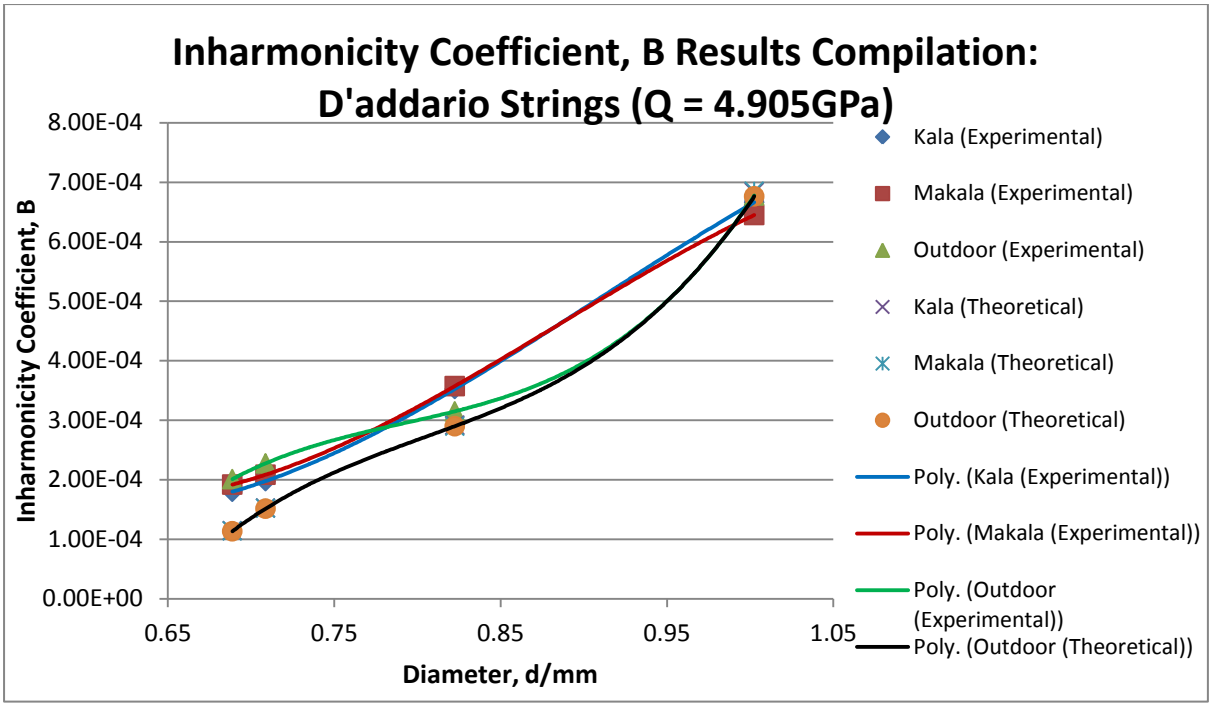

Figure 4.1.11: Plot of Inharmonicity Coefficient, B against diameter, d/mm for the D'addario Strings

Figures 4.1.12 and 4.1.13 show the graphs of B against d with $Q = 4.905GPa$ for both Aquila and D'addario strings respectively.

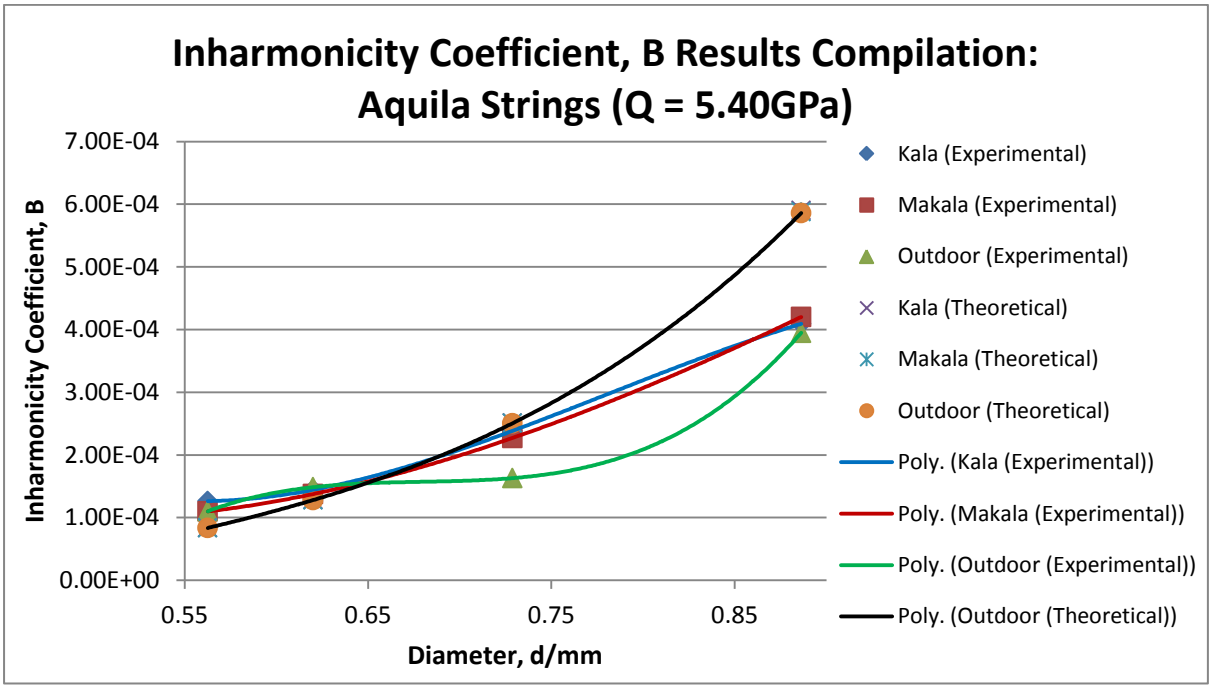

Figure 4.1.12: Plot of Inharmonicity Coefficient, B against diameter, d/mm for the Aquila Strings

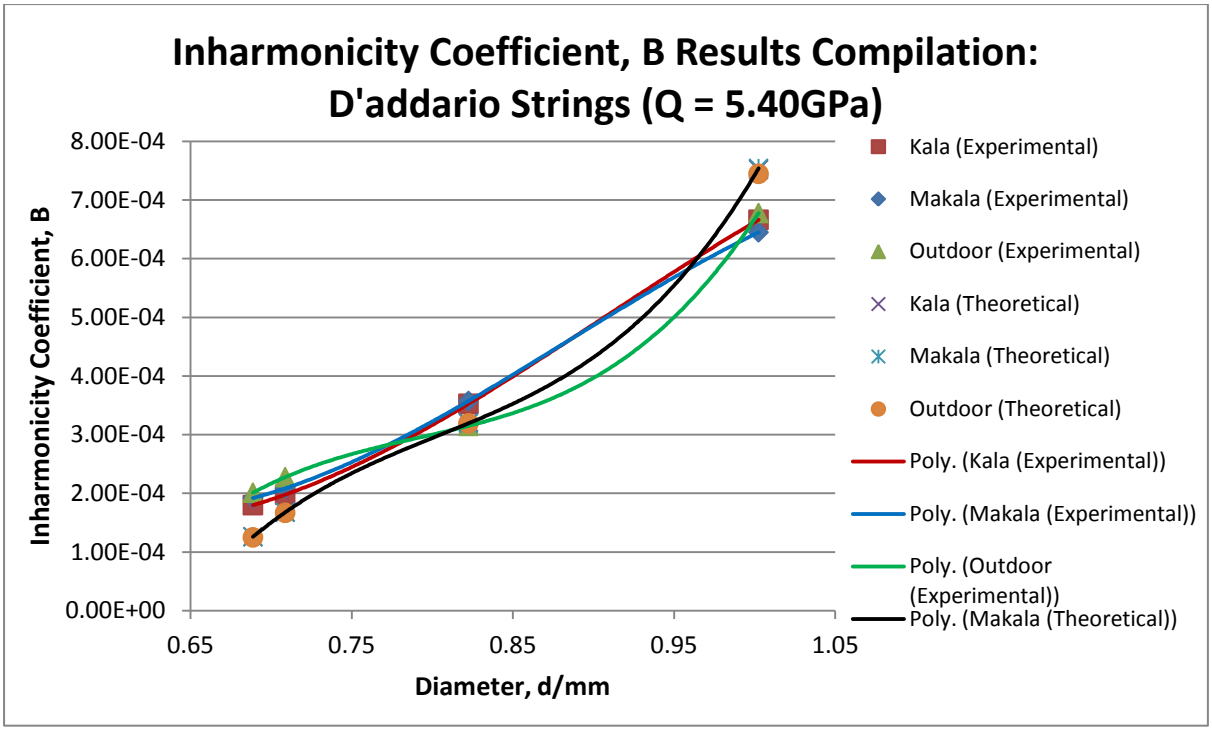

Figure 4.1.13: Plot of Inharmonicity Coefficient, B against diameter, d/mm for the D'addario Strings

From Figures 4.1.8 to 4.1.13, it is observed that the relationship between the inharmonicity coefficient and its diameter models a polynomial to the order of 4 as expected from the equation $B = \left(\frac{\pi^3 Q}{256 {f_1}^2 \sigma l^2}\right) d^4$. Similar to section 4.1.1, the inharmonicity coefficients are seen to increase as the diameters of the strings are increased.

It is noted that the deviation between the experimental values from the theoretical values of strings the Aquila set of were greater in the first method as compared to that in the second method. One possible explanation for this discrepancy is due to the inaccurate values of the tension used in the first method.

(c) Pipa Strings

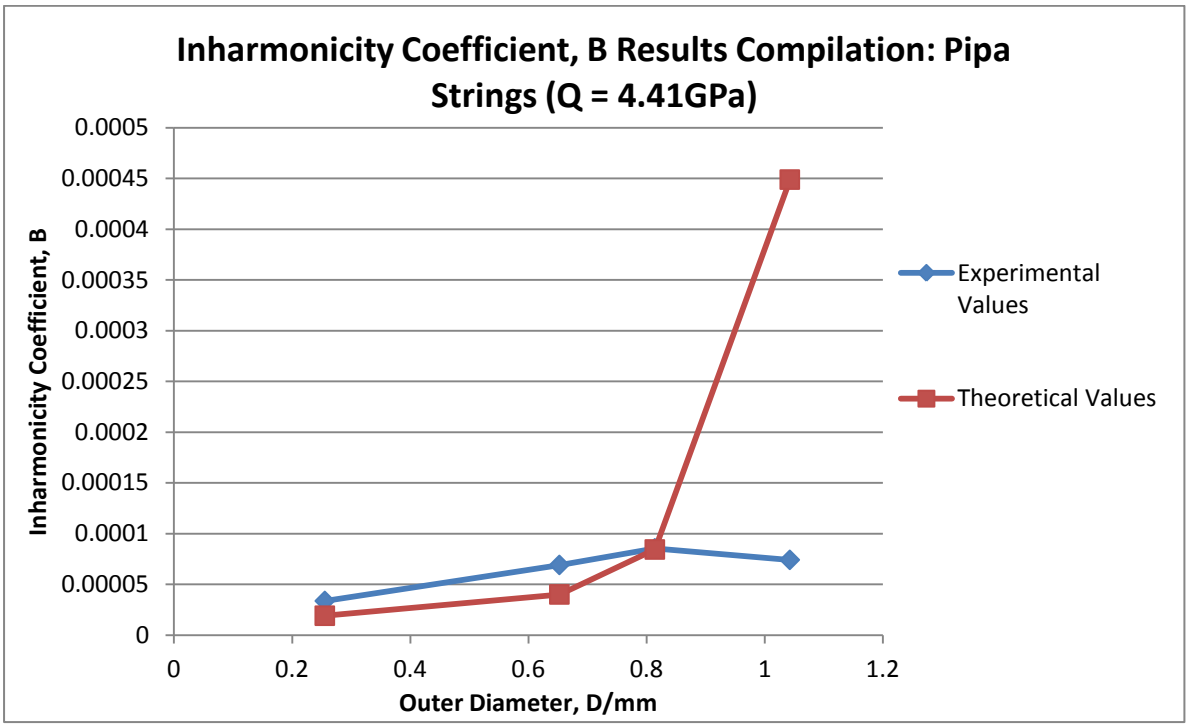

Figure 4.1.14: Plot of Inharmonicity Coefficient, B against diameter, d/mm for Pipa Strings

Figure 4.1.14 is plotted to see the correlation of the points to a straight line fit as predicted by plotting $B = \left(\frac{\pi^3 Q}{256 {f_1}^2 \sigma l^2}\right) d^4$. The trend displayed shows that the inharmonicity coefficients agree with the stiff string model. It is found that the percentage discrepancies between the experimental values and theoretical values were extremely high, ranging from 1.36% to 83.5%. The reasons for these high percentage discrepancies are explained in section 4.5.

(b) Classical Guitar Strings

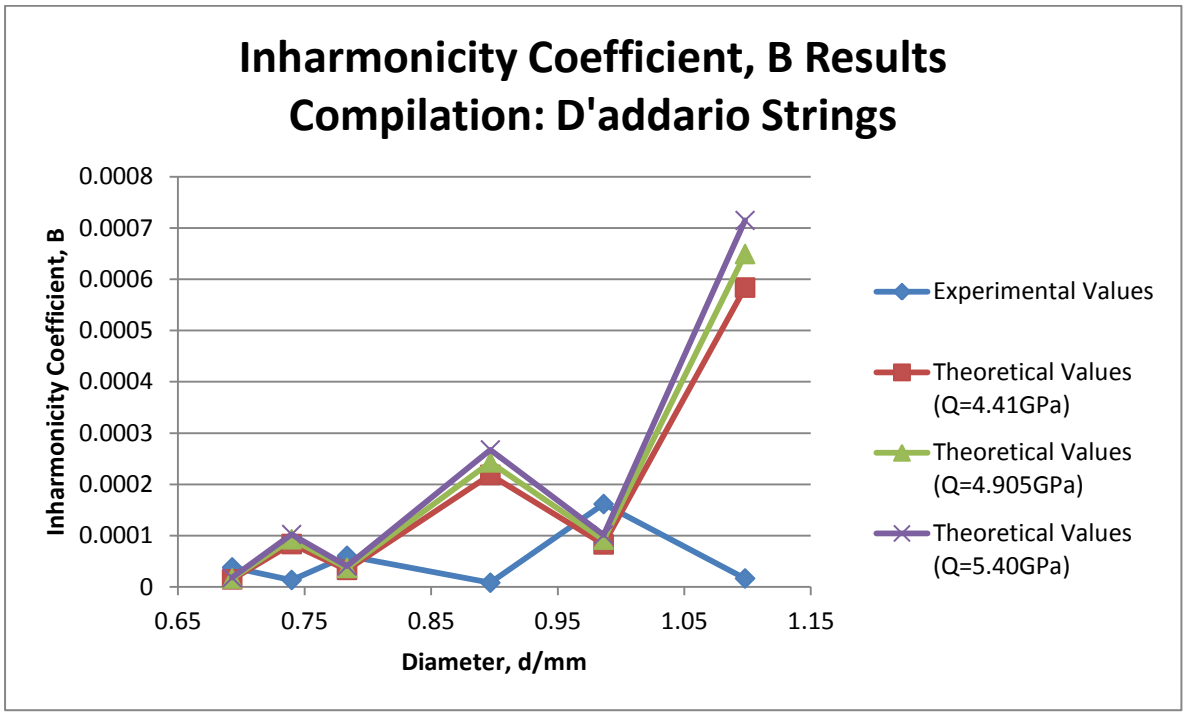

Figure 4.1.15: Plot of Inharmonicity Coefficient, B against diameter, d/mm for Classical Guitar Strings

Figure 4.1.15 is plotted to see the correlation of the points to a straight line fit as predicted by plotting $B = \left(\frac{\pi^3 Q}{256 {f_1}^2 \sigma l^2}\right) d^4$. It is observed that the theoretical values of the first three strings of the classical guitar which is again represented as the first, third and fifth points in Figure 4.1.15 have values less than the experimental values as compared to the plot obtained in Figure 4.1.7. The opposite is seen in the Figure 4.1.7. One possible explanation for this behaviour may be due to the inaccurate choice of density for nylon. More research on this is needed to fully comprehend this behaviour. Nevertheless, their experimental values appear to be closer to the theoretical values as compared to the 4th, 5th and 6th string.

It was observed that the nylon cores of the D3, A2 and E2 wound strings were fibrous and thus, the diameter of the core could not be measured using the micrometer screw gauge. Therefore, the linear densities of the strings used to calculate the theoretical value of B are very inaccurate. The larger percentage discrepancies acquired using this method of calculation proves this.

Similar to the Outdoor Ukulele, several harmonic frequencies determined from the frequency domain graph had values less than the ideal harmonic series and thus, affecting the experimental values of the inharmonicity coefficients.

4.2 Relationship between Harmonic Frequencies and its n^{th} Harmonics

Using the theoretical values of the inharmonicity coefficient from the second method, the theoretical values of the harmonic frequencies were calculated. A graph of harmonic frequencies against harmonics n is then plotted to observe the relationship between the two variables.

4.2.1 Kala Spruce/Rosewood Soprano Ukulele

(a) Aquila AQ-4U New Nylgut® Regular GCEA Set Soprano Strings

Figures 4.2.1 to 4.2.4 show the plots of frequency against harmonics for the A4, E4, C4 and G4 Aquila strings of the Kala Ukulele respectively.

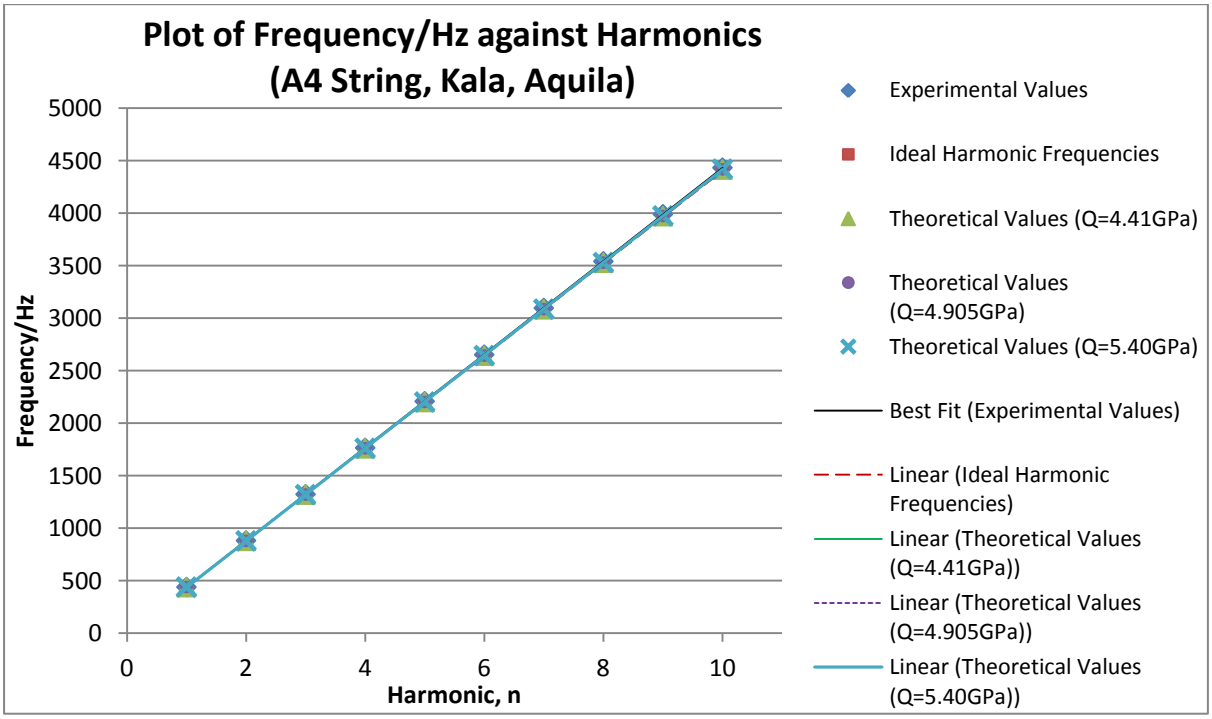

Figure 4.2.1a: Plot of Frequency against Harmonics for the A4 Aquila String for the Kala Ukulele

The experimental, theoretical and ideal harmonic frequencies were found to deviate slightly from each other and it is found that this deviation is increased when the harmonics were increased. The deviation in frequencies cannot be seen clearly from Figure 4.2.1a but an enlarged version showing the 8^{th} to 10^{th} harmonic in Figure 4.2.1b displays this deviation evidently. This is done for all graphs of all instruments.

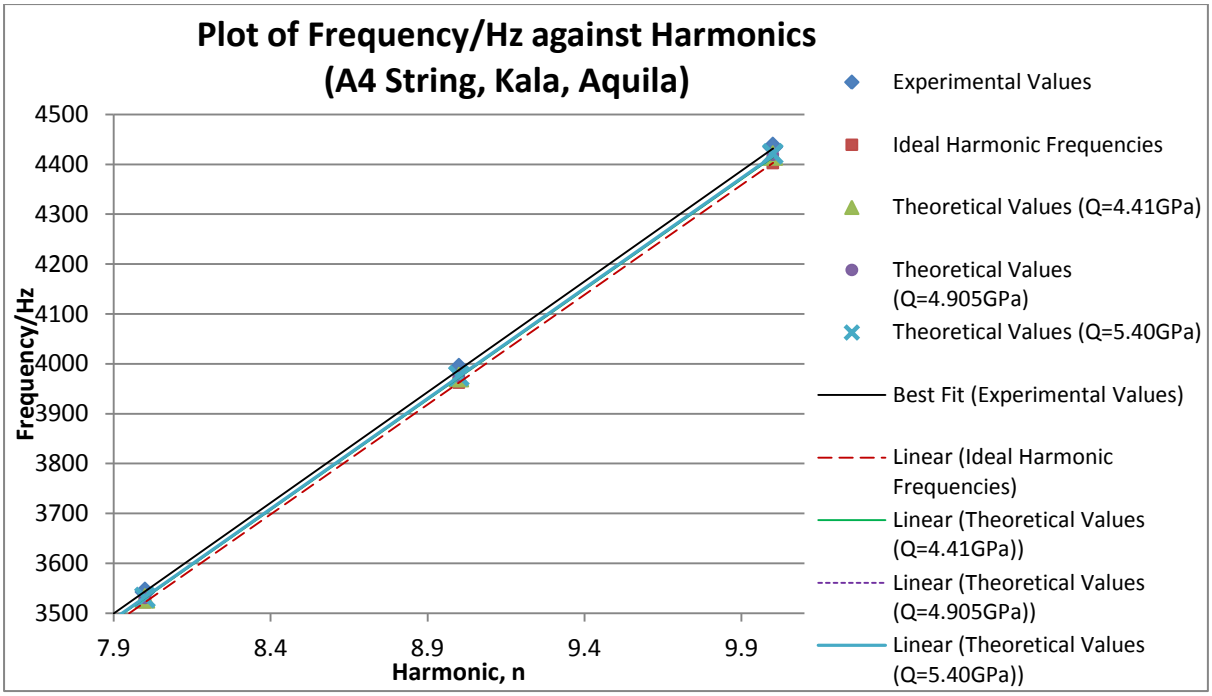

Figure 4.2.1b: Plot of Frequency against Harmonics for the A4 Aquila String for the Kala Ukulele for the 8^{th} to 10^{th} Harmonic

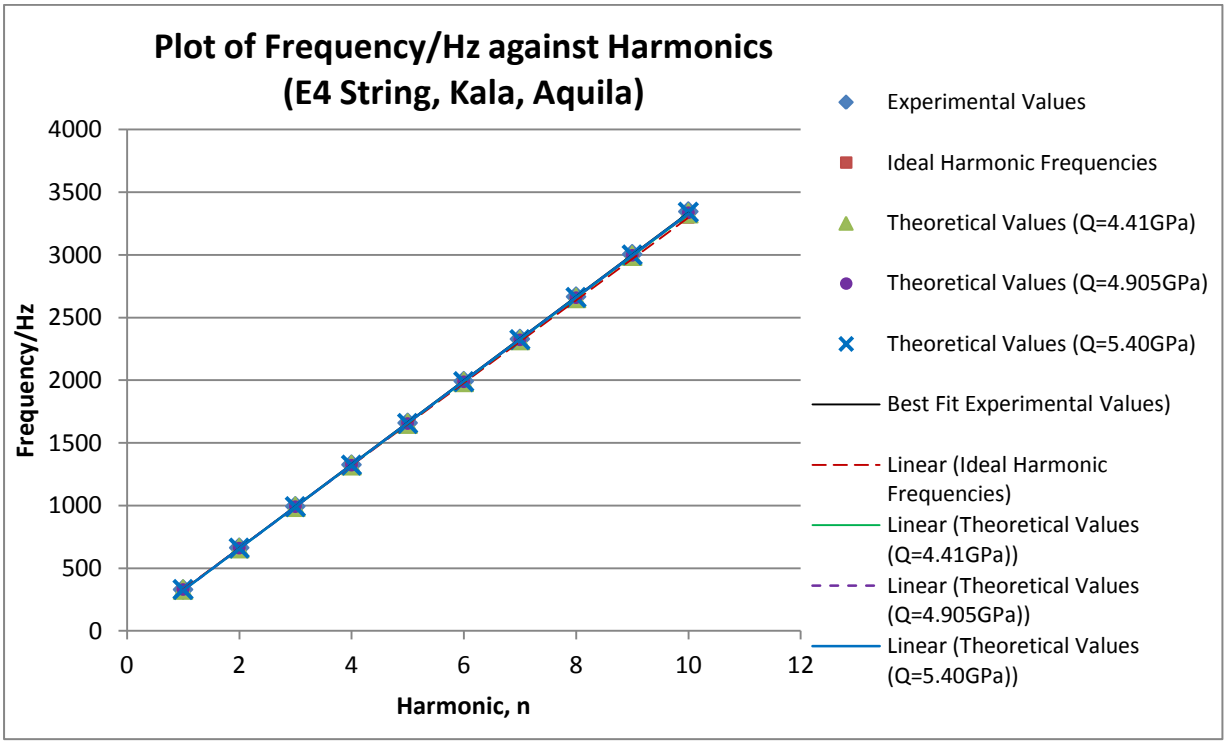

Figure 4.2.2a: Plot of Frequency against Harmonics for the E4 Aquila String for the Kala Ukulele

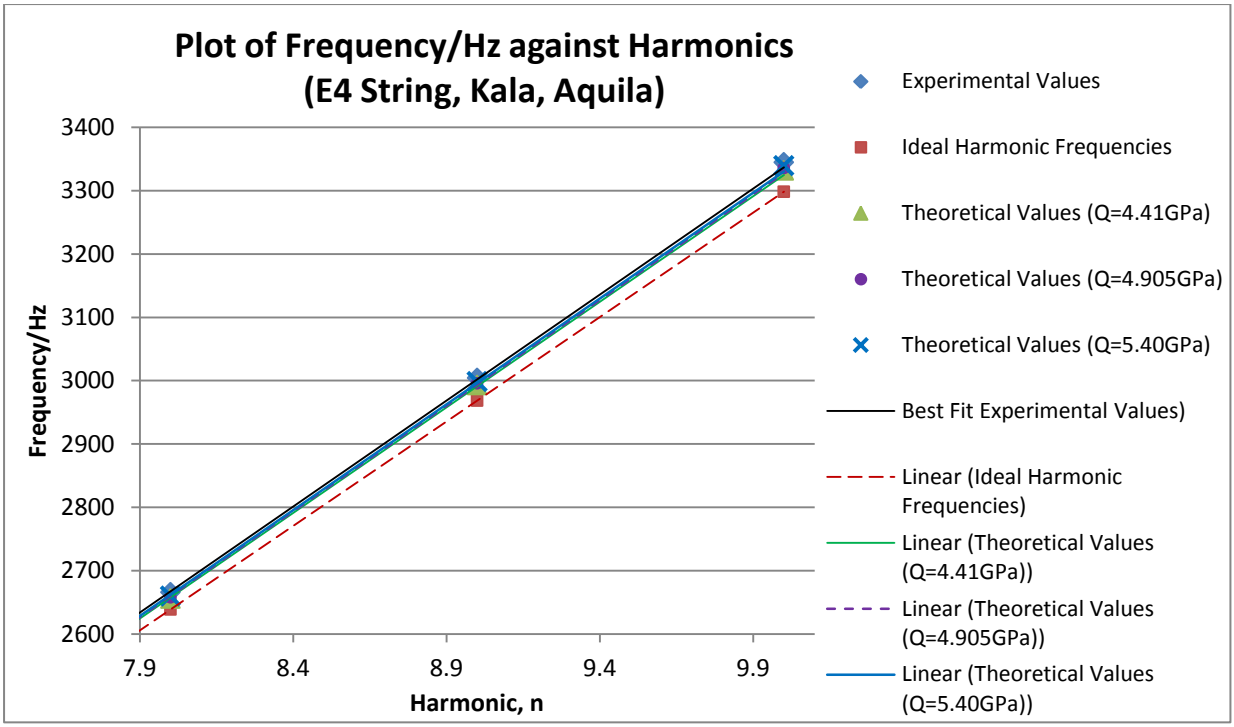

Figure 4.2.2b: Plot of Frequency against Harmonics for the E4 Aquila String for the Kala Ukulele for the 8th to 10th Harmonic

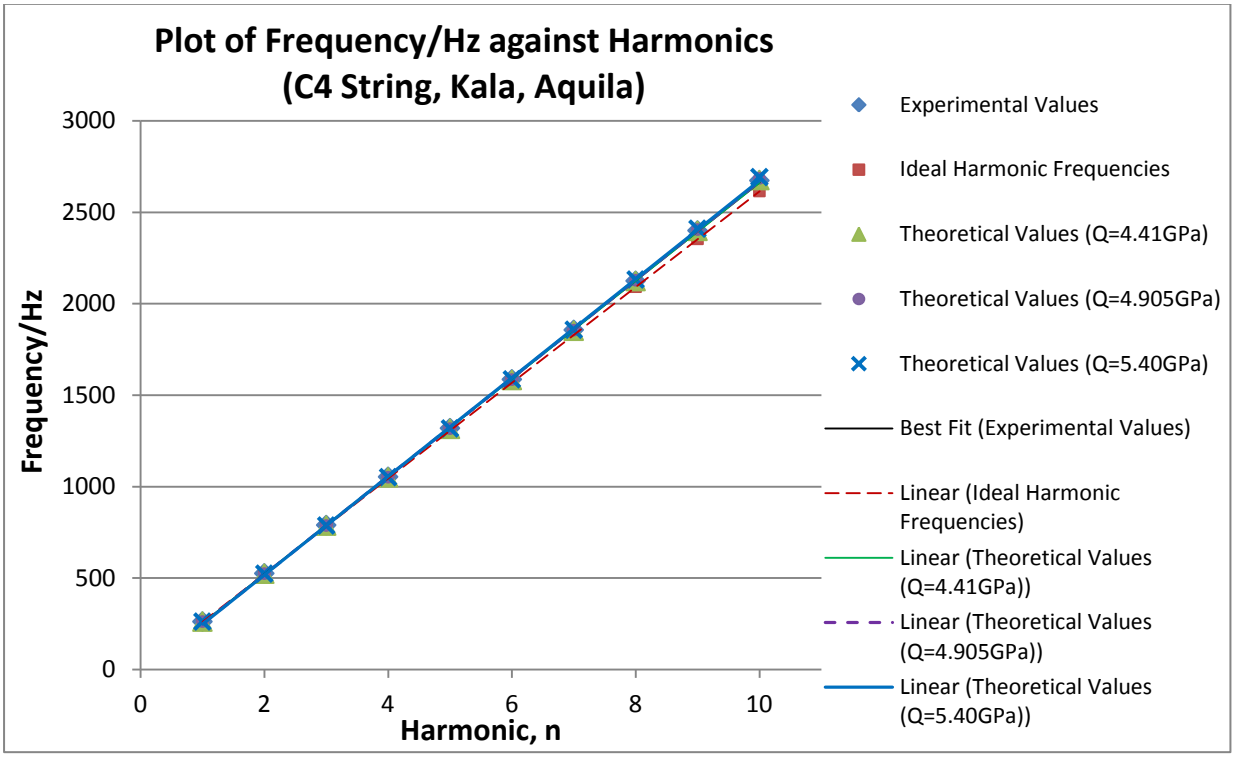

Figure 4.2.3a: Plot of Frequency against Harmonics for the C4 Aquila String for the Kala Ukulele

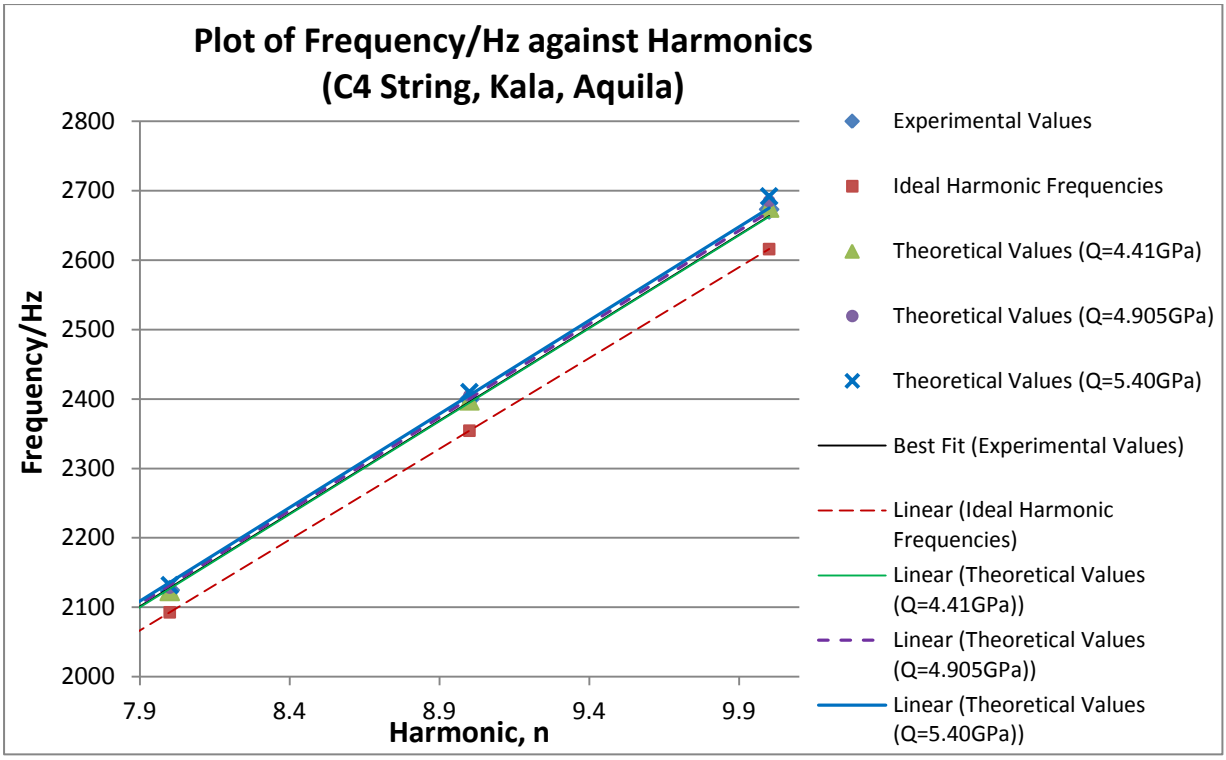

Figure 4.2.3b: Plot of Frequency against Harmonics for the C4 Aquila String for the Kala Ukulele for the 8th to 10th Harmonic

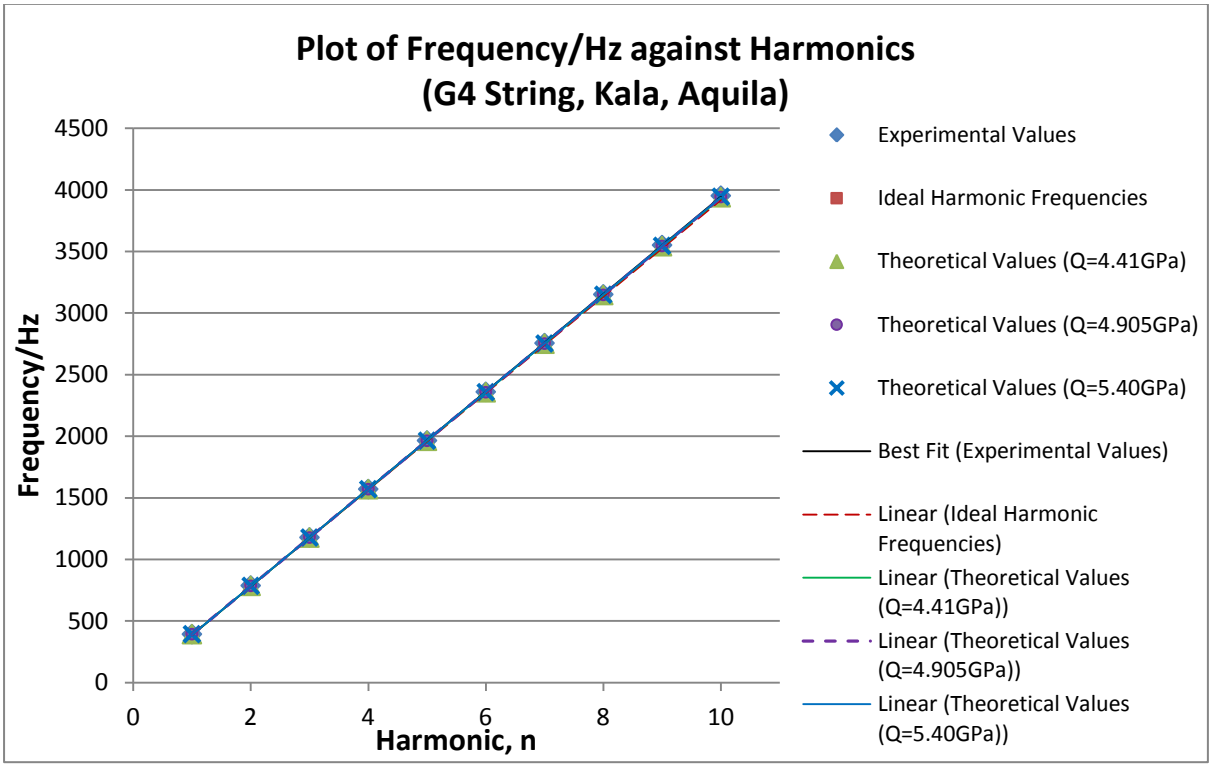

Figure 4.2.4a: Plot of Frequency against Harmonics for the G4 Aquila String for the Kala Ukulele

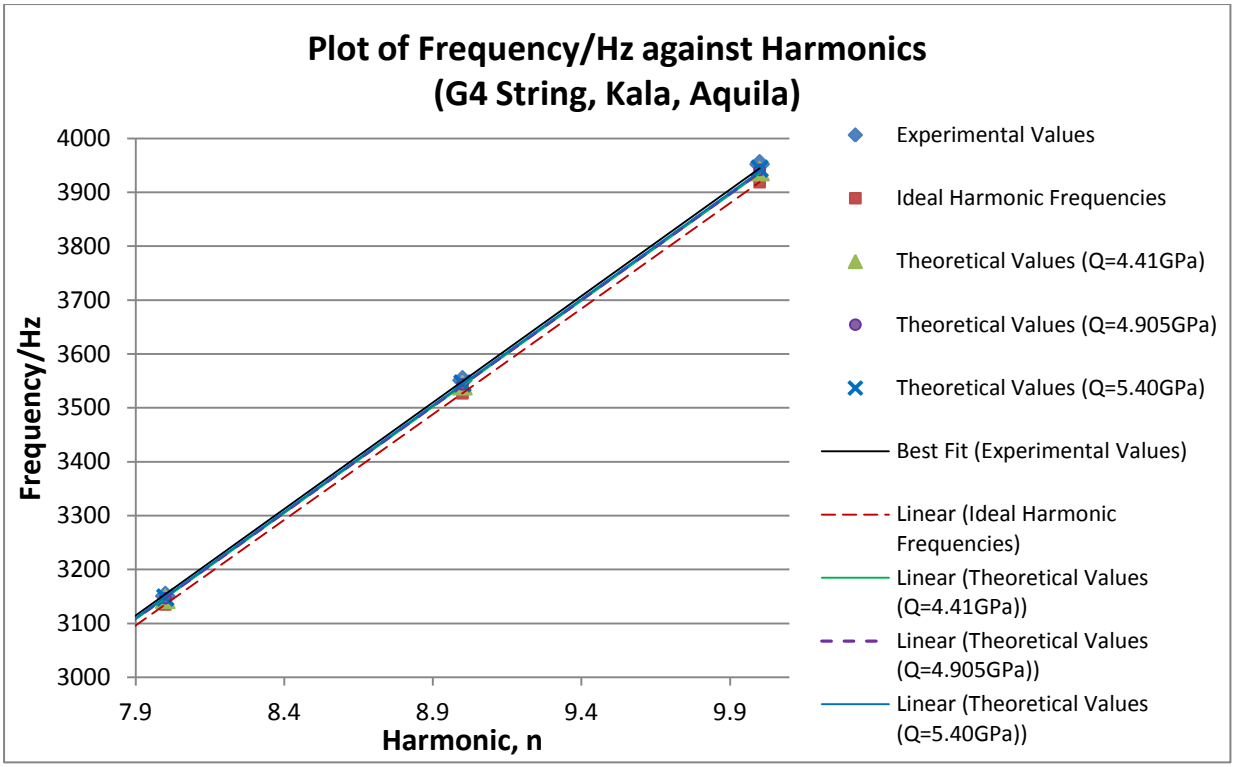

Figure 4.2.4b: Plot of Frequency against Harmonics for the G4 Aquila String for the Kala Ukulele for the 8th to 10th Harmonic

(b) D'Addario T2 Soprano Strings Strings

Figures 4.2.5 to 4.2.8 show the plots of frequency against harmonics for the A4, E4, C4 and G4 D'addario strings of the Kala Ukulele respectively.

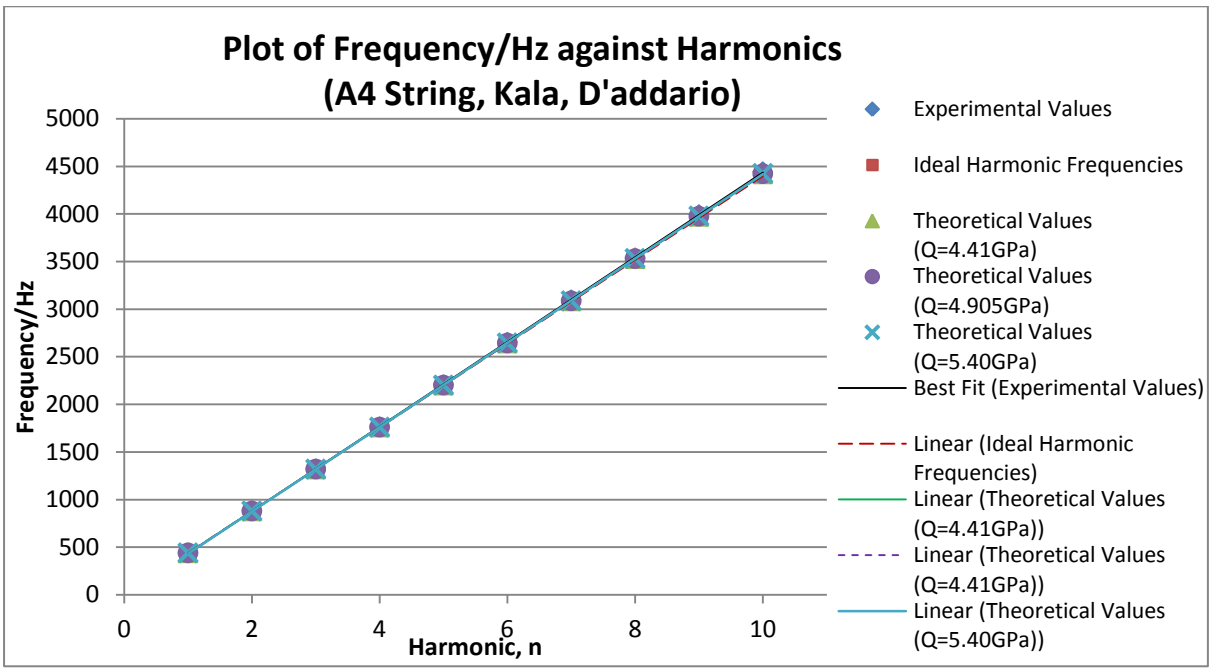

Figure 4.2.5a: Plot of Frequency against Harmonics for the A4 D'addario String for the Kala Ukulele

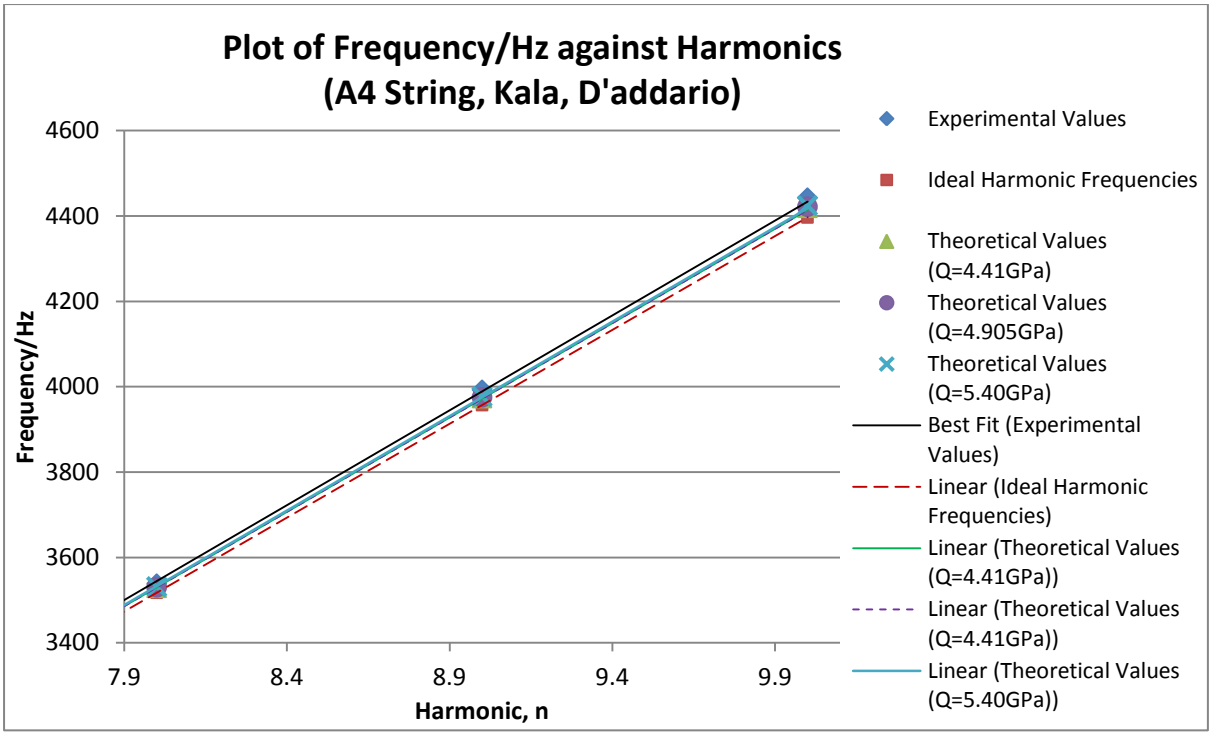

Figure 4.2.5b: Plot of Frequency against Harmonics for the A4 D'addario String for the Kala Ukulele for the 8th to 10th Harmonic

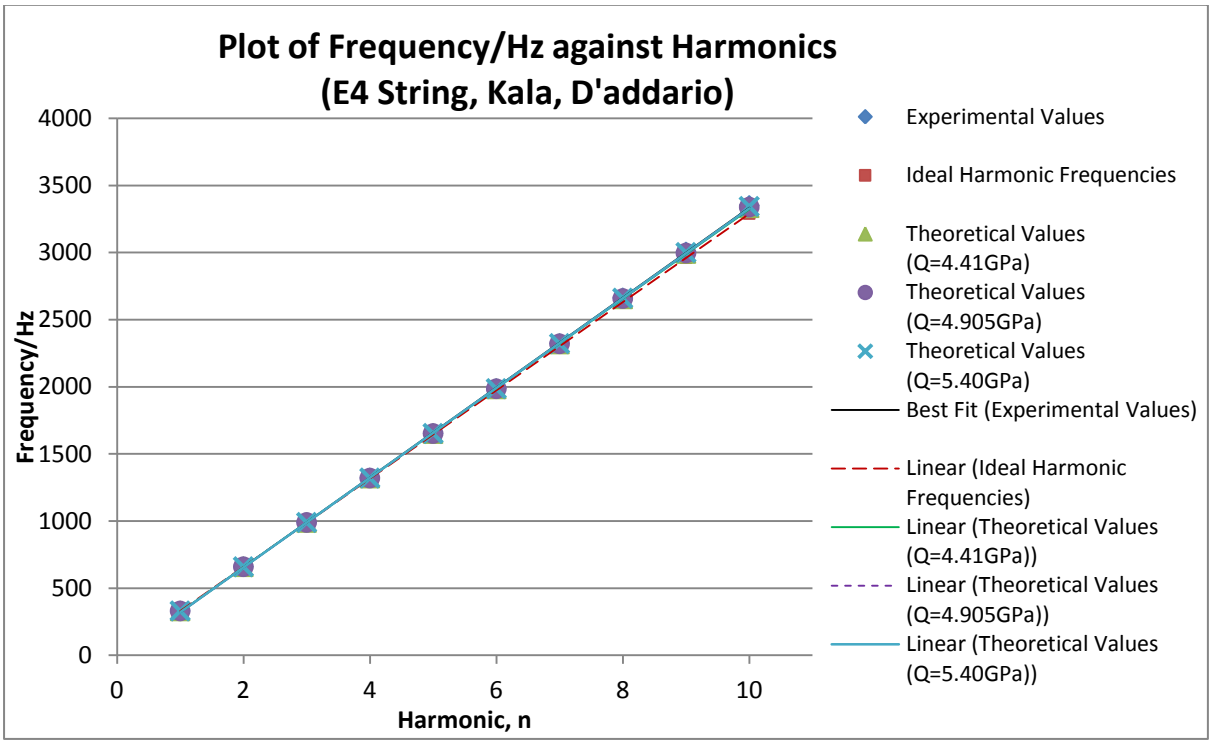

Figure 4.2.6a: Plot of Frequency against Harmonics for the E4 D'addario String for the Kala Ukulele

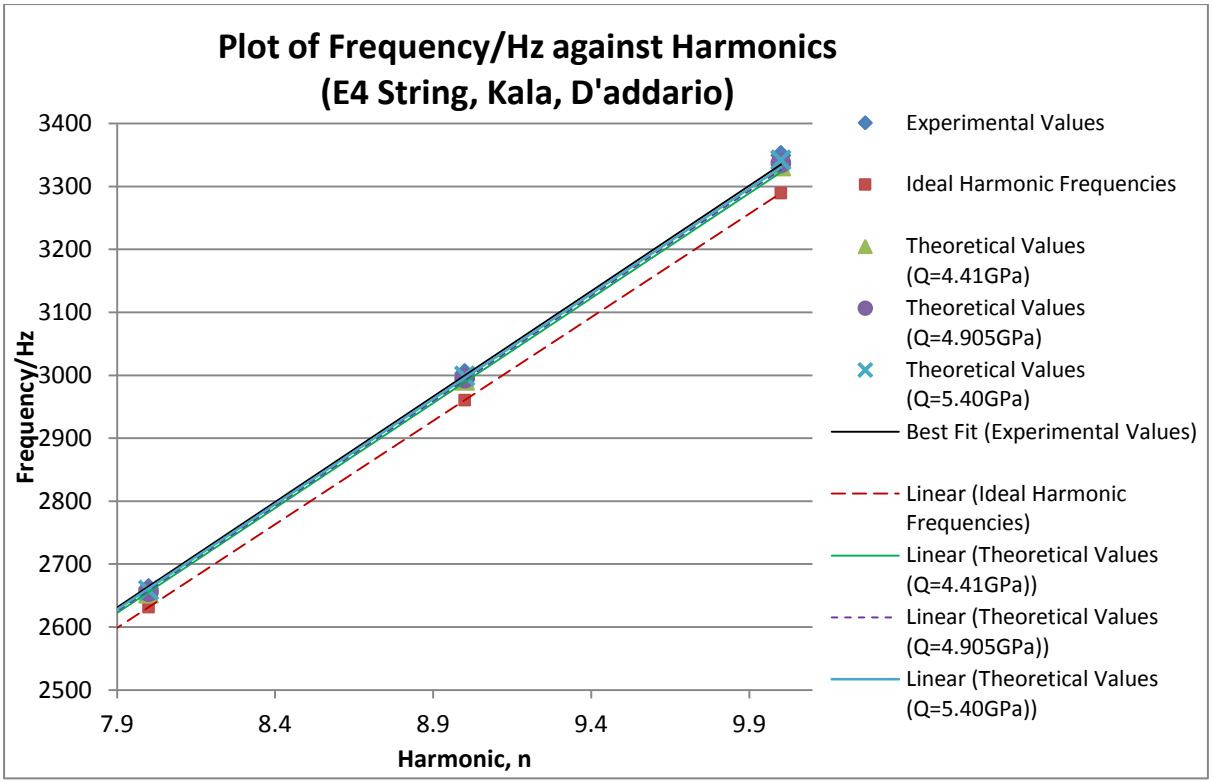

Figure 4.2.6b: Plot of Frequency against Harmonics for the E4 D'addario String for the Kala Ukulele for the 8th to 10th Harmonic

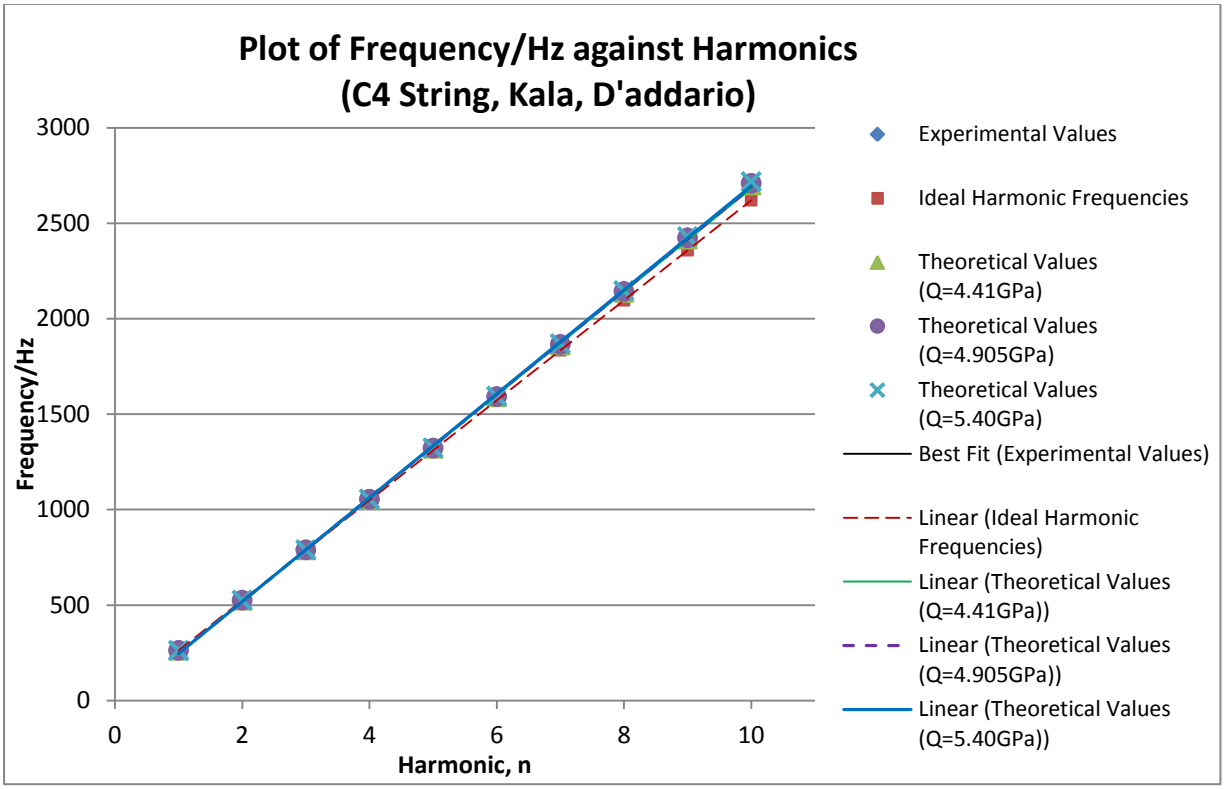

Figure 4.2.7a: Plot of Frequency against Harmonics for the C4 D'addario String for the Kala Ukulele

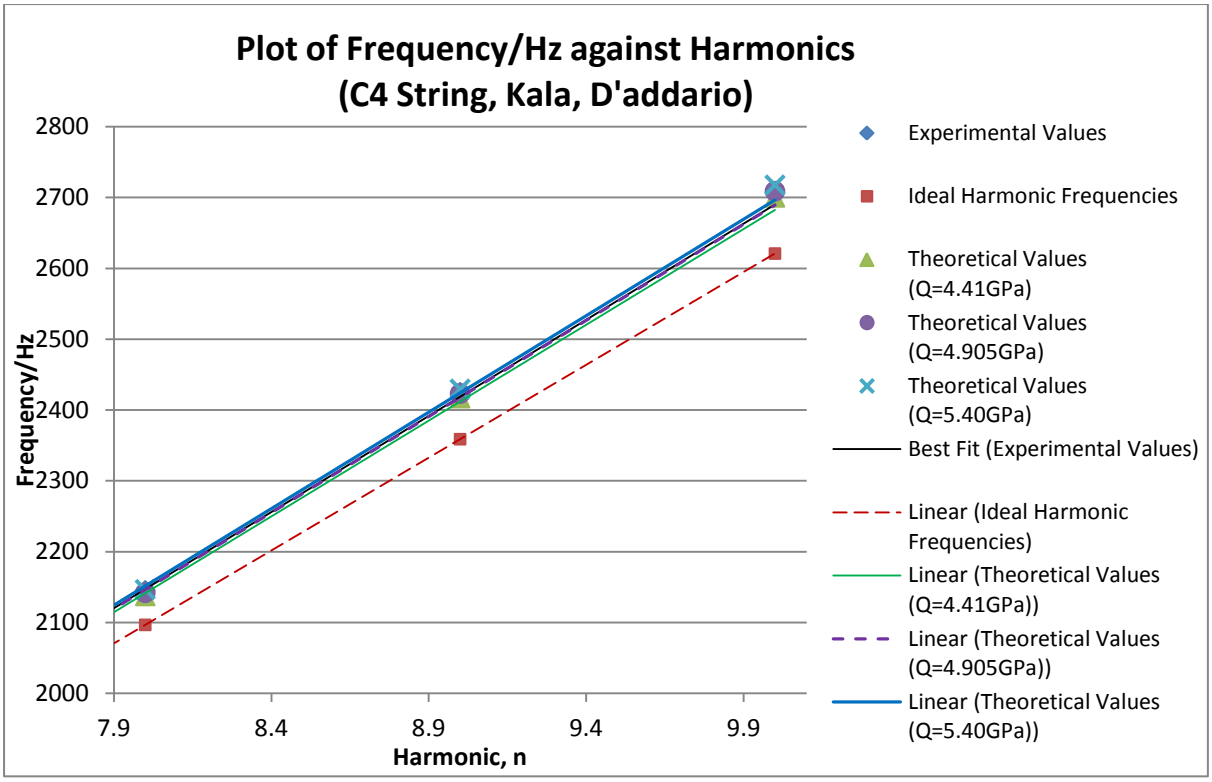

Figure 4.2.7b: Plot of Frequency against Harmonics for the C4 D'addario String for the Kala Ukulele for the 8th to 10th Harmonic

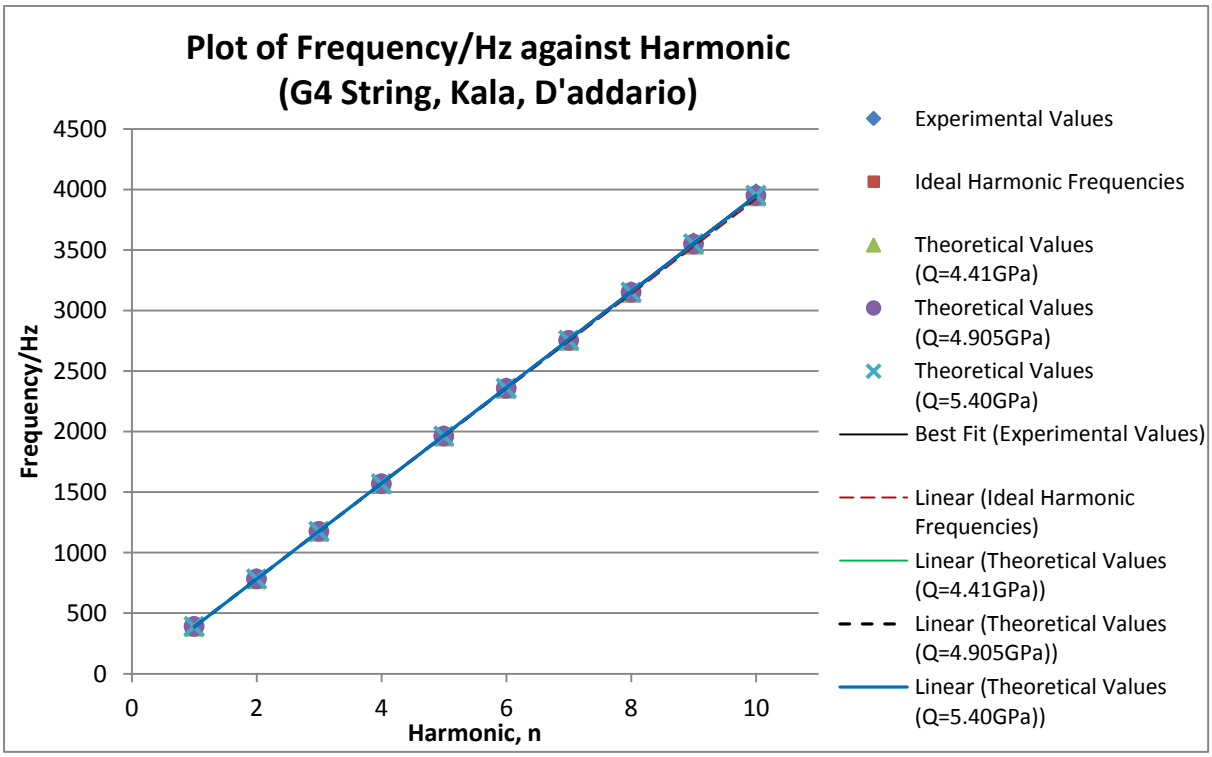

Figure 4.2.8a: Plot of Frequency against Harmonics for the G4 D'addario String for the Kala Ukulele

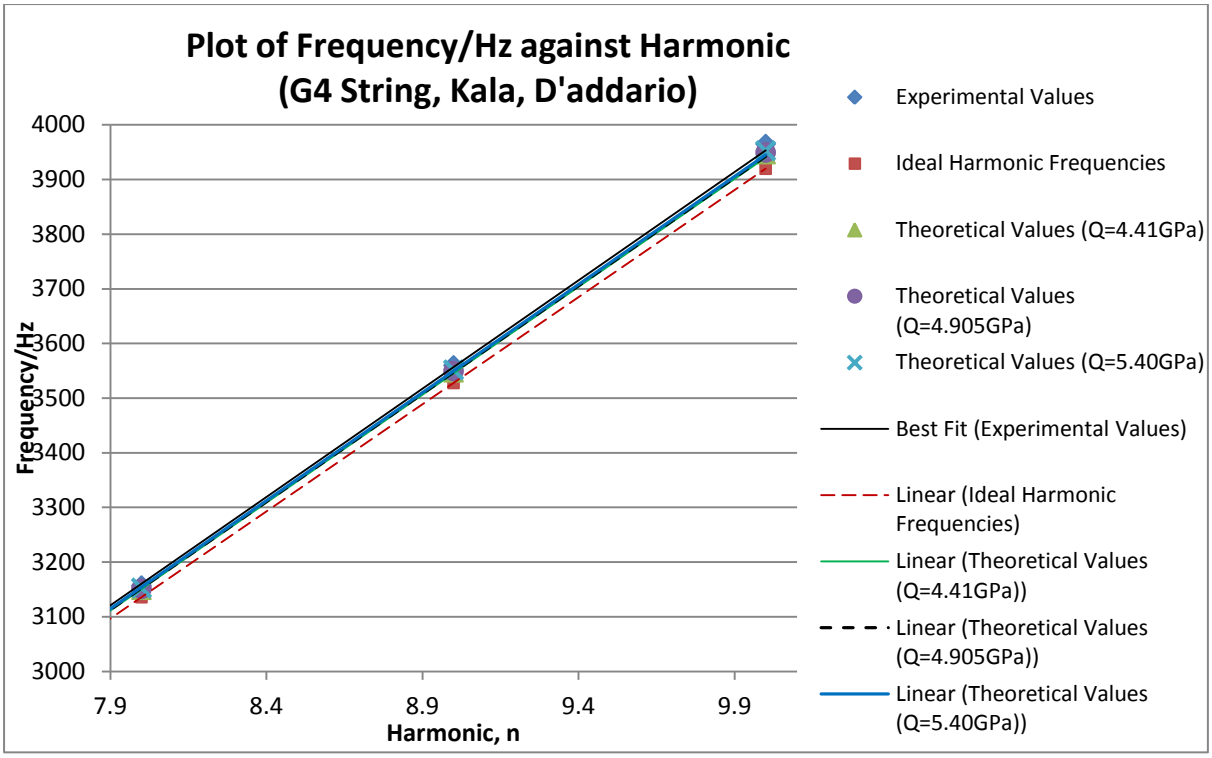

Figure 4.2.8b: Plot of Frequency against Harmonics for the G4 D'addario String for the Kala Ukulele for the 8th to 10th Harmonic

4.2.2 Makala Ukulele

(a) Aquila AQ-4U New Nylgut® Regular GCEA Set Soprano Strings

Figures 4.2.9 to 4.2.12 show the plots of frequency against harmonics for the A4, E4, C4 and G4 Aquila strings of the Makala Ukulele respectively.

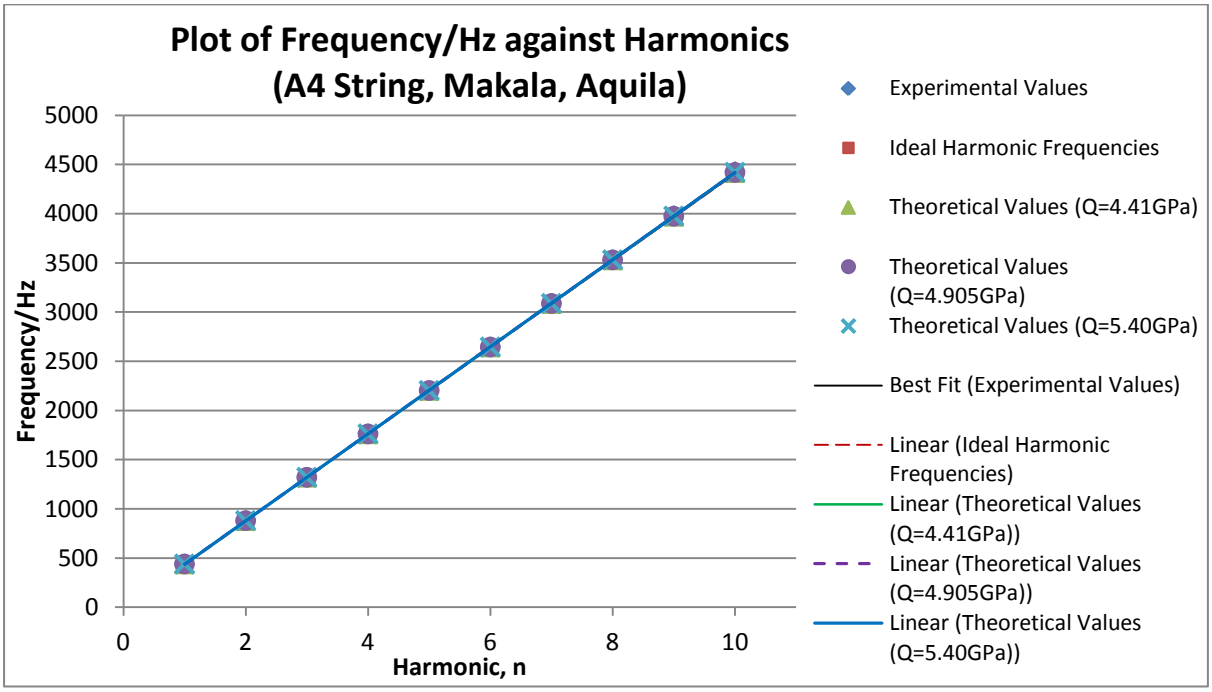

Figure 4.2.9a: Plot of Frequency against Harmonics for the A4 Aquila String for the Makala Ukulele

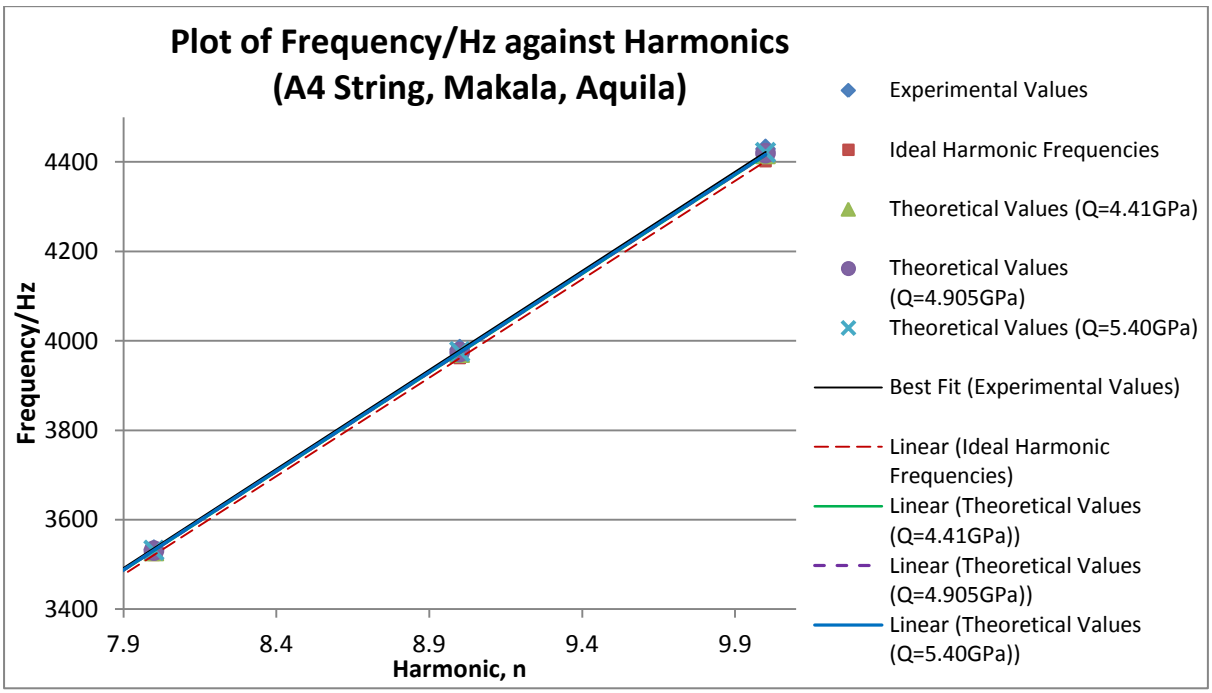

Figure 4.2.9b: Plot of Frequency against Harmonics for the A4 Aquila String for the Makala Ukulele for the 8^{th} to 10^{th} Harmonic

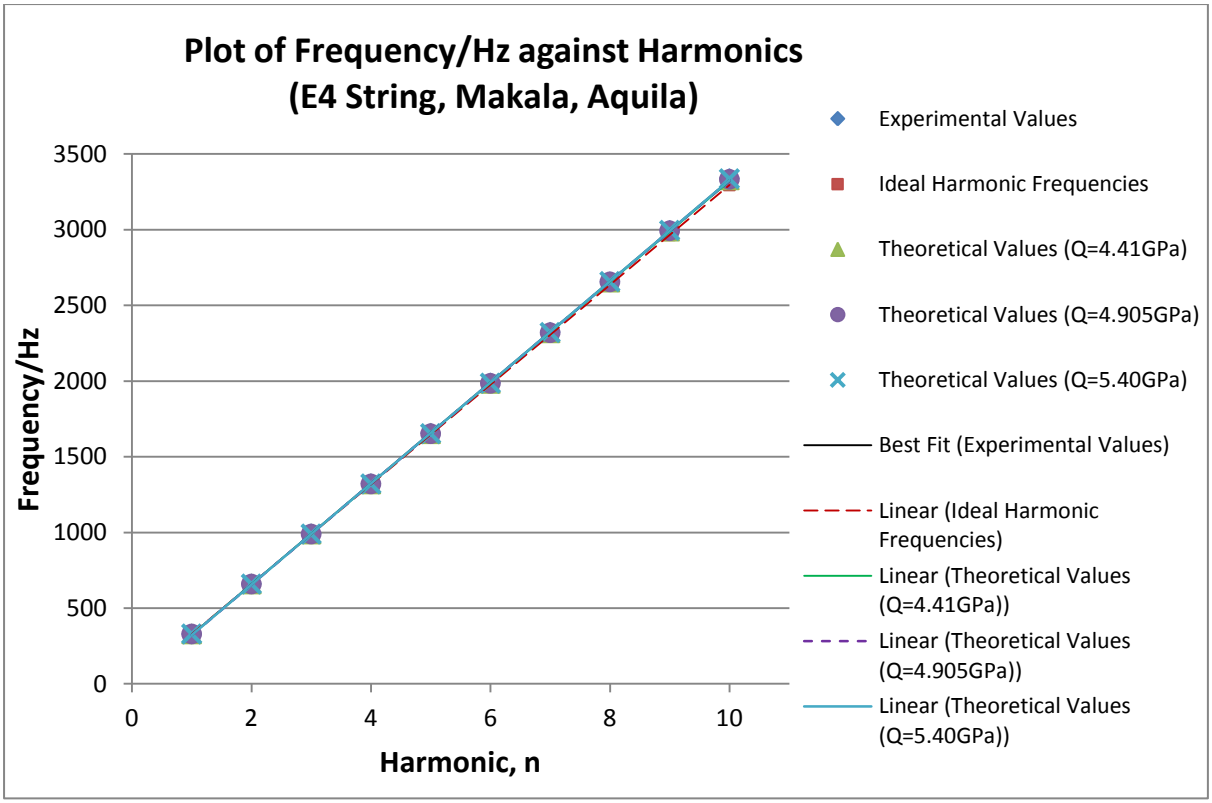

Figure 4.2.10a: Plot of Frequency against Harmonics for the E4 Aquila String for the Makala Ukulele

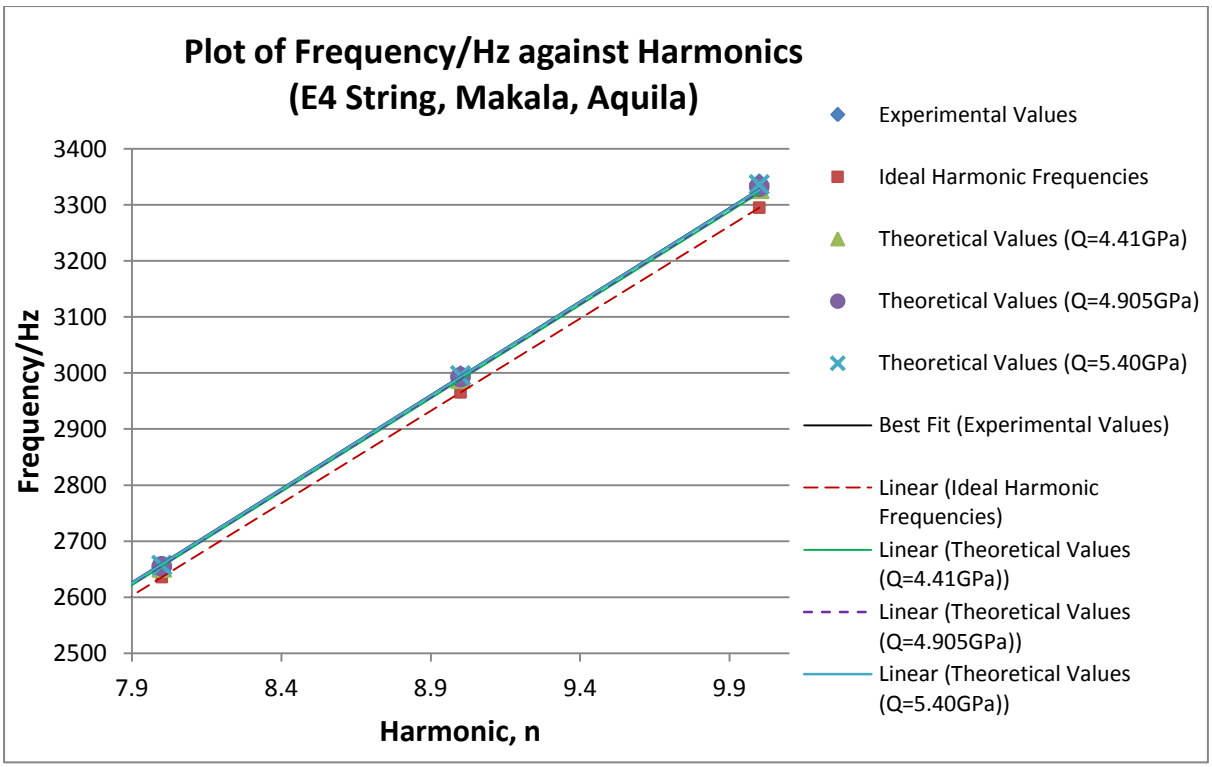

Figure 4.2.10b: Plot of Frequency against Harmonics for the E4 Aquila String for the Makala Ukulele for the 8^{th} to 10^{th} Harmonic

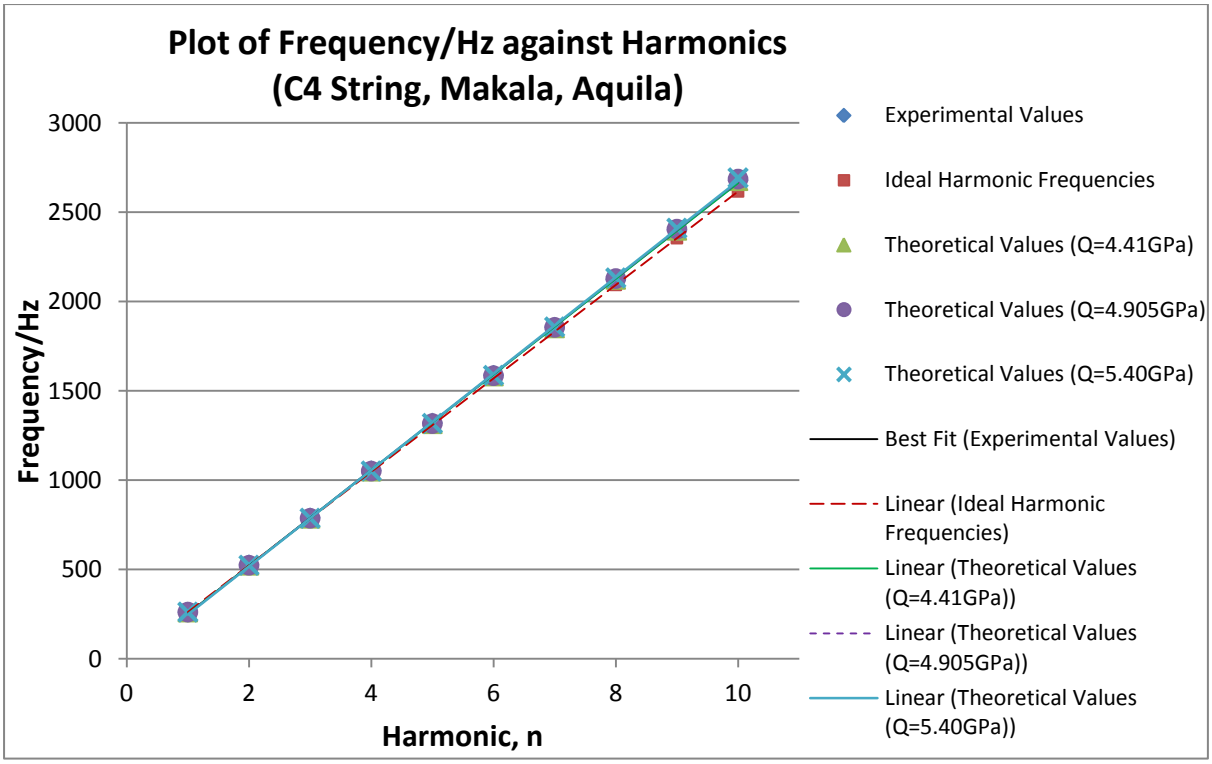

Figure 4.2.11a: Plot of Frequency against Harmonics for the C4 Aquila String for the Makala Ukulele

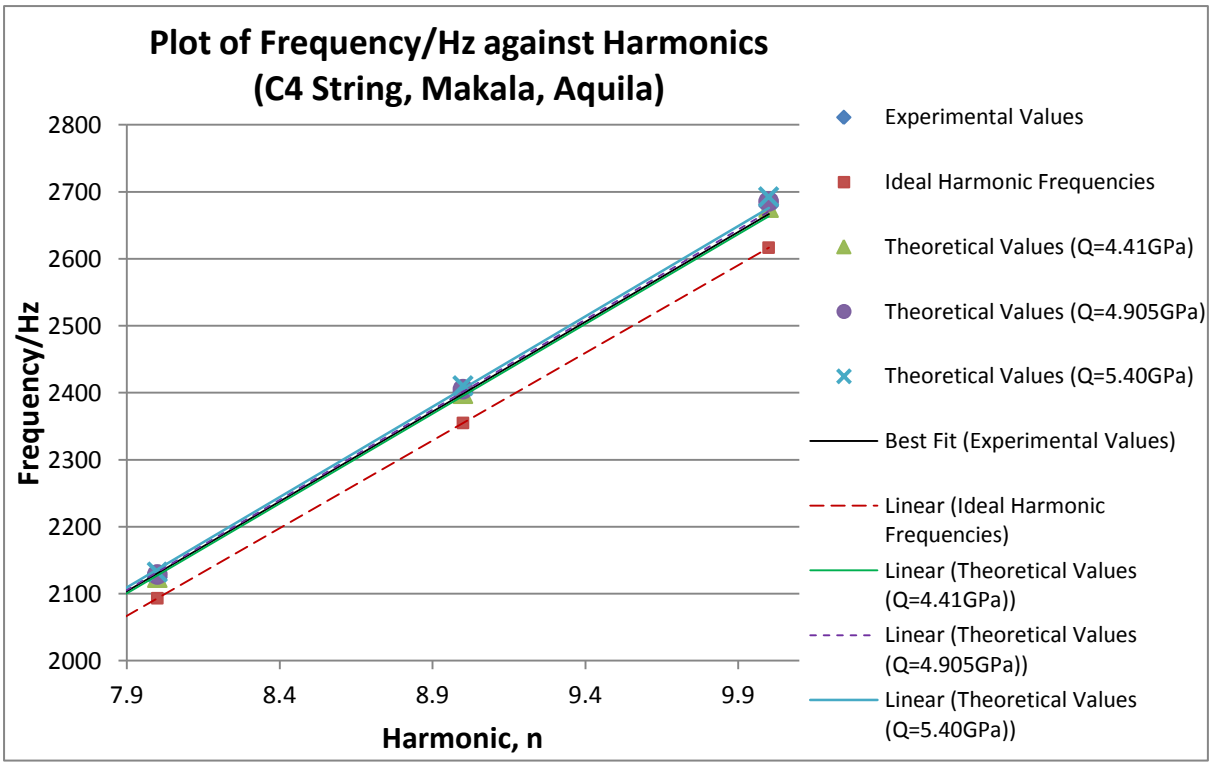

Figure 4.2.11b: Plot of Frequency against Harmonics for the C4 Aquila String for the Makala Ukulele for the 8^{th} to 10^{th} Harmonic

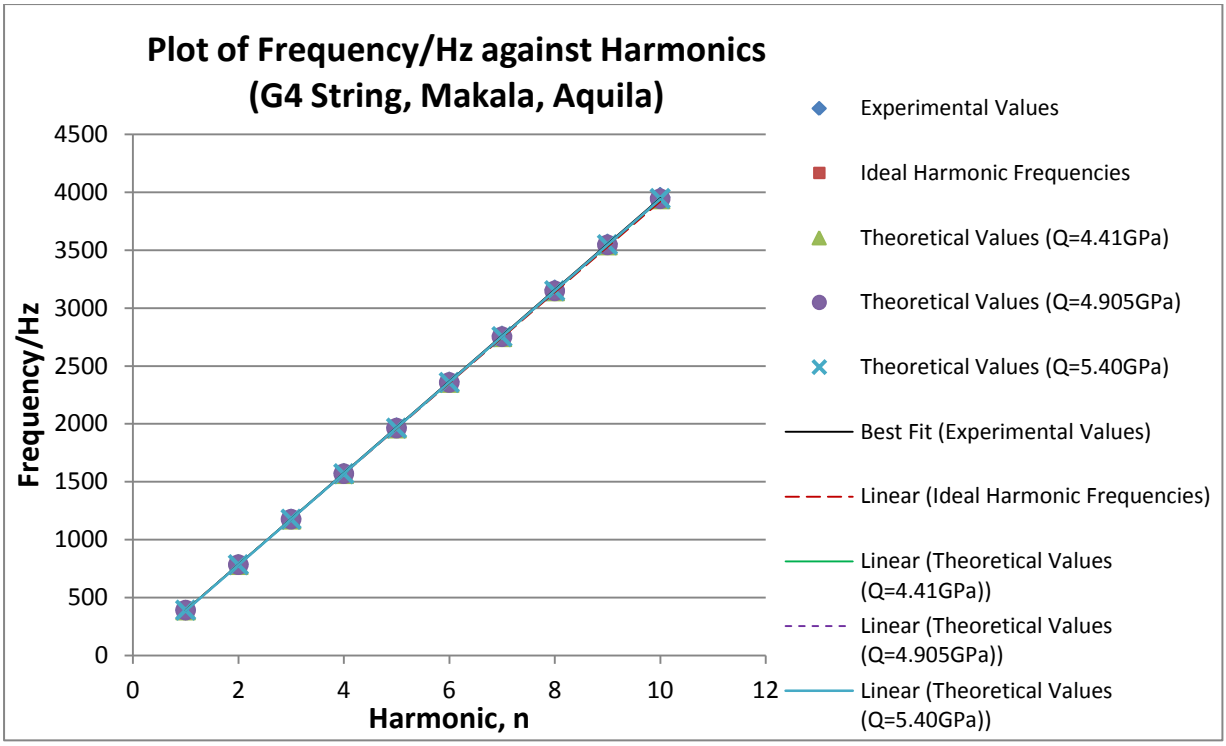

Figure 4.2.12a: Plot of Frequency against Harmonics for the G4 Aquila String for the Makala Ukulele

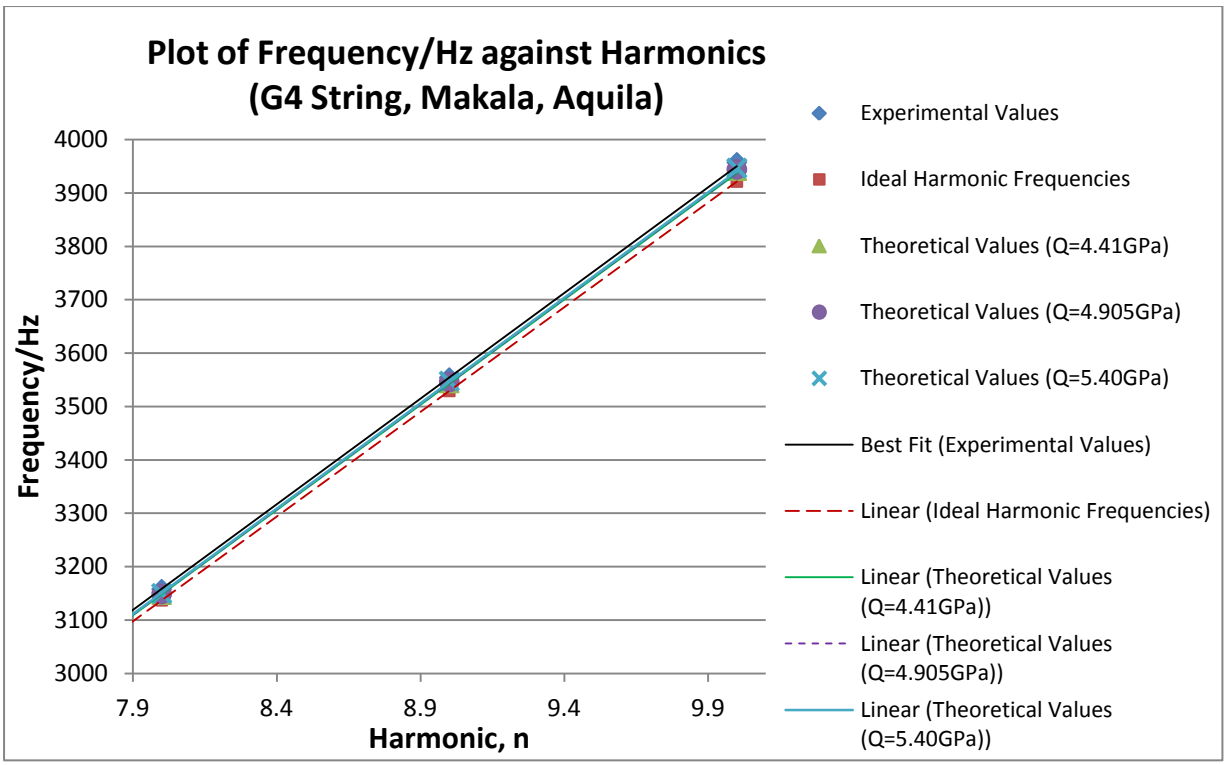

Figure 4.2.12b: Plot of Frequency against Harmonics for the G4 Aquila String for the Makala Ukulele for the 8^{th} to 10^{th} Harmonic

(b) D'Addario T2 Soprano Strings Strings

Figures 4.2.13 to 4.2.16 show the plots of frequency against harmonics for the A4, E4, C4 and G4 D'addario strings of the Makala Ukulele respectively.

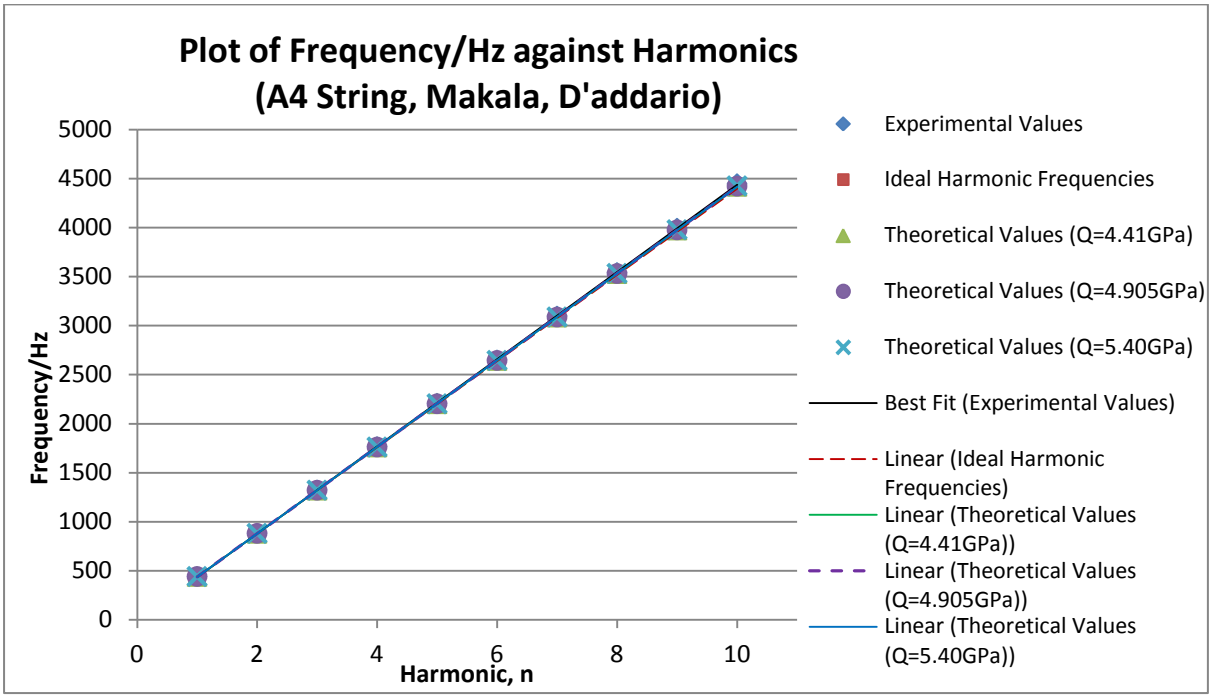

Figure 4.2.13a: Plot of Frequency against Harmonics for the A4 D'addario String for the Makala Ukulele

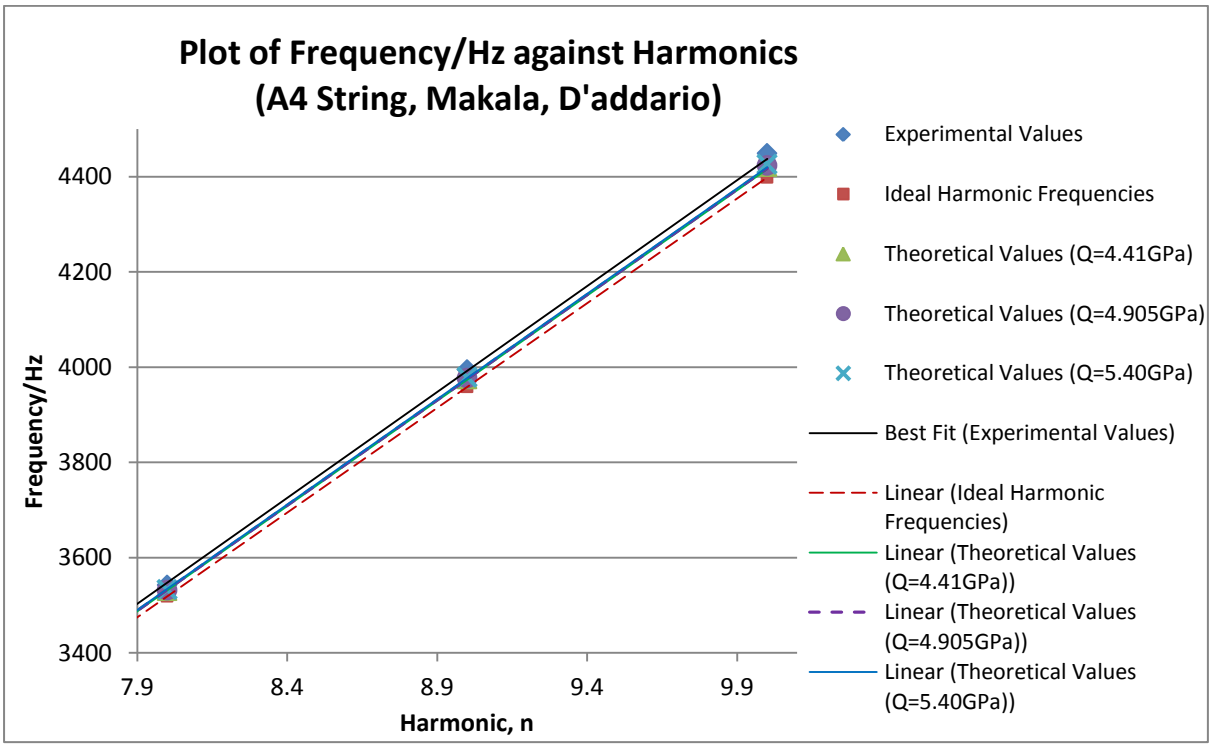

Figure 4.2.13b: Plot of Frequency against Harmonics for the A4 D'addario String for the Makala Ukulele for the 8th to 10th Harmonic

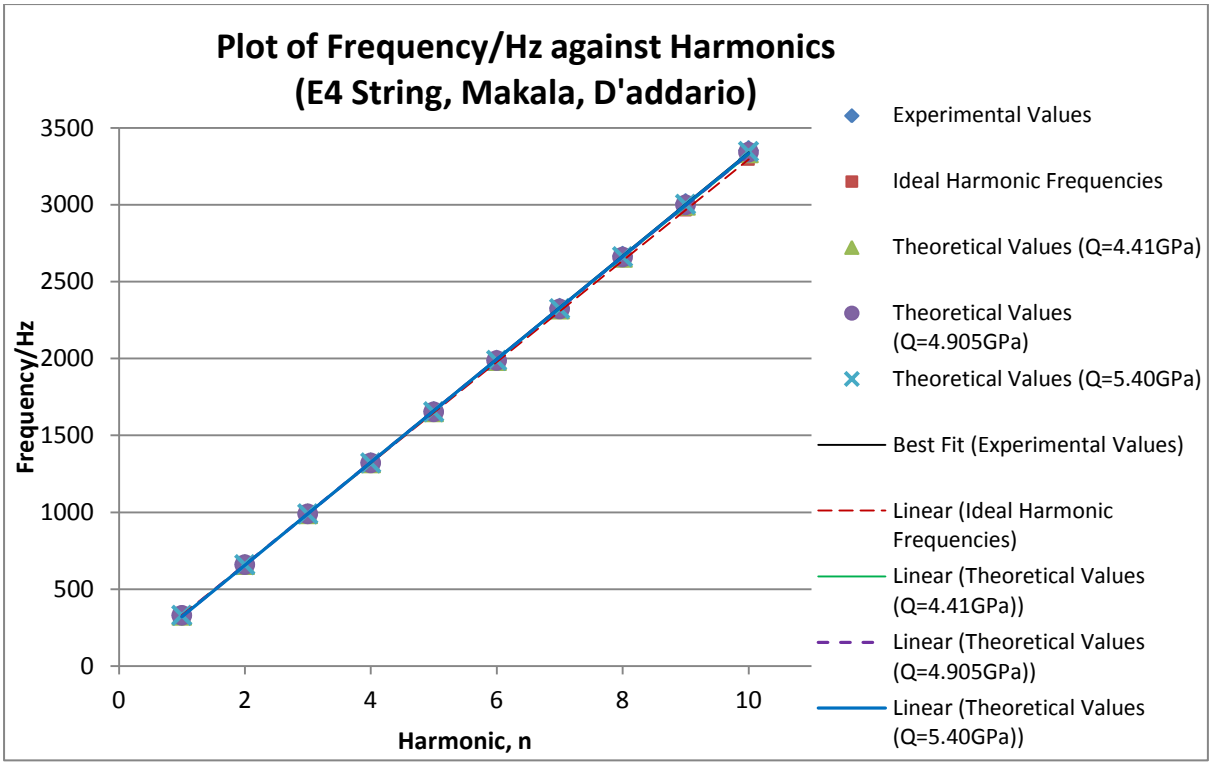

Figure 4.2.14a: Plot of Frequency against Harmonics for the E4 D'addario String for the Makala Ukulele

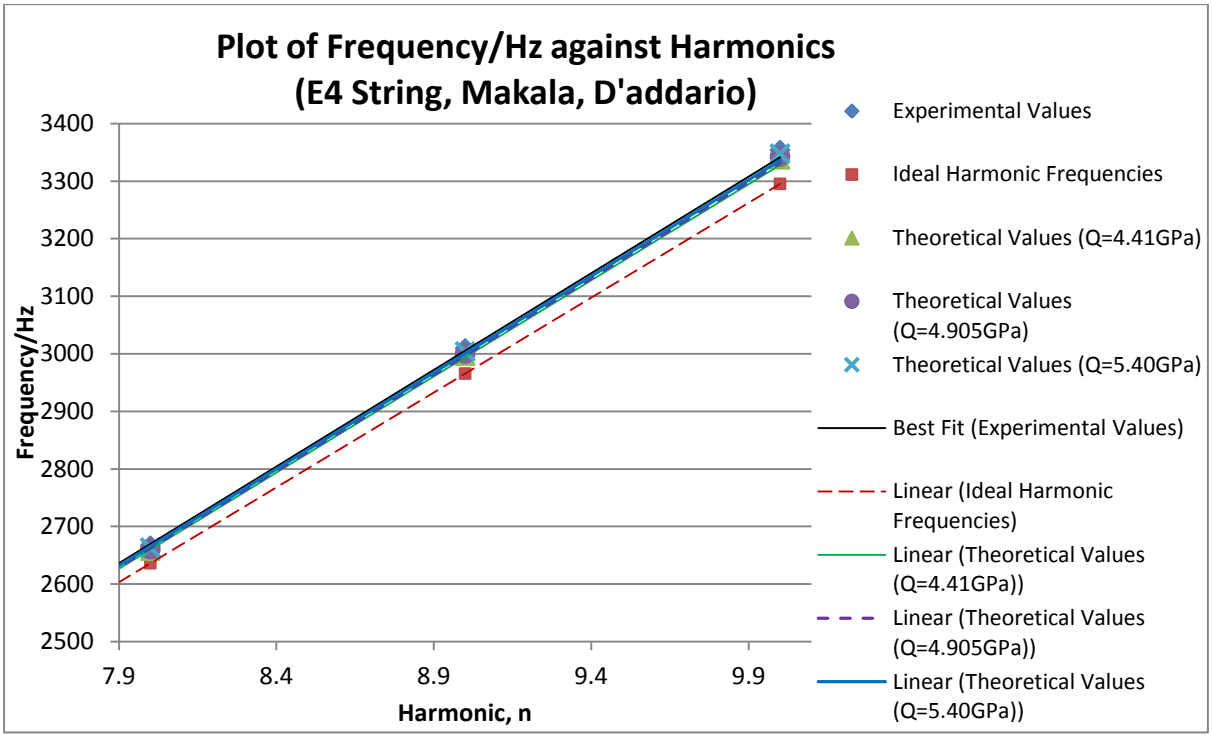

Figure 4.2.14b: Plot of Frequency against Harmonics for the E4 D'addario String for the Makala Ukulele for the 8th to 10th Harmonic

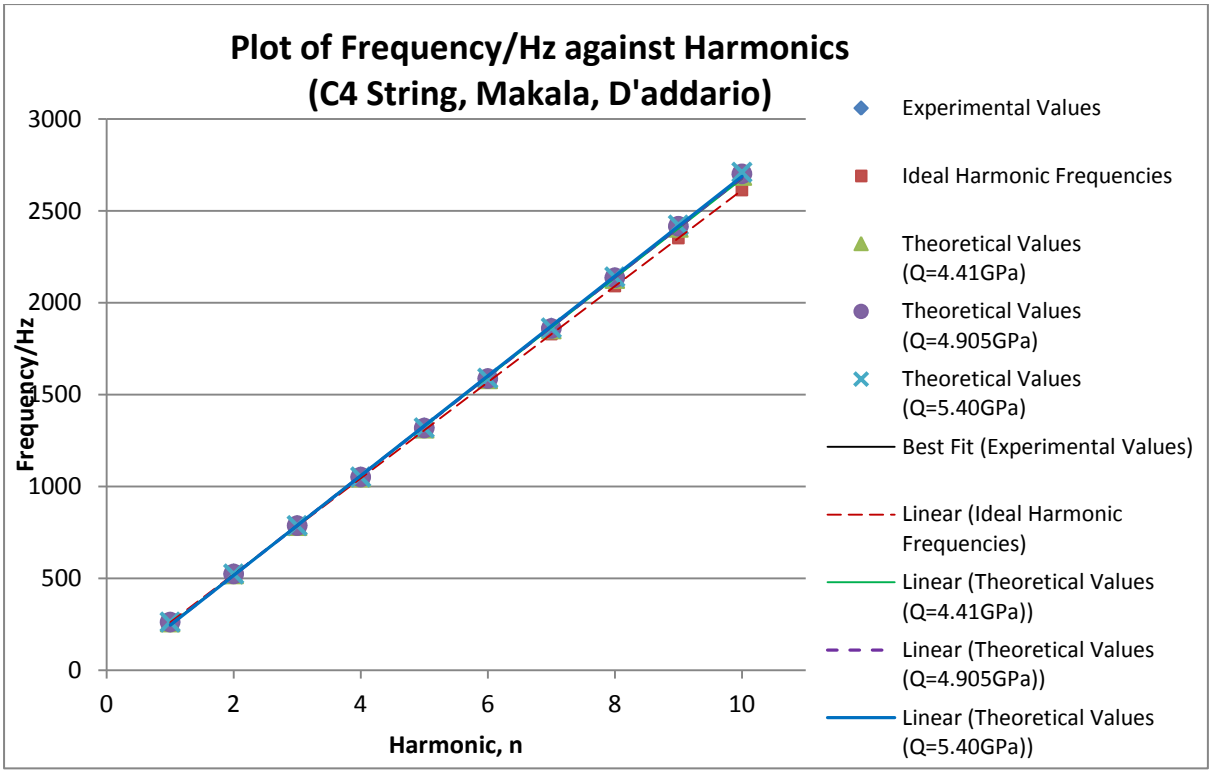

Figure 4.2.15a: Plot of Frequency against Harmonics for the C4 D'addario String for the Makala Ukulele

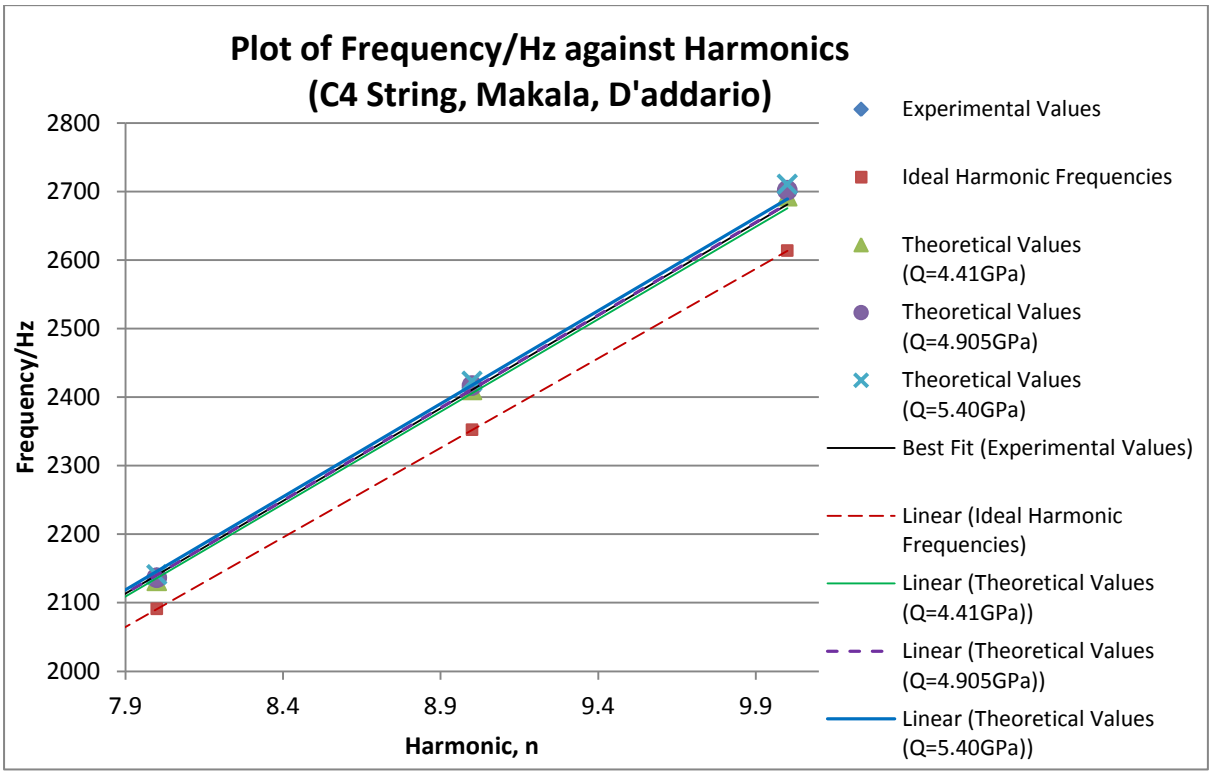

Figure 4.2.15b: Plot of Frequency against Harmonics for the C4 D'addario String for the Makala Ukulele for the 8^{th} to 10^{th} Harmonic

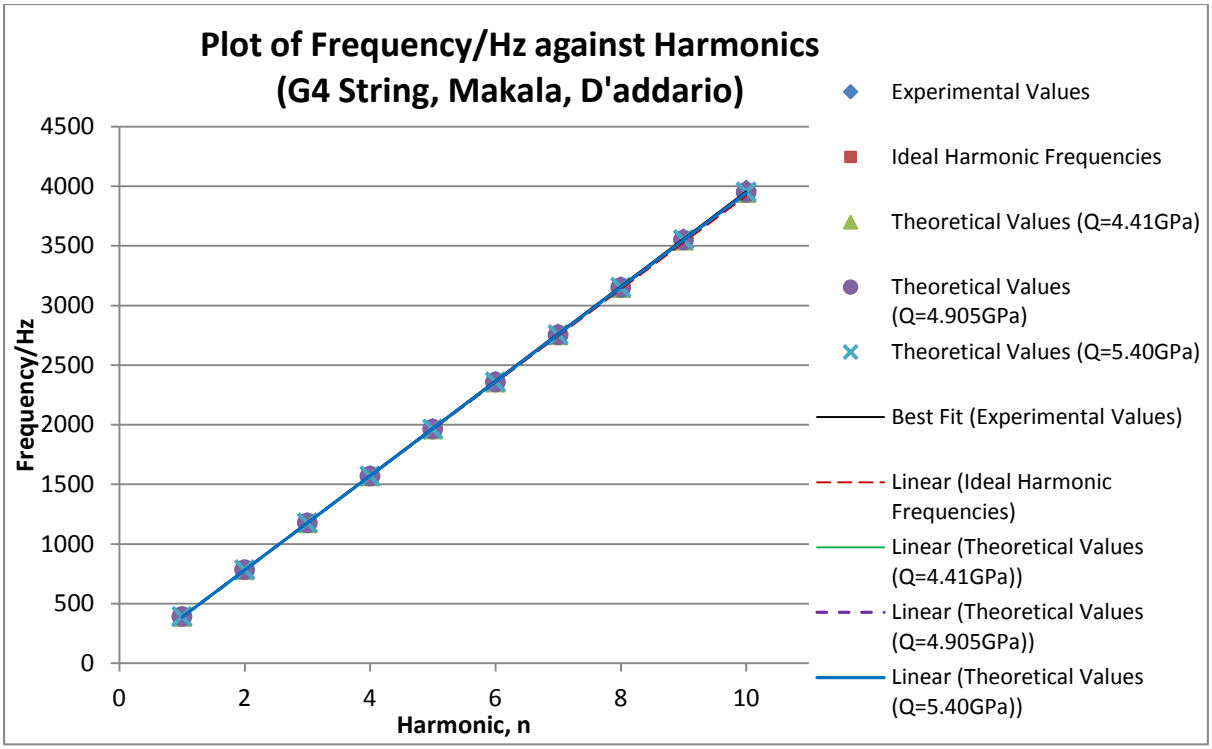

Figure 4.2.16a: Plot of Frequency against Harmonics for the G4 D'addario String for the Makala Ukulele

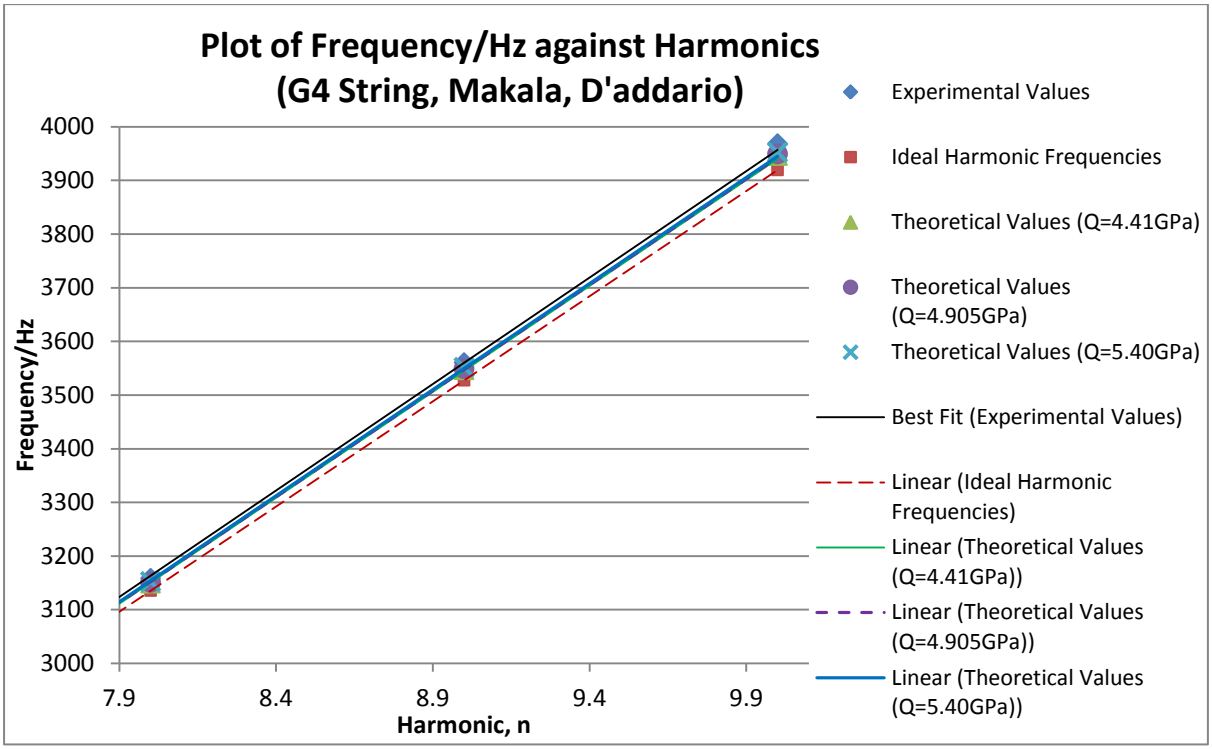

Figure 4.2.16b: Plot of Frequency against Harmonics for the G4 D'addario String for the Makala Ukulele for the 8^{th} to 10^{th} Harmonic

4.2.3 Outdoor Ukulele

(a) Aquila AQ-4U New Nylgut® Regular GCEA Set Soprano Strings

Figures 4.2.17 to 4.2.20 show the plots of frequency against harmonics for the A4, E4, C4 and G4 Aquila strings of the Outdoor Ukulele respectively.

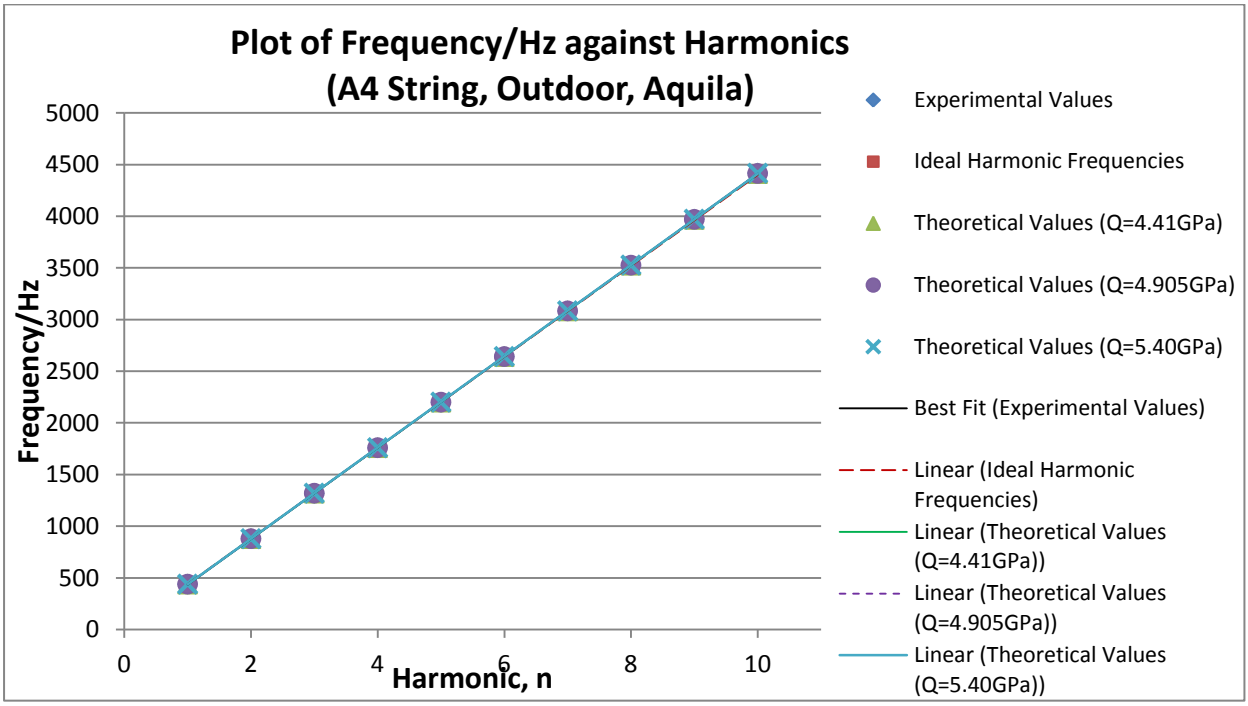

Figure 4.2.17a: Plot of Frequency against Harmonics for the A4 Aquila String for the Outdoor Ukulele

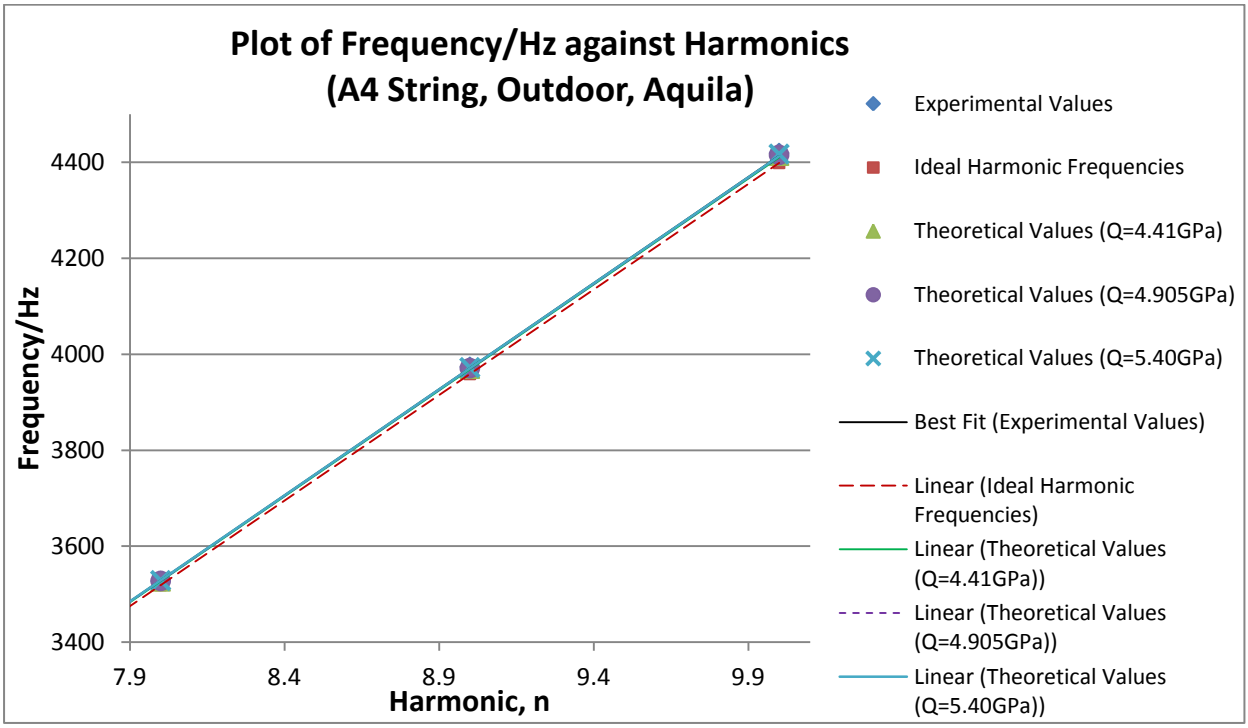

Figure 4.2.17b: Plot of Frequency against Harmonics for the A4 Aquila String for the Outdoor Ukulele for the 8^{th} to 10^{th} Harmonic

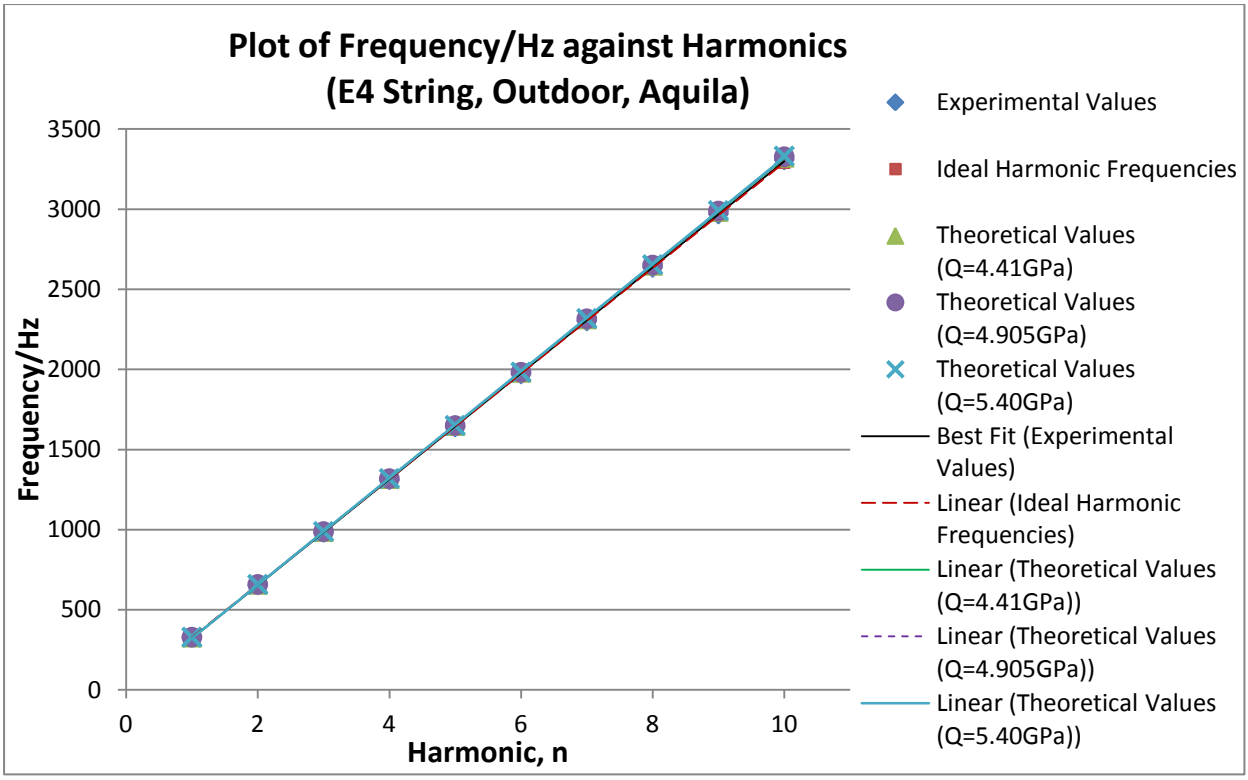

Figure 4.2.18a: Plot of Frequency against Harmonics for the E4 Aquila String for the Outdoor Ukulele

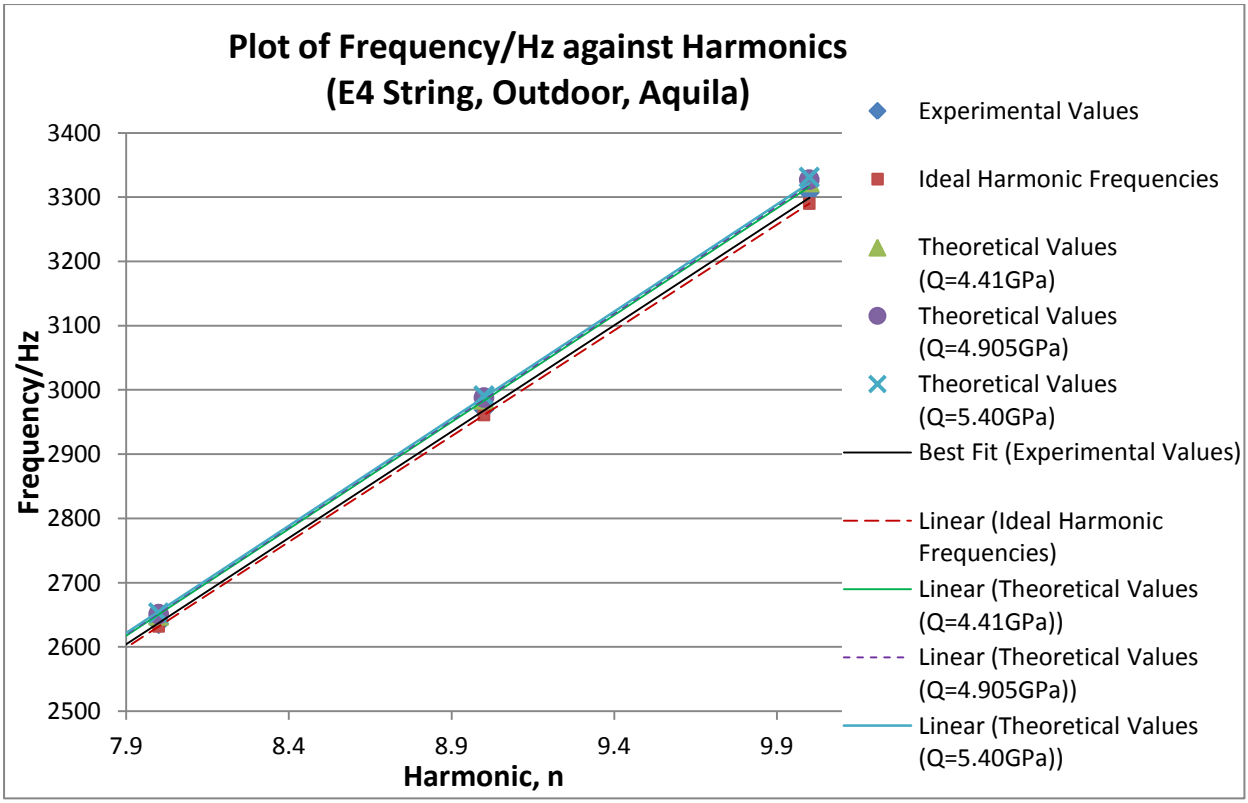

Figure 4.2.18b: Plot of Frequency against Harmonics for the E4 Aquila String for the Outdoor Ukulele for the 8^{th} to 10^{th} Harmonic

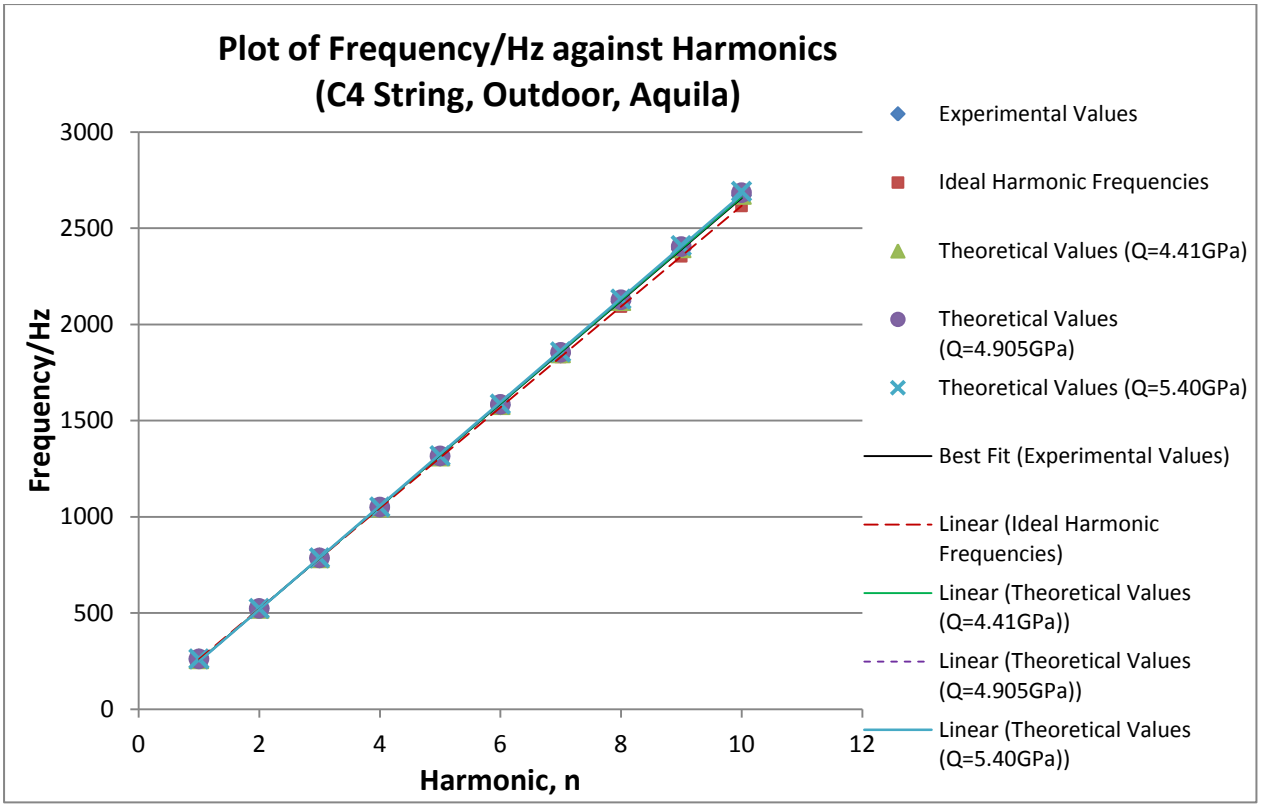

Figure 4.2.19a: Plot of Frequency against Harmonics for the C4 Aquila String for the Outdoor Ukulele

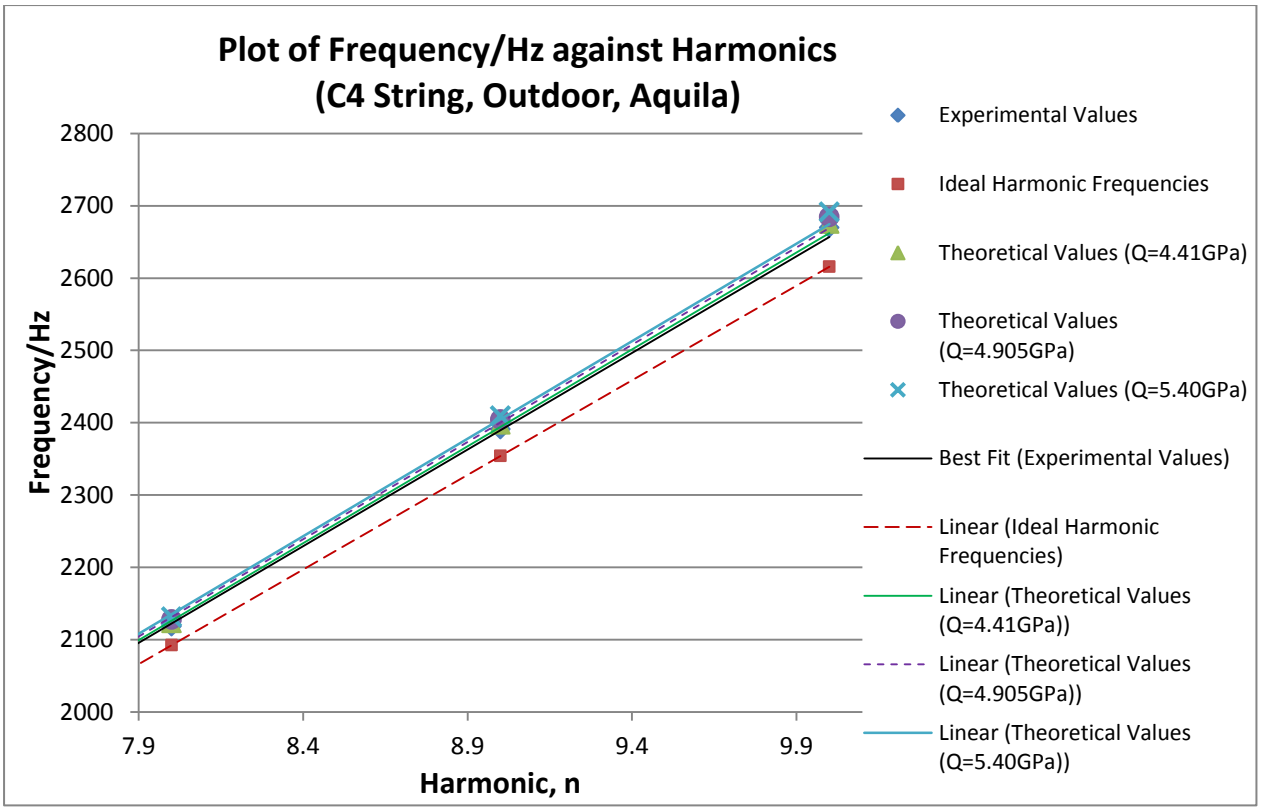

Figure 4.2.19b: Plot of Frequency against Harmonics for the C4 Aquila String for the Outdoor Ukulele for the 8^{th} to 10^{th} Harmonic

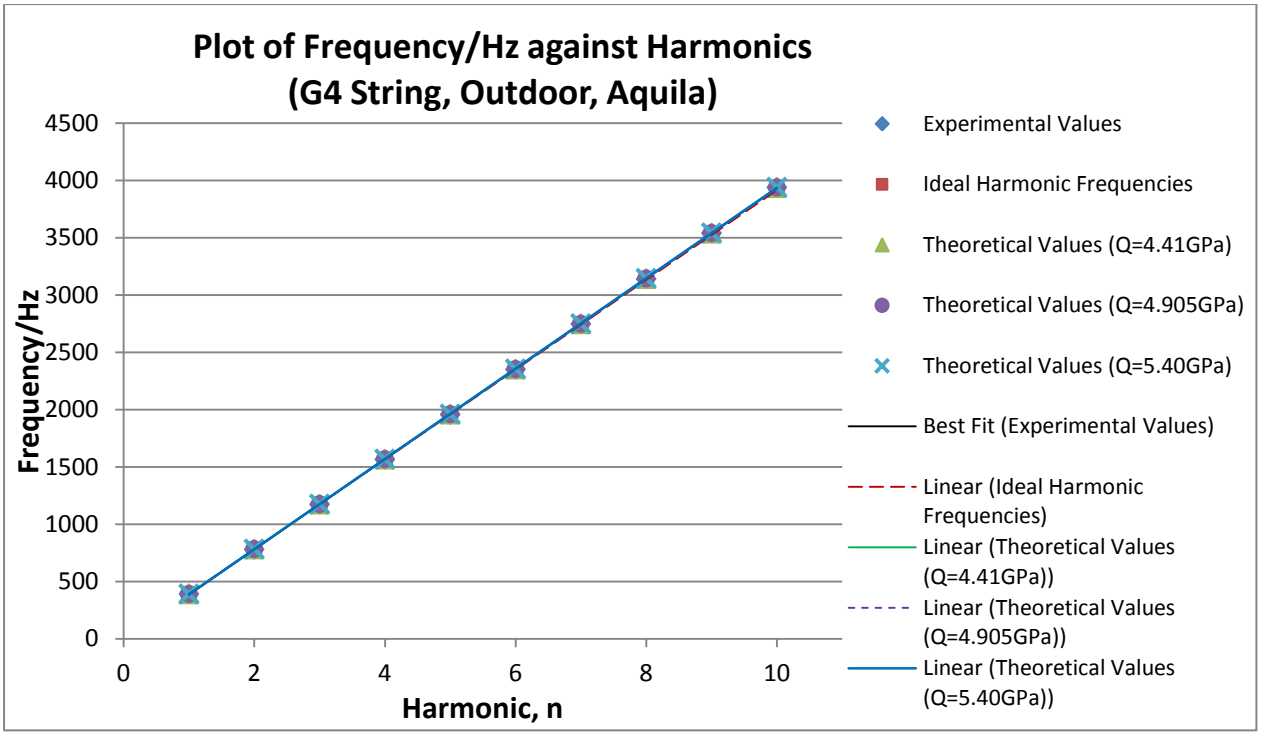

Figure 4.2.20a: Plot of Frequency against Harmonics for the G4 Aquila String for the Outdoor Ukulele

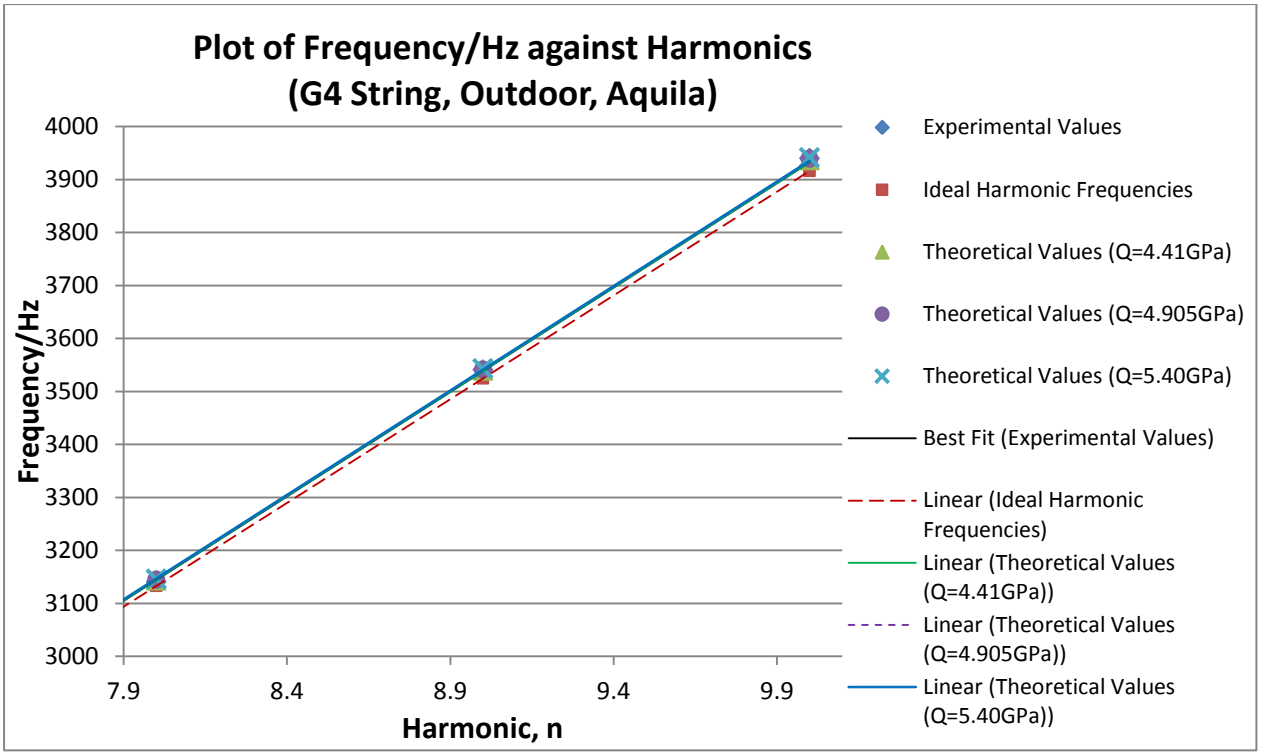

Figure 4.2.20b: Plot of Frequency against Harmonics for the G4 Aquila String for the Outdoor Ukulele for the 8^{th} to 10^{th} Harmonic

(b) D'Addario T2 Soprano Strings Strings

Figures 4.2.21 to 4.2.24 show the plots of frequency against harmonics for the A4, E4, C4 and G4 D'addario strings of the Outdoor Ukulele respectively.

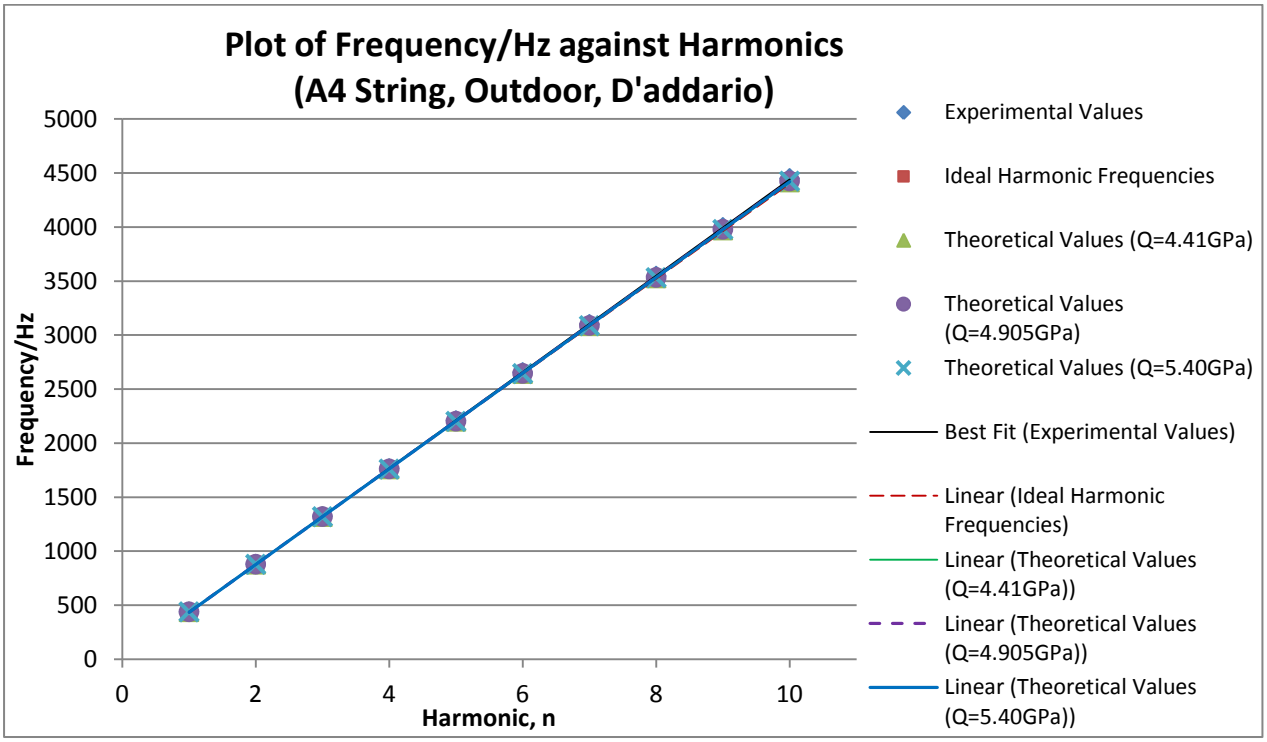

Figure 4.2.21a: Plot of Frequency against Harmonics for the A4 D'addario String for the Outdoor Ukulele

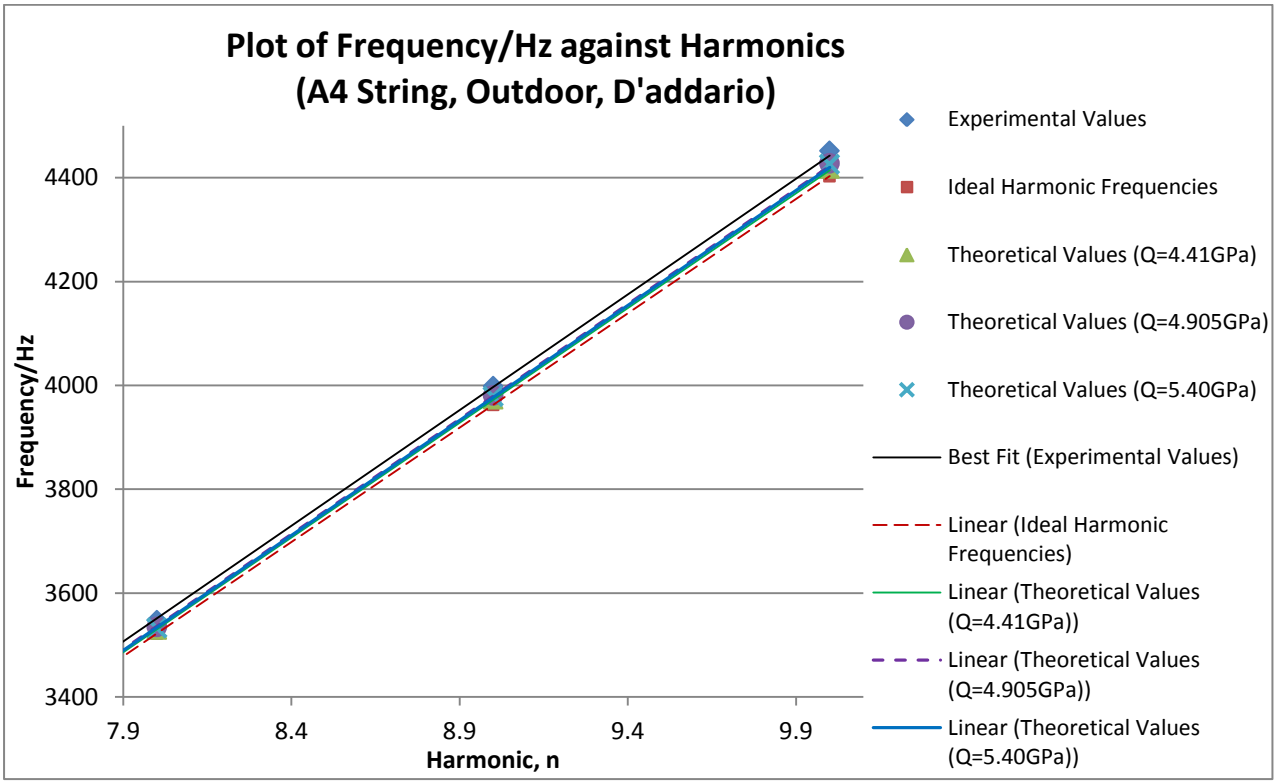

Figure 4.2.21b: Plot of Frequency against Harmonics for the A4 D'addario String for the Outdoor Ukulele for the 8th to 10th Harmonic

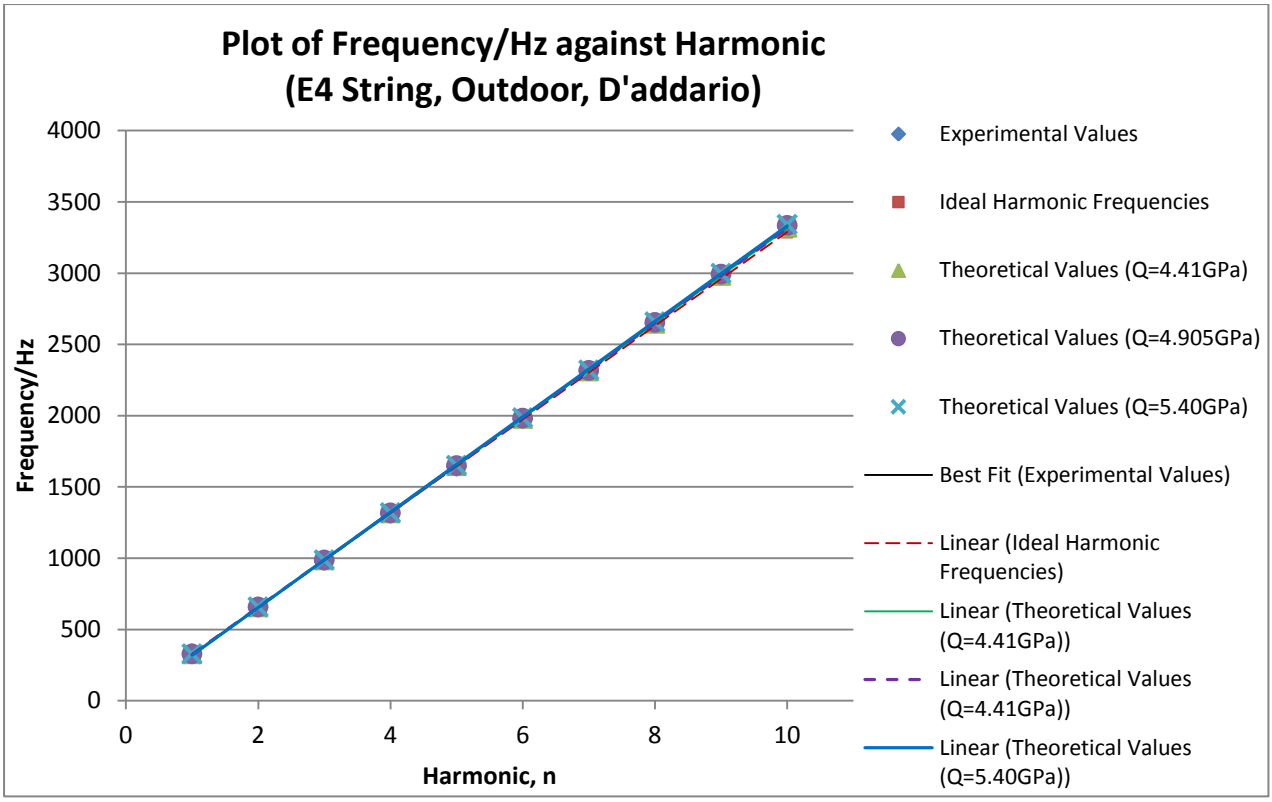

Figure 4.2.22a: Plot of Frequency against Harmonics for the E4 D'addario String for the Outdoor Ukulele

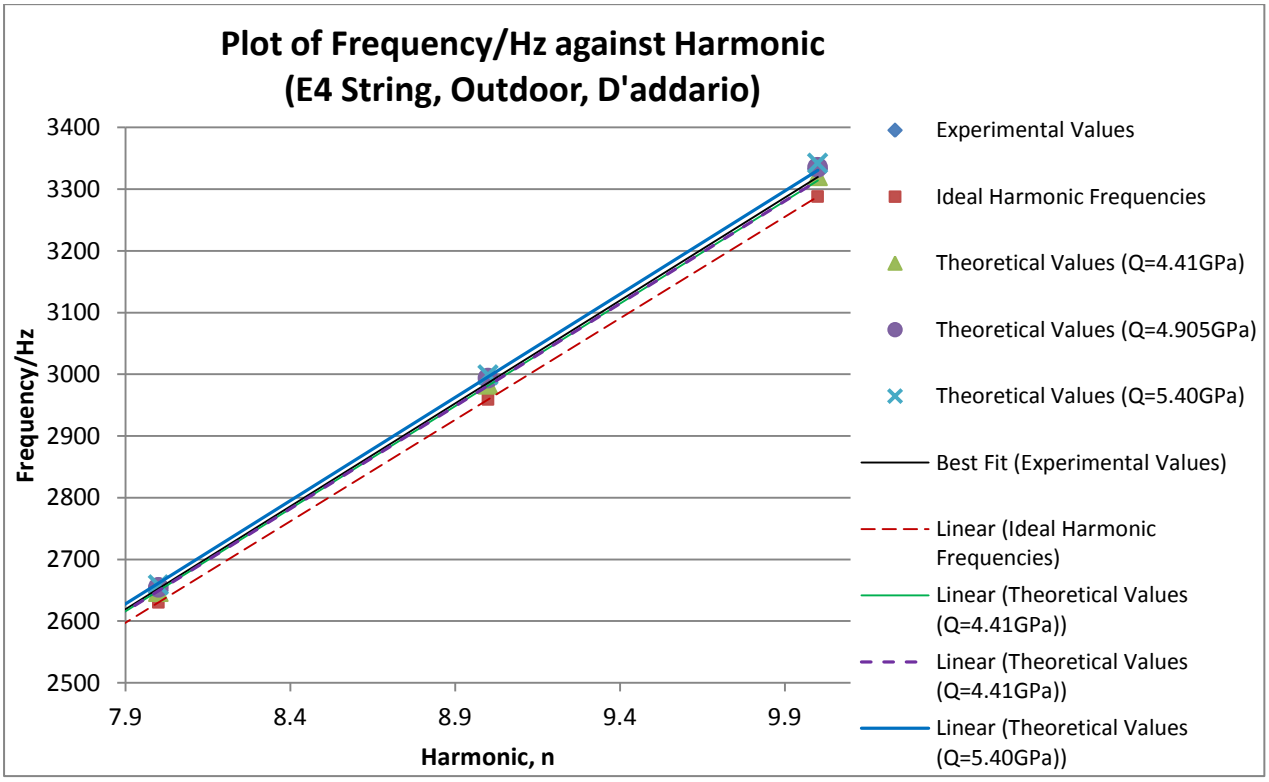

Figure 4.2.22b: Plot of Frequency against Harmonics for the E4 D'addario String for the Outdoor Ukulele for the 8th to 10th Harmonic

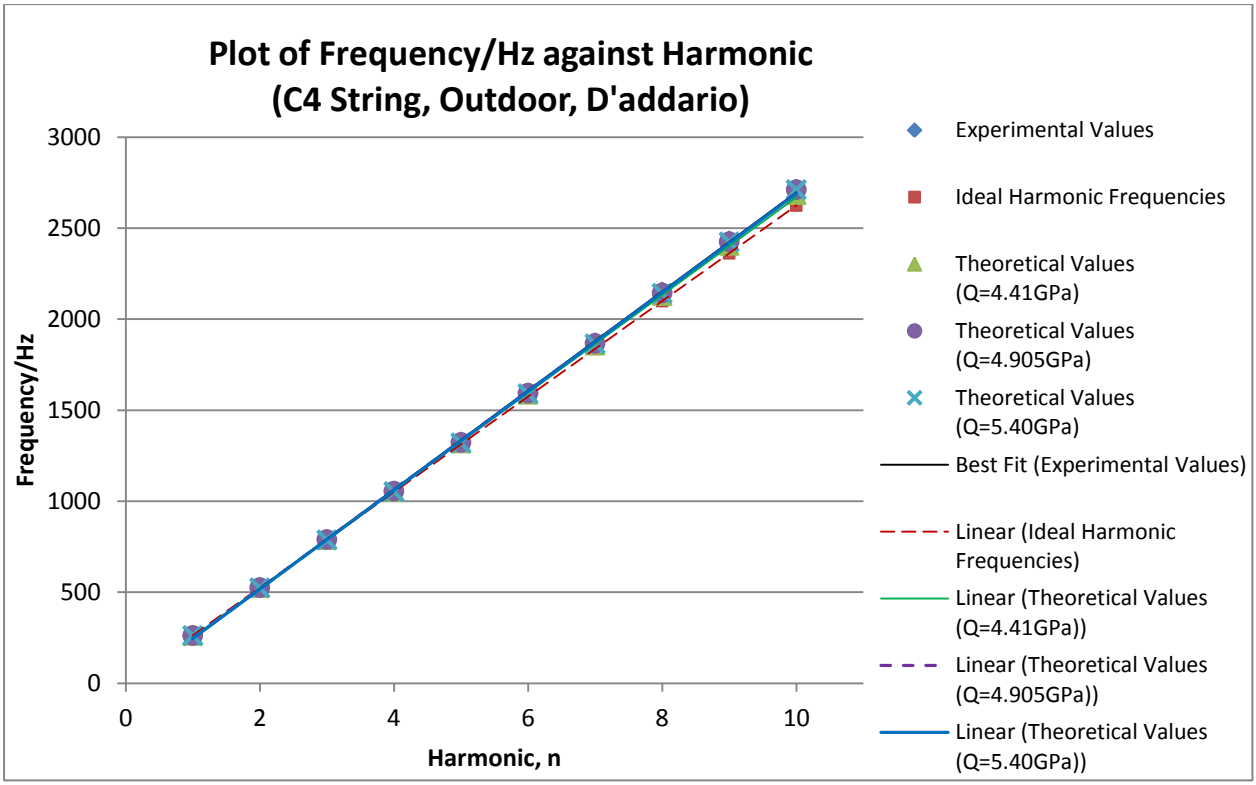

Figure 4.2.23a: Plot of Frequency against Harmonics for the C4 D'addario String for the Outdoor Ukulele

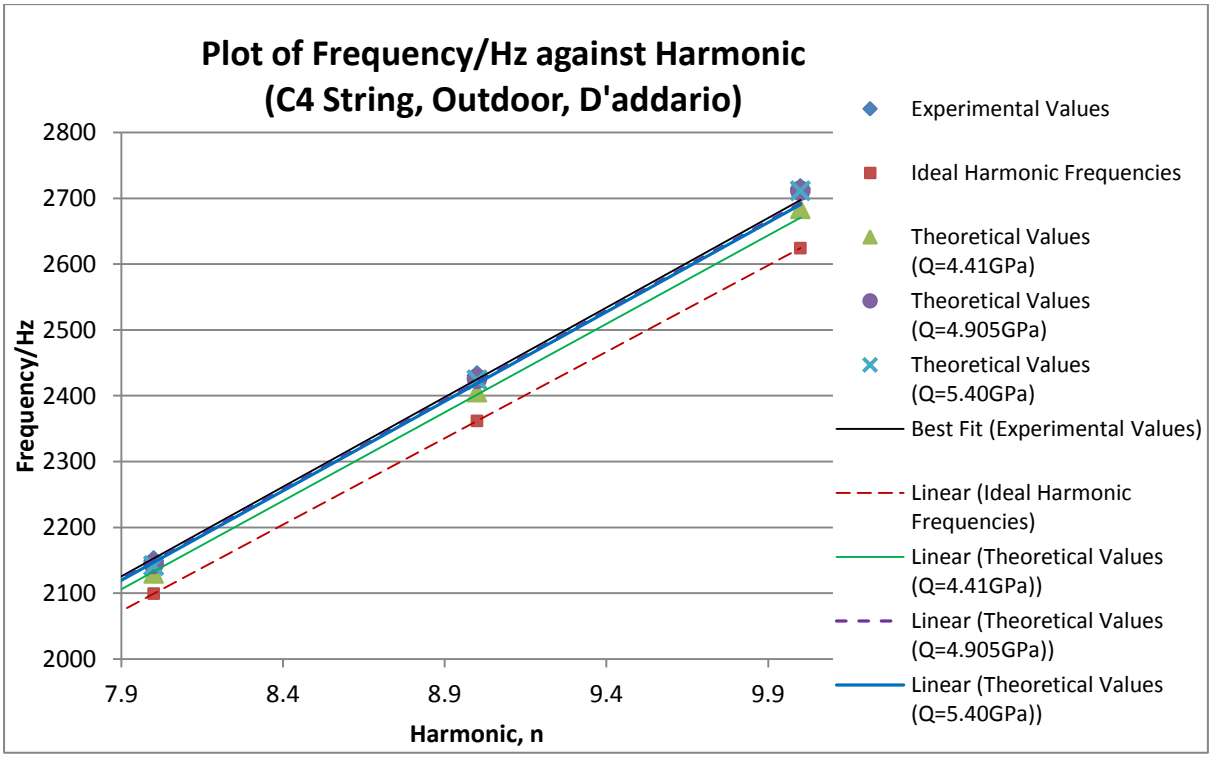

Figure 4.2.23b: Plot of Frequency against Harmonics for the C4 D'addario String for the Outdoor Ukulele for the 8th to 10th Harmonic

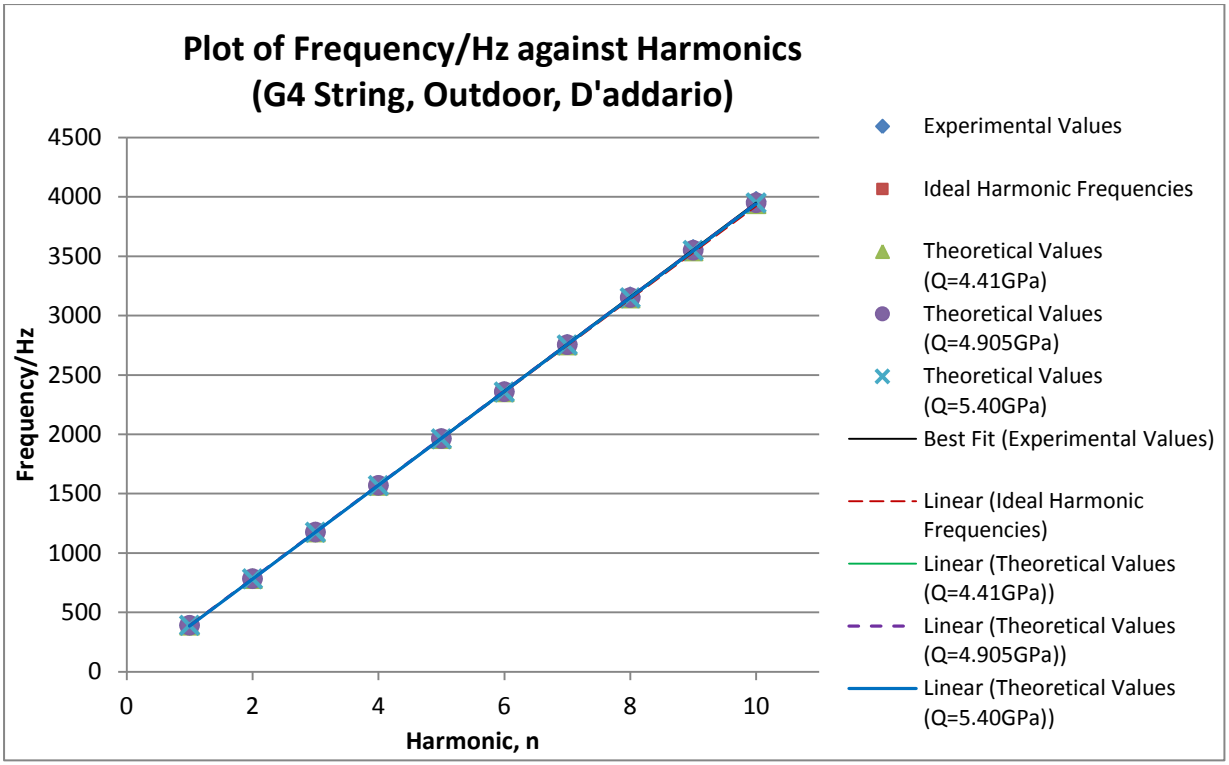

Figure 4.2.24a: Plot of Frequency against Harmonics for the G4 D'addario String for the Outdoor Ukulele

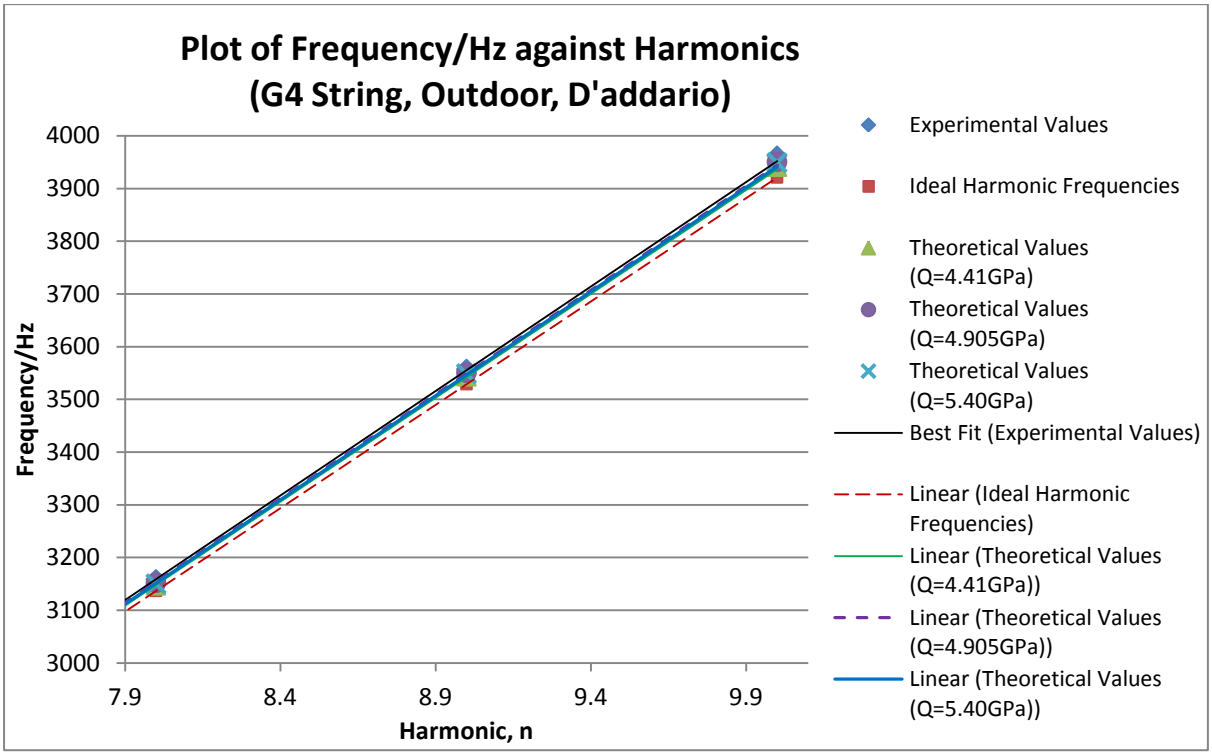

Figure 4.2.24b: Plot of Frequency against Harmonics for the G4 D'addario String for the Outdoor Ukulele for the 8th to 10th Harmonic

4.2.4 Pipa

Figures 4.2.25 to 4.2.28 show the plots of frequency against harmonics for the A3, E3, D3 and A2 strings of the Pipa respectively.

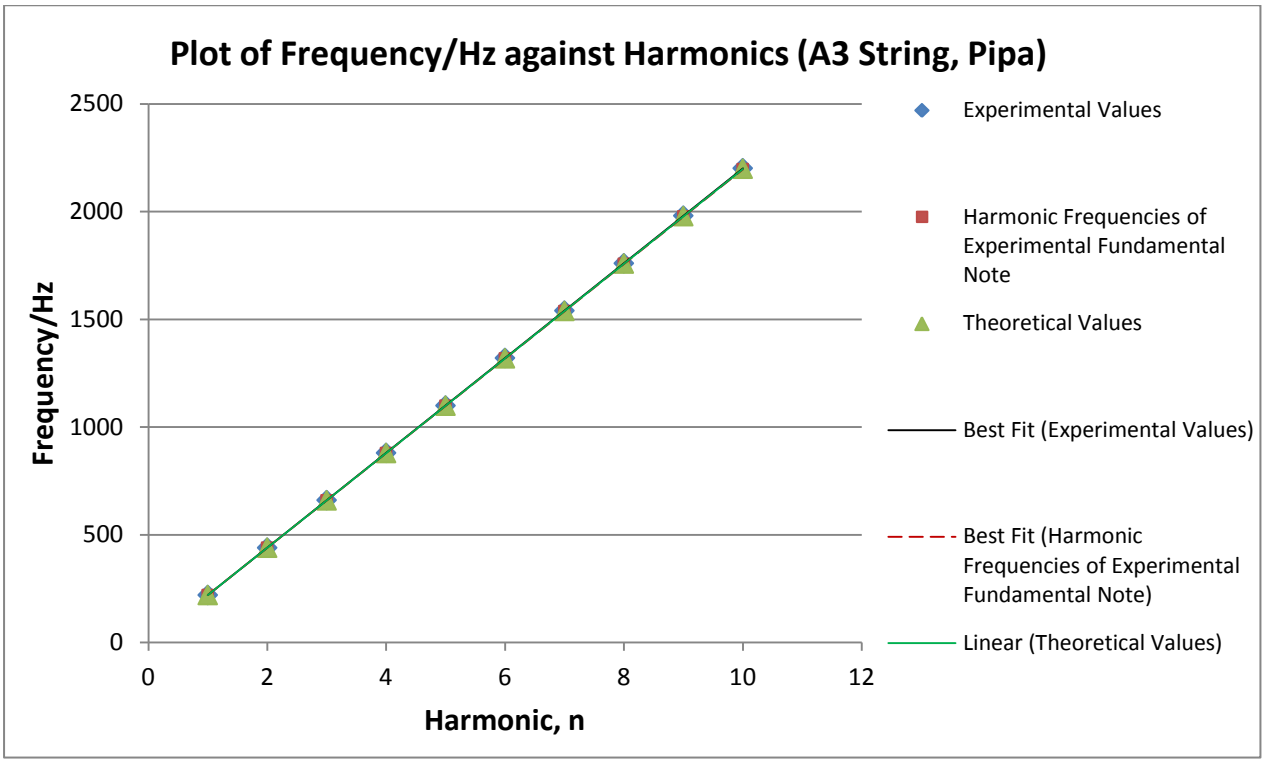

Figure 4.2.25a: Plot of Frequency against Harmonics for the A3 string for the Pipa

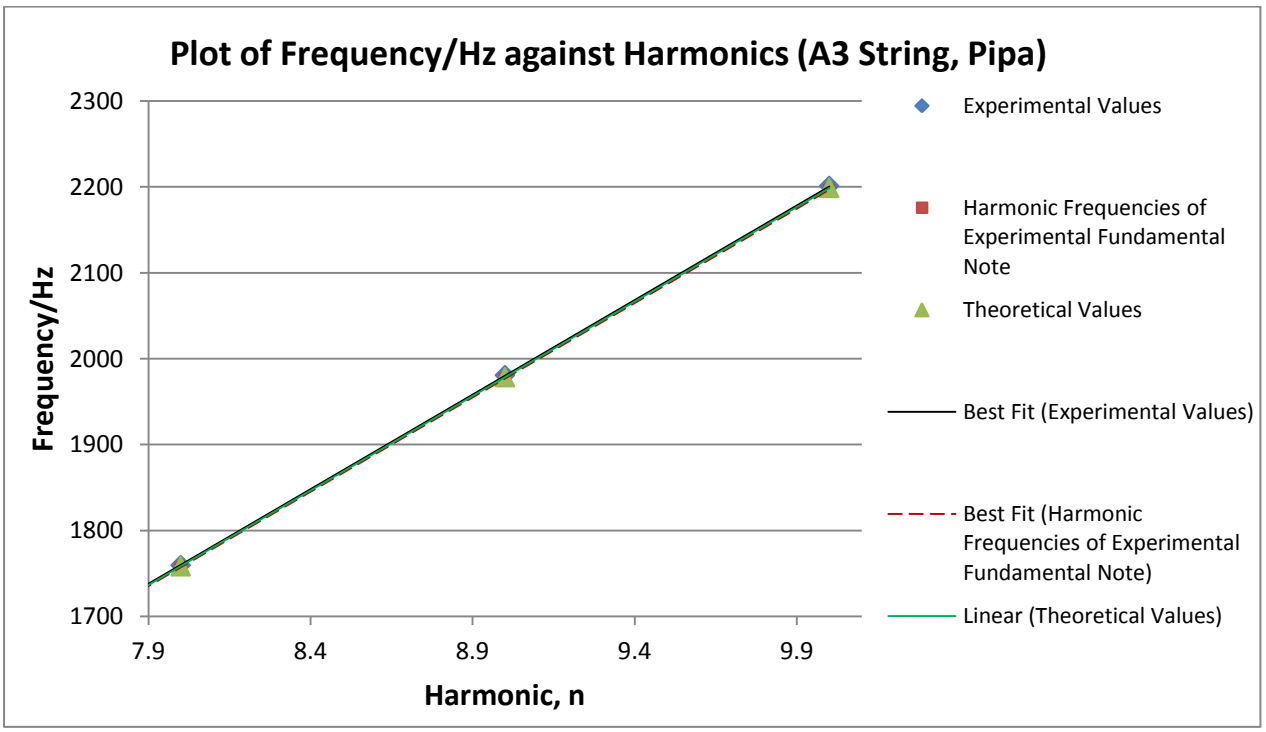

Figure 4.2.256b: Plot of Frequency against Harmonics for the A3 String for the Pipa for the 8th to 10th Harmonic

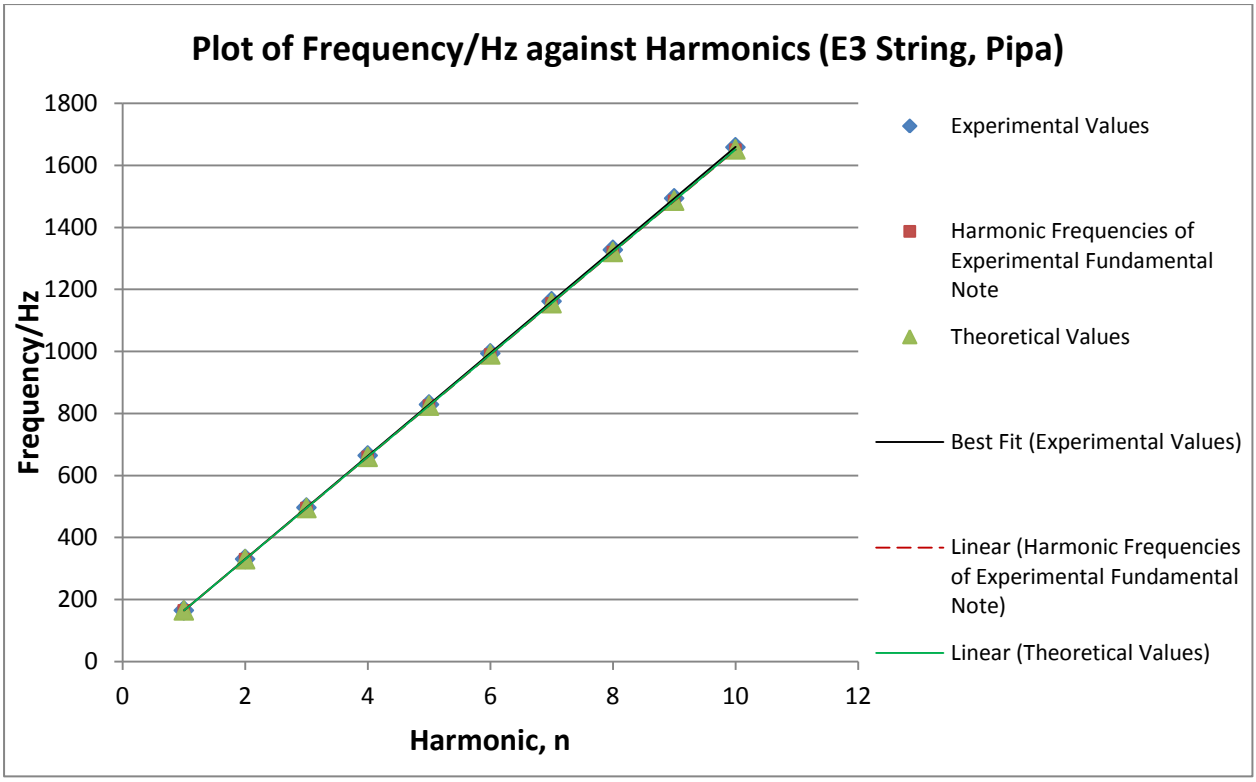

Figure 4.2.26a: Plot of Frequency against Harmonics for the E3 string for the Pipa

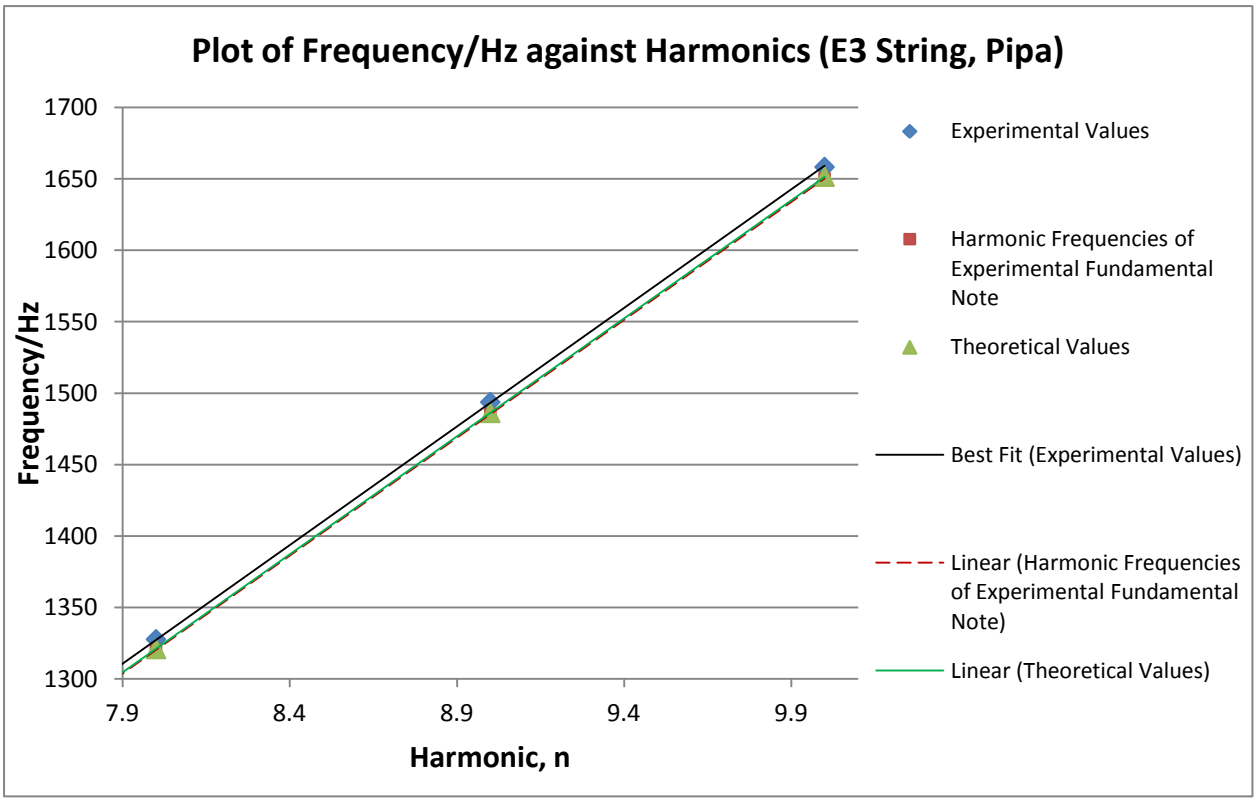

Figure 4.2.26b: Plot of Frequency against Harmonics for the E3 String for the Pipa for the 8^{th} to 10^{th} Harmonic

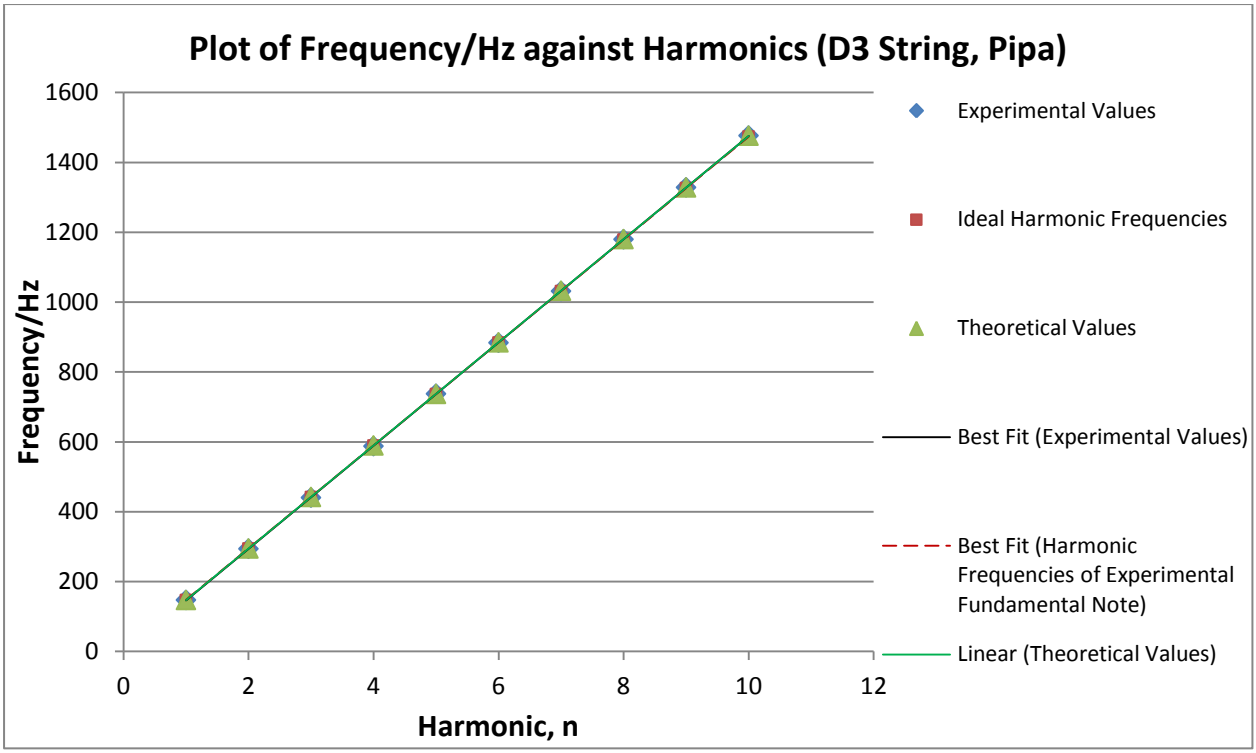

Figure 4.2.27a: Plot of Frequency against Harmonics for the D3 string for the Pipa

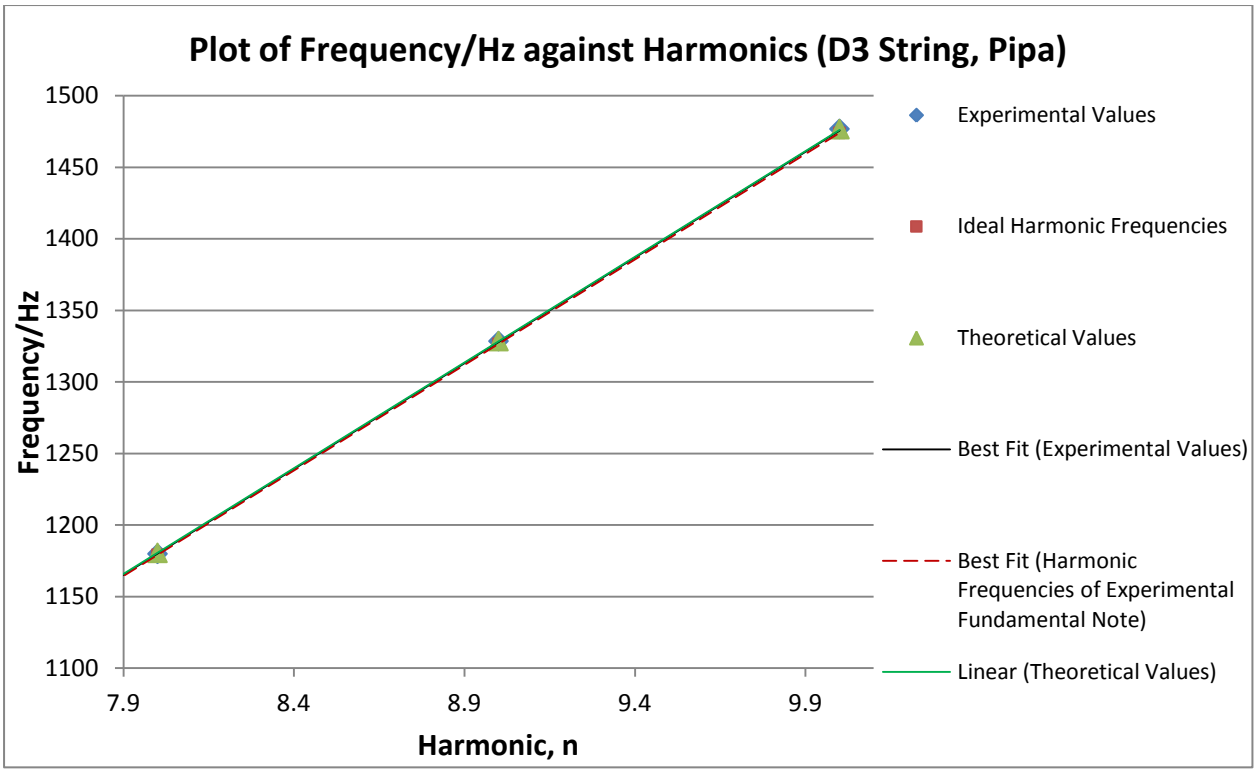

Figure 4.2.27b: Plot of Frequency against Harmonics for the D3 String for the Pipa for the 8^{th} to 10^{th} Harmonic

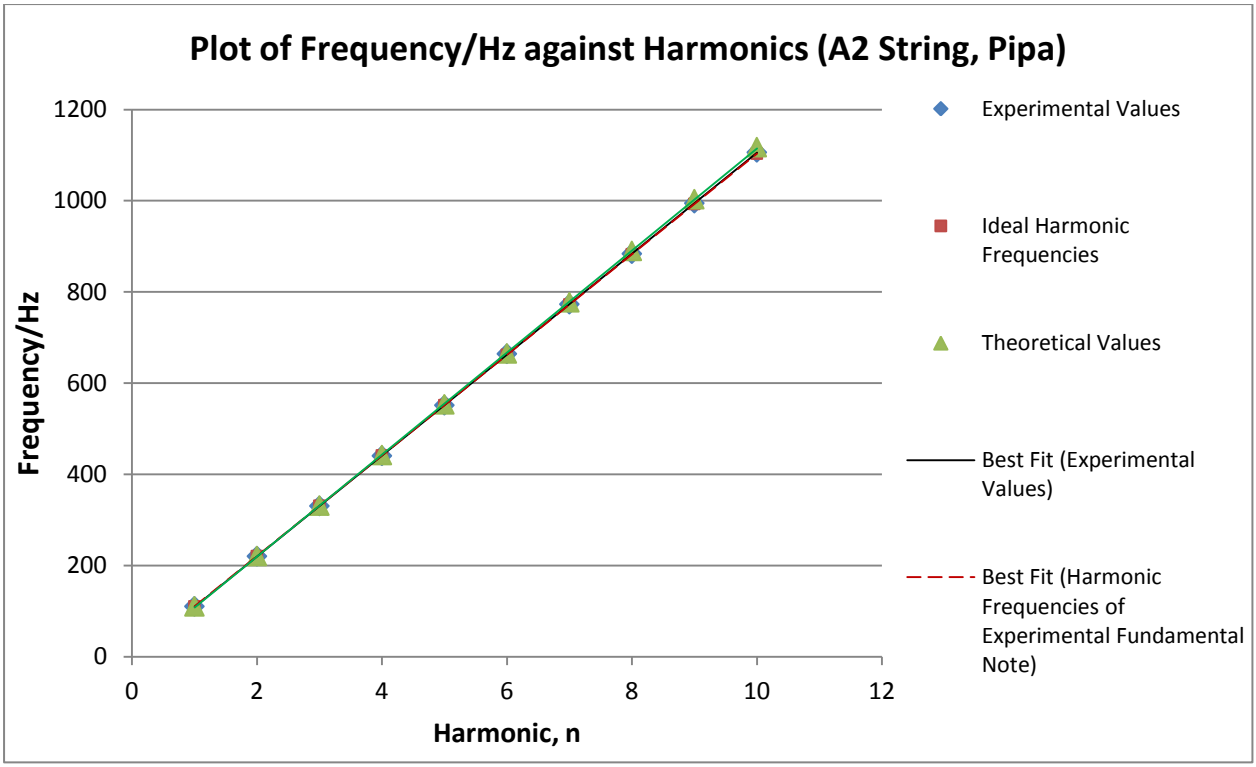

Figure 4.2.28a: Plot of Frequency against Harmonics for the A2 string for the Pipa

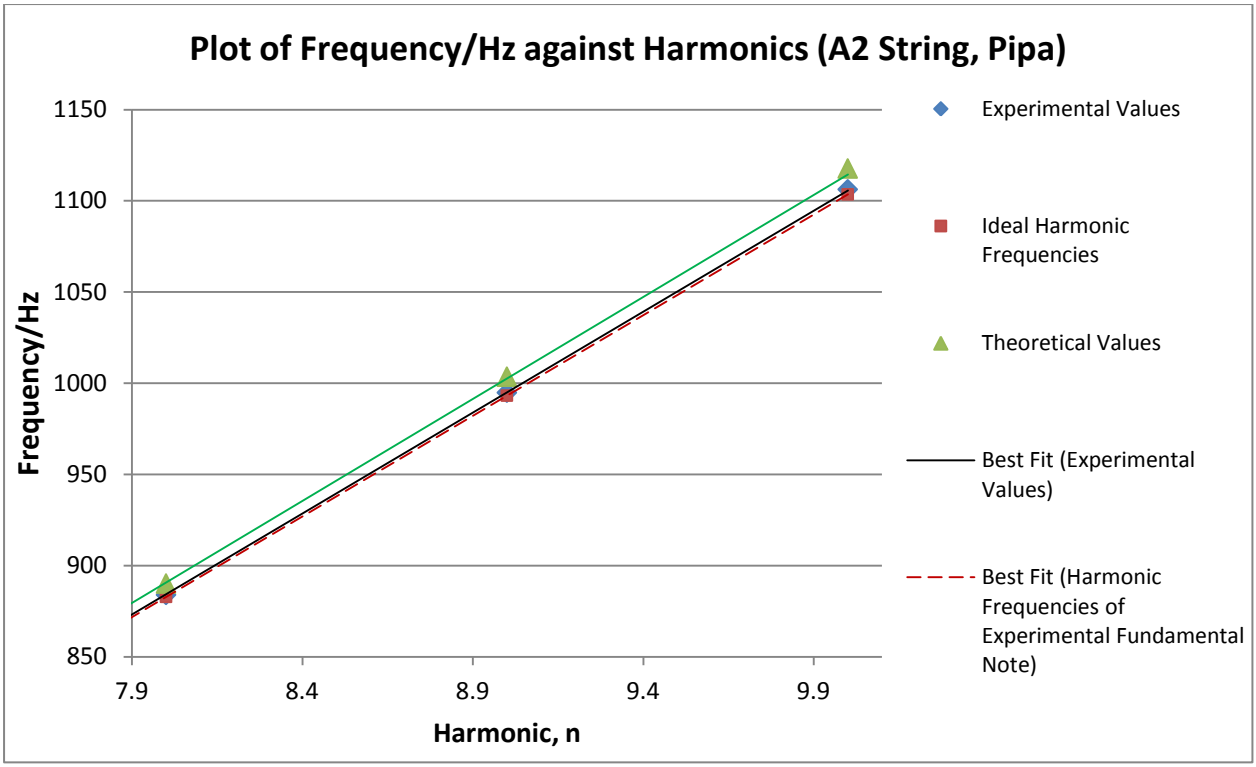

Figure 4.2.28b: Plot of Frequency against Harmonics for the A2 String for the Pipa for the 8th to 10th Harmonic

4.2.5 Classical Guitar

Figures 4.2.29 to 4.2.34 show the plots of frequency against harmonics for the E4, B3, G3, D3 and A2 and E2 strings of the Classical Guitar respectively.

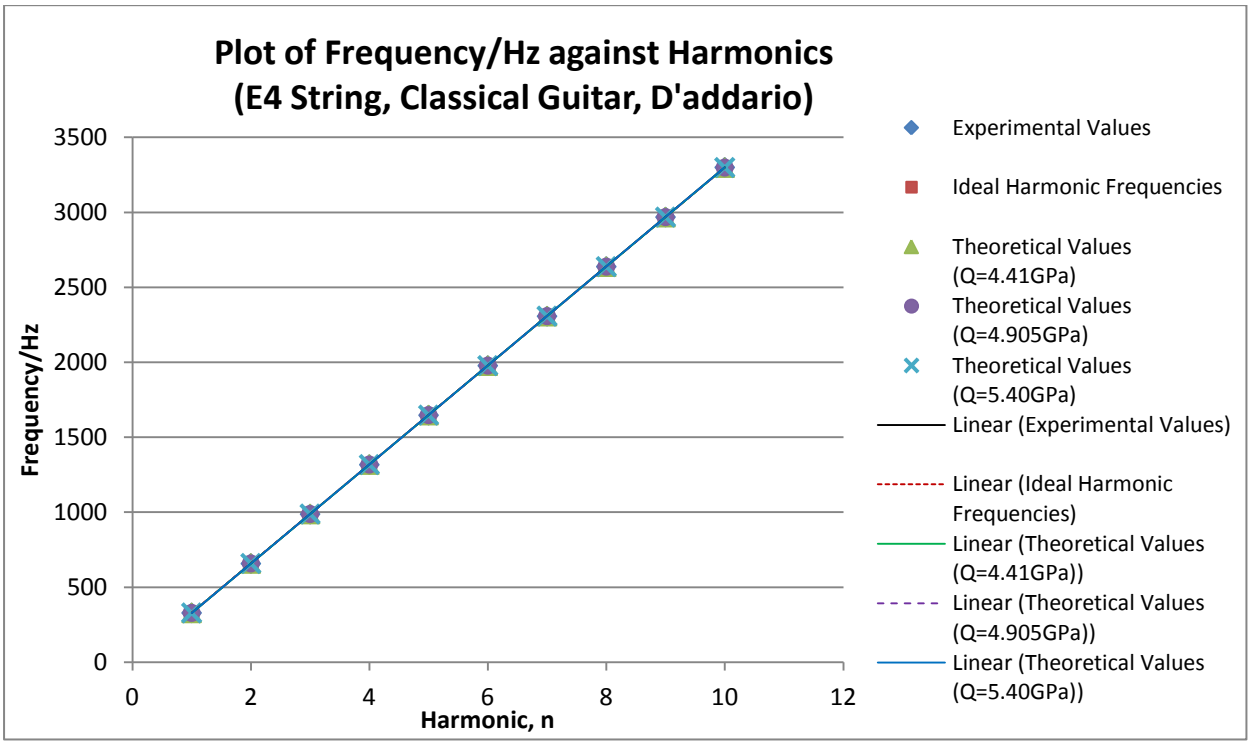

Figure 4.2.29a: Plot of Frequency against Harmonics for the E4 string for the Classical Guitar

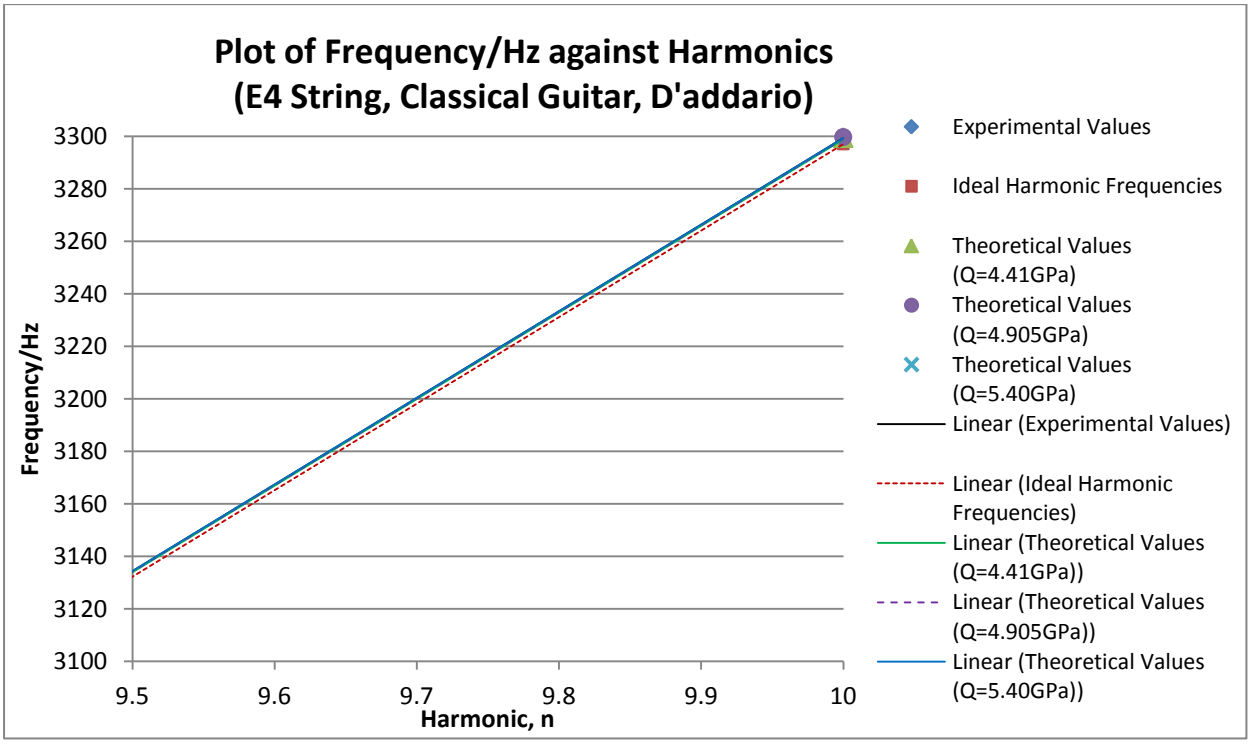

Figure 4.2.29b: Plot of Frequency against Harmonics for the E4 String for the Classical Guitar for the 9.5^{th} and 10^{th} Harmonic

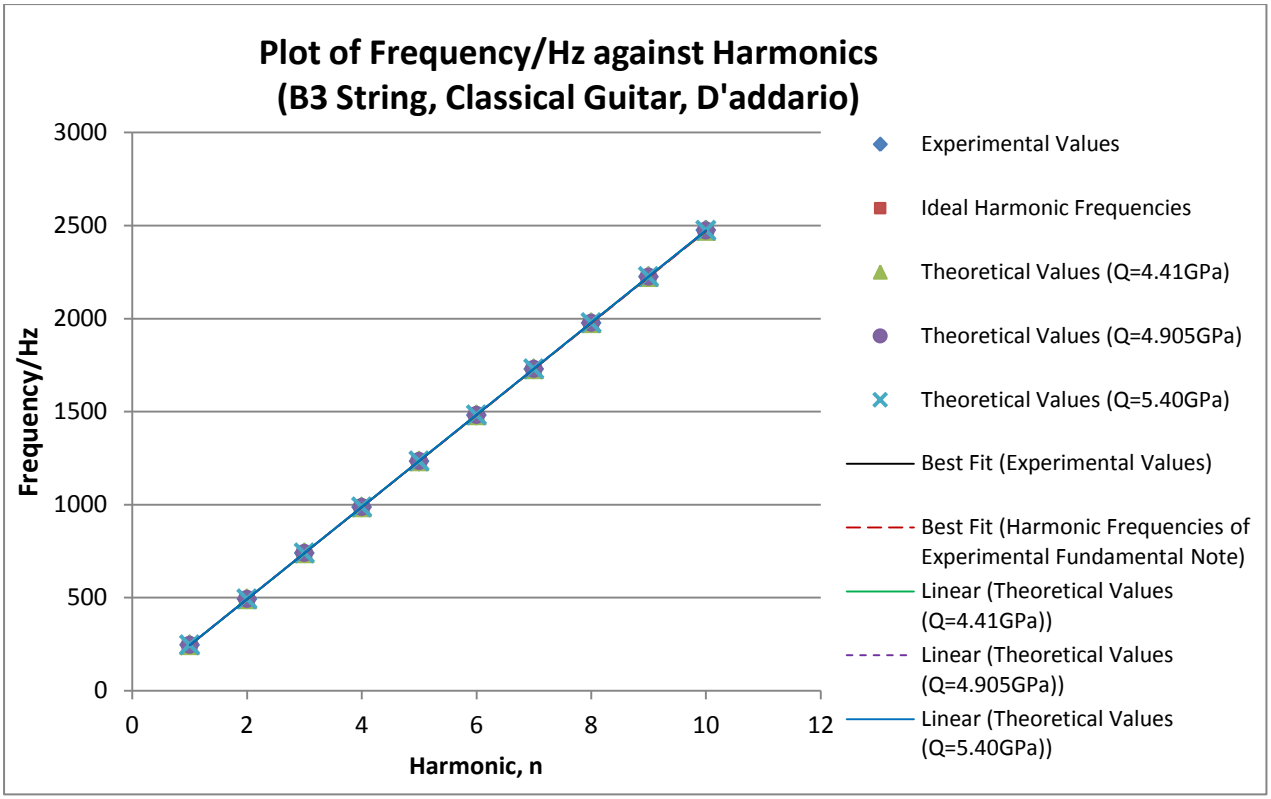

Figure 4.2.30a: Plot of Frequency against Harmonics for the B3 string for the Classical Guitar

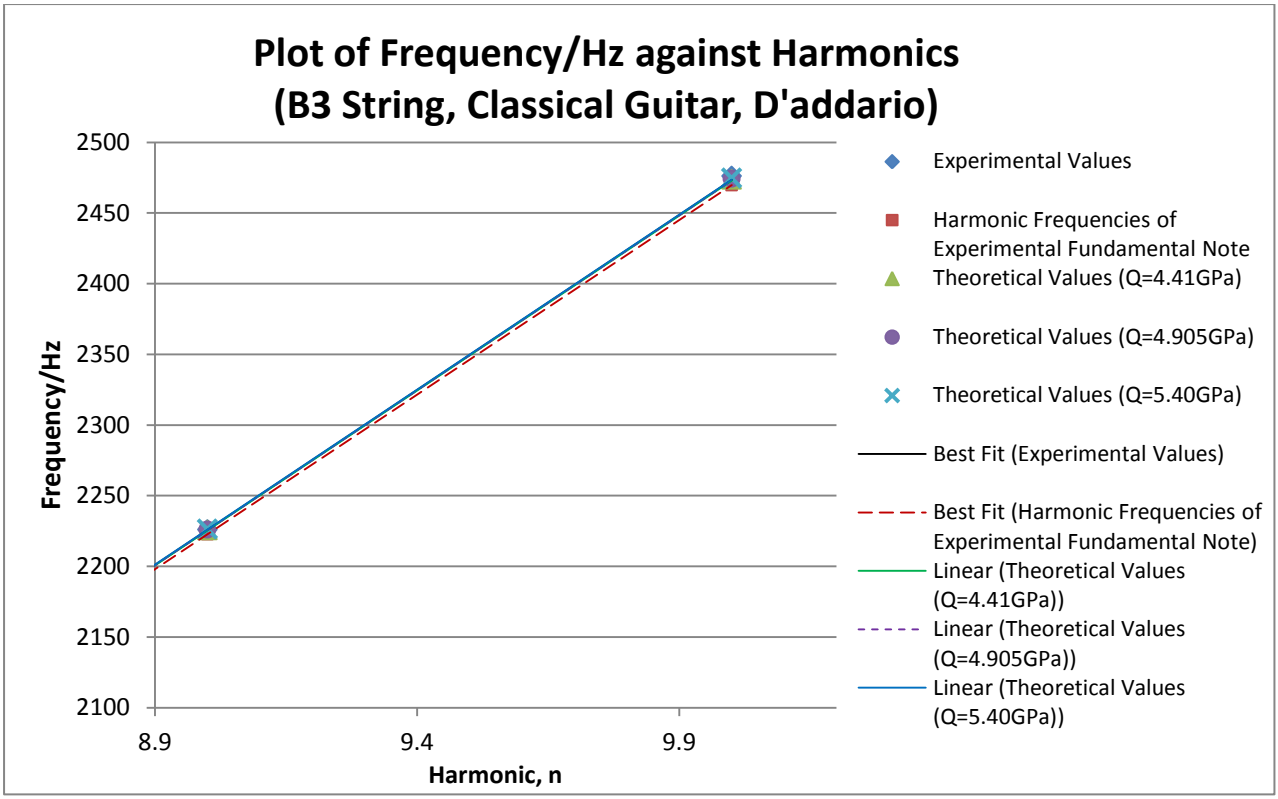

Figure 4.2.30b: Plot of Frequency against Harmonics for the B3 String for the Classical Guitar for the 9^{th} and 10^{th} Harmonic

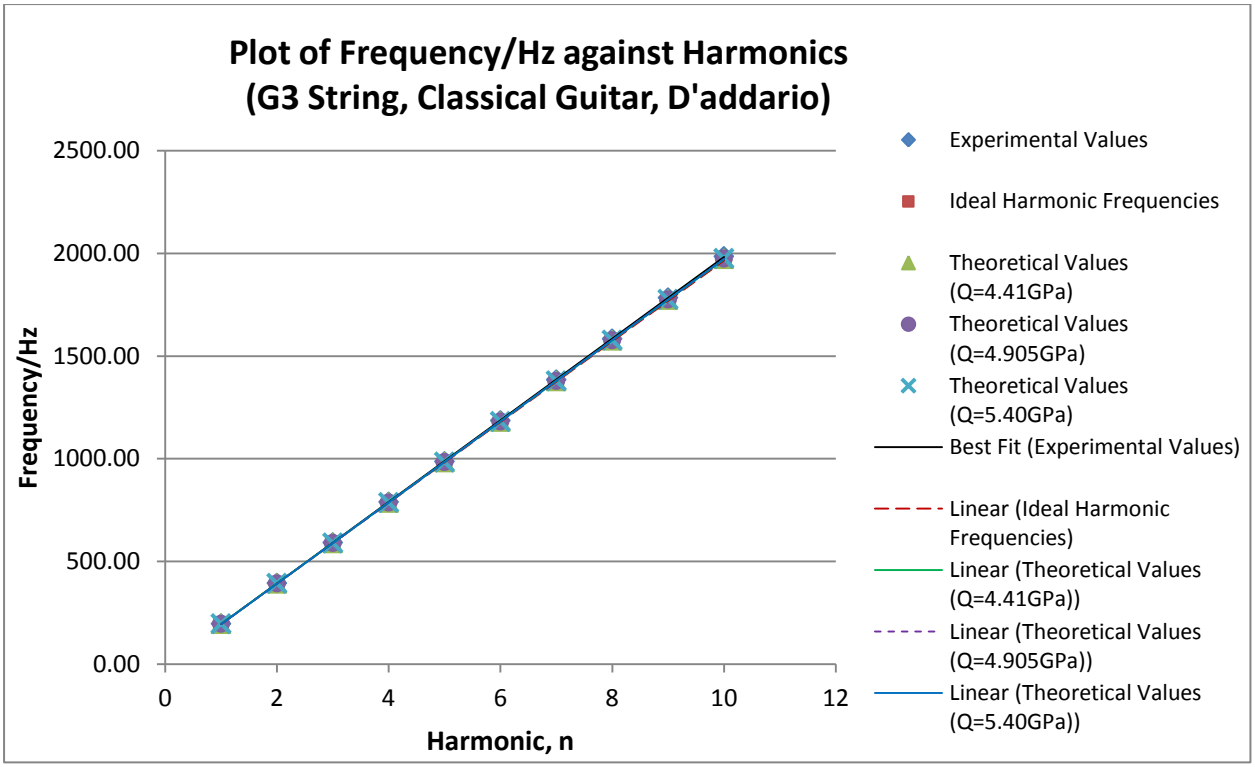

Figure 4.2.31a: Plot of Frequency against Harmonics for the G3 string for the Classical Guitar

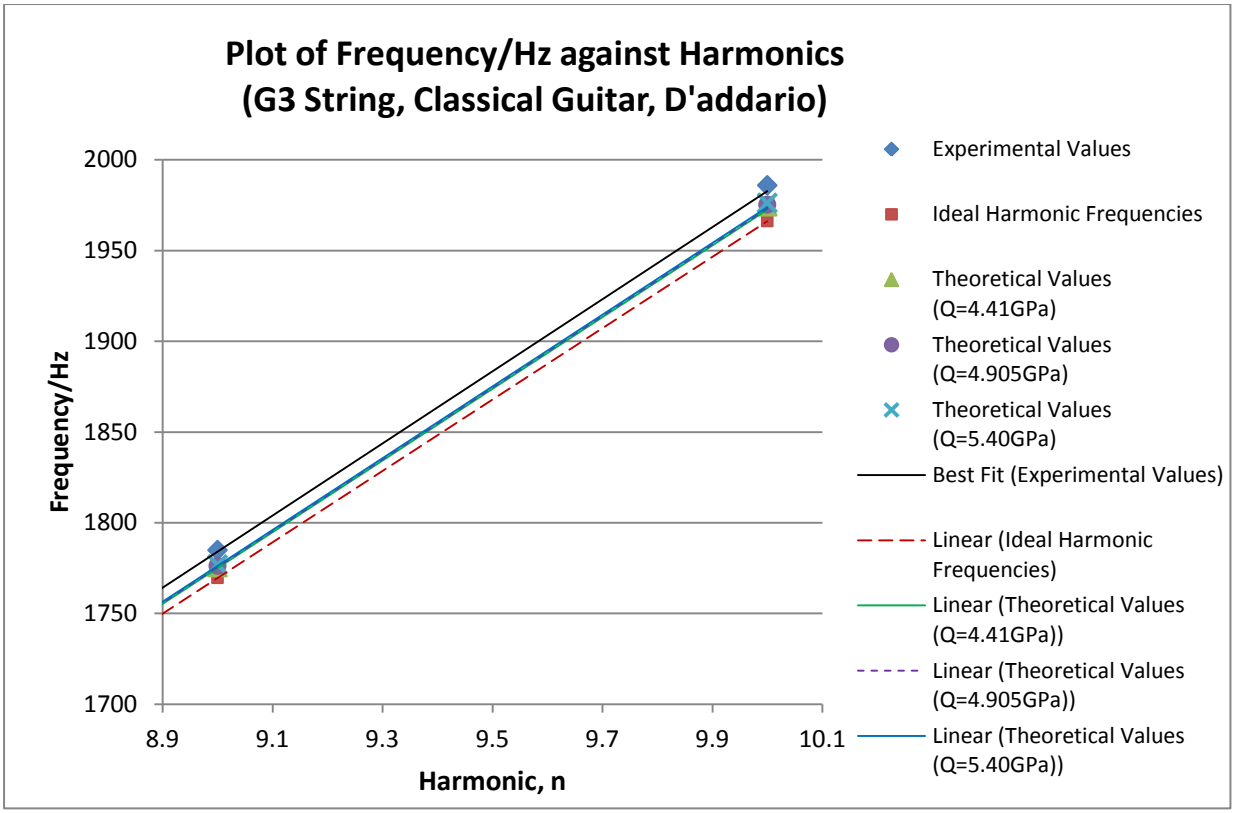

Figure 4.2.31b: Plot of Frequency against Harmonics for the G3 String for the Classical Guitar for the 9^{th} and 10^{th} Harmonic

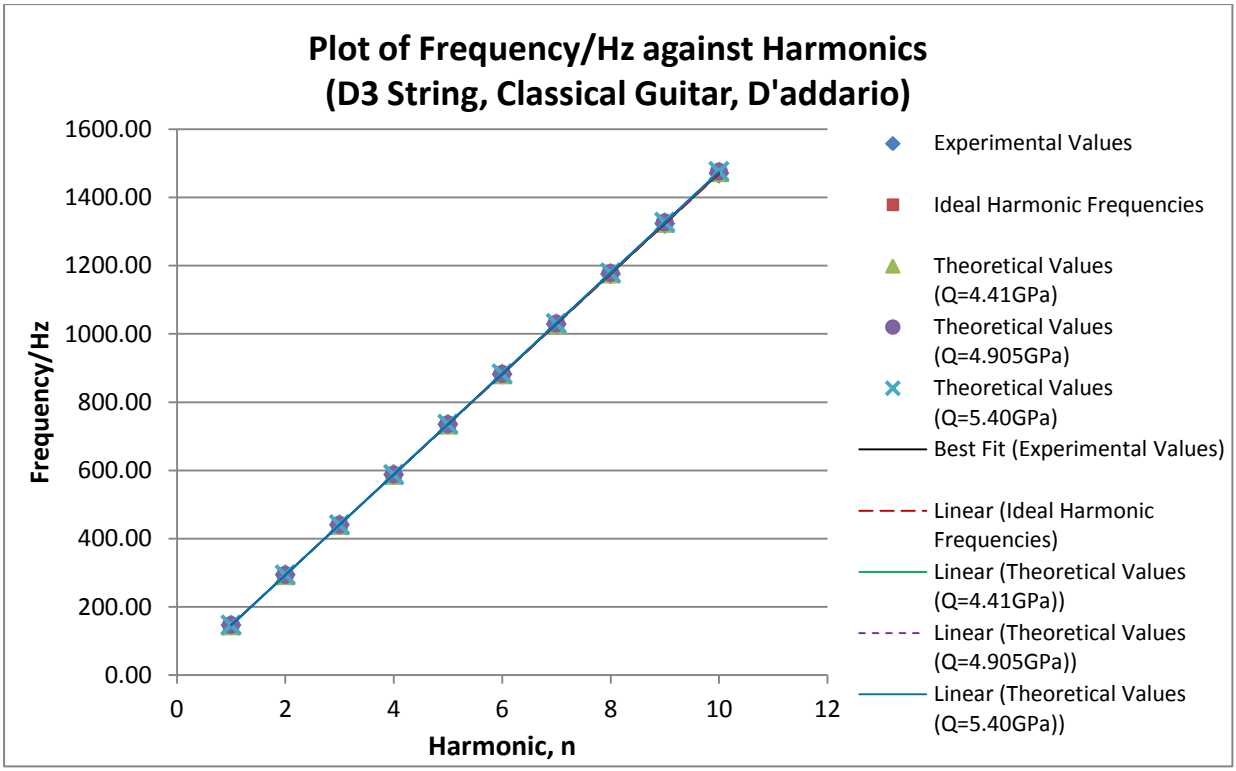

Figure 4.2.32a: Plot of Frequency against Harmonics for the D3 string for the Classical Guitar

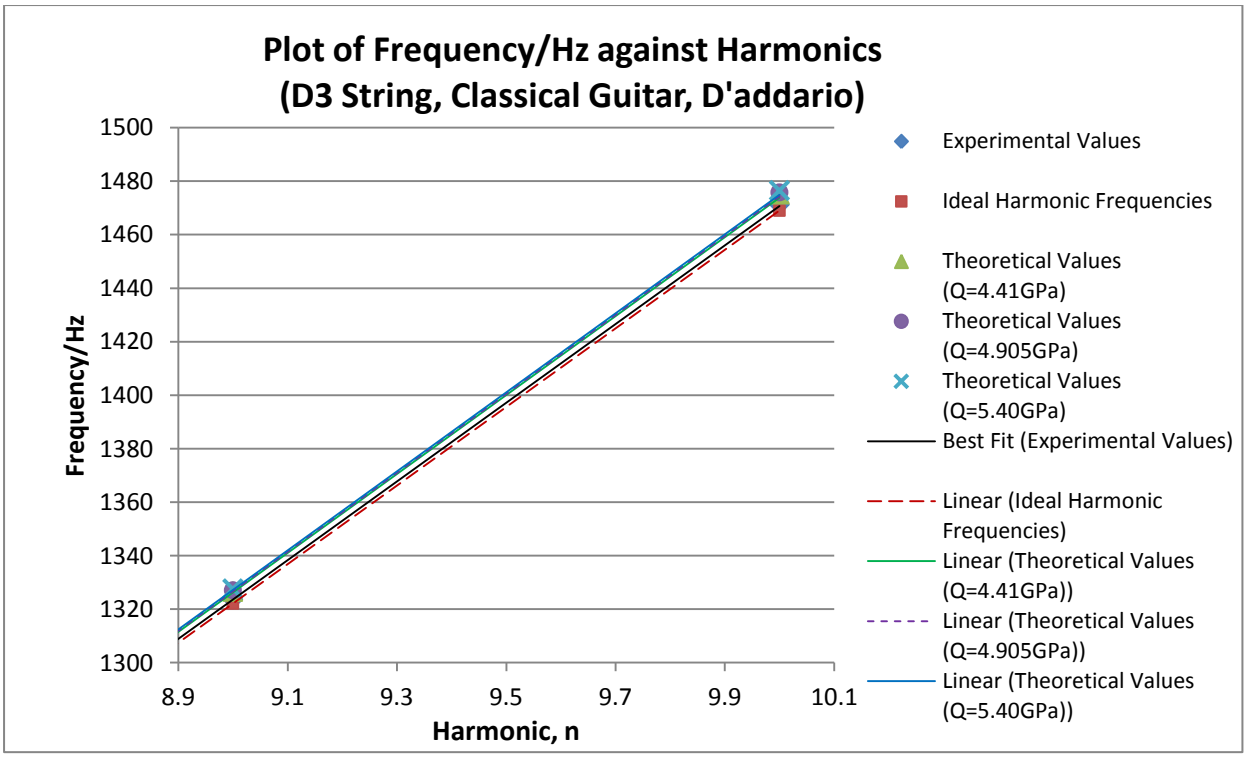

Figure 4.2.32b: Plot of Frequency against Harmonics for the D3 String for the Classical Guitar for the 9^{th} and 10^{th} Harmonic

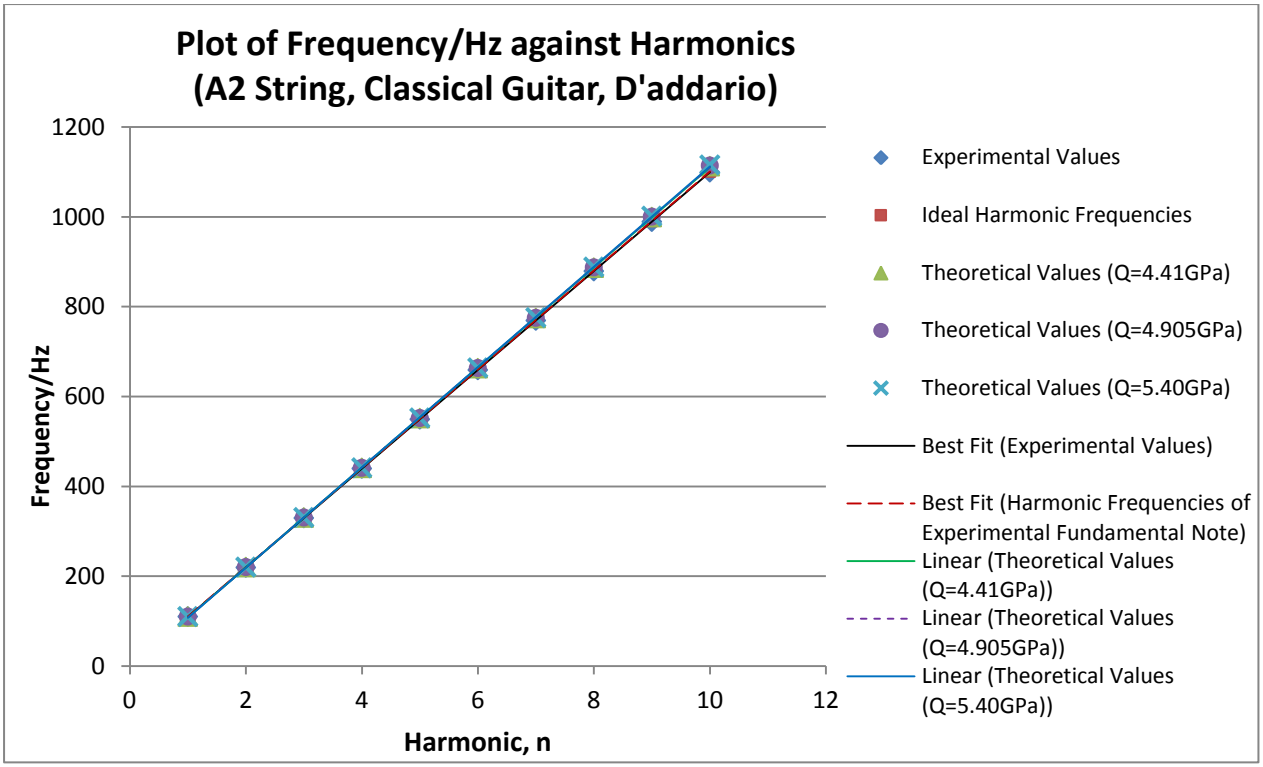

Figure 4.2.33a: Plot of Frequency against Harmonics for the A2 string for the Classical Guitar

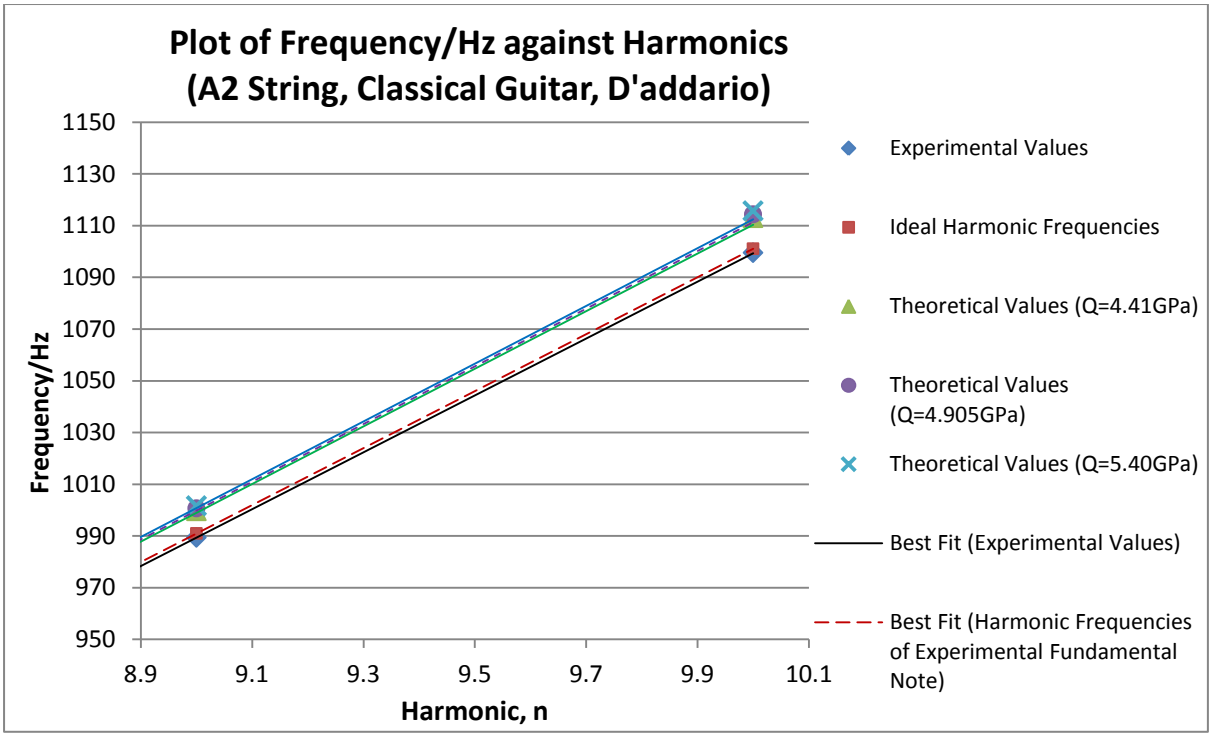

Figure 4.2.33b: Plot of Frequency against Harmonics for the A2 String for the Classical Guitar for the 9^{th} and 10^{th} Harmonic

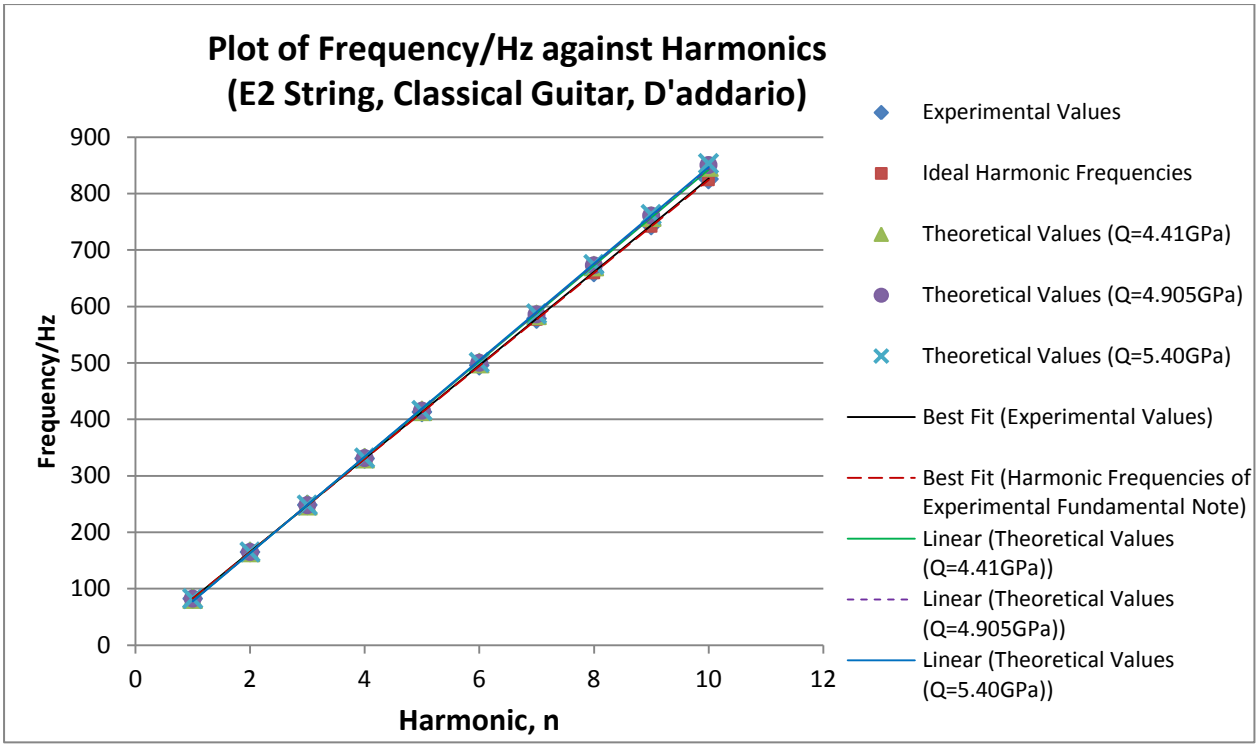

Figure 4.2.34a: Plot of Frequency against Harmonics for the E2 string for the Classical Guitar

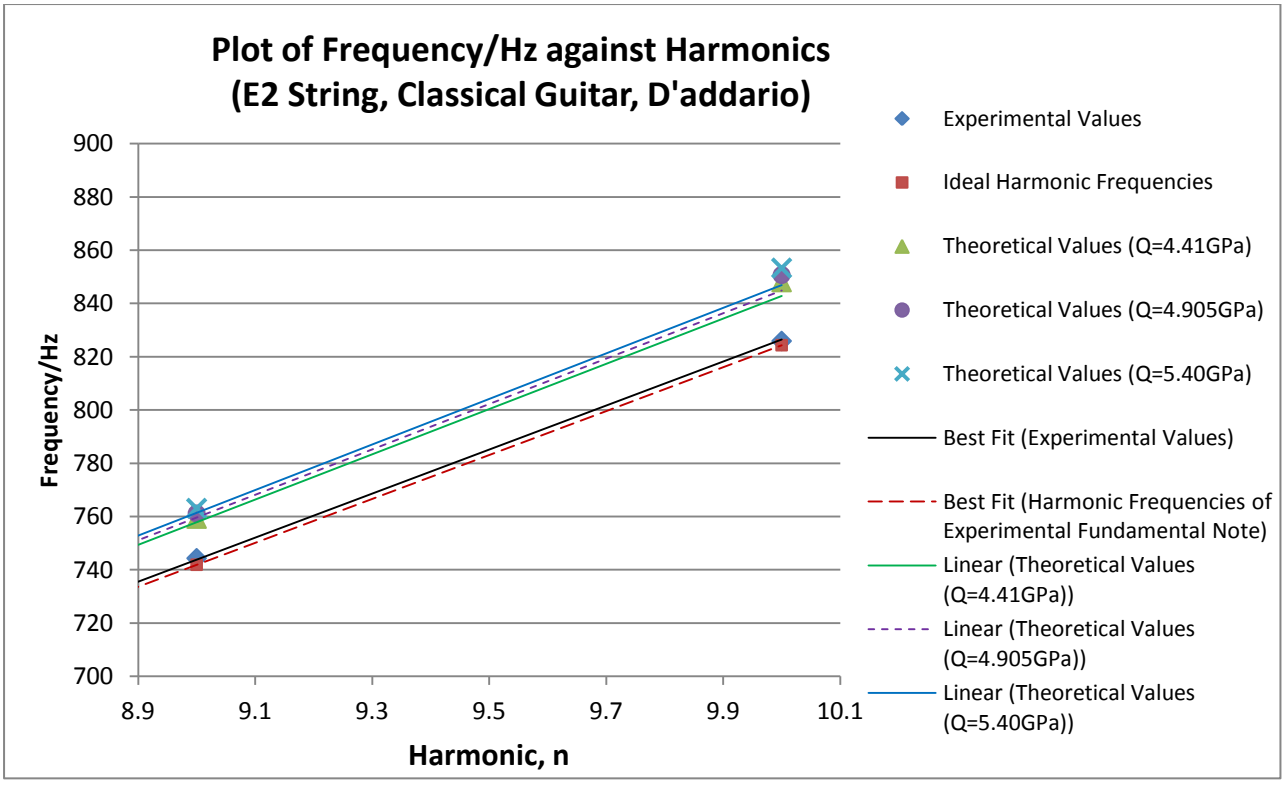

Figure 4.2.34b: Plot of Frequency against Harmonics for the E2 String for the Classical Guitar for the 9^{th} and 10^{th} Harmonic

4.2.6 Discussion on Harmonic Frequencies

Based on all figures in section 4.2.1 to 4.2.5, majority of the plots show a linear relationship between the harmonic frequencies and its harmonics and it can also be seen that the ideal harmonic frequencies have the lowest set of frequencies. This is in agreement with the theory of inharmonicity and the equation $f_n = nf_1(1 + Bn^2)^{\frac{1}{2}}$. It is observed that the experimental frequencies for thicker strings deviate more from the theoretical values as compared to the thinner strings as expected. This is seen in all the C4 strings of the ukuleles, the A2 string of the pipa and the E2 string of the classical guitar.

One abnormality observed is the relatively low frequencies of the A2 string of the classical guitar as compared to the ideal harmonic series and the theoretical frequencies. This is because all the harmonic frequencies obtained from the frequency domain plots had values less than ideal harmonic frequencies and thus giving a lower linear plot than expected.

4.3 Comparisons

4.3.1 Comparing strings within a ukulele

The degree of deviation of the harmonic frequencies from the ideal harmonic series is observed by plotting the graph of $\sqrt{{f_n}^2 - n^2{f_1}^2}$ against n.

(a) Aquila AQ-4U New Nylgut® Regular GCEA Set Soprano Strings

Figures 4.3.1 to 4.3.3 show the comparisons of the four Aquila strings for the Kala, Makala and Outdoor ukulele respectively.

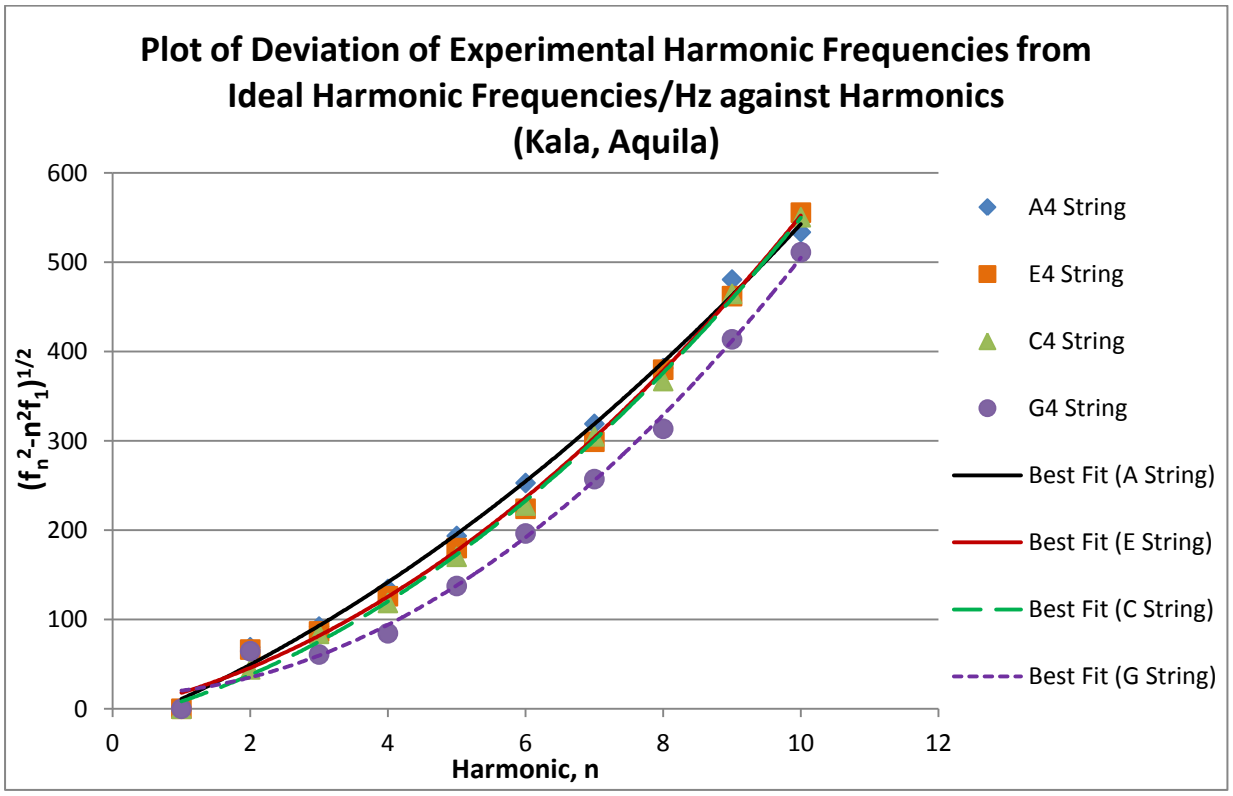

Figure 4.3.1: Plot of $\sqrt{{f_n}^2 - n^2{f_1}^2}$ against n for the Aquila string set on the Kala Ukulele.

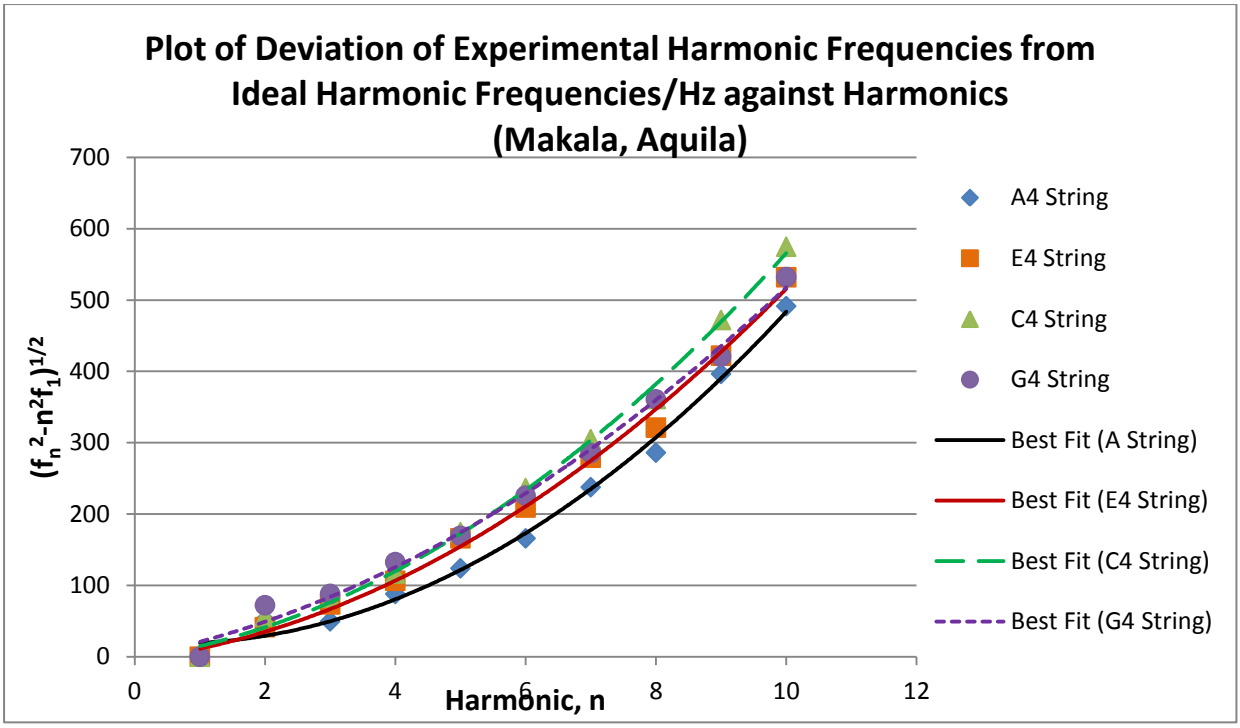

Figure 4.3.2: Plot of $\sqrt{{f_n}^2 - n^2{f_1}^2}$ against n for the Aquila string set on the Makala Ukulele.

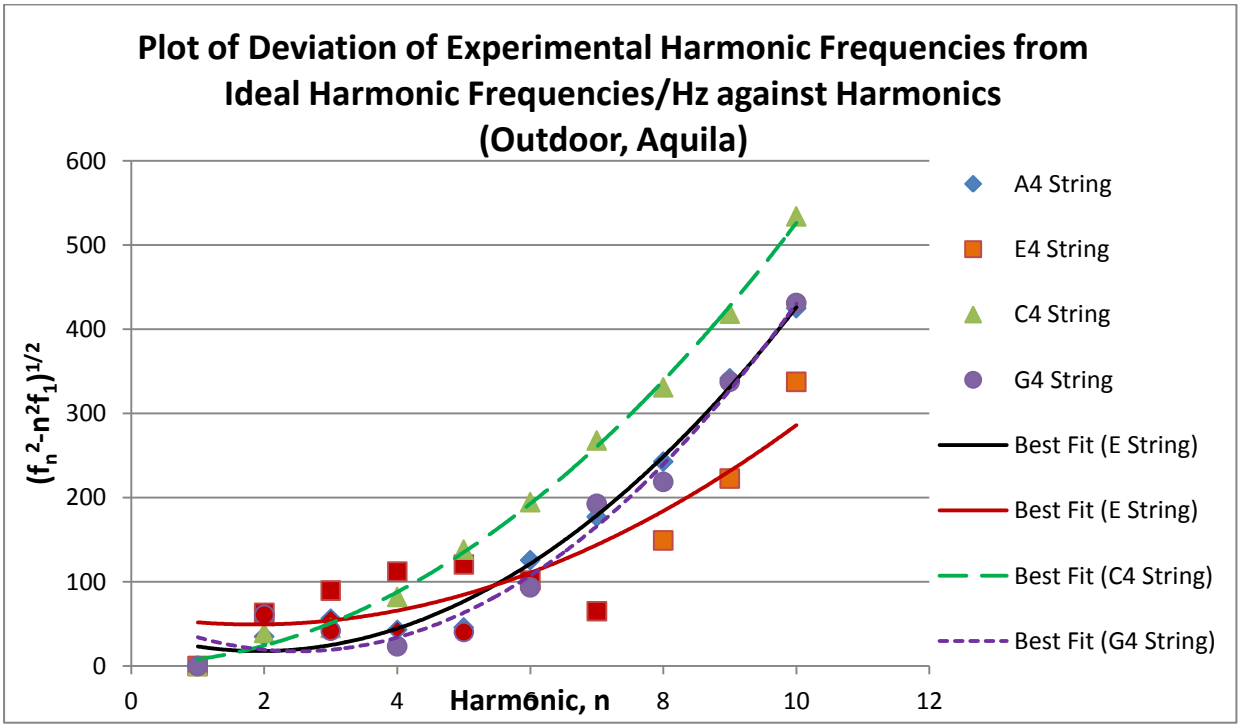

Figure 4.3.3: Plot of $\sqrt{{f_n}^2 - n^2{f_1}^2}$ against n for the Aquila string set on the Outdoor Ukulele.

Several harmonic frequencies of the Outdoor Ukulele were found to have values less than the ideal harmonic frequencies which contradicts the theory of inharmonicity as ${f_n}^2 - n^2{f_1}^2$ will have a negative value. The absolute values of these deviations were taken and are represented as

red data points in Figure 4.3.3. These disparities have affected the inharmonicity coefficients found in section 4.1.

(b) D'Addario T2 Soprano Strings Strings

Figures 4.3.4 to 4.3.6 show the comparisons of the four D'addario strings for the Kala, Makala and Outdoor ukulele respectively.

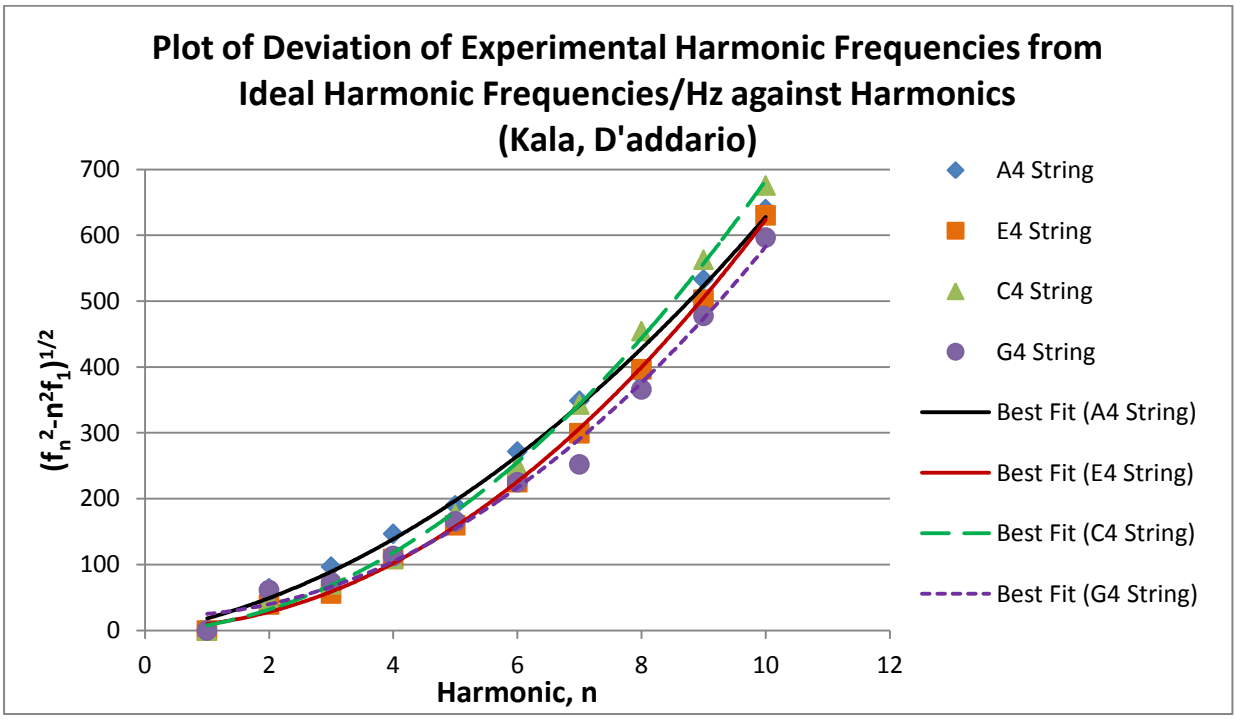

Figure 4.3.4: Plot of $\sqrt{{f_n}^2 - n^2{f_1}^2}$ against n for the D'addario string set on the Kala Ukulele.

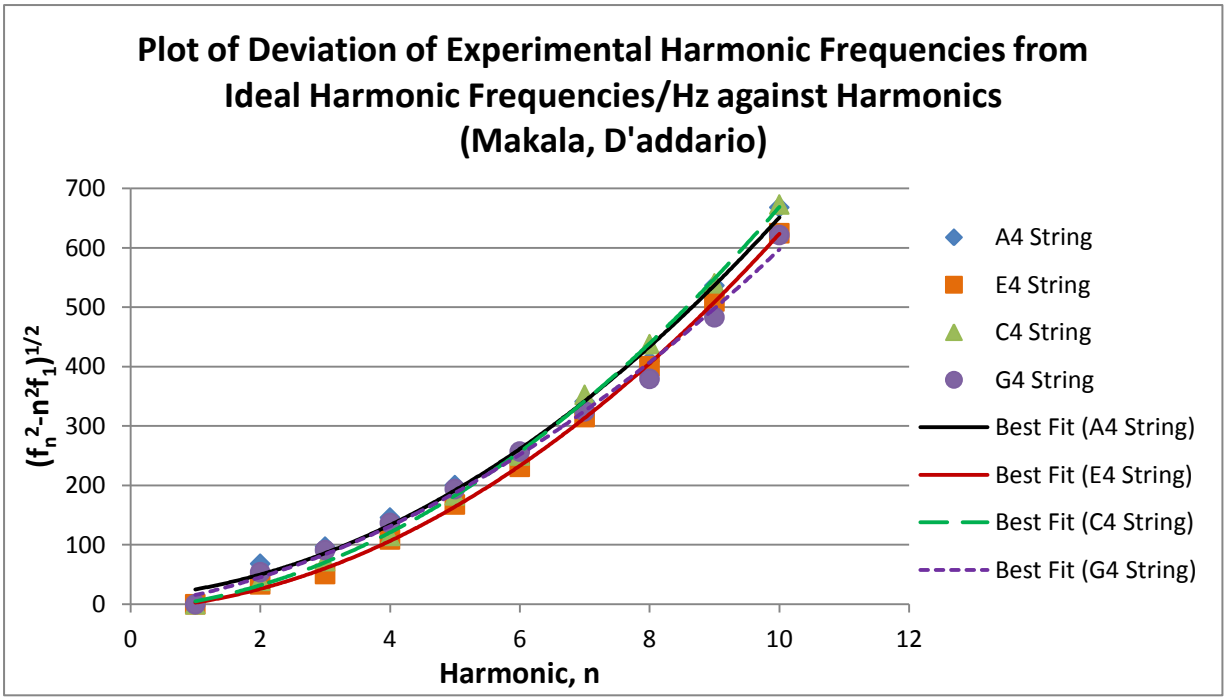

Figure 4.3.5: Plot of $\sqrt{{f_n}^2 - n^2{f_1}^2}$ against n for the D'addario string set on the Makala Ukulele.

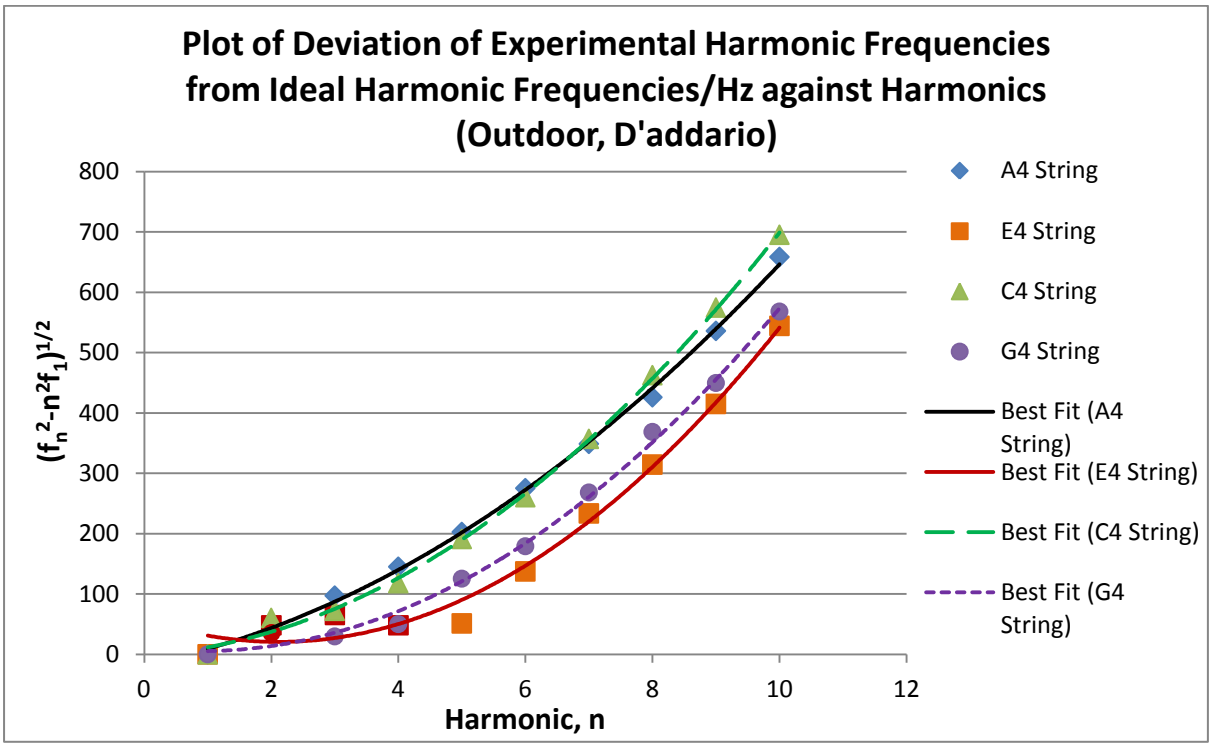

Figure 4.3.6: Plot of $\sqrt{{f_n}^2 - n^2{f_1}^2}$ against n for the D'addario string set on the Outdoor Ukulele.

It is observed that the deviation of experimental frequencies from the ideal harmonic frequencies increases with the increase in nth harmonic. This trend is expected as the deviation is related to the second power of its nth harmonic.

From section 4.1, results have shown that the increase in thickness of strings increases the inharmonicity coefficient. Since the square root of the inharmonicity coefficient is directly proportional to the deviation $\sqrt{{f_n}^2 - n^2{f_1}^2}$, thicker strings are expected to produce larger deviations. The majority of results obtained seem to agree with the theory only at higher partials. In Figure 4.3.1 and Figure 4.3.4, it is found that the A4 string of the Kala Ukulele shows greater deviation at lower harmonics which is not what is expected. This behaviour is also observed in the G4 String of the Makala Ukulele.

Negative deviations were obtained from both plots of the Outdoor ukulele even though different types of strings were used. This suggests that the disparity is purely due to the construction of the Outdoor Ukulele. It is also observed that the E4 string demonstrated these disparities more than the other strings while the C4 string did exhibit any of these disparities.

4.3.2 Comparing ukuleles

The deviations of strings were compared among ukuleles by plotting graphs of $\sqrt{{f_n}^2 - n^2{f_1}^2}$ against n, keeping the type of string variable as a constant for each graph plotted. The graphs obtained are shown in Appendix C. The majority of graphs showed that the Kala and Makala showed larger deviations than the Outdoor Ukulele. The same results were obtained even after neglecting the data points with negative deviation. Therefore, it can be concluded that the Outdoor ukulele exhibits the least amount of deviations.

4.3.3 Comparing string types

The deviations of strings were compared among string types by plotting graphs of $\sqrt{{f_n}^2 - n^2{f_1}^2}$ against n, keeping the type of ukulele variable as a constant for each graph plotted. The graphs obtained are shown in Appendix D. The deviations were found to differ slightly at lower harmonics but the reversed was obtained at higher harmonics. All graphs showed that the Aquila set of strings displayed less deviation at higher harmonics.

4.3.4 Comparing strings of a pipa

Figure 4.3.7 shows the comparisons of the four strings of the Pipa.

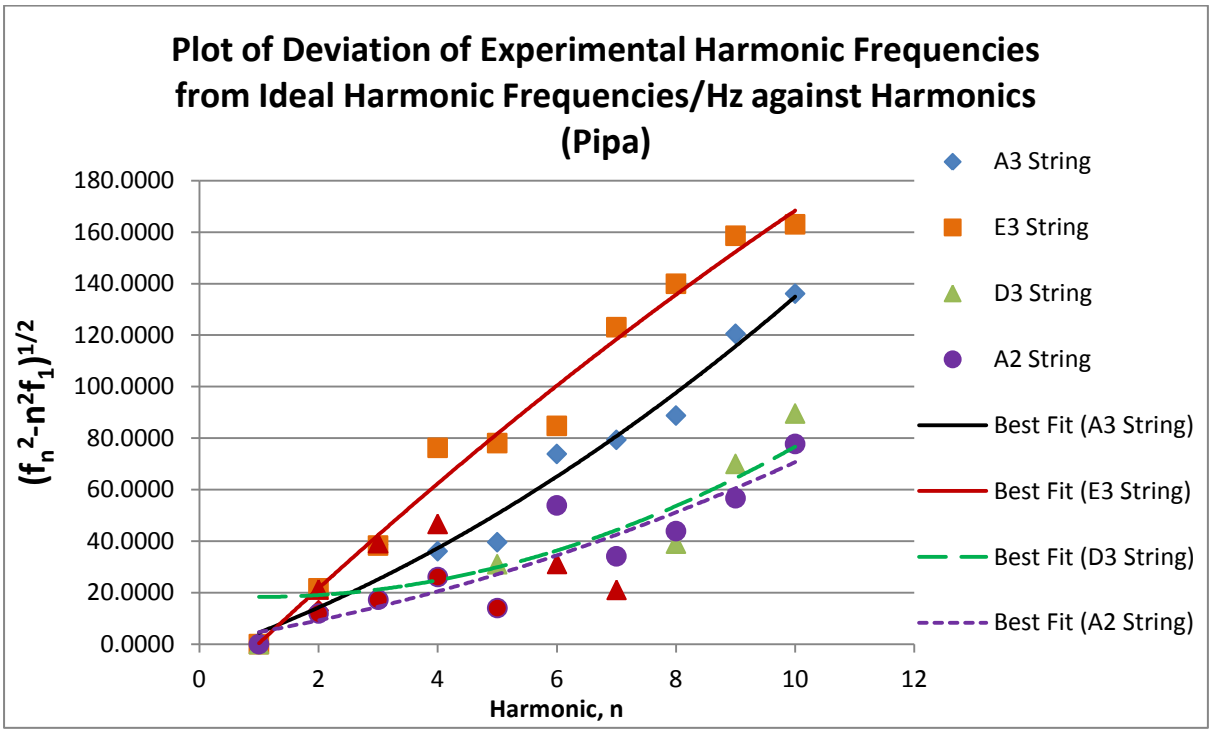

Figure 4.3.7: Plot of $\sqrt{{f_n}^2 - n^2{f_1}^2}$ against n for the strings of a Pipa.

It is observed that the deviation of experimental frequencies from the ideal harmonic frequencies increases with the increase in nth harmonic. Similar to the Outdoor Ukulele, several

harmonic frequencies of the Pipa were found to have values less than the ideal harmonic frequencies and thus producing negative deviations. The absolute values of these deviations were taken and are represented as red data points.

4.3.4 Comparing strings of a Classical Guitar

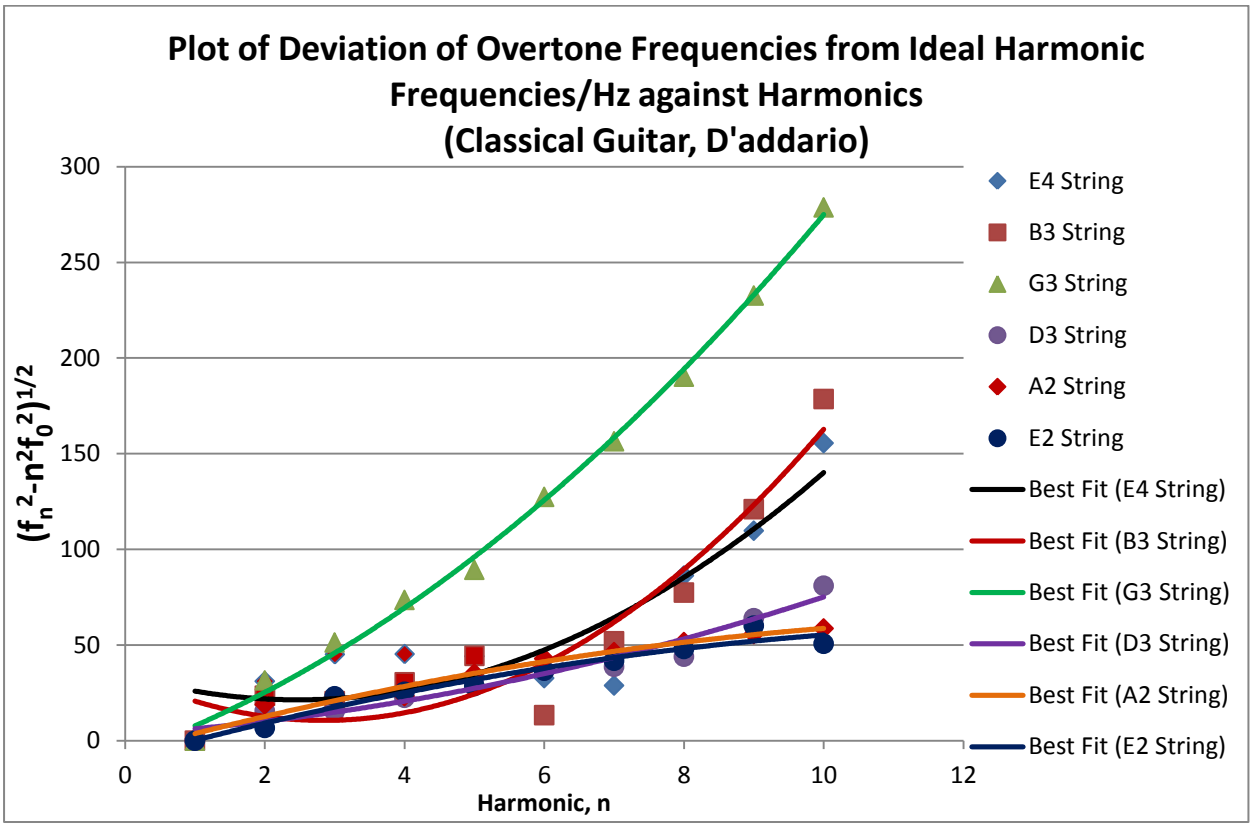

Figure 4.3.8: Plot of $\sqrt{{f_n}^2 - n^2{f_1}^2}$ against n for the strings of a Classical Guitar.

Figure 4.3.8 shows that the deviation of experimental frequencies from the ideal harmonic frequencies increases with the increase in nth harmonic in agreement with the theory of inharmonicity.

4.4 Spectrum Plots

Spectrum plots were plotted for all strings for all instruments used in this project to observe the behavior of harmonic frequencies over time. This is done by dividing each sample into segments of equal periods of time and performing the FFT onto each segment. The amplitudes of the harmonic frequencies were obtained from each segment and then used to plot a 3-dimensional graph over the duration of the sample.

4.4.1 Kala Spruce/Rosewood Soprano Ukulele

(a) Aquila AQ-4U New Nylgut® Regular GCEA Set Soprano Strings

Figures 4.4.1 to 4.4.4 show the spectrum plots of the Kala Ukulele of the A4, E4, C4 and G4 Aquila string respectively.

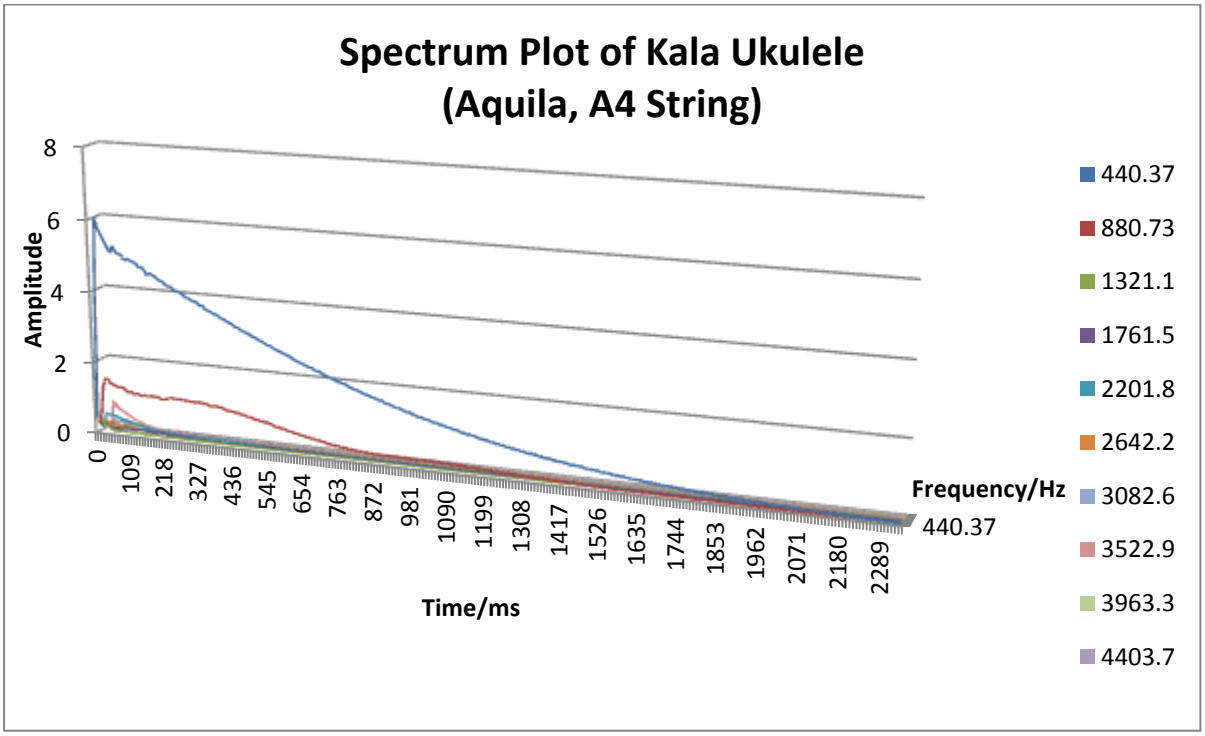

Figure 4.4.1: Spectrum Plot of A4 Aquila String for the Kala Ukulele

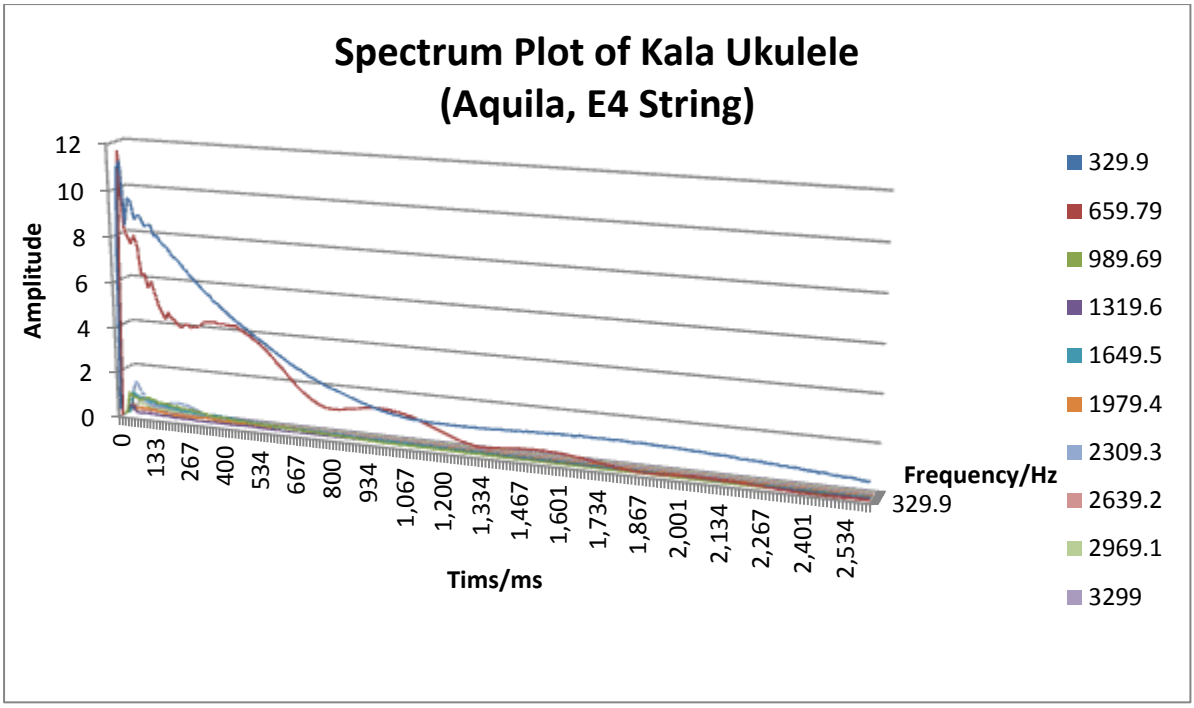

Figure 4.4.2: Spectrum Plot of E4 Aquila String for the Kala Ukulele

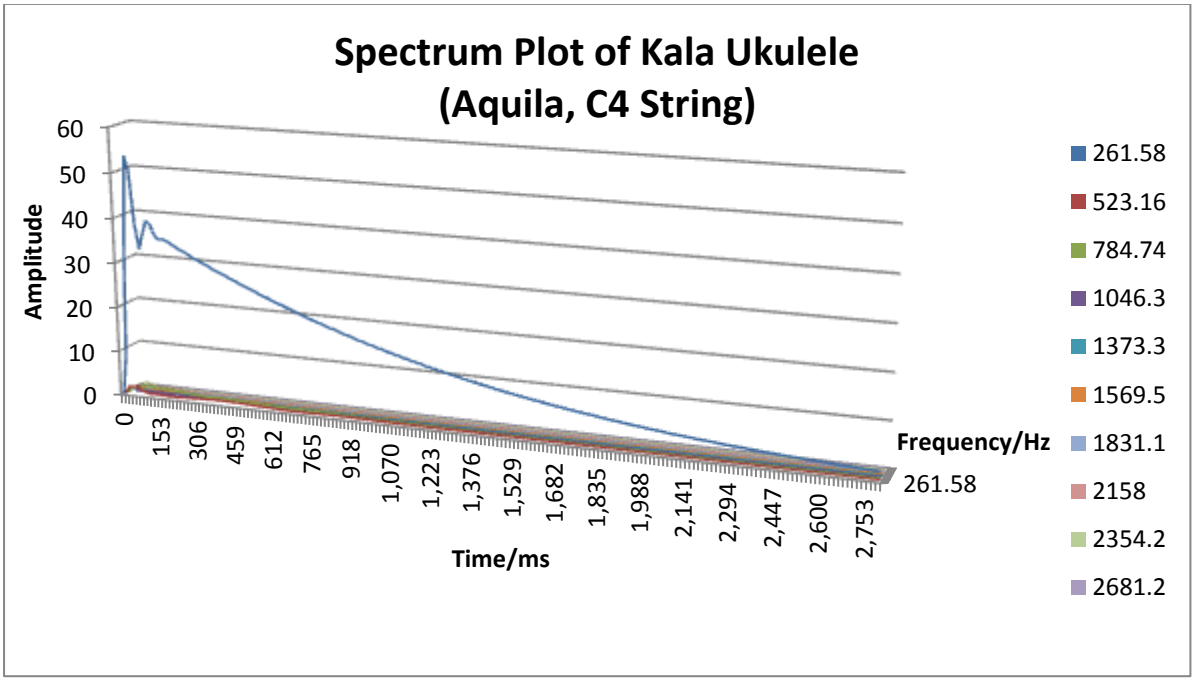

Figure 4.4.3: Spectrum Plot of C4 Aquila String for the Kala Ukulele

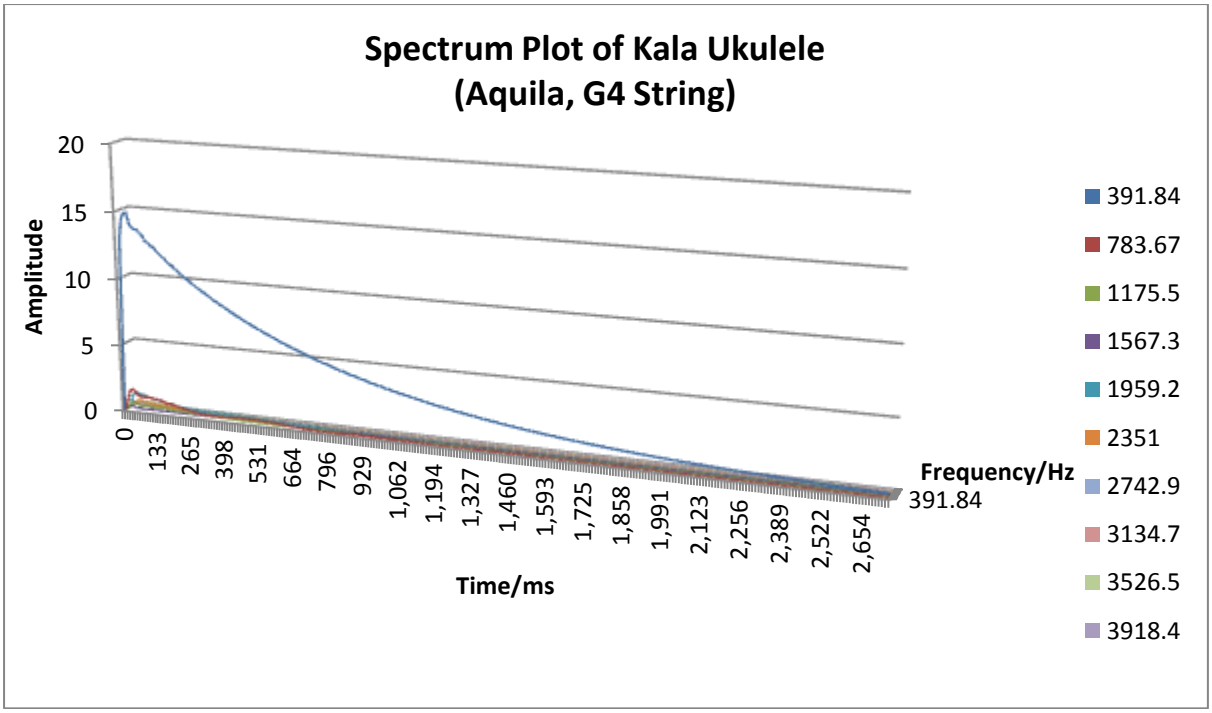

Figure 4.4.4: Spectrum Plot of G4 Aquila String for the Kala Ukulele

(b) D'Addario T2 Soprano Strings Strings

Figures 4.4.5 to 4.4.8 show the spectrum plots of the Kala Ukulele of the A4, E4, C4 and G4 D'addario string respectively.

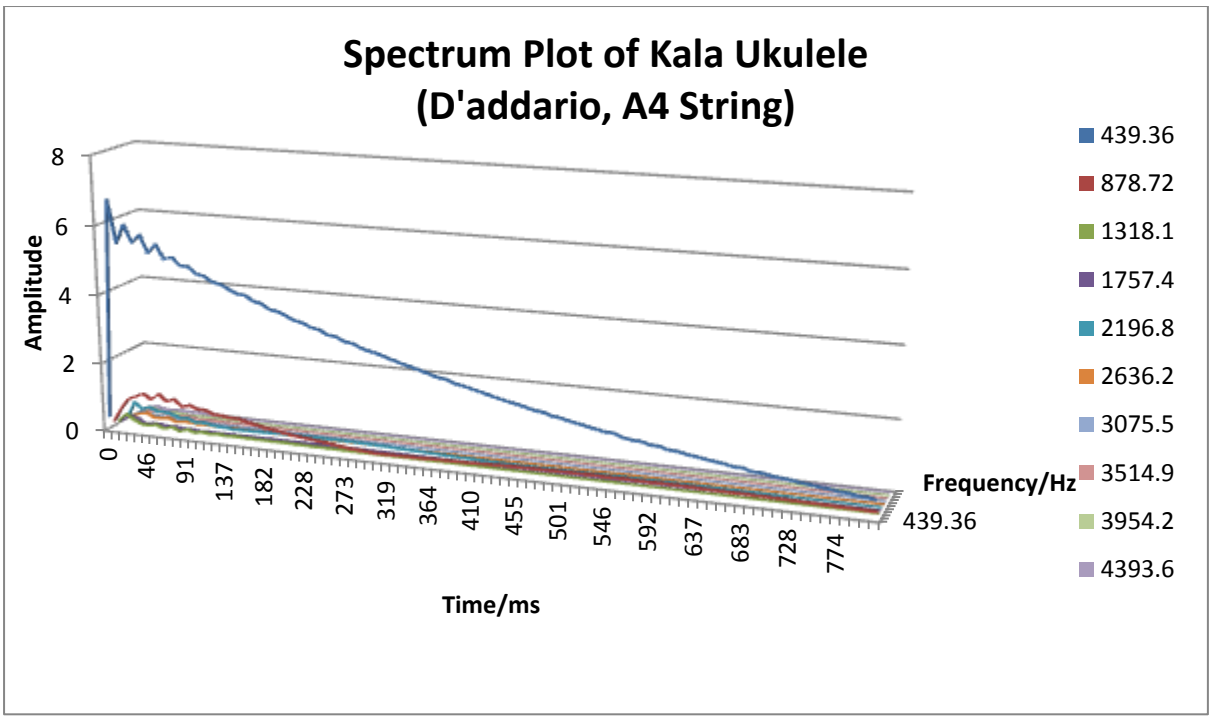

Figure 4.4.5: Spectrum Plot of A4 D'addario String for the Kala Ukulele

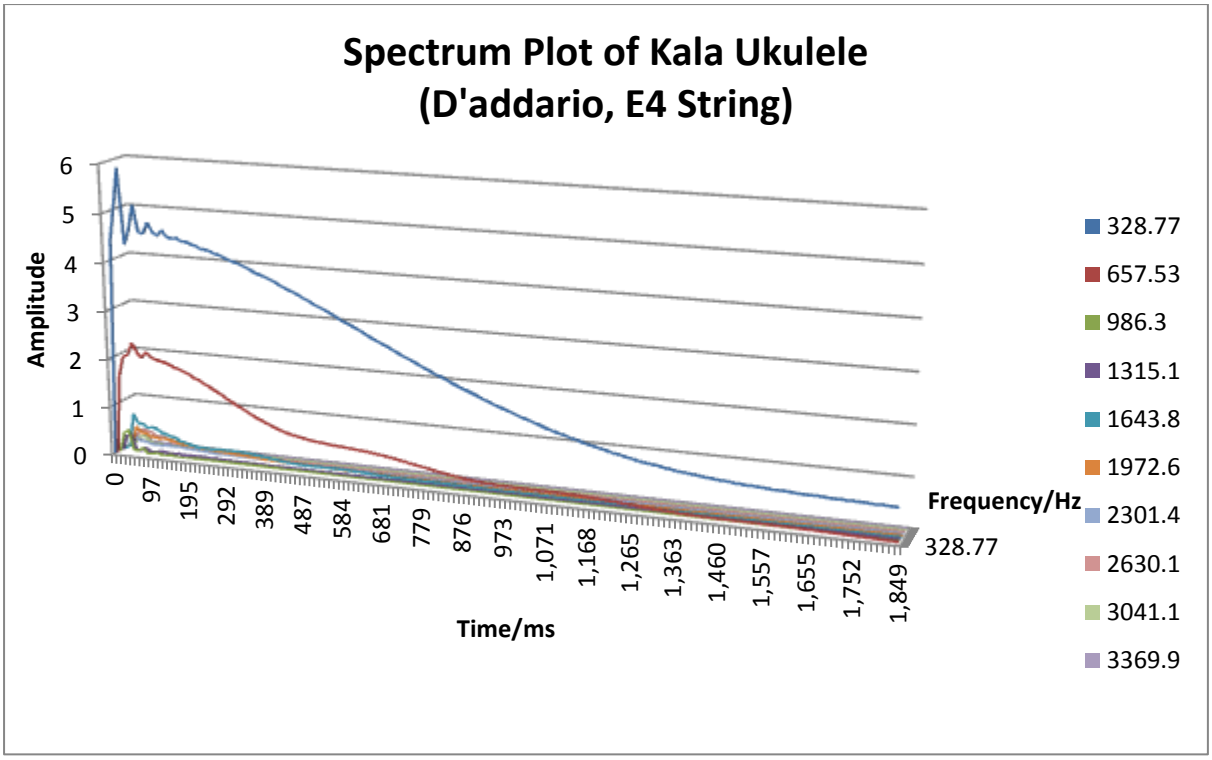

Figure 4.4.6: Spectrum Plot of E4 D'addario String for the Kala Ukulele

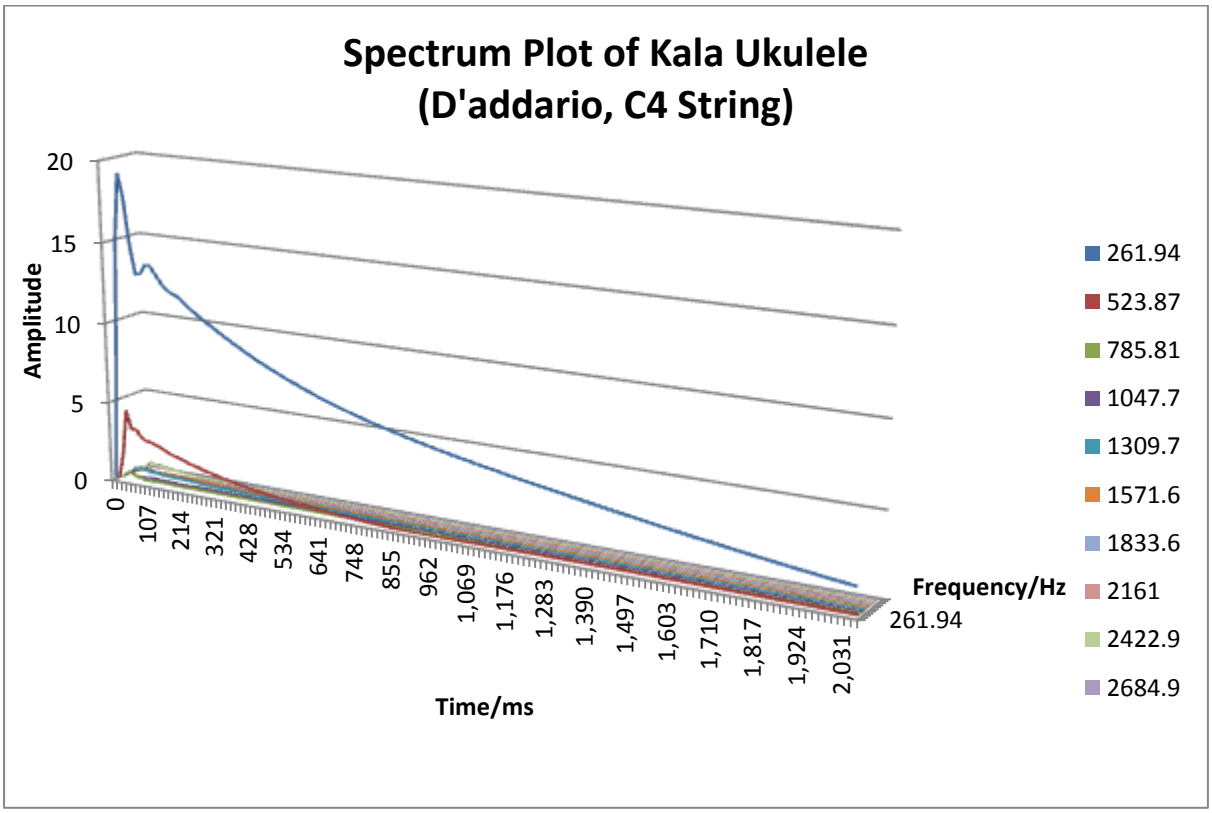

Figure 4.4.7: Spectrum Plot of C4 D'addario String for the Kala Ukulele

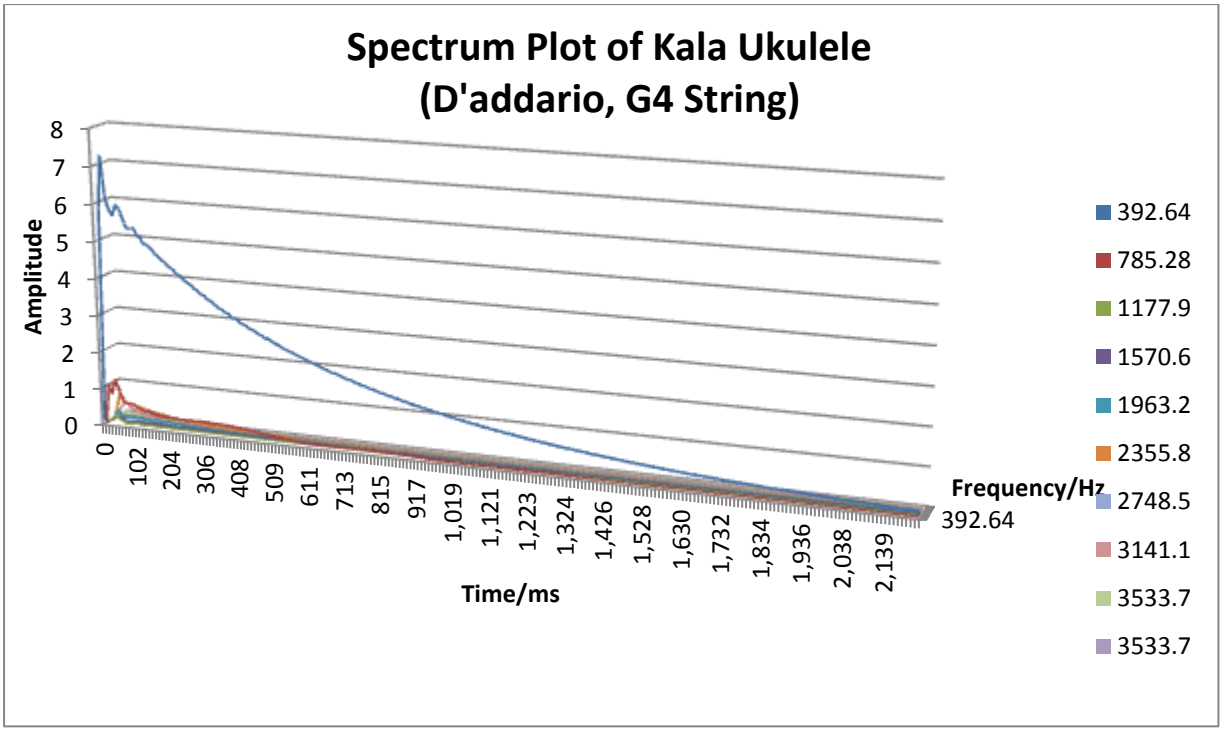

Figure 4.4.8: Spectrum Plot of G4 D'addario String for the Kala Ukulele

4.4.2 Makala Ukulele

(a) Aquila AQ-4U New Nylgut® Regular GCEA Set Soprano Strings

Figures 4.4.9 to 4.4.12 show the spectrum plots of the Makala Ukulele of the A4, E4, C4 and G4 Aquila string respectively.

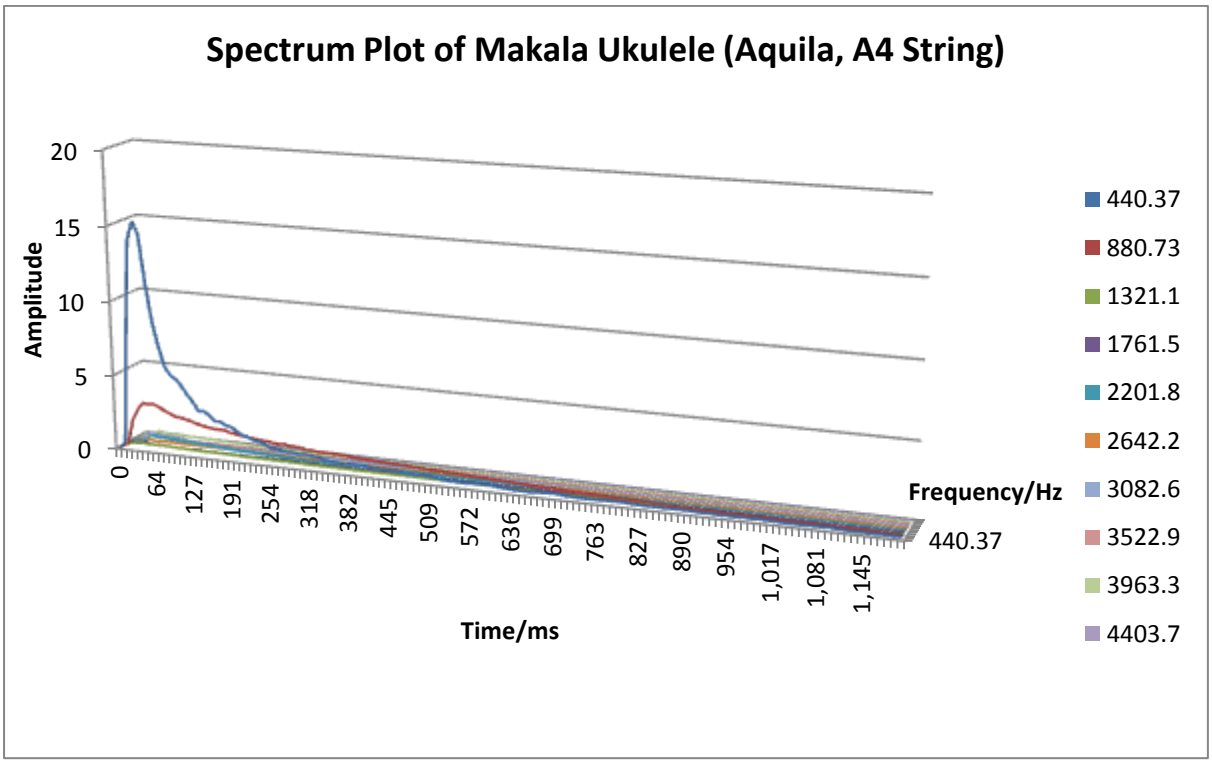

Figure 4.4.9: Spectrum Plot of A4 Aquila String for the Makala Ukulele

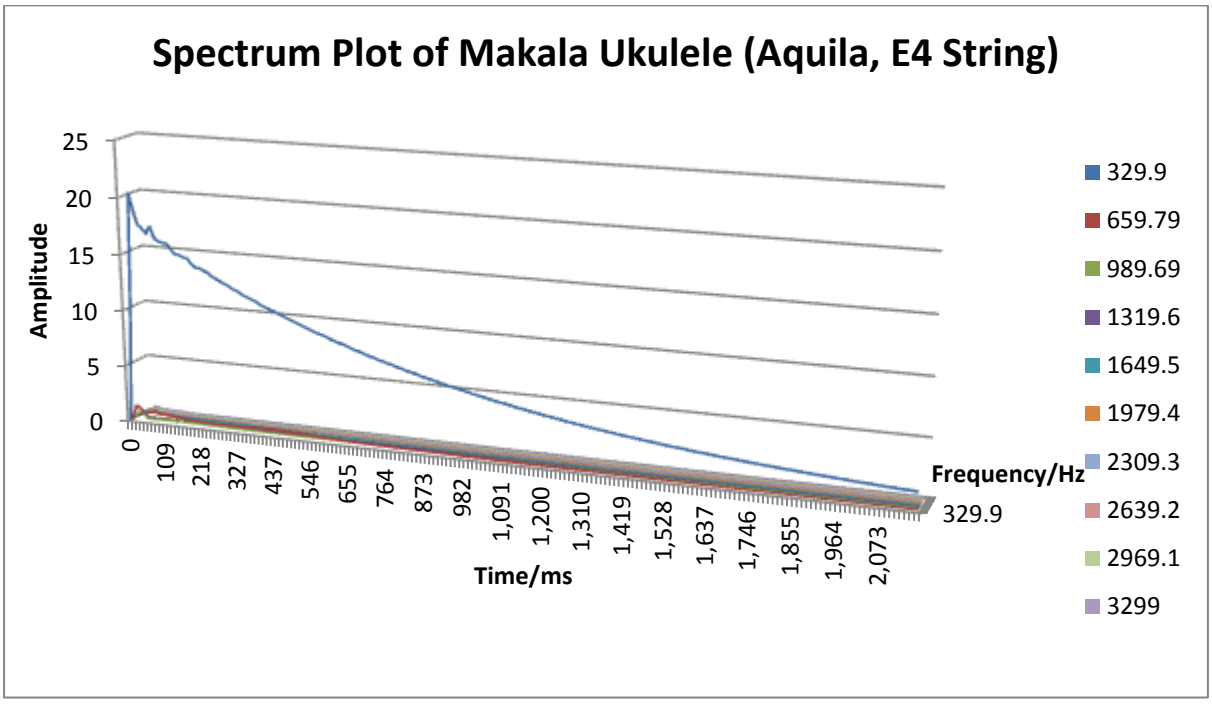

Figure 4.4.10: Spectrum Plot of E4 Aquila String for the Makala Ukulele

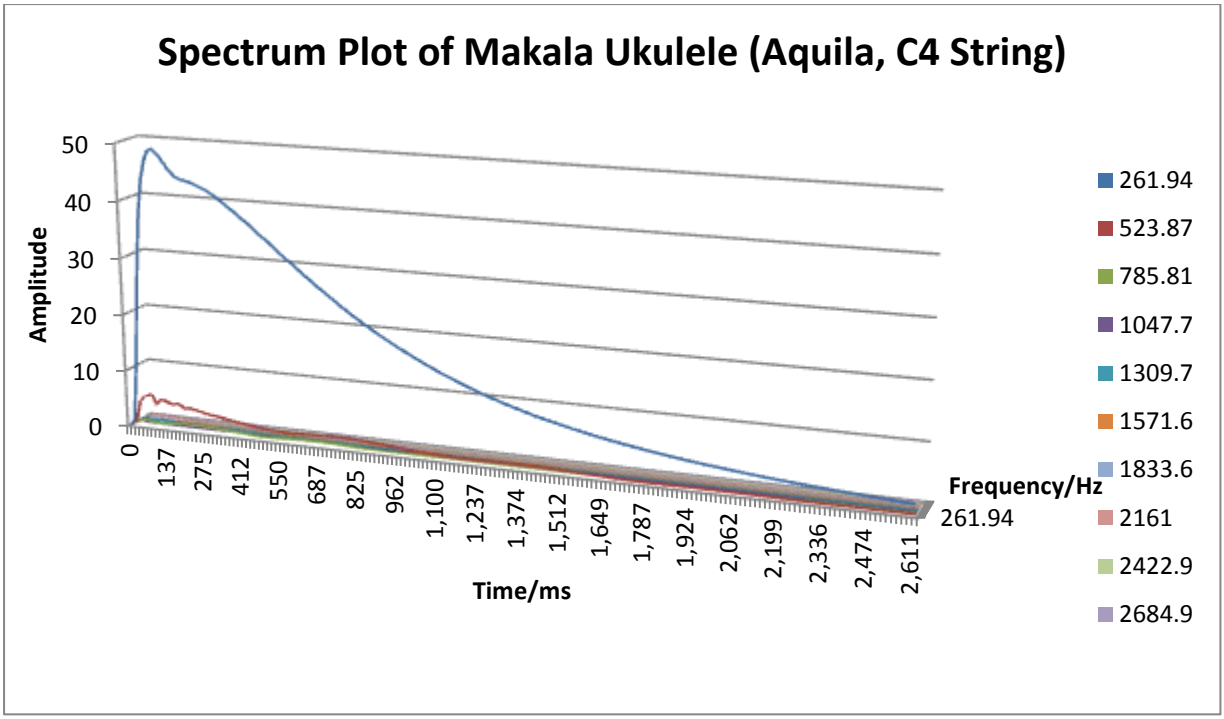

Figure 4.4.11: Spectrum Plot of C4 Aquila String for the Makala Ukulele

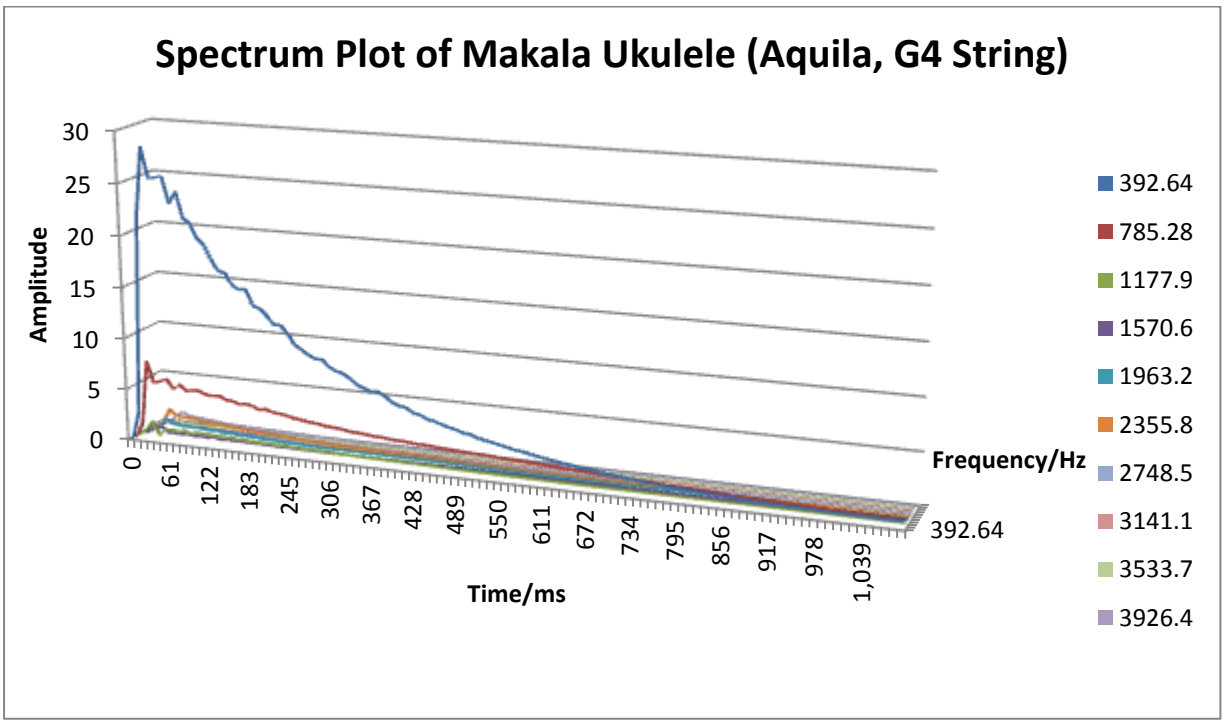

Figure 4.4.12: Spectrum Plot of G4 Aquila String for the Makala Ukulele

(b) D'Addario T2 Soprano Strings Strings

Figures 4.4.13 to 4.4.16 show the spectrum plots of the Makala Ukulele of the A4, E4, C4 and G4 D'addario string respectively.

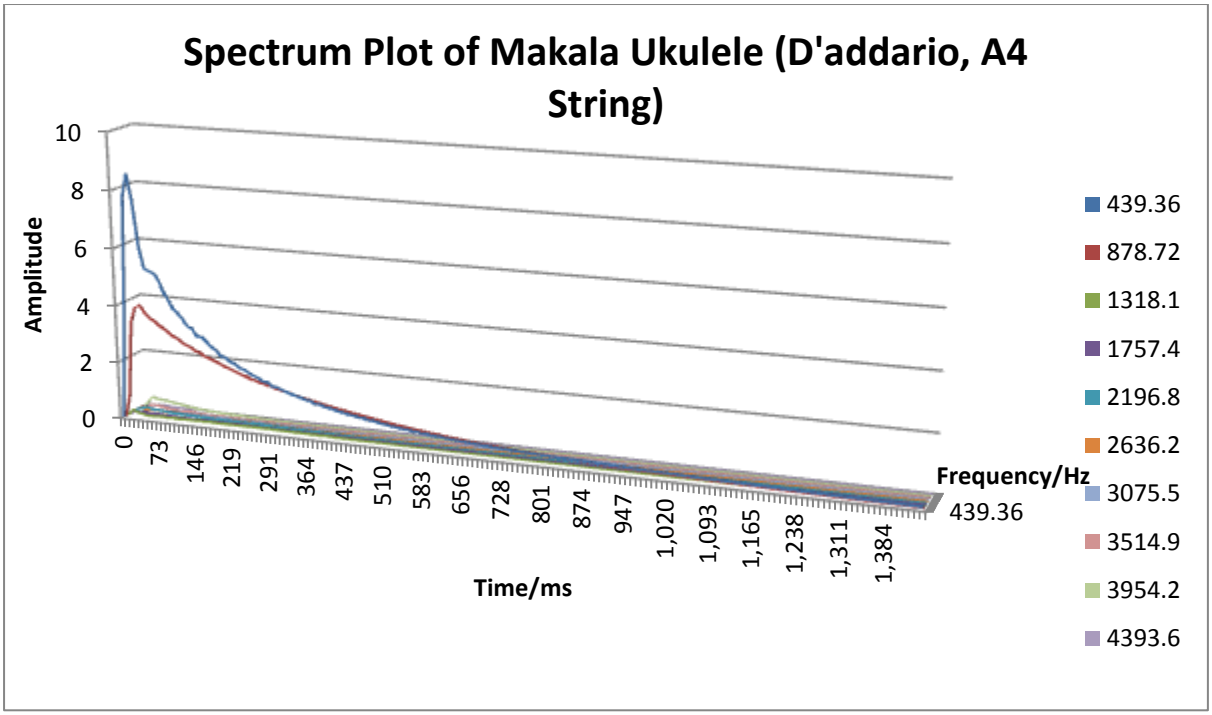

Figure 4.4.13: Spectrum Plot of A4 D'addario String for the Makala Ukulele

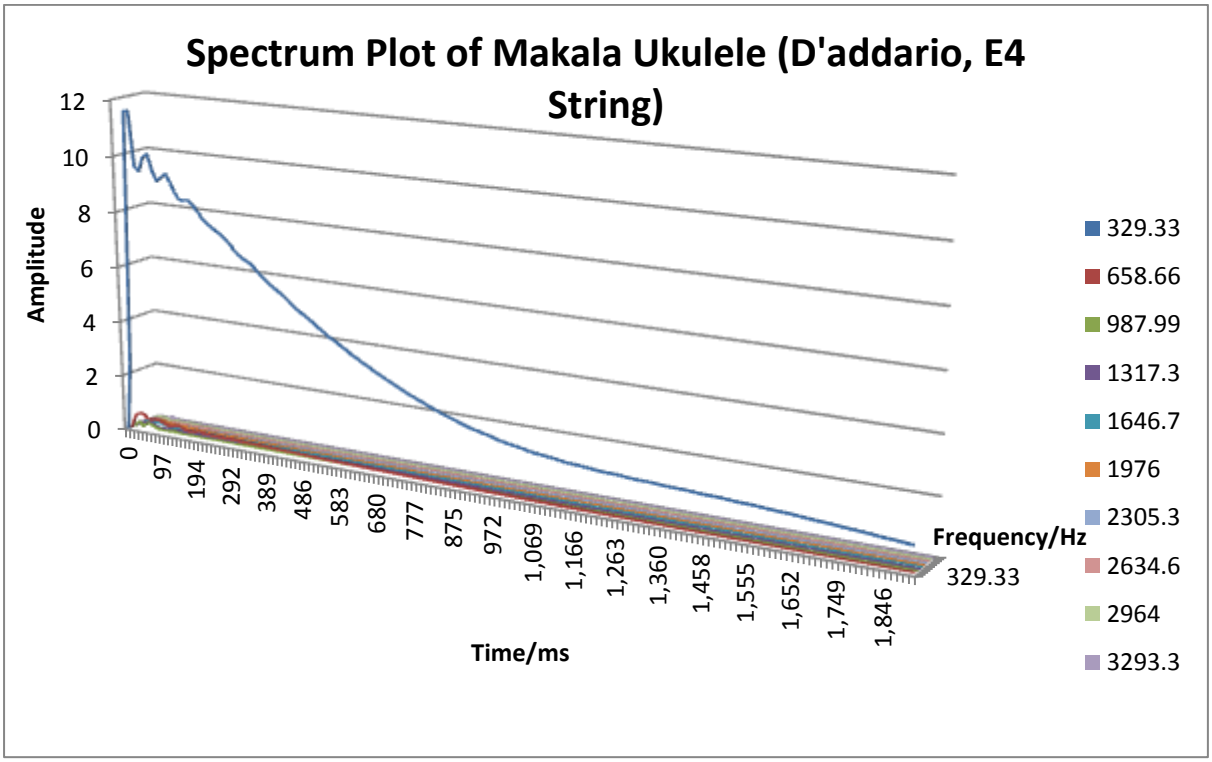

Figure 4.4.14: Spectrum Plot of E4 D'addario String for the Makala Ukulele

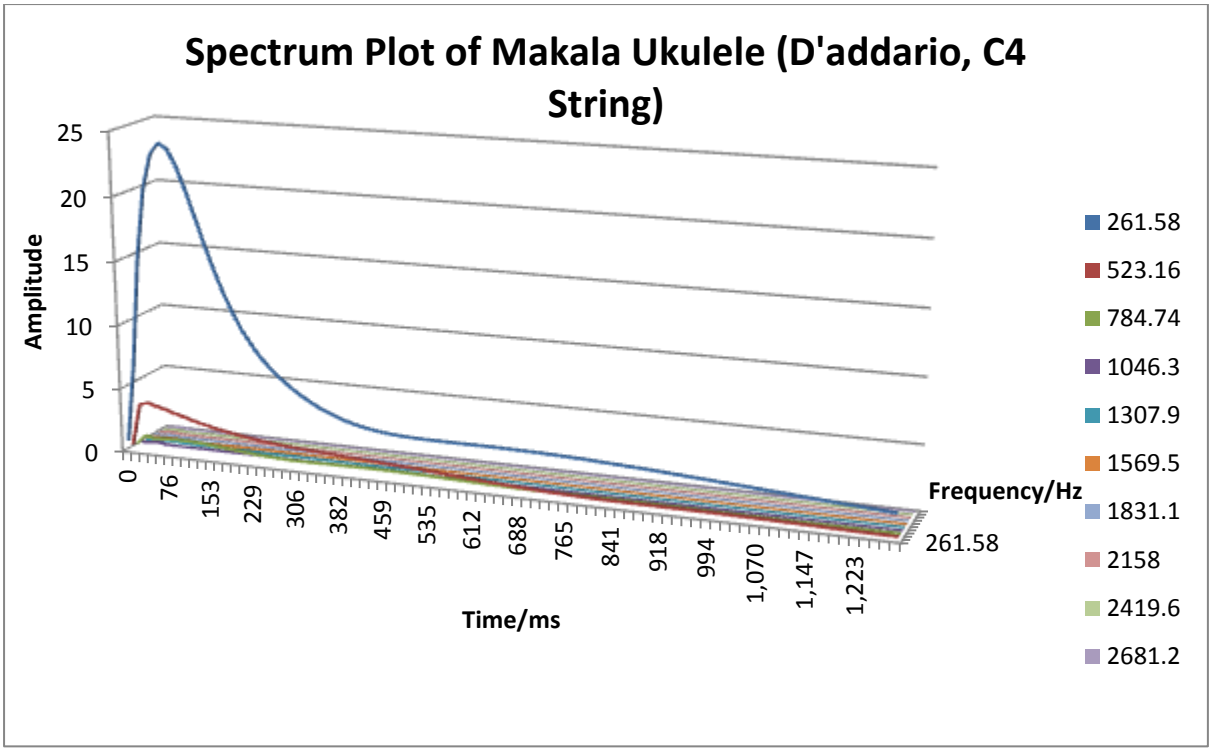

Figure 4.4.15: Spectrum Plot of C4 D'addario String for the Makala Ukulele

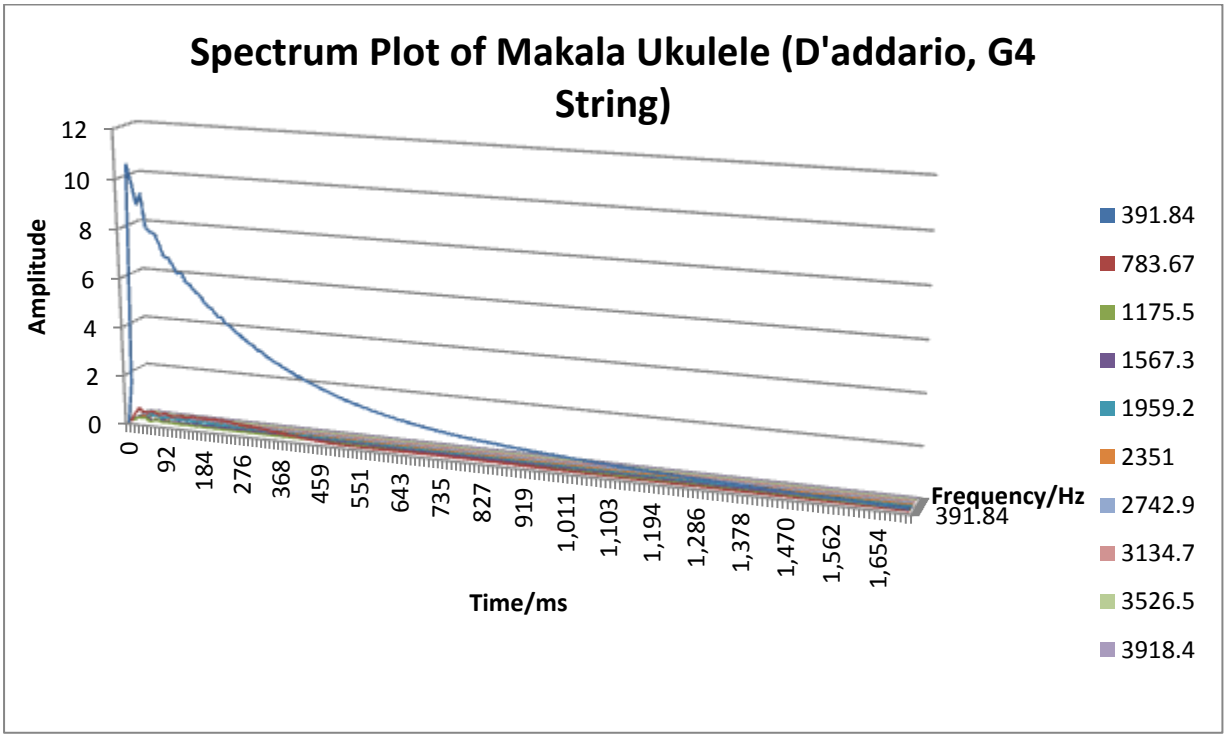

Figure 4.4.16: Spectrum Plot of G4 D'addario String for the Makala Ukulele

4.4.3 Outdoor Ukulele

(a) Aquila AQ-4U New Nylgut® Regular GCEA Set Soprano Strings

Figures 4.4.17 to 4.4.20 show the spectrum plots of the Outdoor Ukulele of the A4, E4, C4 and G4 Aquila string respectively.

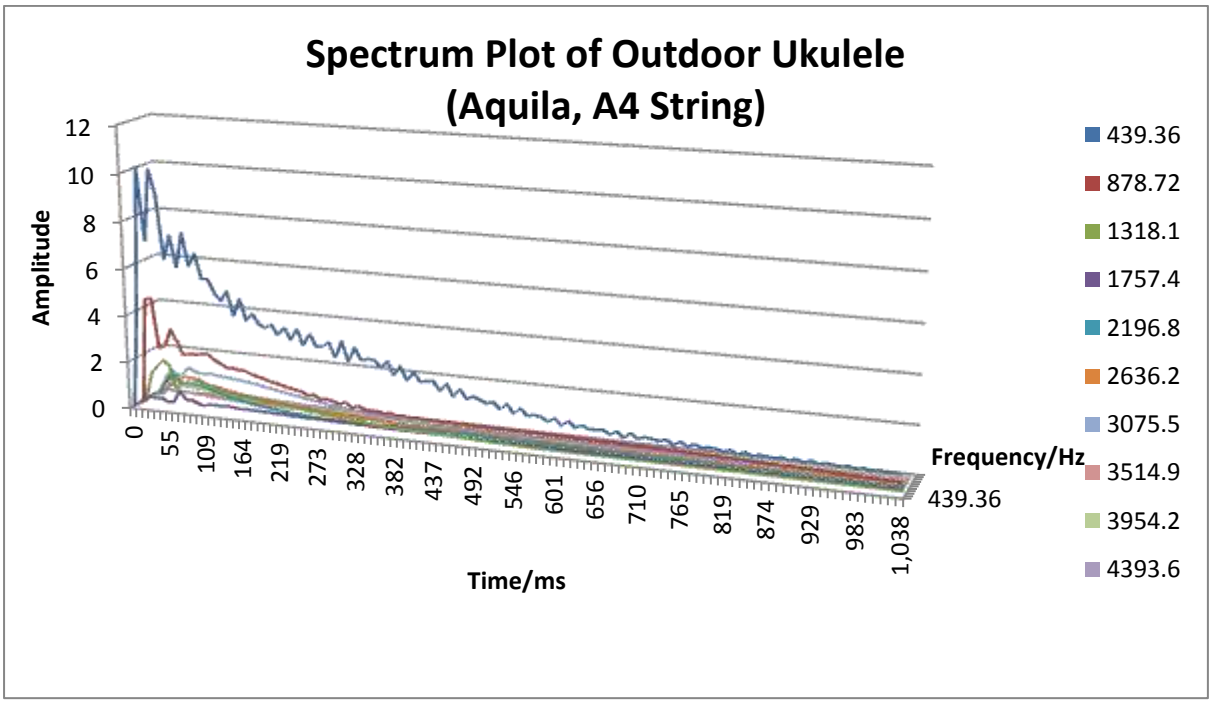

Figure 4.4.17 : Spectrum Plot of A4 Aquila String for the Outdoor Ukulele

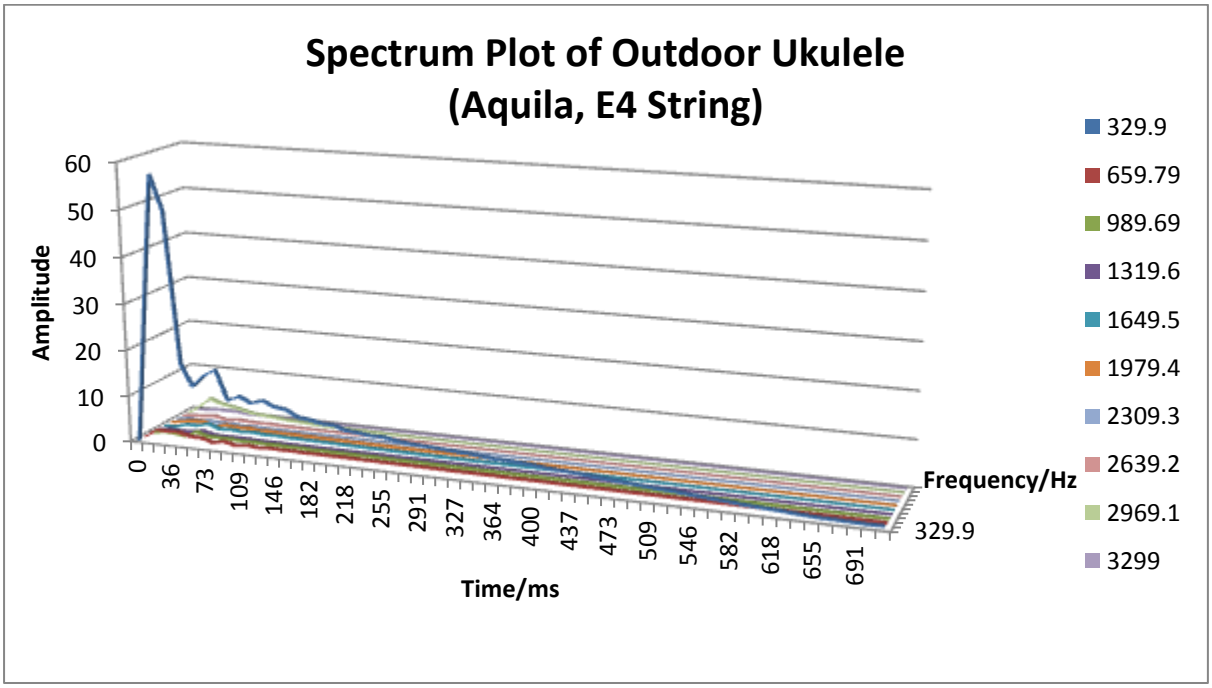

Figure 4.4.18: Spectrum Plot of E4 Aquila String for the Outdoor Ukulele

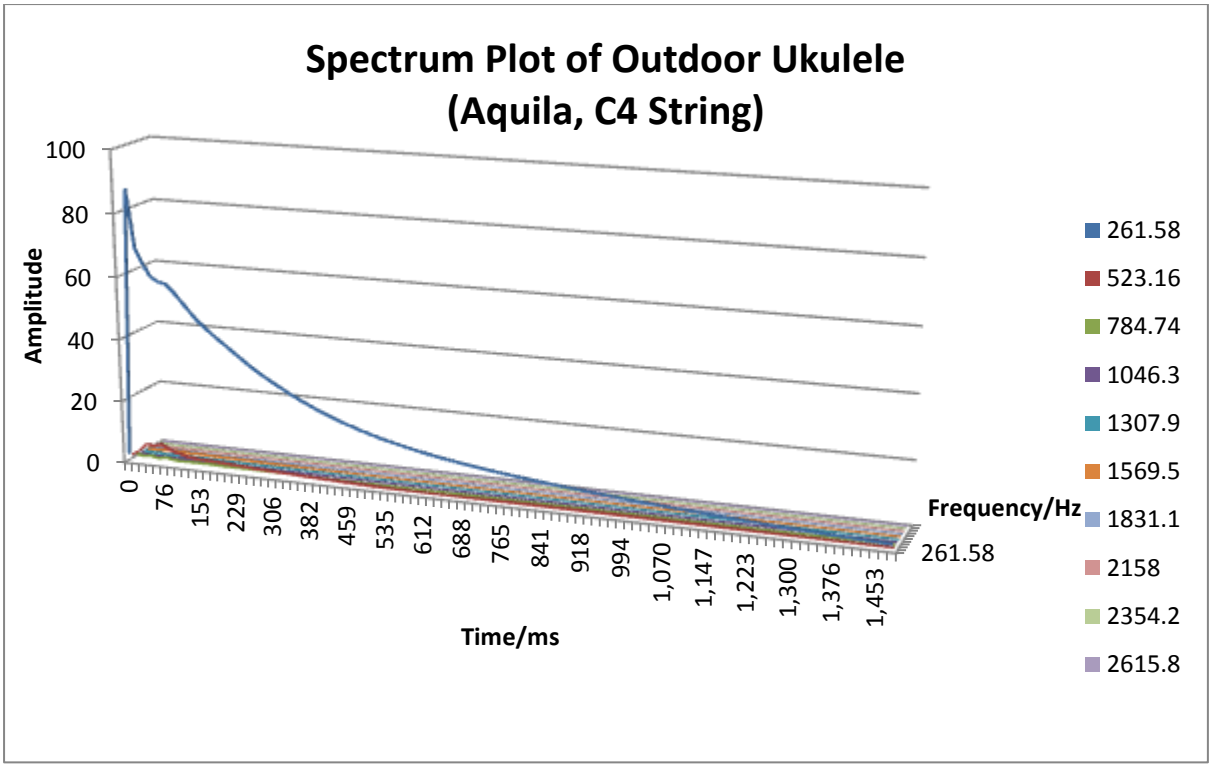

Figure 4.4.19: Spectrum Plot of C4 Aquila String for the Outdoor Ukulele

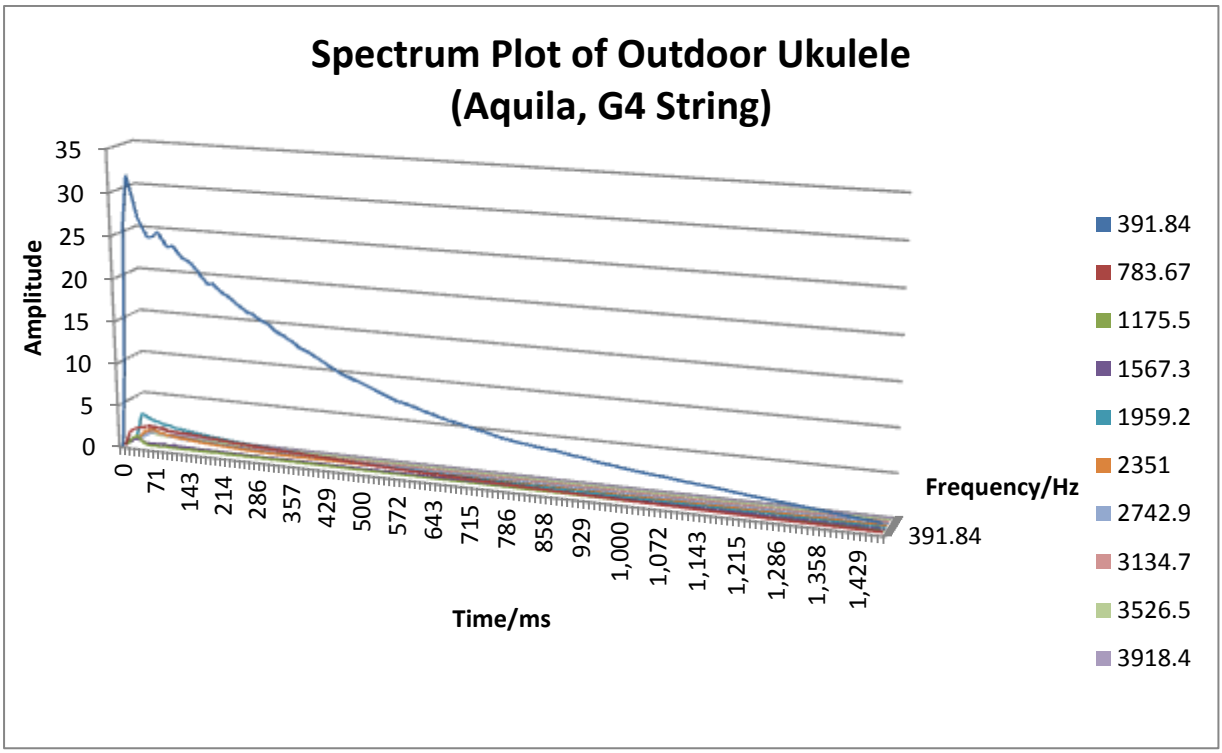

Figure 4.4.20: Spectrum Plot of G4 Aquila String for the Outdoor Ukulele

(b) D'Addario T2 Soprano Strings Strings

Figures 4.4.21 to 4.4.24 show the spectrum plots of the Outdoor Ukulele of the A4, E4, C4 and G4 D'addario string respectively.

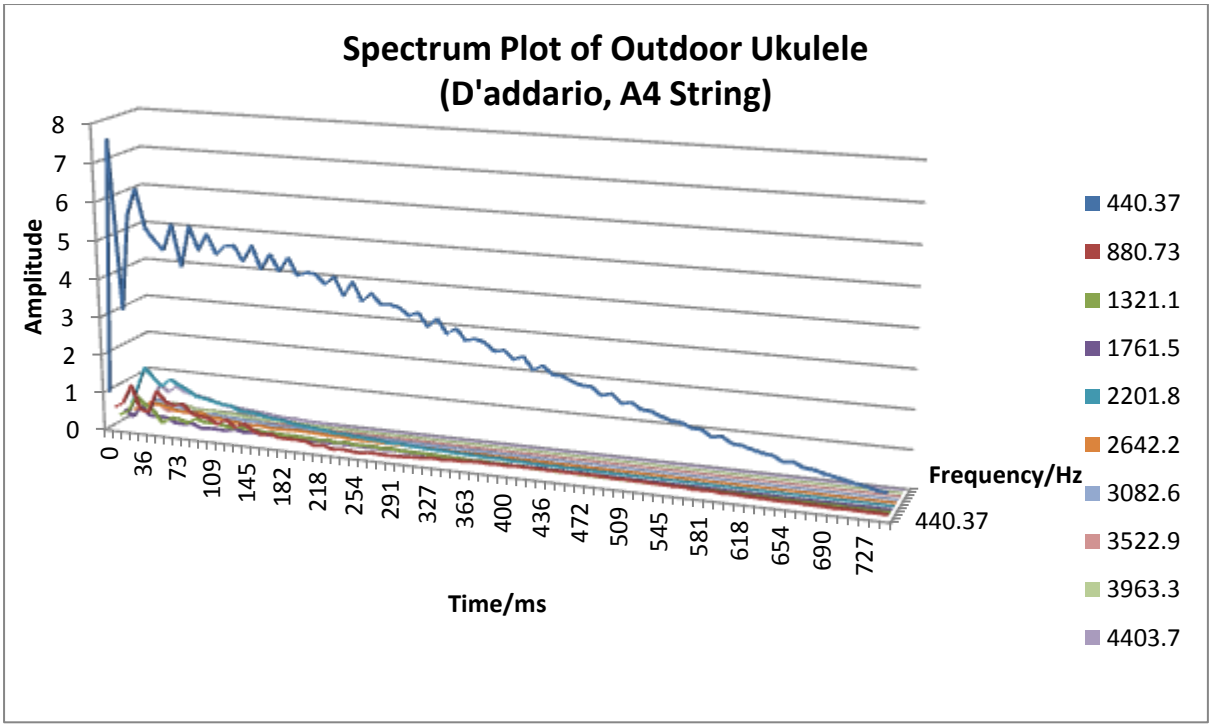

Figure 4.4.21: Spectrum Plot of A4 D'addario String for the Outdoor Ukulele

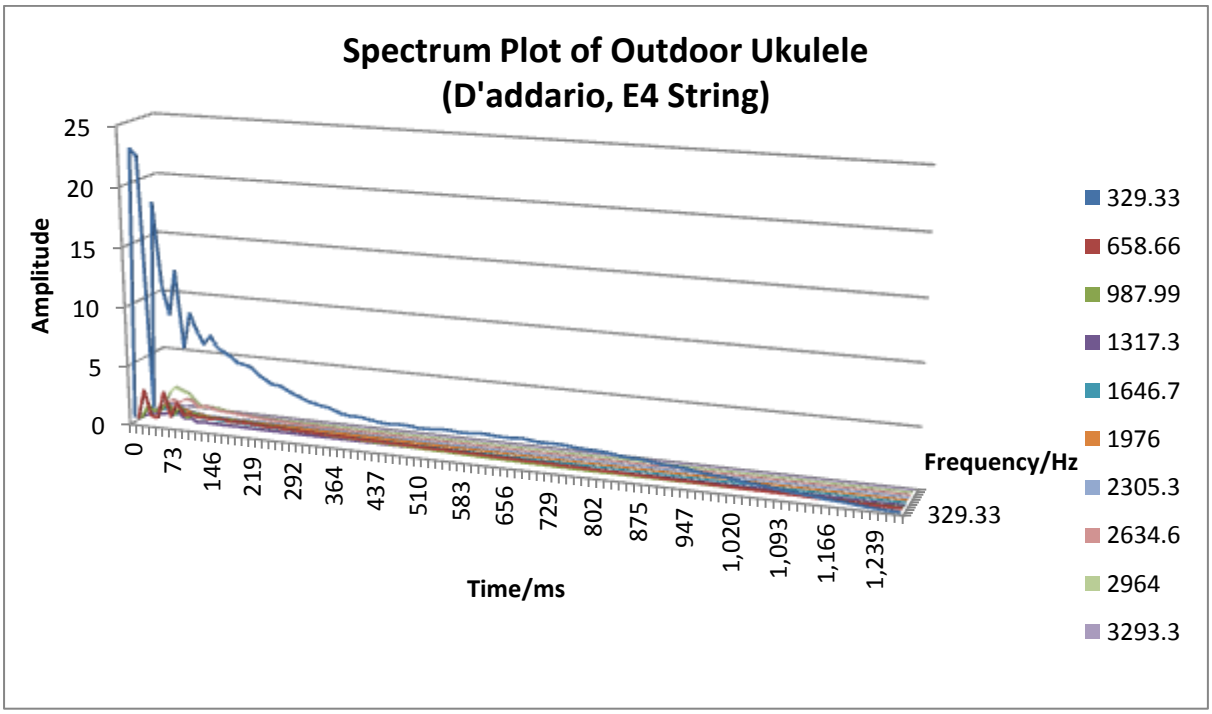

Figure 4.4.22: Spectrum Plot of E4 D'addario String for the Outdoor Ukulele

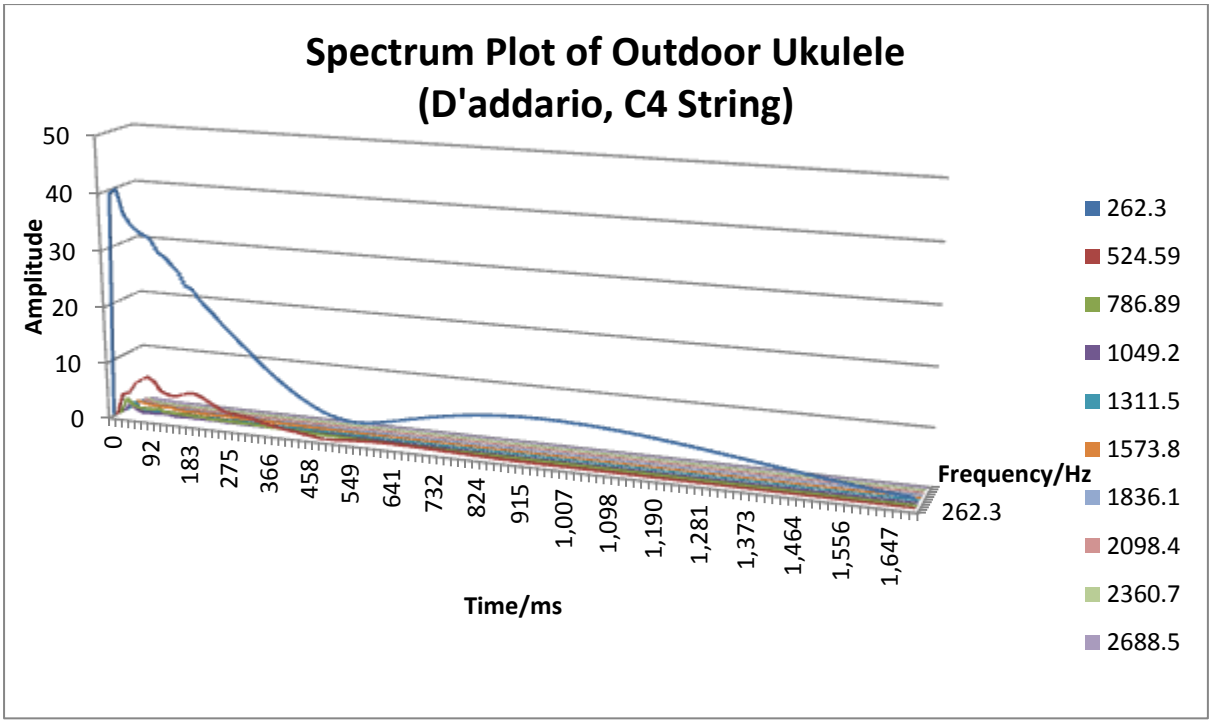

Figure 4.4.23: Spectrum Plot of C4 D'addario String for the Outdoor Ukulele

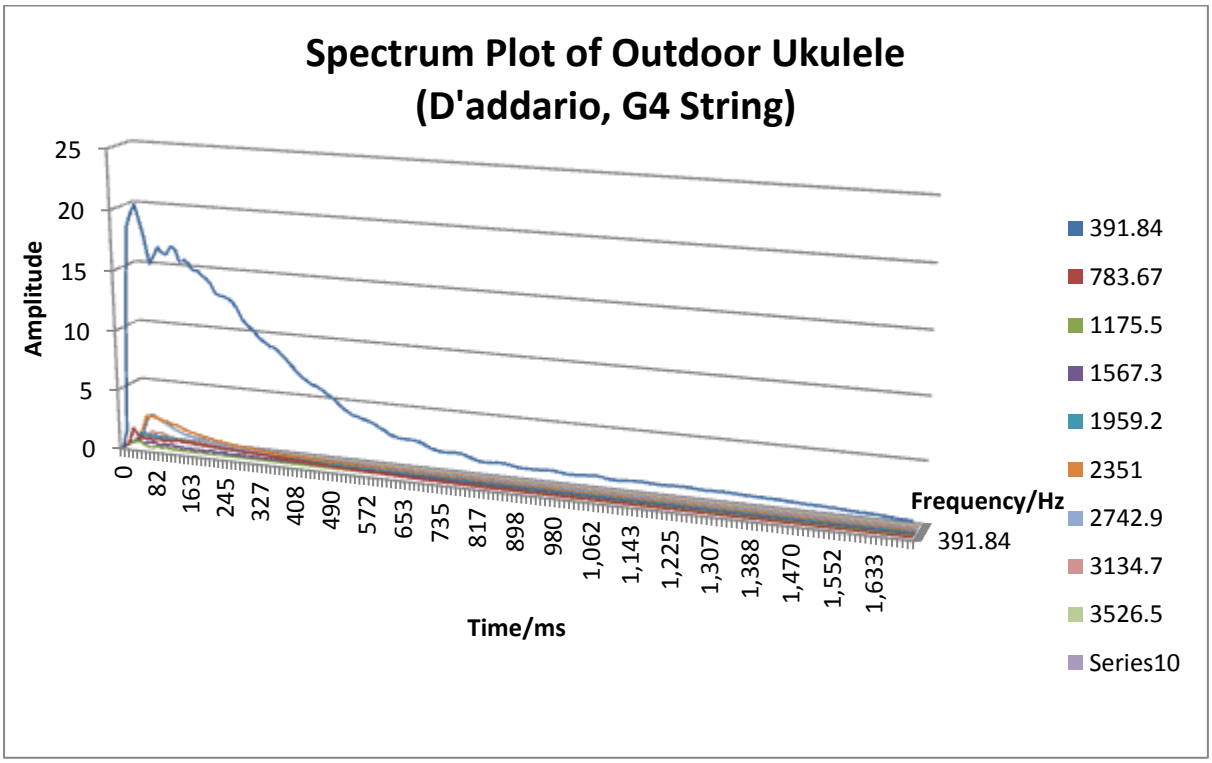

Figure 4.4.24: Spectrum Plot of G4 D'addario String for the Outdoor Ukulele

4.4.4 Spruce Wood Shanghai Pipa

Figures 4.4.25 to 4.4.28 show the spectrum plots of the Pipa of the A3, E3, D3 and A2 string respectively.

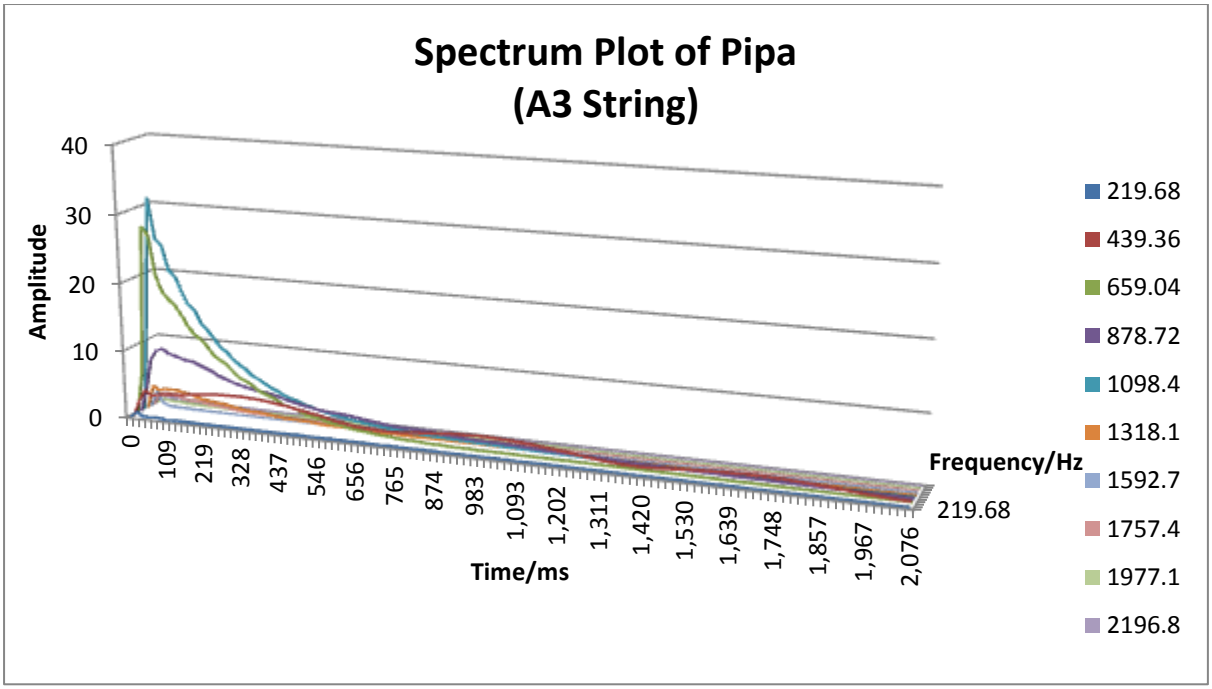

Figure 4.4.25: Spectrum Plot of A3 String for the Pipa

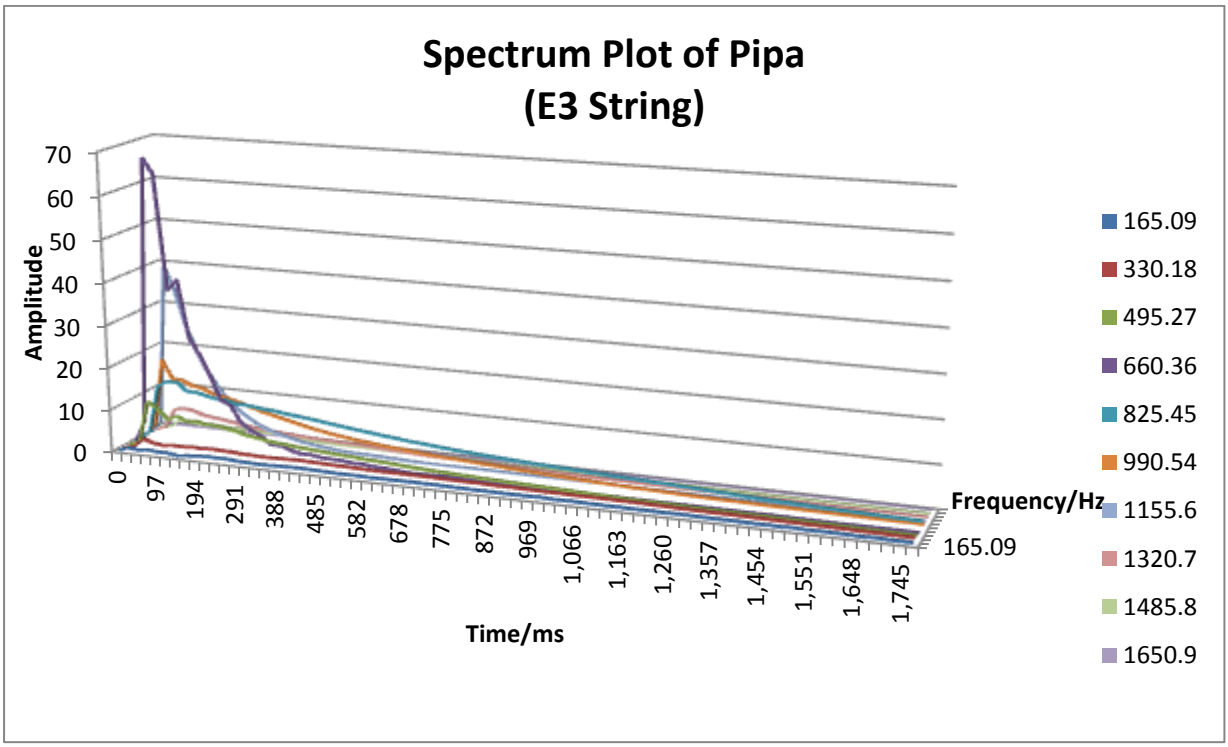

Figure 4.4.26: Spectrum Plot of E3 String for the Pipa

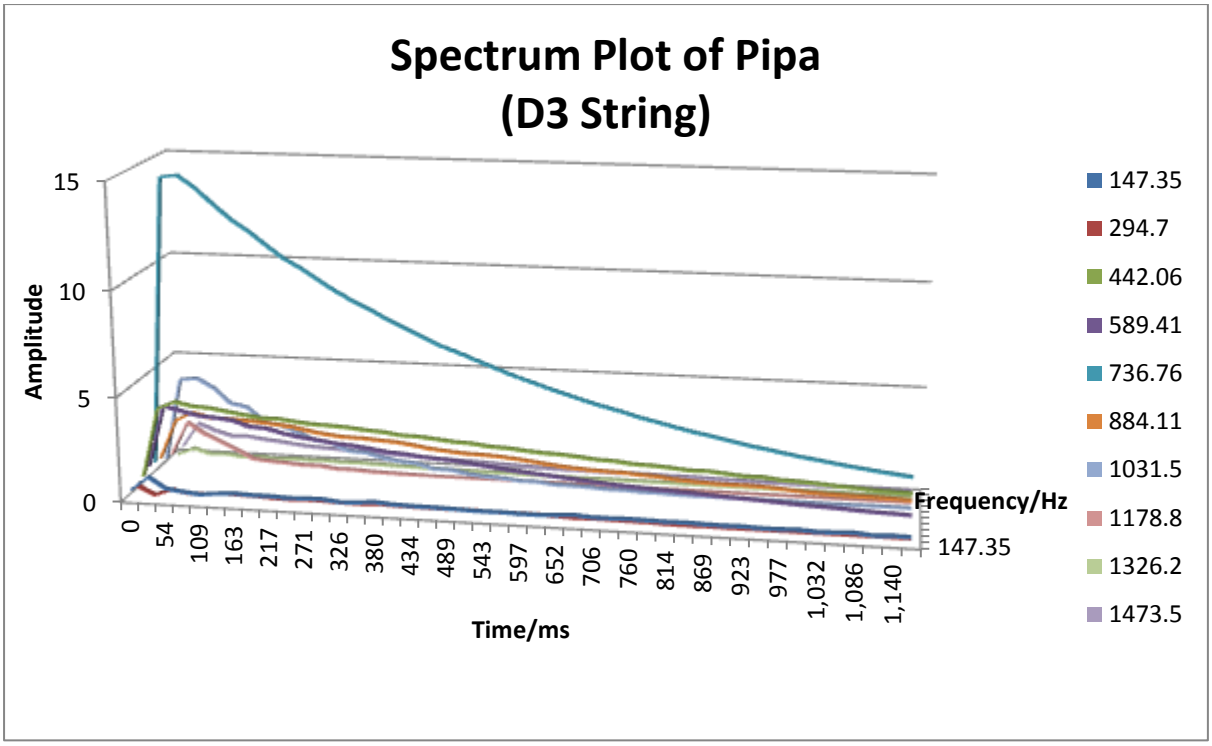

Figure 4.4.27: Spectrum Plot of D3 String for the Pipa

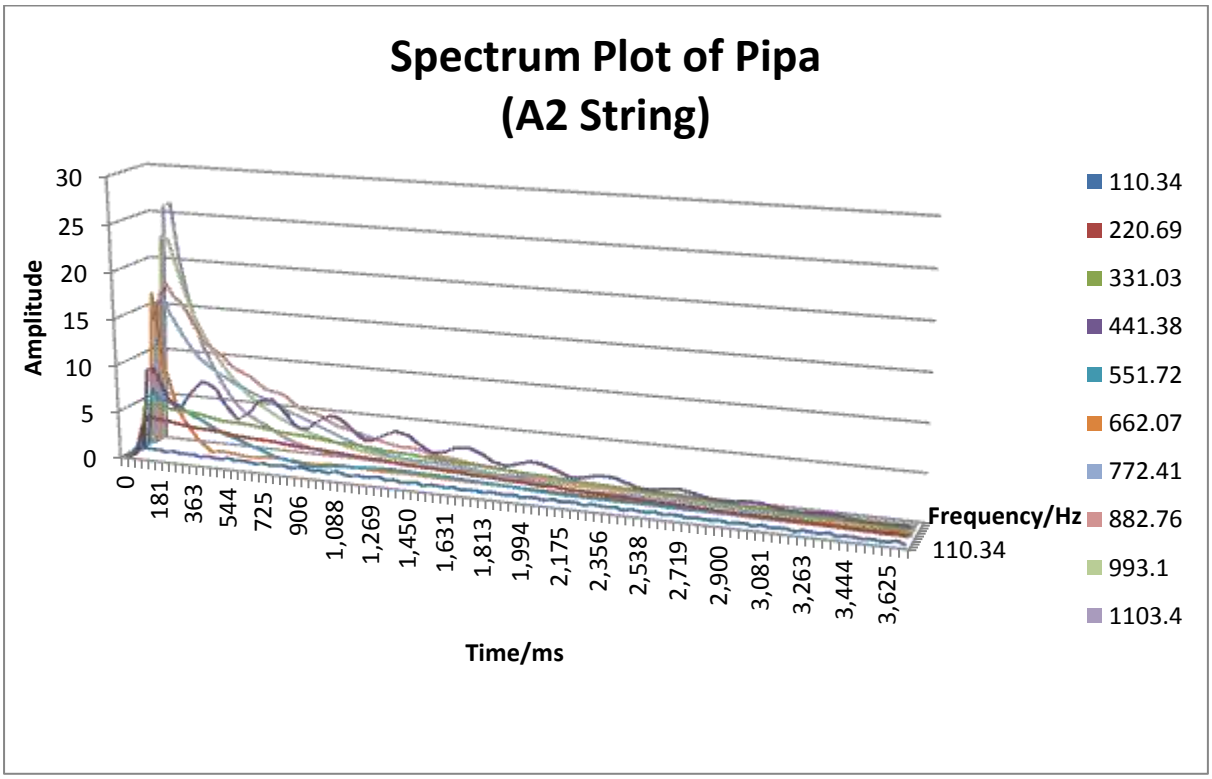

Figure 4.4.28: Spectrum Plot of A2 String for the Pipa

4.4.5 CG151S Yamaha Classical Guitar

Figures 4.4.29 to 4.4.34 show the spectrum plots of the Classical Guitar of the E4, B3, G3, D3, A2 and E2 Aquila string respectively.

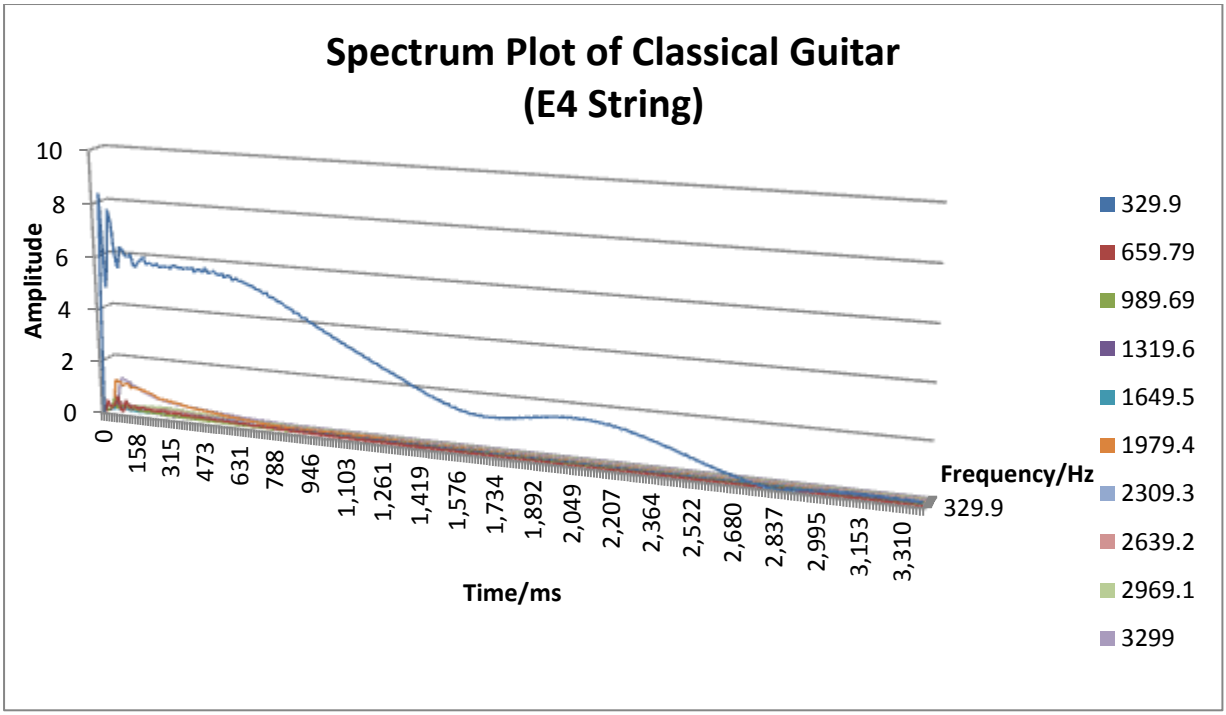

Figure 4.4.29: Spectrum Plot of E4 String for the Classical Guitar

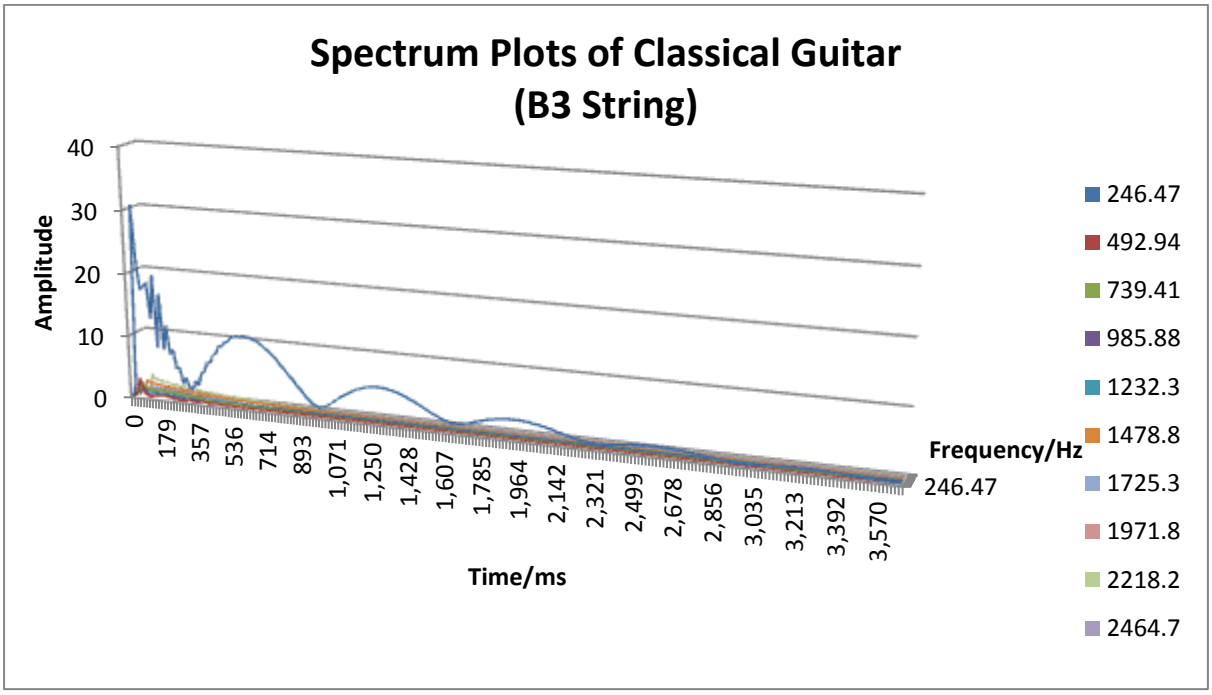

Figure 4.4.30: Spectrum Plot of B3 String for the Classical Guitar

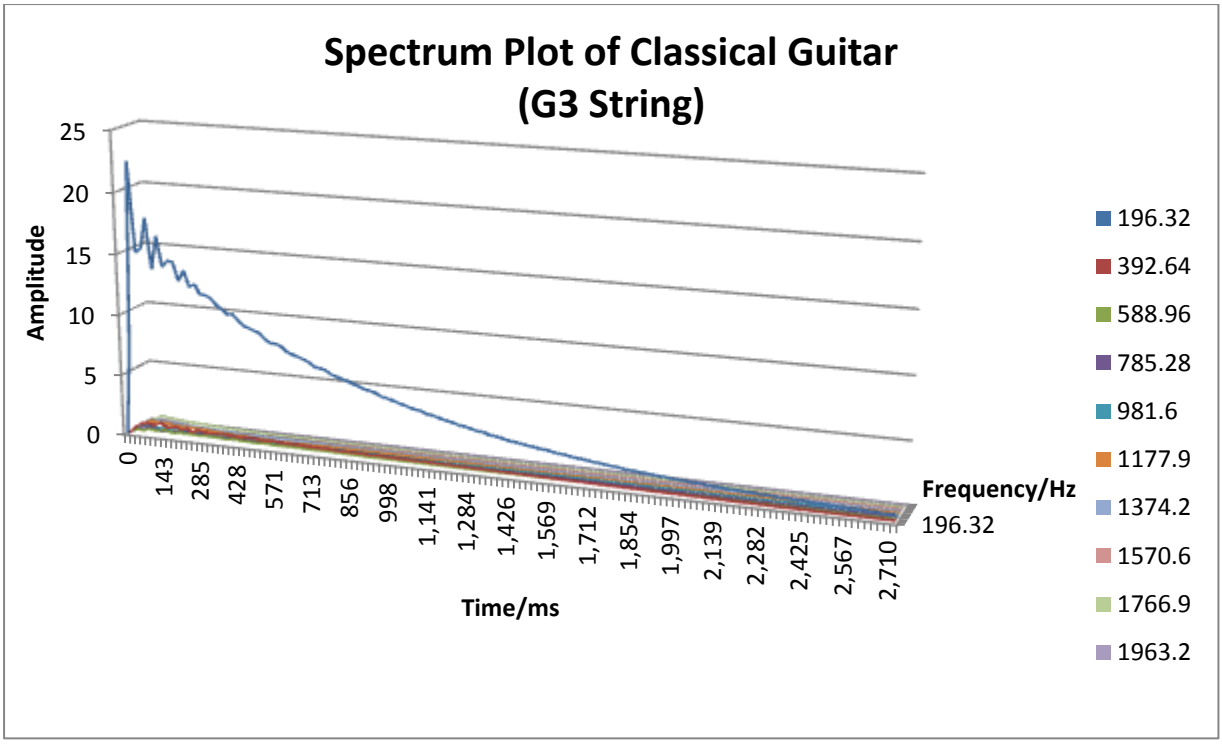

Figure 4.4.31: Spectrum Plot of G3 String for the Classical Guitar

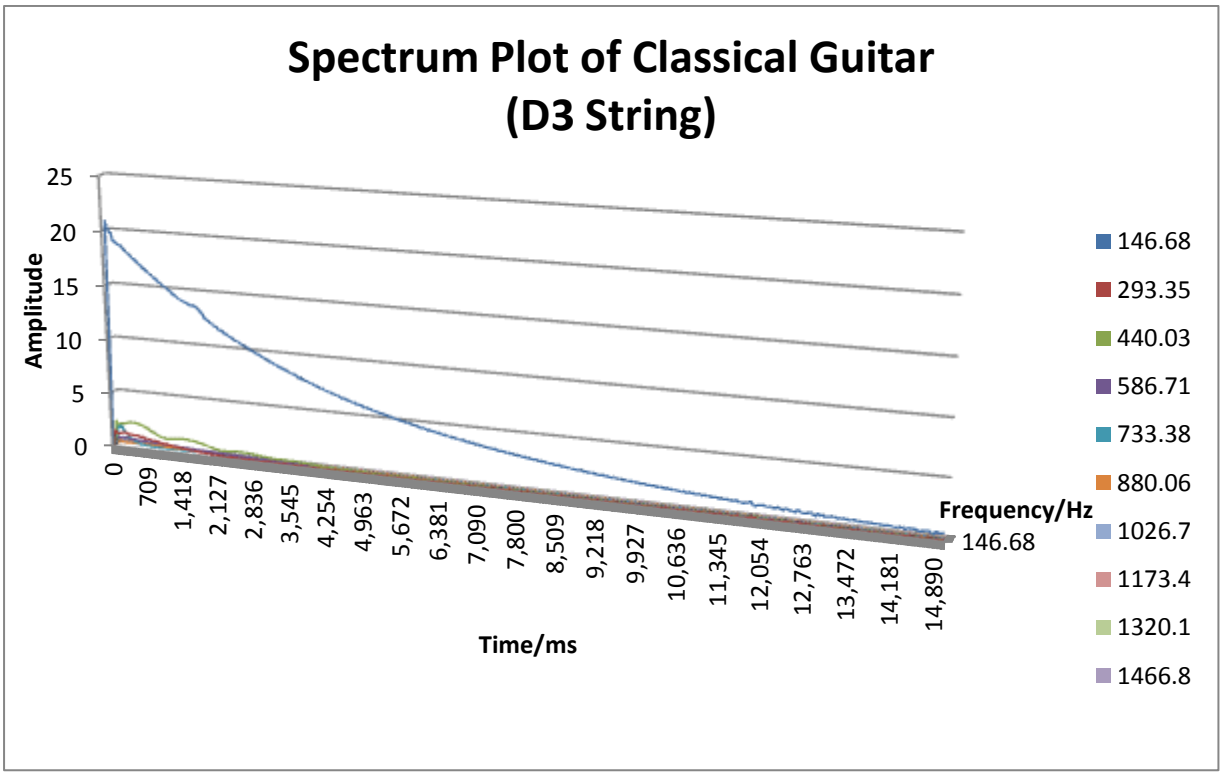

Figure 4.4.32: Spectrum Plot of D3 String for the Classical Guitar

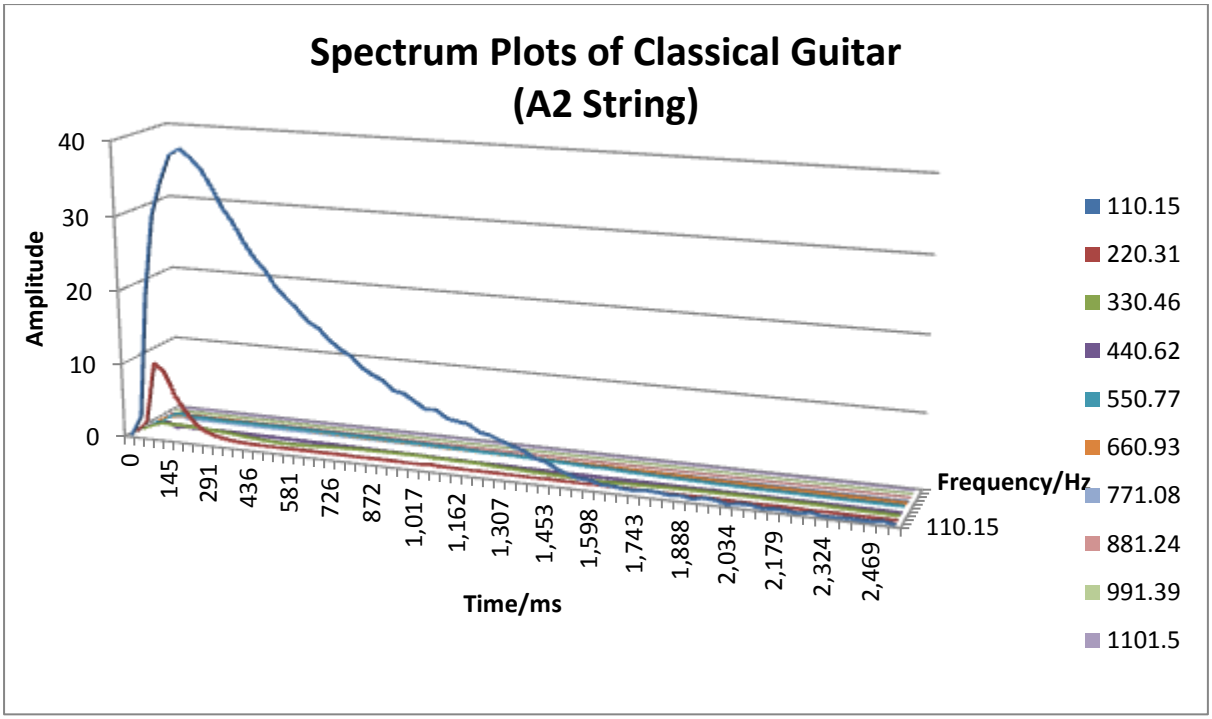

Figure 4.4.33: Spectrum Plot of A2 String for the Classical Guitar

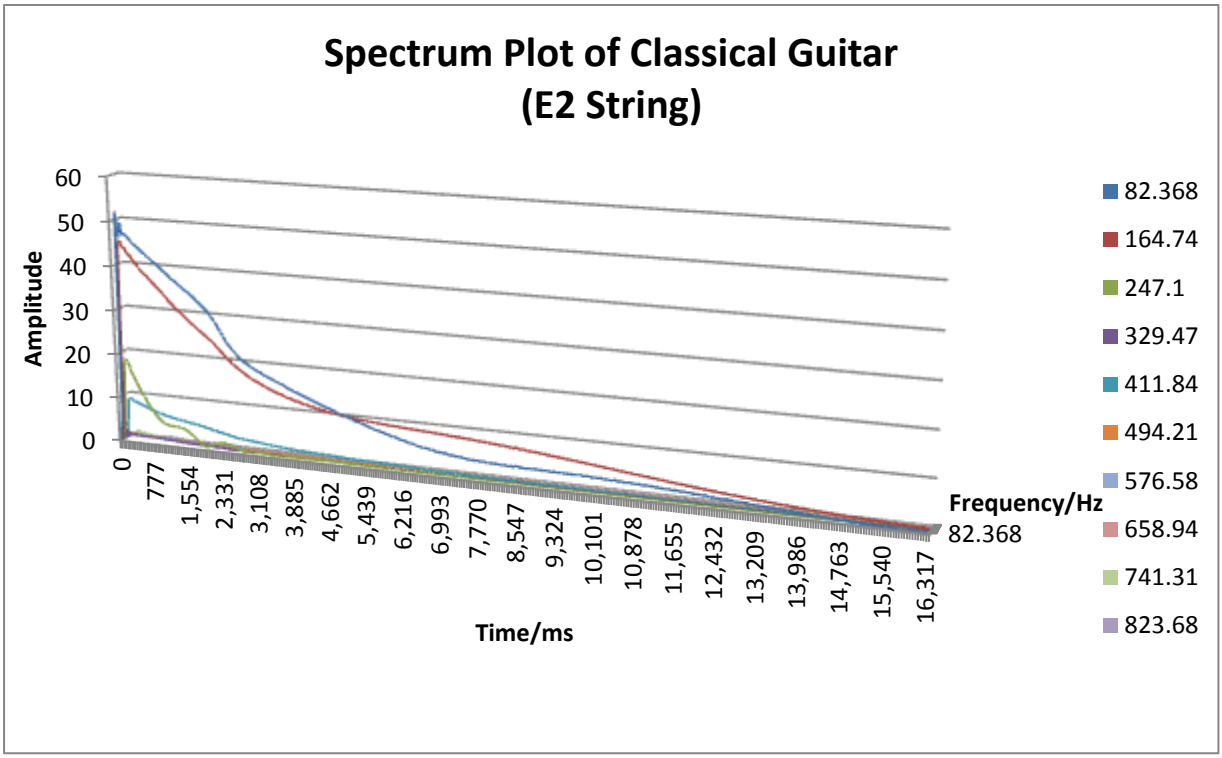

Figure 4.4.34: Spectrum Plot of E2 String for the Classical Guitar

4.4.6 Discussion on Spectrum Plots

Based on the spectrum plots of the ukuleles, it can be seen that all ukulele strings have similar plots in which the amplitudes of the first harmonic is seen to be the largest, followed by the second harmonic. It has also been noted that the thickest string produces the highest amplitudes which lasts for a longer period of time as compared to the remaining strings. In addition, the frequencies generally tend to fluctuate a little when it is first plucked but stabilizes after a certain period of time. However, the frequencies of the Outdoor Ukulele were seen to fluctuate more than the typical wooden ukulele.

The spectrum plots of the classical guitar are seen to be comparable to the spectrum plots of the ukulele. Similar to the ukulele, the frequency of the first harmonic has the largest amplitude and the thicker strings produce higher amplitudes which appear to be louder to perceivers.

The pipa has a more complex spectrum of harmonic frequencies than the ukulele and classical guitar. The higher harmonics of the pipa are seen to have larger amplitudes whereas the first two harmonics are seen to have much smaller amplitudes. This explains the perceived high pitch and bright sounds of the pipa. The difference in spectrum plots may be attributed to the varied shape, size and strings of the pipa, ukulele and guitar.

4.5 Discussion

Young's Modulus and Linear Density

The deviations between the theoretical values and experimental values of the inharmonicity coefficient of the ukulele strings can be attributed to the assumption that the strings used were completely made out of nylon. In actuality, this is not the case. The Aquila New Nylgut set of strings are not completely nylon nor are they gut strings but rather a plastic compound of three different components which exhibit characteristics similar to the nylon and gut strings[18]. The D'addario T2 strings, on the other hand, is said to be crafted from a dense monofilament material which is similar to nylon [19]. The Young's modulus and linear density used in these calculations may differ quite significantly from the actual values of the strings. The same goes for the strings of the Pipa and bass strings of the classical guitar as they are rather complex strings**.** There is also a possibility that the Young's Modulus for each type of string differs slightly. However, this contribution may have very little impact on the overall results. It is clear that further analyses on these strings are needed.

Problems with the Pipa and Classical Guitar

When determining the experimental inharmonicity coefficients of the strings of the pipa and the bass strings of the classical guitar, it was noted that there were a few values which lies out of the trend. In the case of the pipa, this could have been due to the difference in plucking style as it was harder to pluck the strings with the same position using the fake fingernail. Another possible reason for this is the presence of dirt in the windings which may slightly increase the frequencies of strings at higher harmonics.

Problem with Theoretical Model for Wound Strings

The discrepancies in this project may be due to the fact that a lot of approximations were used not just in terms of constants but as well as the model used. Fletcher created his model based on piano strings and made approximations which may not be applicable for the analysis of other types of strings. In his analysis, Fletcher assumed that the windings were very small and treated the cross sectional area of the windings as a sheaf of metal. However, this approximation may contribute to the percentage discrepancy especially for strings with larger diameters. If each loop of winding were treated as a torus instead, it is found that the percentage discrepancy for the A2 string decreased by 10%.

Comparison of Ukulele Strings with Trebles Strings of Classical Guitar

The inharmonicity coefficients of the ukulele strings ranges from 1.1×10^{-4} to 6.8×10^{-4} whereas the inharmonicity coefficients of the treble classical guitar strings were found to range from 3.0×10^{-5} to 1.6×10^{-4}. In general, the ukulele strings have smaller diameters than the treble classical guitar strings which explains the larger values obtained for the classical guitar.

As for strings which have nylon cores wound with copper, the values were found be even smaller ranging from 8.0×10^{-6} to 1.6×10^{-5}. The pipa strings which have steel cores wrapped with nylon have values higher than the bass strings of the classical guitar that is from 3.3×10^{-5} to 8.5×10^{-5}.

Due to the lack of research in nylon strings, the results obtained could not be compared with any other external theoretical values. Thus, this project has provided a rough gauge as to what the magnitudes of inharmonicity coefficient of nylon strings should be.

Chapter 5

CONCLUSION

The inharmonicity of ukulele, pipa and classical guitar strings is studied through the standard method of harmonic analysis, the Fast Fourier Transform (FFT). The degree of inharmonicity in stings is also analyzed by varying the thickness of the strings, type of instrument used and the type of strings. In addition, the inharmonicity coefficients of strings which contained nylon were determined and analyzed. Although these strings may not fit the stiff string model proposed by Fletcher completely, it can be seen that these strings generally agree with the model. Adjustments to this model may be required in order to be applied to nylon strings.

Investigations on the frequencies of the ukulele, pipa and classical guitar strings were made. The deviation of harmonic frequencies from the ideal harmonic frequencies were also examined and compared across strings of different thickness, quality and type of instrument. It is found that the results acquired from these two analyses generally agree with the stiff string model although several outliers were obtained. The spectrum plots produced also provided information on the behavior of harmonic frequencies over time which may be used as reference in the synthesis of sounds.

Overall, the objectives of this project were carried out successfully and this paper offers a good platform for further research.

References

[1] Olson, H. F. (1967). *Music, physics and engineering* (Vol. 1769). Courier Dover Publications.Culver,

[2] Encyclopedia Britannica: Pipa. http://www.britannica.com/EBchecked/topic/459043/pipa (accessed 21 Mar 2014)

[3] Chen, Y. H., & Huang, C. F. (2011). Sound Synthesis of the Pipa Based on Computed Timbre Analysis and Physical Modeling. *Selected Topics in Signal Processing, IEEE Journal of*, *5*(6), 1170-1179.

[4] Chin, S. H. L., & Berger, J. (2010). Analysis of Pitch Perception of Inharmonicity in Pipa Strings Using Response Surface Methodology. *Journal of New Music Research*, *39*(1), 63-73.

[5] Parts of Classical Guitar. http://en.wikibooks.org/wiki/Guitar/Classical_Guitar (accessed 31 Mar 2014)

[6] Design of a Classical Guitar. http://www.designofaclassicalguitar.com/acoustic-principles.php (accessed 31 Mar 2014)

[7] Jahnel, F. (2000). *Manual of guitar technology: The history and technology of plucked string instruments*. Bold Strummer Limited.

[8] Modeling the wave motion of a guitar. http://www.forskningsradet.no/servlet/Satellite(accessed 17 Mar 2014)

[9] Fletcher, N. H., & Rossing, T. D. (1998). *The physics of musical instruments*. Springer.

[10] Rossing, T. D., Moore, F. R., & Wheeler, P. A. (1990). *The science of sound*(Vol. 2). Reading, MA: Addison-Wesley.

[11] Feldman, J. (2007) *Solution of the Wave Equation by Separation of Variable.* University of British Columbia: Notes from the Mathematics Department 267 2007-2007. Available at: http://www.math.ubc.ca/~feldman/m267/separation.pdf (accessed 18 Mar 2014)

[12] Young, H. D., & Freedman, R. A. (2006). *Sears and Zemansky's university physics* (Vol. 1). Pearson education.

[13] Fletcher, H. (2005). Normal vibration frequencies of a stiff piano string. *The Journal of the Acoustical Society of America*, *36*(1), 203-209.

[14] Feuer, A., & Goodwin, G. C. (1996). *Sampling in digital signal processing and control*. Springer.

[15] Fast Fourier Transform (FFT): http://www.cmlab.csie.ntu.edu.tw/cml/dsp/training/coding/transform/fft.html (accessed 20 Mar 2014)

[16] Kala Spruce/Rosewood Soprano Ukulele and Makala Soprano.

[17] Outdoor Ukulele. http://outdoorukulele.com/

[18] Aquila Strings. http://www.aquilausa.com/uke_strings.html, http://www.aquilastringschina.com/Our_products.html

[19] D'addario T2 Titanium Strings. http://www.daddario.com/DADProductDetail.Page?ActiveID=3769&productid=254&productname=EJ87S_Titanium_Ukulele__Soprano

[20] Spruce Wood Starter Pipa. http://www.easonmusicstore.com/webshaper/store/viewProd.asp?pkProductItem=101

[21] Classical Guitar. http://en.wikibooks.org/wiki/Guitar/Classical_Guitar

[22] CG151S Yamaha Classical Guitar http://sg.yamaha.com/en/products/musical-instruments/guitars-basses/cl-guitars/cg/cg151s/

[23] D'addario Pro-Arte Nylon, Normal Tension Classical Guitar Strings http://www.daddario.com/DADProductDetail.Page?ActiveID=3769&productid=213&productname=EJ45_Pro_Arte_Nylon__Normal_Tension

[24]Elejabarrieta, M. J., Ezcurra, A., & Santamarıa, C. (2002). Coupled modes of the resonance box of the guitar. *The Journal of the Acoustical Society of America*, *111*(5), 2283-2292.

[25] Keane, M. (2004). Understanding the complex nature of piano tones. *Acoustics Research Centre. Available fro m http://www. acoustics. auckland. ac. nz/research/research_files/keane_nzas04. pdf*.

Appendix A: Code for Signal Processing

Code used for performing FFT and plotting graphs in time and frequency domains

```
%Load File KalaAA.wav
file='KalaAA.wav';
[y,Fs,bits]=wavread(file);

%Number of samples in file
Nsamps=length(y);

%Generate time domain values
t=(1/Fs)*(1:Nsamps);

%Applying FFT function on sampled data array y
y_fft=abs(fft(y));   %Retain only Magnitude
y_fft=y_fft(1:Nsamps);
y=y(1:Nsamps);   %For later parts analysis

%Generate frequency domain values
f=Fs*(0:Nsamps-1)/Nsamps;

%Plot Sound File in Time Domain
plot(t,y)
xlabel('Time(s)')
ylabel('Amplitude')
title('Amplitude(dB) in Time Domain(s)')

%Plot Sound File in Frequency Domain
plot(f,y_fft)
xlim([0 <set to a frequency slightly higher than largest expected frequency>])
xlabel('Frequency(Hz)')
ylabel('Amplitude')
title('Spectral Power(Watts/Hz) in Frequency Domain(Hz)')
```

Appendix B: Code for Spectrum Plots

```
%Load File MakalaAA.wav
% Select destination folder
file = 'C:\Users\kirstenwong\Documents\Semester 1\Honours Project\WAV Files\MakalaAA.wav';
dest = 'C:\Users\kirstenwong\Documents\Semester 1\Honours Project\CSV Files\MakalaAA.csv';

%Fundamental frequency of sample
freq = 440.43;

% Read the wav file
[y,Fs,bits] = wavread(file);

% Calculate the number of samples in 4 wavelengths
section_size = round((Fs / freq) * 4);

% Calculate the exact number of samples we'll be expecting
size_y = numel(y);

% Discard the beginning of the samples to round it up evenly
% Multiple of section_size
l = floor(size_y / section_size) * section_size;
y = y((size_y - l + 1):size_y);
size_y = l;
section_count = size_y / section_size;

% Process each section_size-ed section of the PCM sample
sections = reshape(y, section_size, []);

% The frequencies of the frequencies buckets
ret = Fs * (0:section_size - 1) / section_size;
ret = [[0] ret]';

% Process each section in turn
for i = 1:section_count
        y = sections(:,i);

        % The start time for this group of samples
        t = (i - 1) * (section_size / Fs);

        % Perform FFT
        y_fft = abs(fft(y));
        y_fft = y_fft(1:section_size);

        ret = [ret [[t]; y_fft]];
end

%Save file in .csv format
csvwrite(dest, ret)
```

Appendix C: Comparing Ukuleles

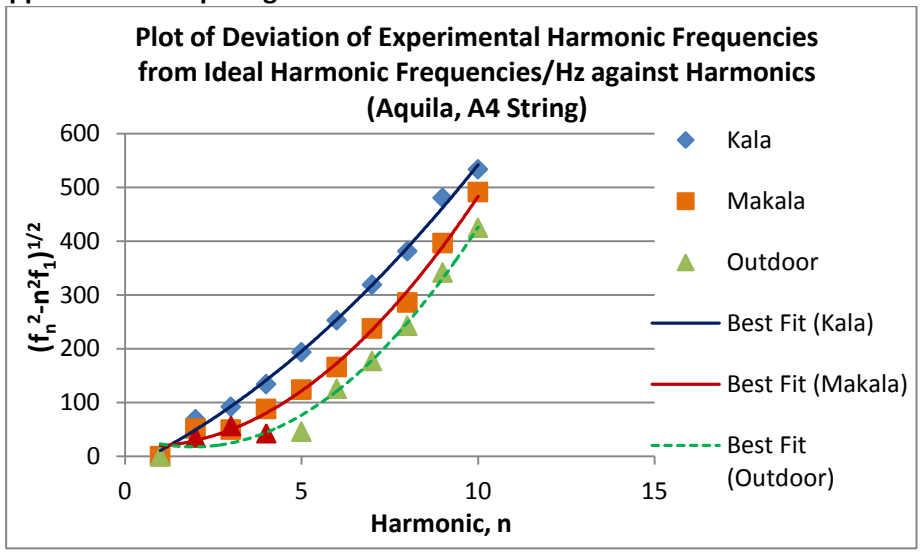

Figure 5.1: Plot of $\sqrt{{f_n}^2 - n^2{f_1}^2}$ against n for the A4 Aquila string set.

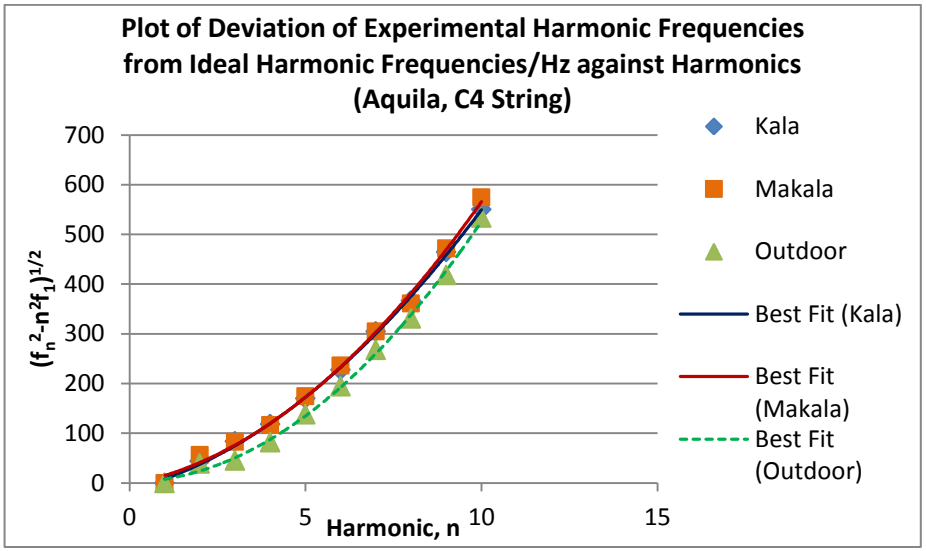

Figure 5.3: Plot of $\sqrt{{f_n}^2 - n^2{f_1}^2}$ against n for the C4 Aquila string set.

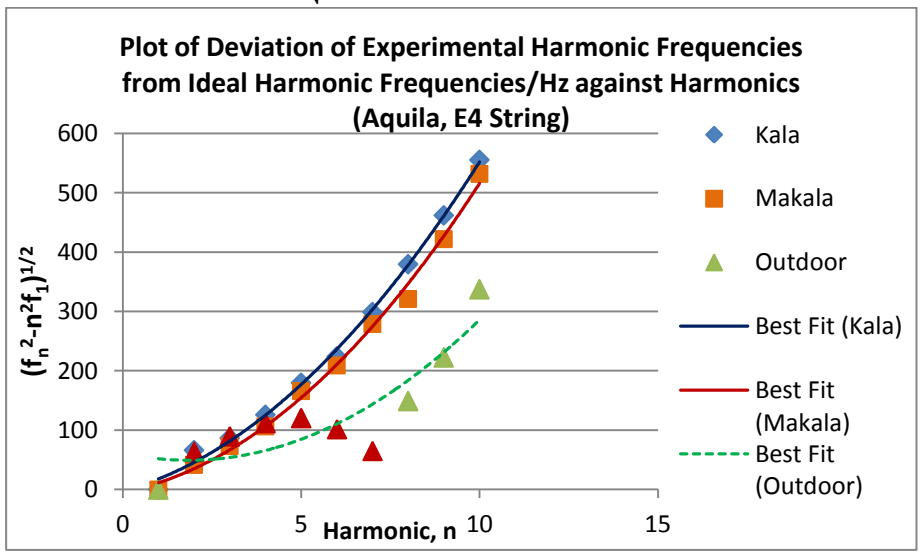

Figure 5.2: Plot of $\sqrt{{f_n}^2 - n^2{f_1}^2}$ against n for the E4 Aquila string set.

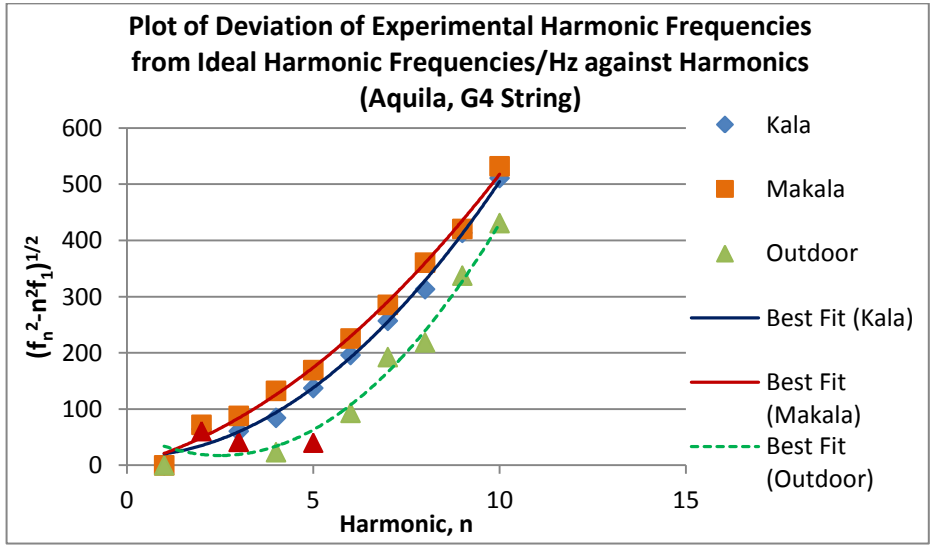

Figure 5.4: Plot of $\sqrt{{f_n}^2 - n^2{f_1}^2}$ against n for the G4 Aquila string set.

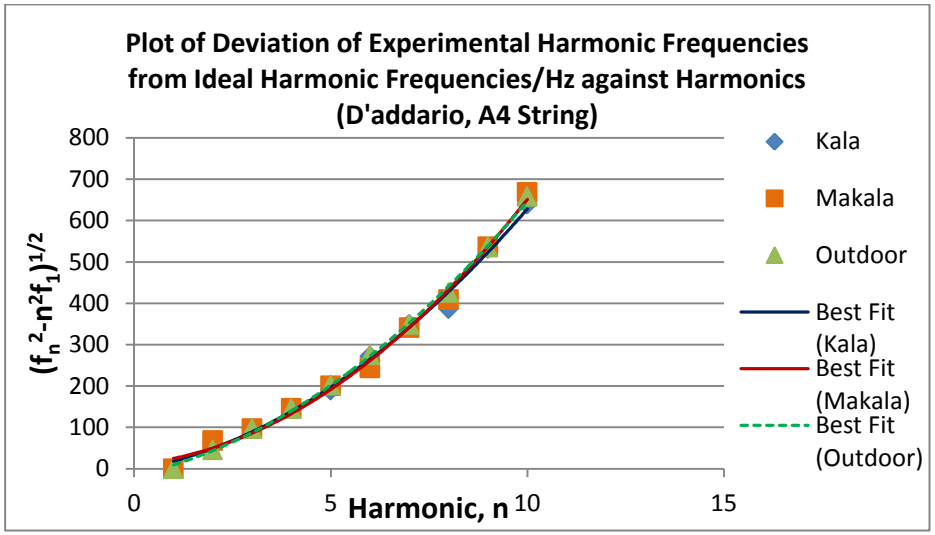

Figure 5.5: Plot of $\sqrt{{f_n}^2 - n^2{f_1}^2}$ against n for the A4 D'addario string set.

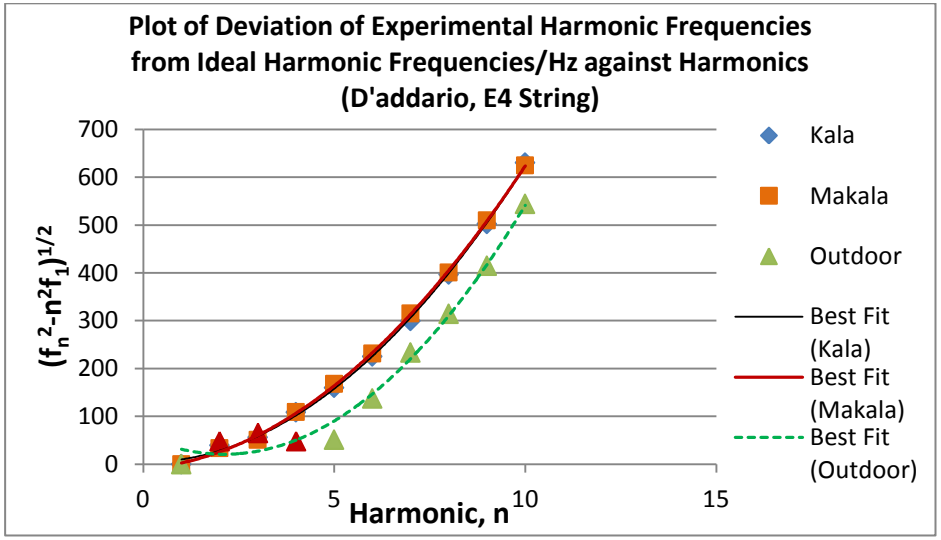

Figure 5.6: Plot of $\sqrt{{f_n}^2 - n^2{f_1}^2}$ against n for the E4 D'addario string set

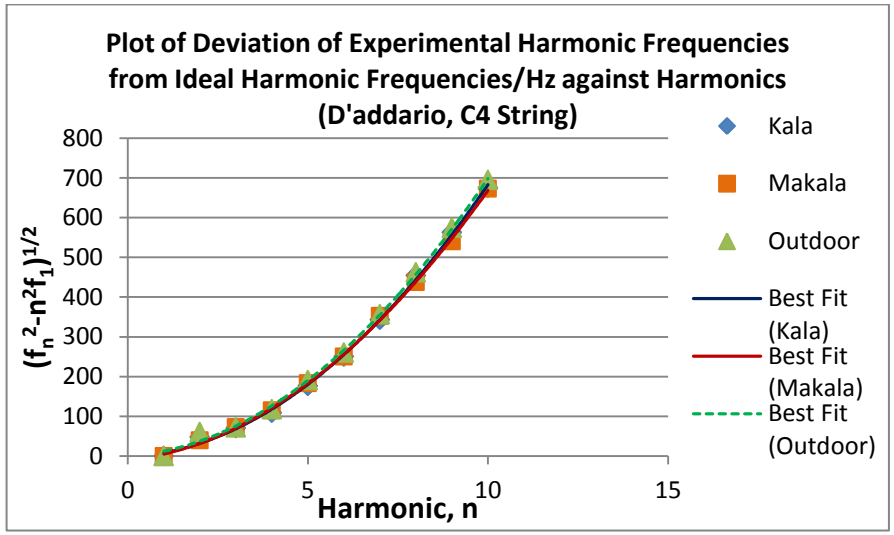

Figure 5.7: Plot of $\sqrt{{f_n}^2 - n^2{f_1}^2}$ against n for the C4 D'addario string set

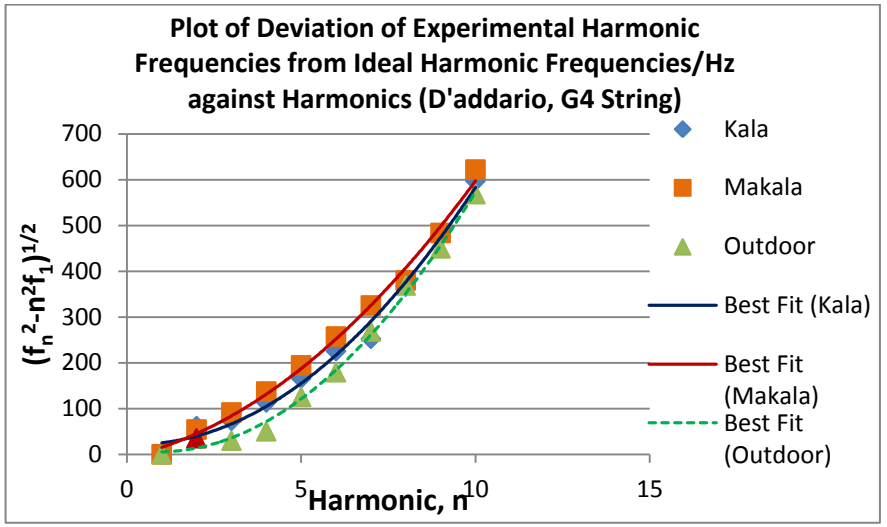

Figure 5.8: Plot of $\sqrt{{f_n}^2 - n^2{f_1}^2}$ against n for the G4 D'addario string set

Appendix D: Comparing String Types

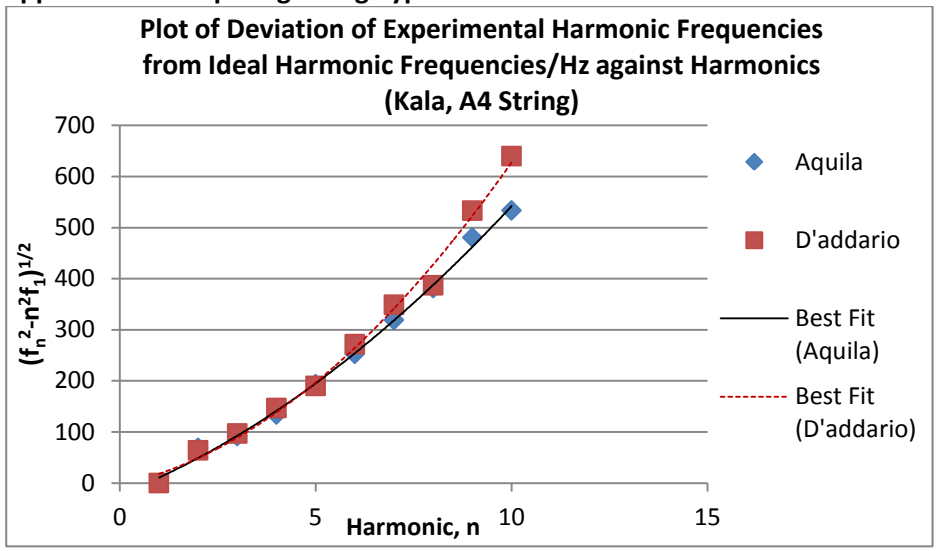

Figure 5.9: Plot of $\sqrt{{f_n}^2 - n^2{f_1}^2}$ against n for the A4 String of the Kala ukulele.

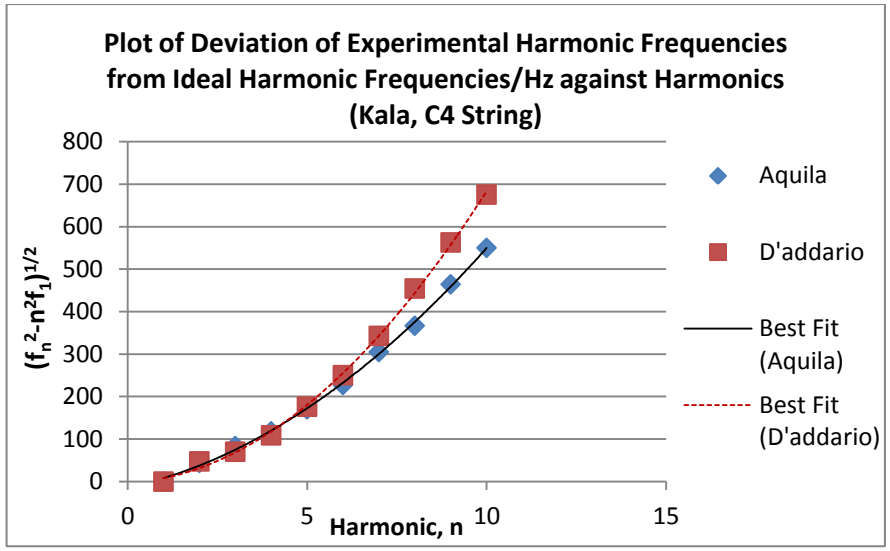

Figure 5.11: Plot of $\sqrt{{f_n}^2 - n^2{f_1}^2}$ against n for the C4 String of the Kala ukulele.

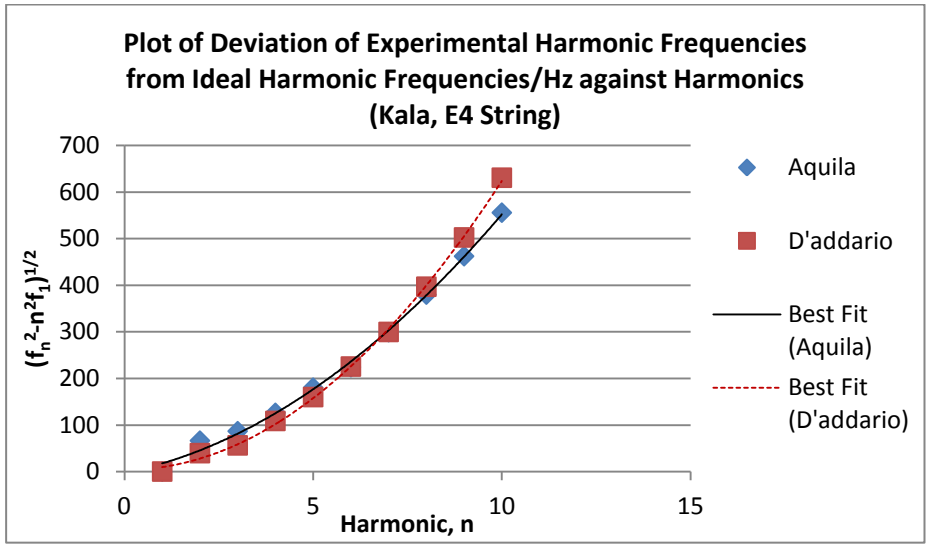

Figure 5.10: Plot of $\sqrt{{f_n}^2 - n^2{f_1}^2}$ against n for the E4 String of the Kala ukulele.

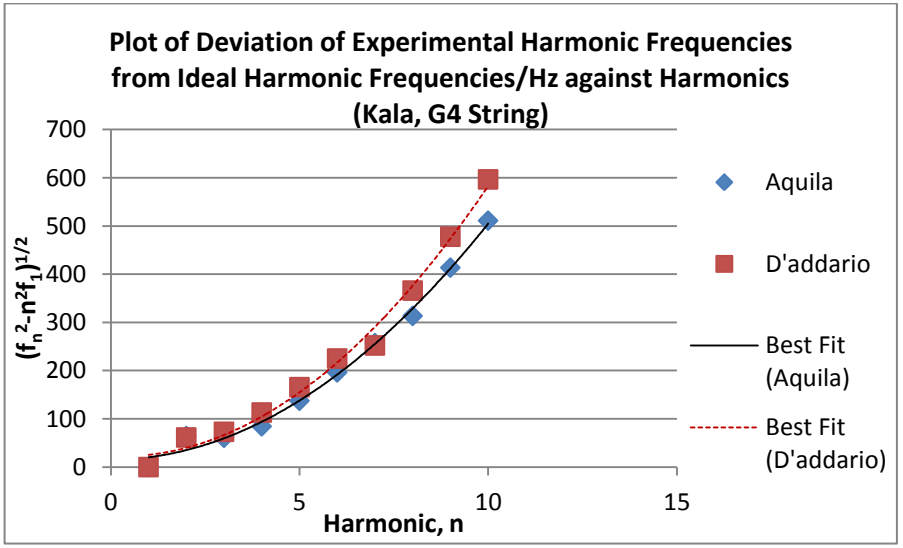

Figure 5.12: Plot of $\sqrt{{f_n}^2 - n^2{f_1}^2}$ against n for the G4 String of the Kala ukulele.

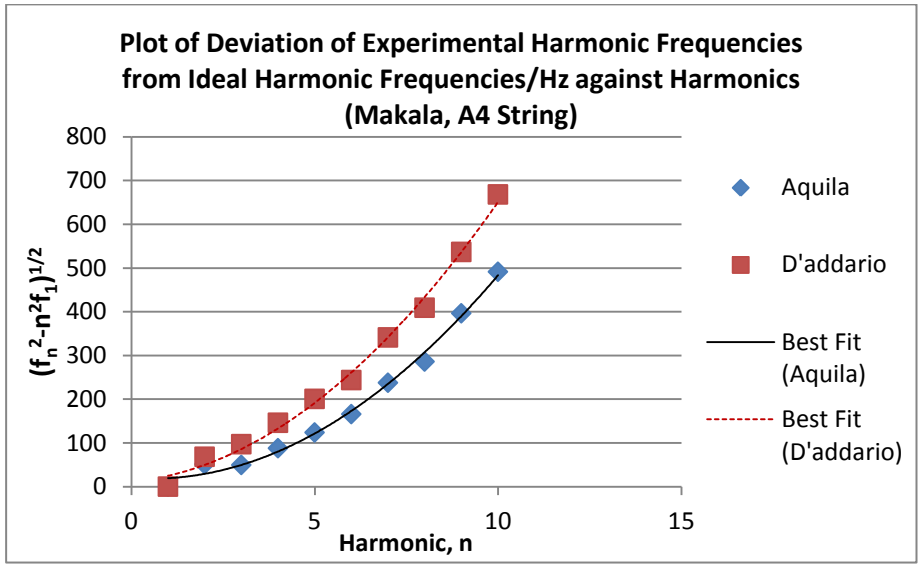

Figure 5.13: Plot of $\sqrt{{f_n}^2 - n^2{f_1}^2}$ against n for the A4 String of the Makala ukulele.

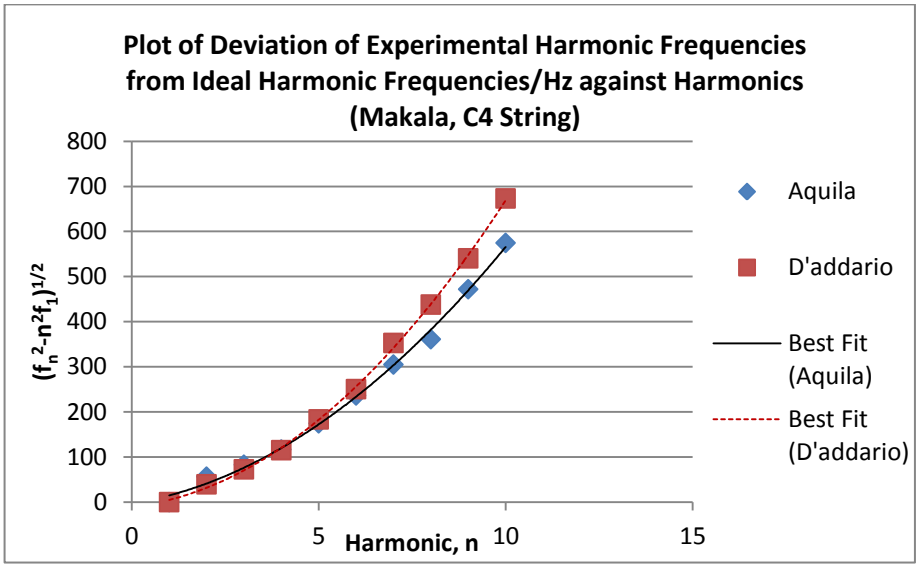

Figure 5.15: Plot of $\sqrt{{f_n}^2 - n^2{f_1}^2}$ against n for the C4 String of the Makala ukulele.

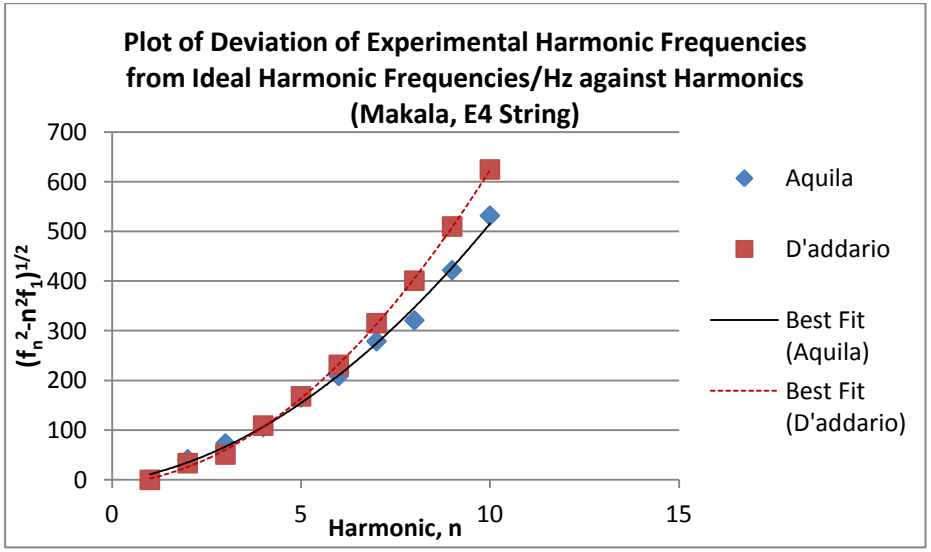

Figure 5.14: Plot of $\sqrt{{f_n}^2 - n^2{f_1}^2}$ against n for the E4 String of the Makala ukulele.

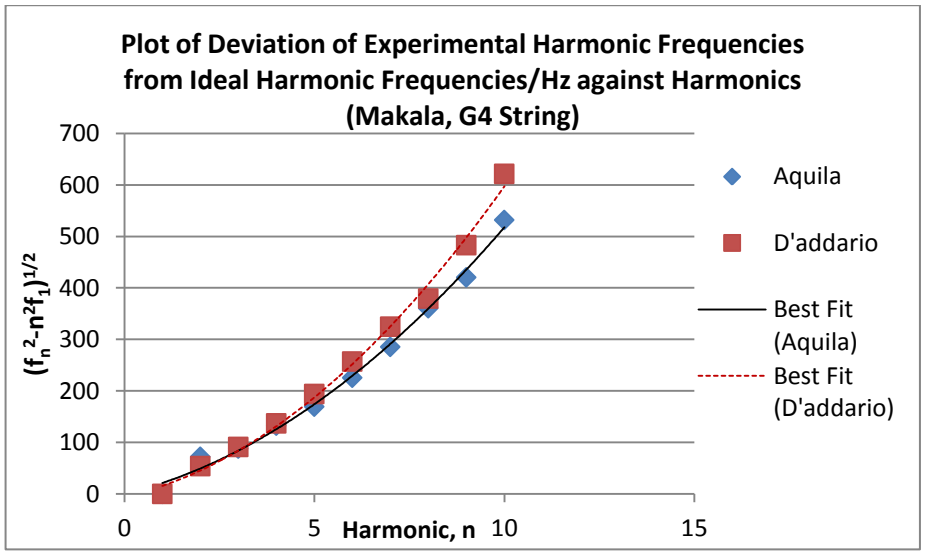

Figure 5.16: Plot of $\sqrt{{f_n}^2 - n^2{f_1}^2}$ against n for the G4 String of the Makala ukulele.

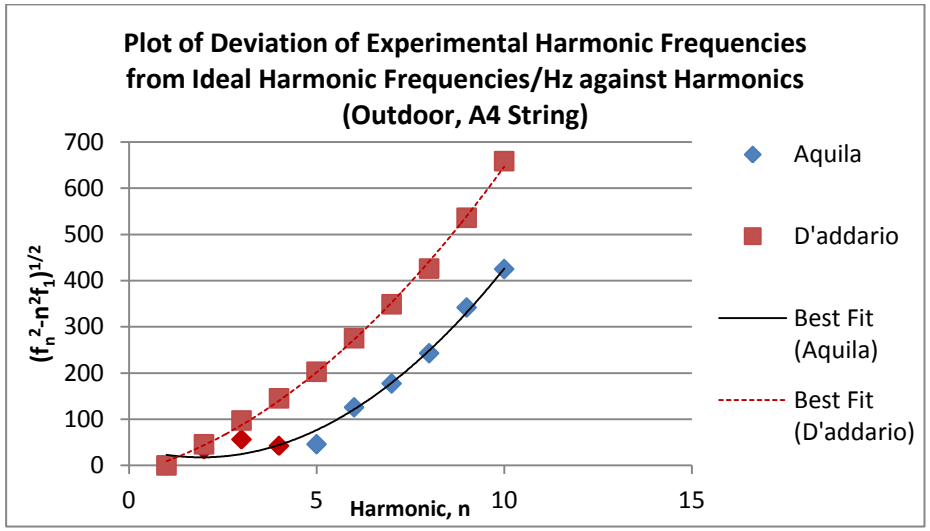

Figure 5.17: Plot of $\sqrt{{f_n}^2 - n^2{f_1}^2}$ against n for the A4 String of the Outdoor ukulele.

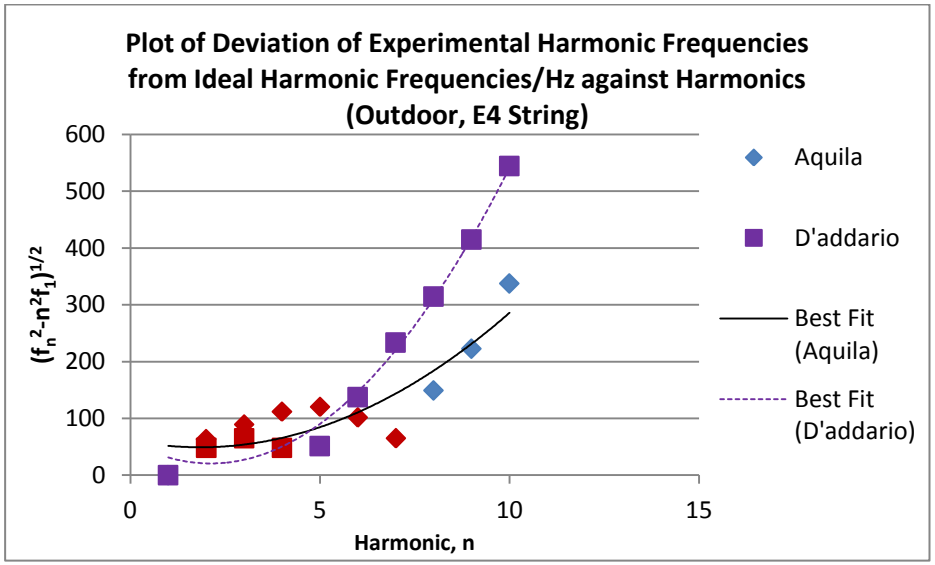

Figure 5.18: Plot of $\sqrt{{f_n}^2 - n^2{f_1}^2}$ against n for the E4 String of the Outdoor ukulele.

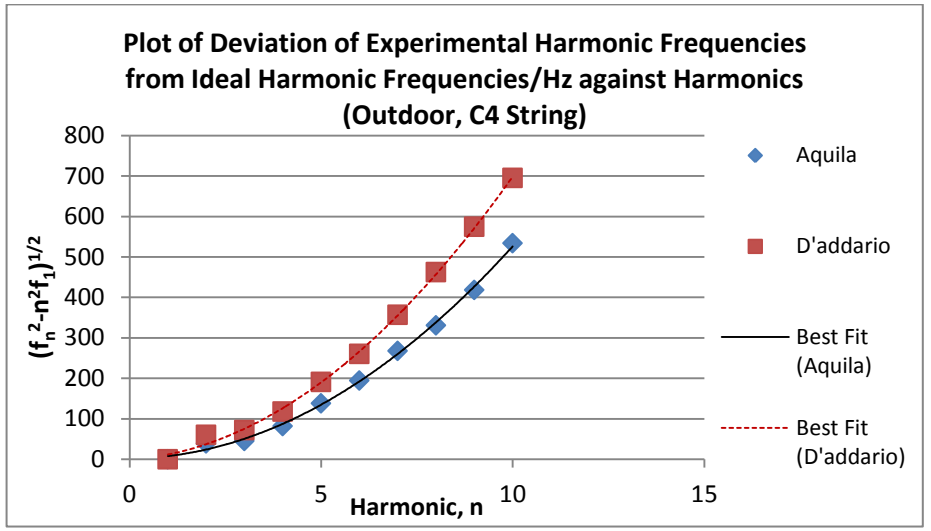

Figure 5.19: Plot of $\sqrt{{f_n}^2 - n^2{f_1}^2}$ against n for the C4 String of the Outdoor ukulele.

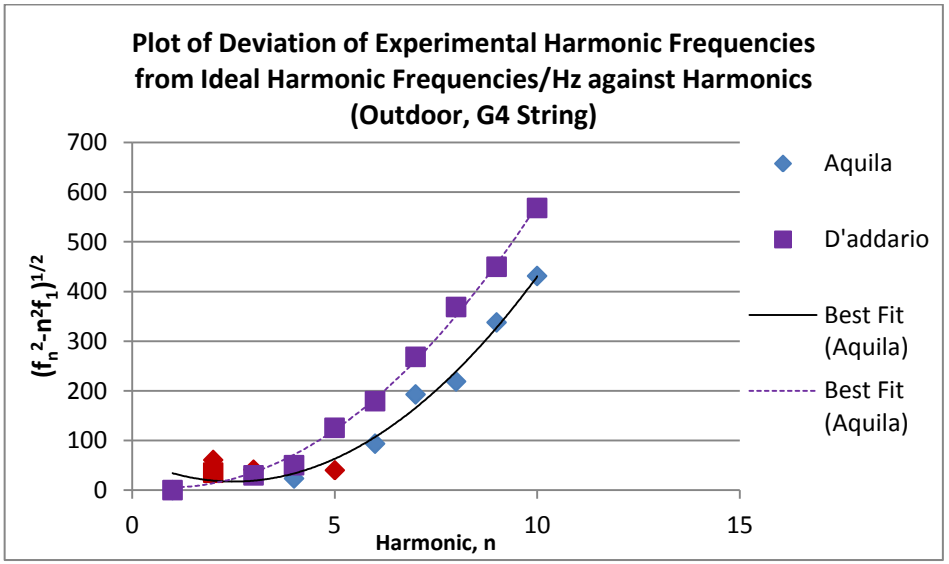

Figure 5.20: Plot of $\sqrt{{f_n}^2 - n^2{f_1}^2}$ against n for the G4 String of the Outdoor ukulele.